UNIVERSITY OF CALIFORNIA
SANTA CRUZ

DEEP SEA CORALS AS PALEOPROXIES FOR THE CENTRAL NORTH PACIFIC OVER THE LAST ~12,000 YEARS: STUDY OF $\delta^{13}C$, $\delta^{15}N$, AND BIOGEOCHEMICAL SHIFTS

A dissertation submitted in partial satisfaction
of the requirements for the degree of

DOCTOR OF PHILOSOPHY

in

OCEAN SCIENCES

by

Danielle S. Glynn

December 2022

The Dissertation of Danielle S. Glynn is approved:

_____
Professor Matthew McCarthy, chair

_____
Professor Christina Ravelo

_____
Nancy Prouty, Ph.D.

_____
Thomas Guilderson, Ph.D.

_____
Peter Biehl
Vice Provost and Dean of Graduate Studies

Table of Contents

List of Figures

List of Appendix Supplemental Figures

Page #

List of Appendix Tables

ABSTRACT

Deep sea corals as paleo proxies for the central North Pacific over the last ~12,000 years: Study of $\delta^{13}C$, $\delta^{15}N$, and biogeochemical shifts

Danielle Glynn

This thesis explored the use of bulk stable nitrogen ($\delta^{15}N$) and carbon ($\delta^{13}C$) isotope records from central Pacific proteinaceous deep-sea corals to create novel multi-millennial scale, sub-decadal resolution records of export production in this ocean region. I used live collected and subfossil coral specimens from both the central North Pacific Subtropical Gyre and Line Islands, to explore how coral isotope records can reconstruct climate forced changes in oceanography in very different areas of the Pacific, as well as to explore the limits of isotope records and coral skeleton preservation over time.

My thesis is organized in three parts. In the first chapter, I used three *Kulamanamana haumeaae* specimens from the main Hawaiian Islands to create ~5000 year record of North Pacific Subtropical Gyre (NPSG) export production $\delta^{15}N$ and $\delta^{13}C$ history, greatly expanding previous coral records (by ~4000 years) into the Mid-Holocene. These bulk isotope records revealed a very different oceanic regime during the mid-Holocene, with higher $\delta^{15}N$ values indicative enhanced flow of source waters bearing signatures of denitrification from the eastern Pacific. Further, these new $\delta^{15}N$ data confirmed that the extremely low present day $\delta^{15}N$ values recorded by deep sea corals (~8‰) are unprecedented for the NPSG, at least within the past five millennia. My data also suggested that the coupling or decoupling of $\delta^{15}N$ and $\delta^{13}C$

values may be an important new tool for understanding the ocean's response to climate shifts. During most biogeochemical regimes shifts in this period, $\delta^{15}N$ and $\delta^{13}C$ trends were synchronous (similar to recent coral records), consistent with nutrient concentration and isotopic values acting together with plankton community shifts. However, several distinctly decoupled regimes also appear, indicating unusual mechanisms must have been at work. Phytoplankton species composition and nutrient source changes are hypothesized as the dominant mechanisms which controlled the coupling and decoupling of $\delta^{15}N$ and $\delta^{13}C$ values, likely primarily influenced by changing oceanographic conditions (e.g., stratification versus entrainment).

Chapter 2 was a methodological study, aimed at understanding the extent in time over which proteinaceous coral records from this region can be extended. Specifically, this study examined the relative changes due to degradation in subfossil corals, asking to what degree bulk versus compound-specific isotope values remain viable over multi-millennial time scales. This chapter examined one of the oldest deep sea *K. haumeaae* corals ever collected and the specifics of proteinaceous skeleton preservation over ~10 kyrs on the seafloor. I compared amino acid (AA) molar composition and isotope pattern changes, together with bulk $\delta^{13}C$ and $\delta^{15}N$ values in a subfossil (~9.6-11.6 kyrs BP) coral skeleton with a live collected specimen from the same region (Cross Seamount, Hawaii). I aimed to understand the effects of long-duration benthic oxic exposure on AAs and organic preservation in a subfossil coral. This study shows that while bulk isotope values are dramatically altered in a clear diagenetic outer zone, likely due to carbonate deposition and

protein-structural degradation, most of the AA isotopic data remains almost entirely unaltered. Some notable results included nearly ~50% of glycine loss over ~10 kyrs, likely due to abiotic water based hydrolysis of the protein matrix, which nevertheless does not appreciably shift glycine's isotope values. Despite changes to molecular composition, compound-specific isotope analysis of amino acids (CSIA-AA) data patterns remained almost entirely unchanged in inner coral layers. This indicates that in contrast to bulk isotope data, CSIA-AA data can reconstruct paleo-oceanographic biogeochemical and ecosystem information in subfossil corals beyond the clear outer diagenetic horizon, which is easily identifiable from an evaluation of C/N ratios and the ΣV degradation proxy.

My last chapter, switched back to paleo-oceanographic application for a very different region in the equatorial Pacific (Kingman Reef, Line Islands), one for which no prior proteinaceous coral records exist for the most recent two millennia. I examined the bulk $\delta^{13}C$ and $\delta^{15}N$ values and CSIA-AA $\delta^{15}N$ values of both a live-collected and subfossil specimen to determine how export production isotope values have changed in response to climate shifts through the last ~2000 years. I proposed shifts in both $\delta^{13}C$ and $\delta^{15}N$ values are fundamentally driven by changing current dynamics, with an alternation between dominance by two water sources: western Pacific waters in the North Equatorial Countercurrent, and east Pacific waters in the North Equatorial Current with distinctly different nutrient concentrations and isotopic signatures. I utilized modern day El Niño Southern Oscillation patterns as a model to interpret the overall data, e.g. lower $\delta^{13}C$ and $\delta^{15}N$ values are indicative of more El

Niño-like (warmer/wetter) conditions, with smaller-celled prokaryotic phytoplankton communities, and advection from the west Pacific. These changes in current dynamics recorded in my new records and are likely related to shifts in the Intertropical Convergence Zone, which is the major source of ocean stratification due to controls on precipitation and climate in the region.

Overall, by combining both new methodological work utilizing CSIA-AA to determine preservation state, and a novel set of coral archive records, my thesis expanded the utility of and potential application of deep sea coral archives, while specifically greatly expanding the biogeochemical history of oceanic change in two separate central Pacific regions. My thesis examined time periods and regions for which no such prior records exist, showing that both modern and subfossil specimens can provide high resolution information of Pacific Ocean variability through the Holocene.

Dedication

This work was made possible through the collaboration of those who study ocean biogeochemistry, namely the McCarthy Lab and Stable Isotope Lab of the University of California, Santa Cruz. Thank you to my advisor Matthew McCarthy, and committee members Christina Ravelo, Nancy Prouty, and Thomas Guilderson. Thank you to my coauthors Kelton McMahon and Owen Sherwood and the crew and pilots who helped collect the corals used in this dissertation. I also had much assistance from the Ocean Sciences department, namely Phoebe Lam and Rondi Robison. Thank you to the fellow lab managers, workers, and fellow graduate students such as Stephanie, Elizabeth, Collin, Dyke, Jessie, Wilson, Hope, Natasha, Fabian, Eve, Taylor, and John. Thanks to the undergraduate students who also helped me over the years during the summer program; namely Samantha Kaplan, Arash Jalali-Sohi, Kevin Miles, Lourdes Gomez, and Zoe Wright. Finally gratitude towards my friends and family who helped me see through the long process of getting my PhD. I wish my father was still alive to see me get my doctorate. Also much love to Joe Murray, my significant other who pushed me along into finishing the graduate program and all the others who helped me through the years.

Introduction

1. Motivation: Paleo-oceanography using deep sea corals

With the drastic changes in climate occurring due to human activities, the study of climate and ocean sciences has become increasingly important. By studying Earth and ocean history, humanity can gain an understanding of the underlying mechanisms and processes which link climate change to specific earth, ocean, and ecosystem processes, in order to better predict how climate may evolve in the future. Paleo-oceanography is most broadly the study of the ocean's history, and aims to provide insights on how the ocean as a system has evolved over the past, often in response to climate forcing, with key areas of focus including phytoplankton communities and nutrient dynamics. By understanding past ecosystem changes it becomes easier to both understand present day changes as well as improve predictions of future environmental shifts.

Since the deglaciation ended ~12 kys ago and the Holocene began, global climate has warmed dramatically and human civilizations proliferated to create a substantial impact on the global environment. More recently, climate is shifting rapidly again, with ongoing warming beginning approximately after the 1850s. In order to put modern day climatic changes into perspective, it is necessary to have tools to examine the natural range of variability of past ocean ecosystems, in order to evaluate ongoing shifts and impacts. One way to do this is to utilize *paleo proxies,* which are specific data types that paleo-climatologists gather from natural recorders of climate variability, such as tree rings, ice cores, ocean sediments, and different

types of corals, which collectively are referred to as *paleo archives*. By reconstructing climate-driven shifts in ocean conditions through the usage of oceanic proxies measured in archives such as sediments and corals, the natural variation of ecosystems such as the oligotrophic open ocean can be revealed. My thesis is focused on using deep sea proteinaceous corals as archives for isotopic information, developing this combination to elucidate ocean change over several different periods over the course of the Holocene in the North Pacific Subtropical Gyre (Hawaiian corals spanning 1-5 kyrs and ~10-12 kyrs) and the central equatorial Pacific (Kingman Reef corals spanning the most recent 2 kyrs).

Deep sea corals are fundamentally different from the more familiar photosynthetic varieties of corals found in tropical reef ecosystems. They come in many varieties, and can form calcite and/or proteinaceous skeletons. Proteinaceous deep sea corals which are the focus of my thesis survive in the dark depths of the ocean by the consumption of falling organic matter that originates ultimately from surface phytoplankton populations. Whereas tree rings can record the signature of precipitation in their growth layers, deep sea coral skeletons record in their growth layers the changes in the sinking particle food sources which track nutrient dynamics and phytoplankton communities. By sending down robotic vehicles it is possible to collect both living and dead-collected (subfossil) coral skeletons for analysis. The chemical signatures recorded in the near-annual proteinaceous layers can then be used to understand the history of nutrients and phytoplankton at very high resolution (~4-10 years per 0.1 mm).

The gold coral *K. Haumeaae* utilized for this study is a particularly long-lived variety, with colony ages up to ~2700 years and a growth rate of ~36 ± 20 μm per year (Roark et al. 2009). This makes them particularly useful recorders of the chemical signatures of sinking organic matter over time to reveal the changes in oceanic conditions, which reveals changes in oceanic carbon storage and food web dynamics. Using live-collected and subfossil specimens from near the Hawaiian Islands (Lanikai and Cross Seamount) and equatorial Pacific (Kingman Reef, Line Islands) the main work in this thesis focused on multiple millennia of oceanic history in these regions, which showed changes in oceanic nutrients and phytoplankton communities through time. Due to their ubiquitous distribution on seamounts throughout the global oceans, proteinaceous deep sea corals are important potential paleo archives, with the ability to provide high resolution data spanning important oceanographic regimes that influence global climate conditions. Therefore I examined how far into the past isotope proxies can be used in subfossil corals and what they suggest for past oceanic ecosystems.

2. Study Sites: Subtropical Gyre and Equatorial North Pacific

Open ocean regions are critical for understanding both global and oceanic climate change, yet they are also complex regions that are very difficult to study using typical paleo archives such as sediment cores. These regions are typically lower in both nutrients and phytoplankton biomass than areas near the coasts, and yet they comprise most of the surface area of the earth, comprising the largest of all ocean biomes and biogeochemical provinces. Due to coupled ocean-atmosphere

teleconnections, the Pacific Ocean region in this study has a substantial influence on global climate dynamics and experiences oscillations in sea surface temperatures and stratification on a variety of different timescales. However, studying long term changes at high resolution in such open ocean regions is difficult based on many traditional sediment cores records, primarily due to the low rate of sedimentation. Utilizing sediment cores, the most common ocean archive, may only provide a single isotopic data point representing hundreds to thousands years, due to a combination of slow sedimentation rates and bioturbation. In region with seamounts, deep sea corals can overcome these issues as they provide high resolution data within their near-annual growth layers and are particularly useful for open ocean ecosystems.

In my dissertation I focus on two different systems, first the North Pacific Subtropical Gyre (near the Hawaiian Islands), and second the tropical equatorial central Pacific (near the Line Islands). The North Pacific Subtropical Gyre (NPSG) is characterized by complete utilization of nitrate in the surface waters, intensive nutrient recycling, and diazotrophic phytoplankton communities which can fix nitrogen (Karl et al. 2002). As oligotrophic gyre ecosystems appear to be expanding due to warming temperatures (Polovina et al. 2008), by studying the Holocene it becomes possible to determine whether natural variability can plausibly account for any part of current change through examining whether such conditions occurred previously. Prior to this dissertation, published deep sea coral records existed for only the most recent millennium (Sherwood et al. 2014, McMahon et al. 2015). In my

thesis I provide a further ~4000 years of NPSG history into the Mid-Holocene (0-5 kyrs) as well as a record from the early Holocene (~10-12 kyrs ago).

The second site is in the central equatorial Pacific (CEP). Kingman Reef is not in the central gyre, but instead on a borderline between the gyre and the region influenced by equatorial upwelling, and so is heavily impacted by the major currents from the east and west Pacific, which change in strength and latitude due to shifts in climate, such as the well-known El Niño Southern Oscillation (Johnson et al. 2002). In the CEP temperature and precipitation control phytoplankton biomass, with warmer and wetter conditions facilitating less chlorophyll and smaller celled organisms (Yan et al. 2011), with a strengthened North Equatorial Counter Current from the west Pacific. Conversely, cooler and drier conditions correspond to a strengthened advection from the more nutrient rich eastern Pacific (Johnson et al. 2002), facilitating more productivity such as from larger celled organisms like diatoms. There have not been any prior deep sea coral records developed for the CEP region, and only one sediment core record exists from the region, which lacks the most recent few millennia (Altabet 2001). This new data set therefore represents the first isotopic records for the most recent two millennia of changing equatorial Pacific current dynamics. The new data can provide information on water mass changes in nutrients linked to larger climatic dynamics.

3. Tools: Bulk and compound specific AA Stable Isotopes ($\delta^{15}N$ and $\delta^{13}C$)

Stable isotopes, both of total samples and individual amino acids, are the primary analytical toolset of my thesis. Most elements exist in two or more forms, known as isotopes, which differ due to slight differences in atomic weight, causing different isotopes to behave slightly differently in chemical reactions and physical processes. This is a process known as fractionation, where typically a lighter isotope reacts faster than a heavier isotope in biologic processes. Different environments are often characterized by predictable isotopic signatures and different phytoplankton groups may also have distinct signatures due to their photosynthetic processes. "Bulk" isotope analysis examines the isotope ratios of entire samples, in this case of skeleton powder. These bulk measurements are useful as very high resolution data records can be readily created, and yet at the same time bulk isotope values are intrinsically limited due to being the product of both nutrient shifts and trophic changes. In contrast, examining the isotopes of individual amino acids provides more specific information regarding source nutrients, trophic structure, and phytoplankton community composition.

Bulk nitrogen (N) isotope ratios ($\delta^{15}N$) is well established as a biogeochemical tool to track the $\delta^{15}N$ value of primary exported marine organic matter and its multiple isotopic influencers. The $\delta^{15}N$ value is impacted by 1) the degree of source nitrate utilization by autotrophs (Rafter and Charles, 2012), 2) N sources (terrigenous inputs and N fixation; e.g. Guilderson et al., 2013), and 3) N sinks (denitrification and anammox; Dubois et al., 2011), and 4) attendant adjustments in the concentration

(Altabet et al., 1991) and $\delta^{15}N$ of supplied nitrate (Rafter et al., 2012). For deep sea corals in the open ocean and equatorial Pacific, these proxies ultimately record $\delta^{15}N$ signatures related to changes in nitrate isotopic values, revealing information on possible nitrogen fixation changes, physical current changes, and plankton food web dynamics of the surface waters. Primarily, I used bulk $\delta^{15}N$ values to understand shifts in central Pacific current dynamics, linked to trade winds and sea surface temperature shifts.

Bulk $\delta^{13}C$ values are linked to a larger set of possible drivers, yet ultimately are complimentary to $\delta^{15}N$ data, typically forced by similar mechanisms. The ocean absorbs CO_2 through physical as well as biological processes, creating distinct carbon (C) isotope values ($\delta^{13}C$) which differ between oceanographic regions and phytoplankton community composition. There are clear latitudinal gradients in phytoplankton $\delta^{13}C$ values, with higher values found within the equatorial upwelling zone near the equator (though with little <2‰ interannual variability in the central equatorial Pacific) and values decline into the subtropical gyres (Magozzi et al. 2017). Different phytoplankton groups have unique carbon isotope fractionations during photosynthesis (Laws et al., 1995; Rau et al., 1996), and thus a shifting phytoplankton community composition can be a major driver behind changes in $\delta^{13}C$ values of export production recorded in deep sea corals over time (McMahon et al., 2015). Thus this dissertation uses bulk $\delta^{13}C$ values primarily to investigate multi-millennial changes in phytoplankton communities, typically related to shifts in the relative proportion of smaller celled cyanobacteria (lower values) and larger celled diatom

based communities (higher values). The oscillation between dominance of these two groups is in turn related to nutrient abundance and/or N fixation, which allows both $\delta^{13}C$ and $\delta^{15}N$ shifts to be used together to evaluate hypotheses about ocean change.

A more novel method used for this dissertation is compound-specific isotope analysis of amino acids (CSIA-AA), which analyze the isotope ratios of the basic AA building blocks of the proteinaceous skeleton of *K. haumeaae* corals. This technique is explained in the chapters which follow, but ultimately it is based on the differential biochemical and metabolic fractionation of specific AA groups. For example, there are specific amino acids which are only produced by phytoplankton at the base of the food web that experience little to no change upon being consumed by other organisms, thus more directly tracking source nutrient conditions and phytoplankton compositional changes. These are known as source (nitrogen) and essential (carbon) amino acids. Others are modified due to trophic transfer and have a distinct fractionation effect which can be utilized to examine changes in trophic position, microbial resynthesis, or changing phytoplankton community compositions. By utilizing CSIA-AA as a complimentary approach to bulk isotope analysis, this study examines changes in nutrients and phytoplankton dynamics for time periods and regions not previously examined in such high resolution, as well as furthers the application of utilizing deep sea corals as paleo proxies for the Holocene by examining the extent of degradation of the proteinaceous matrix after multi-millennial periods on the seafloor.

In addition to studying isotopic changes, a final approach utilized is examining the molecular compositional changes of the different amino acids, which we used in a method focused chapter to evaluate the preservation and degradation state of a subfossil coral. Most previous studies have only utilized live-collected corals, so one of the key goals of part of this thesis is testing the long term fidelity of *K. Haumeaae* subfossil corals. Due to the very long colony lifespans (thousands of years) and protected status of these gold coral species, by using the dead subfossil skeletons it may be possible to extend records without the destructive harvesting required of living specimens. However, prior to this thesis the long term preservation or degradation status after millennial timespans on the seafloor without an outer living colony had not been studied in depth. My 2nd chapter therefore ground truths our data by looking at possible degradative signatures that might convolute the isotopic data. Specifically, by looking at both molecular changes as well as isotopic shifts in certain amino acids, we further validate the utility of even subfossil corals to reveal environmental signatures.

4. Chapter Summary

Using these tools, this dissertation consists of three chapters. **Chapter 1** examines a 5000 year record of $\delta^{15}N$ and $\delta^{13}C$ oceanic history from Lanikai, Oahu, Hawaii, vastly extending previous coral records which only touched upon the most recent millennia (Sherwood et al. 2014, McMahon et al. 2015). My results reveal multiple large isotopic shifts in both $\delta^{15}N$ and $\delta^{13}C$ values similar to or even larger in magnitude to those linked to rapid ongoing climate change in the last 150 yrs. This

suggests that part of the modern day trends could be due to natural variability. While typically $\delta^{15}N$ and $\delta^{13}C$ trends were coupled (i.e., in the same direction), there were distinct periods where this was not the case, suggesting that oceanographic forcing and ecosystem responses controlling $\delta^{15}N$ and $\delta^{13}C$ values of export production were substantially different earlier in the Holocene compared to mechanisms controlling the present day system.

Chapter 2 compares bulk and CSIA-AA data from a live collected coral from Cross Seamount, Hawaii with a subfossil specimen from ~9.6-12 kyrs ago. This second chapter examines the degradative effects of seawater intrusion to the coral skeleton by looking at bulk $\delta^{15}N$ and $\delta^{13}C$ values, as well as CSIA-AA and molecular percentage (mol%) data to examine which amino acids are preserved or changed over the multi-millennial time frame. This study discovered an overall loss of glycine over time as well as a clear diagenetic horizon in the outermost layers which caused elevated isotopic values and higher C/N values alongside signatures of microbial resynthesis. Beyond that horizon, this chapter indicates that at least CSIA-AA values likely can still preserve original isotope values, and so environmental information, even after millennia upon the seafloor.

Finally, Chapter 3 examines a different location in the equatorial North Pacific using a live and subfossil specimen from Kingman Reef, Line Islands to examine ~2000 years of bulk $\delta^{15}N$ and $\delta^{13}C$ values along with CSIA-AA $\delta^{15}N$ data, with the ultimate goal of determining the history of nutrients and phytoplankton community shifts, which in turn are related to changes in current dynamics and variability in the

precipitation Southern Oscillation Index. Specifically, I hypothesize that shifts to higher $\delta^{15}N$ and $\delta^{13}C$ values are linked to enhanced flow of more nutrient rich waters from the eastern Pacific, resulting in more relative diatom contribution in export production, while in contrast lower $\delta^{15}N$ and $\delta^{13}C$ values are suggestive of enhanced western Pacific advection containing signatures of smaller celled prokaryotic and possibly diazotrophic phytoplankton populations. My data ultimately links isotopic variability with changes in current dynamics related to the Intertropical Convergence Zone.

Taken as a whole, this dissertation greatly extends previous coral records in time and for unique locations, while providing the first detailed information regarding the fidelity of these archives over long time scales. This component represents the first detailed study of degradation and preservation of CSIA-AA and bulk isotope data in coral skeletons, and my data therefore expands the overall utility of using subfossil *K. Haumeaae* corals as archives to study Holocene climate by discovering the key structural, molecular and isotopic changes that occur through time. Overall, my data clearly show several periods of major change in both $\delta^{15}N$ and $\delta^{13}C$ values over the last 5000 years similar in magnitude to changes in the Anthropocene (since the Industrial Revolution), however in general the past changes appear to have occurred over much longer (~millennial) timescales. My new data links isotopic changes to climatic variability, in order to provide an improved understanding of NPSG and CEP oceanographic changes over multi-millennial timescales.

Chapter 1

Major shifts in nutrient and phytoplankton dynamics in the North Pacific Subtropical Gyre over the last 5000 years revealed by high-resolution proteinaceous deep-sea coral $\delta^{15}N$ and $\delta^{13}C$ records

The results presented in this chapter are published in Earth and Planetary Science Letters as an article by Danielle S. Glynn and co-authors as follows:

Glynn, D. S., McMahon, K. W., Guilderson, T. P., & McCarthy, M. D. (2019). Major shifts in nutrient and phytoplankton dynamics in the North Pacific Subtropical Gyre over the last 5000 years revealed by high-resolution proteinaceous deep-sea coral $\delta^{15}N$ and $\delta^{13}C$ records. *Earth and Planetary Science Letters*, **515**, 145-153.

Abstract

The North Pacific Subtropical Gyre (NPSG) is the largest continuous ecosystem on Earth and is a critical component of global oceanic biogeochemical cycling and carbon sequestration. We report here multi-millennial-scale, sub-decadal-resolution records of bulk stable nitrogen ($\delta^{15}N$) and carbon ($\delta^{13}C$) isotope records from proteinaceous deep-sea corals. Data from three *Kulamanamana haumeaae* specimens from the main Hawaiian Islands extend the coral-based time-series back ~5000 years for the NPSG and bypass constraints of low resolution sediment cores in this oligotrophic ocean region. We interpret these records in terms of shifting biogeochemical cycles and plankton community structure, with a main goal of placing the extraordinarily rapid ecosystem biogeochemical changes documented by recent coral records during the Anthropocene in a context of broader Late-Holocene variability.

During intervals where new data overlaps with previous records, there is strong correspondence in isotope values, indicating that this older data represents a

direct extension of Anthropocene records. These results reveal multiple large isotopic shifts in both $\delta^{15}N$ and $\delta^{13}C$ values similar to or larger in magnitude to those reported in the last 150 years. This shows that large fluctuations in the isotopic composition of export production in this region are not unique to the recent past, but have occurred multiple times through the Mid- to Late-Holocene. However, these earlier isotopic shifts occurred over much longer time intervals (~millennial vs. decadal). Further, the $\delta^{15}N$ data confirm that the extremely low present day $\delta^{15}N$ values recorded by deep sea corals (~8‰) are unprecedented for the NPSG, at least within the past five millennia.

Together these records reveal centennial to millennial-scale oscillations in NPSG biogeochemical cycles. Further, these data also suggest a number of independent biogeochemical regimes during which $\delta^{15}N$ and $\delta^{13}C$ trends were synchronous (similar to recent coral records) or distinctly decoupled. We propose that phytoplankton species composition and nutrient source changes are the dominant mechanisms controlling the coupling and de-coupling of $\delta^{15}N$ and $\delta^{13}C$ values, likely primarily influenced by changing oceanographic conditions (e.g., stratification vs. entrainment). The decoupling observed in the past further suggests that oceanographic forcing and ecosystem responses controlling $\delta^{15}N$ and $\delta^{13}C$ values of export production have been substantially different earlier in the Holocene compared to mechanisms controlling the present day system.

1. Introduction

Modern subtropical gyres are characterized by low nutrient concentrations and low primary production, with biogeochemical cycles typically dominated by microbial loop dynamics (Karl, 1999). These oligotrophic gyre systems comprise around 60% of the global oceans and are critical components of the global marine biogeochemical balance (Karl, 1999). It is now recognized that aggregate open-ocean oligotrophic regions, due to their vast extent, contribute the bulk of marine productivity and account for a substantial amount of global ocean export (Karl et al., 1997; Martin et al., 1987).

The North Pacific Subtropical Gyre (NPSG) is the largest contiguous ecosystem on earth, and remote sensing indicates that it is rapidly expanding (Polovina et al., 2008). In contrast to global trends of declining marine productivity, phytoplankton communities of the NPSG are increasing in both biomass and productivity (Boyce et al., 2010; Corno et al., 2007; Karl et al., 2001). This is due to changes in plankton community structure, which appear to be linked to the addition of new nutrient sources from expanding communities of nitrogen-fixing diazotrophs, selected for by increased stratification (Karl et al., 1997; Karl et al., 2001; Karl et al., 2011). As such, understanding how algal community structure and nutrient supply have responded to physical forcing in the past is critical to understanding future changes in the ecosystem dynamics of these critical open ocean systems. As part of the Hawaiian Ocean Time-Series (HOT) program, instrumental observations taken at Station ALOHA (22°45’N, 158°W) suggest that variability in physical and biological

attributes of the NPSG are coupled to inter-annual climate variability superimposed upon longer term, basin-wide variability (Corno et al., 2007; Di Lorenzo et al., 2008). While much can be gained from detailed instrumental records at ALOHA and other time-series stations, the short timescale of these records is inadequate to understand the coupling of biogeochemical cycles to long term climate forcing. Further, the low sedimentation rate in oligotrophic regions, such as the NPSG, means the entire Holocene is recorded in ~10 cm of bioturbated sediments, leading at best to uncertain, low resolution sediment records.

Cosmopolitan deep-sea proteinaceous corals are unique biogenic archives that can provide centennial to millennial-scale records at sub-decadal resolution of past ocean conditions. These azooxanthellate corals are low-order consumers which feed on recently exported particulate organic matter (POM), and record the isotopic signatures of this food source into the accretionary growth layers of proteinaceous skeletons (Roark et al., 2009; Sherwood et al., 2014; McMahon et al., 2017). The horny proteinaceous skeleton is composed of a fibrillar protein framework (Ehrlich et al., 2006) that is resistant to degradation (Sherwood et al., 2006). The Hawaiian gold coral *Kulamanamana haumeaae,* a colonial zoanthid, is extraordinarily long-lived, thus providing a bioarchive on multi-millennial time scales for the NPSG region with average radial growth rates in the low tens of microns per year (Guilderson et al., 2013; Roark et al., 2009).

Previous deep-sea coral records from the NPSG Hawaiian Islands spanning the last ~1000 years have shown dramatic decreases in both nitrogen ($\delta^{15}N$;

Sherwood et al. 2014) and carbon ($\delta^{13}C$; McMahon et al. 2015) isotopic values since the Little Ice Age (~1850 CE) by ~1.5‰ and ~1.2‰ for $\delta^{15}N$ and Suess-corrected $\delta^{13}C$ respectively. These data indicate that both $\delta^{15}N$ and $\delta^{13}C$ values of exported primary production have strongly decreased, commensurate with 20th century warming and gyre expansion. Sherwood et al. (2014) used a multi-proxy compound-specific stable isotope approach to show that the declining deep-sea coral $\delta^{15}N$ values were indicative of an increase in the relative contribution of nitrogen fixation supporting export production in the NPSG over the last 150 yrs. McMahon et al. (2015) then used a compound-specific stable isotope $\delta^{13}C$ fingerprinting approach to show a concurrent shift towards more N_2-fixing cyanobacteria in the phytoplankton community supporting export production over this time period, consistent with the conclusions of Sherwood and co-authors.

Together, these records indicate dramatic responses in both broad algal community structure and fundamental biogeochemical cycles to shifting climate states of the NPSG. Specifically, these data have suggested: 1) direct coupling in major changes of primary production $\delta^{15}N$ and $\delta^{13}C$ values over the last ~1000 years, 2) that present primary production $\delta^{15}N$ and $\delta^{13}C$ values are the lowest in at least a millennium, 3) the variability in $\delta^{15}N$ and $\delta^{13}C$ of export production is driven primarily by algal community structure shifts, and 4) that stratification may be a major driver for these changes in plankton community dynamics (Sherwood et al., 2014; McMahon et al., 2015). However, in order to assess these hypotheses within the broader context of the Holocene, longer records are required to better understand

the potential drivers for recent variability and to potentially facilitate predictions of ecosystem responses to future change.

The main goal of this study was to determine if the dramatic changes documented in the last 150 years are in fact unique or if similar coupled $\delta^{15}N$ and $\delta^{13}C$ shifts are typical on millennial timescales. To answer these objectives, we report bulk stable nitrogen and carbon isotope records extending into the Mid-Holocene (~5000 years ago), from proteinaceous deep-sea coral specimens collected from offshore Oahu, Hawaii. Proteinaceous deep-sea coral skeletons' bulk $\delta^{15}N$ and $\delta^{13}C$ stable isotope values are a reliable proxy of baseline isotope dynamics represented by source and essential amino acid values (e.g., Schiff et al., 2014; Sherwood et al., 2014; McMahon et al., 2015; 2017). These new records are used to examine the stability of historical baselines in export production $\delta^{15}N$ and $\delta^{13}C$ values.

2. Materials and Methods:

Three sub-fossil *K. haumeaae* deep-sea coral samples were collected from ~400 m depth offshore of Lanikai on the island of Oahu, Hawaii (21° 24.4' N, 157° 38.6' W; Fig. 1-1). In the results and discussion below, we refer to individual specimens as Lanikai 1, 2, and 3 (L1, L2, and L3). Skeletons were washed with seawater then fresh water before being air-dried on deck. Cross section disks ~0.7 cm thick were cut from close to the basal attachment, polished, and mounted onto glass plates. A computerized Merchanteck micromill was used to isolate 2-3 mg of proteinaceous coral skeleton at 0.1 mm increments along radial transects from the

outer edge to the center. The disk radius for L1, L2, and L3 were 17.5, 13.0, and 27.6 mm respectively. A subset of samples (1-2 mg each, 5-6 per coral) were acidified in 1 N HCl for 20 hours under refrigerated conditions, filtered onto a 0.22 μM GFF which was then dried overnight at 45ºC before being scraped off into a tin capsule for EA analysis.

Bulk $\delta^{15}N$ and $\delta^{13}C$ analyses were conducted on ~0.3 mg raw material using a Carlo Erba 1108 elemental analyzer coupled to a ThermoFinningan Delta Plus XP isotope ratio mass spectrometer at the UCSC Stable Isotope Laboratory, following the lab's standard bulk stable isotope protocols (which can be found at this link: *https://websites.pmc.ucsc.edu/~silab/EA_Protocol.php/*). Results are reported in conventional per mil (‰) notation relative to air and VPDB standards for $\delta^{15}N$ and $\delta^{13}C$, respectively. Laboratory error is 0.2‰ for both $\delta^{15}N$ and $\delta^{13}C$, with duplicate coral analyses (n=28) indicating 0.11‰ and 0.14‰ reproducibility for $\delta^{15}N$ and $\delta^{13}C$, respectively. Coral C:N values have a C:N laboratory error of 0.1 as determined from repeated measurements of co-analyzed acetanilide.

Radiocarbon analyses were performed on 7-11 acid-pretreated sub-samples per specimen. Age-models were determined for each specimen using Bacon, a Bayesian modeling approach (Blaauw and Christensen 2011), with Marine13 (Reimer et al., 2013), with more information available in supplemental materials. Isotopic regime shifts were detected using the methodology of Rodionov (2004), with a significance level of 0.1, cut off length of 10, and a Huber's weight parameter of 1.

The regime shift program uses a sequential t-test to determine regimes and can detect shifts in both the mean level of fluctuations and the variance (Rodionov 2004).

For comparison with published bulk sediment $\delta^{15}N$ records, marine sediment cores whose chronology were ^{14}C based were updated using Marine13 (Reimer et al., 2013; details in supplementary file). The $\delta^{15}N$ records from the NICOPP database (Tesdal et al., 2013) were differenced against the mean of each individual record for the last 6000 years, and datasets were combined to determine a regional, composite response. Sediment records were restricted to those that had more than two $\delta^{15}N$ sampling points in the last six millennia. Simple bivariate linear regressions were performed using JMP Pro® version 12 on both coral and sediment records to examine long-term trends and probabilities.

3. Results:

3.1 Timescale and Resolution

The 95% confidence interval for the individual age models averaged 98 ± 15 years (Fig. 1-S1, Table 1-1). The L1 record (1510 to 220 CE) partially overlaps with the coral record from an adjacent location (M; fig. 1-1B) in Sherwood et al. (2014) but extends the record by nearly 1000 years. L1 had an estimated average radial growth rate of 14 μm yr^{-1}, such that isotope samples averaged 7 years. The L2 coral spanned ~565 years (-20 to -580 CE) with a growth rate of 21 μm yr^{-1} and isotope data averaging 5 years. L3 was the oldest coral and spanned ~1420 years (-1540 to -

2960 CE). L3 had an estimated growth rate of 19 μm yr^{-1}, with isotope data averaging 5 years. See appendix data for radiocarbon results (Table 1-1).

3.2 Stable Isotope Results

Stable isotope data and C:N ratios as a function of radial distance and age are reported in Appendix Table 1-2.

3.3 C:N Ratio and Acidification Test as a Screening Tool

All samples from the live-collected Makapu'u coral skeleton in Sherwood et al., (2014) have an invariant C:N ratio of 2.86 ± 0.04, consistent with the 2.8-3.0 range previously reported for modern specimens (Druffel et al., 1995). A C:N of 2.86 ± 0.04 therefore represents the expected range for fresh coral skeletal material. While the average of all C:N values for the three fossil Lanikai corals are within error of this value (L1 2.89 ± 0.09, L2 2.90 ± 0.15, and L3 2.92 ± 0.06), there is also a persistent increase in C:N values for some samples in the outermost layers (Table 1-2). Comparison of acidified versus non-acidified duplicate samples from all three corals shows increases in both C:N and $\delta^{13}C$ values in only the outermost layers (Fig. 1-S2, Table 1-2), with the distance of this effect increasing with time since the death of the colony and thus, seawater exposure time. The youngest fossil coral specimen (L1) showed no difference between acidified and non-acidified samples $\delta^{13}C$ values, however elevated C:N ratios in the outer 1.3 mm may suggest some skeletal degradation. For skeletons L2 and L3 the outer 1 mm $\delta^{13}C$ bulk values average +

0.8‰ more positive compared with acidified samples. Differences in $\delta^{13}C$ decline steadily toward the coral center, and both acidified vs. non-acidified values overlap within error in L2 by 2.2 mm and in L3 by 3.9 mm.

Based on these results and to be conservative in our interpretation, we have excluded samples from layers in which the C:N values or $\delta^{13}C$ values were influenced by acidification (Fig. 1-S2, red shading). Further, throughout the entire remaining data set any sample for which C:N values were outside analytical error (±0.1) of the live collected Makapu'u coral values (<2.72 or >3.0) were excluded (Table 1-2). In the remaining data set (for which all samples had C/N values consistent with fresh coral skeletal material) when data for each coral is considered independently there remains a weak correlation between $\delta^{13}C$ and C:N ratio for two specimens (L1, R^2= 0.23; L2, R^2= 0.12). Therefore, while we cannot rule out the influence of diagenesis in our data set, the magnitude of potential $^{\delta 13}C$ influence based on these regressions (~0.2‰ and ~0.1‰ of total $\delta^{13}C$ record variation, respectively) is very similar to analytical error relative to the larger coral $\delta^{13}C$ record trends and so should not influence the interpretations reported below.

3.4 Nitrogen Stable Isotopes

L1 $\delta^{15}N$ values overlap data from a specimen from nearby Makapu'u, presented in Sherwood et al. (2014), for nearly 170 years (Fig. 1-2A). L1 $\delta^{15}N$ values vary by ~2‰ from a low of 8.8‰ in 240 CE to a high of 10.8‰ in 1400 CE. There appears to be $\delta^{15}N$ oscillations around 9.4 ± 0.3‰ (n=66) between 220 CE and 580

CE, followed by a large increase of ~1.2‰ from 660 CE to a high of 10.3‰ in 680 CE. $\delta^{15}N$ values then decline to an average of 9.9 ± 0.2‰ (710 CE and 1260 CE, n=62) before increasing ~0.8‰ over the next two decades to overlap Makapu'u values.

The L2 coral (-70 to -580 CE) exhibits no clear secular trend but has substantial oscillations (range ~1.6‰) about the mean $\delta^{15}N$ value of 9.2 ± 0.3‰ (n=101, Fig. 1-2A), similar to the values at the start of L1 300 years later. Regime detection (Fig. 1-S3) notes periods of high $\delta^{15}N$ values during -420 to -450 CE (9.8 ± 0.2‰, n=6) and -300 to -340 CE (9.5 ± 0.1‰, n=10). The highest $\delta^{15}N$ value was 10.0‰ (-430 CE). Lower $\delta^{15}N$ values occurred between -190 and -100 CE (8.8 ± 0.4‰, n=18), reaching 8.4‰ in -180 CE.

The Mid-Holocene L3 coral (-1650 to -2960 CE) has substantially more positive $\delta^{15}N$ values (10.8 ± 0.3‰, n=225) compared to all of the Late-Holocene and near modern coral data (Fig. 1-2A). From -2940 to -2600 CE $\delta^{15}N$ increases 0.02‰ decade^{-1} (R^2= 0.51, P<0.0001) from 10.3‰ to 10.9‰, while reaching its lowest value of 10.0‰ in a brief excursion near -2720 CE.

3.5 Carbon Isotope Results

We observe a ~2‰ total range in coral $\delta^{13}C$ values, with low $\delta^{13}C$ values very similar to present day occurring multiple times since the Mid-Holocene (in L1 ~200 CE; in L2 ~-800 CE; in L3 ~-2800 CE, Fig. 1-3A). L1 $\delta^{13}C$ values begin low at -17.1 ± 0.1‰ (n=43) between 220 - 460 CE, before increasing by ~0.4‰ over the next few

decades to an average of -16.7 ± 0.1‰ (480 – 1400 CE, n=110). L1 coral $\delta^{13}C$ values overlap within 0.3‰ with previously published Makapu'u $\delta^{13}C$ records from 1230 - 1400 CE (McMahon et al., 2015).

The L2 $\delta^{13}C$ values range by ~1‰ from a low of -16.9‰ (-370 CE) to -15.8% (-80 CE) over the length of the ~510 year record (Fig 3A). From a relatively stable 16.6 ± 0.1‰ (n=27, -580 - -430CE), $\delta^{13}C$ values increase towards the outer layers of the coral at a rate of 0.01‰ per decade (R^2= 0.48, P<0.0001). The L2 record indicates a large isotopic discontinuity in $\delta^{13}C$ values from the end of L2 to the more recent L1 $\delta^{13}C$ record.

The Mid-Holocene L3 record (-1650 to -2960 CE) is marked by a large and statistically significant, nearly unidirectional, $\delta^{13}C$ shift of ~1.6‰ (~0.01‰ decade^{-1}, R^2= 0.84, p <0.0001) with values ranging from -15.2‰ (-1540 CE) to -17.2‰ (-2860 CE) (Fig. 1-3A). Regime detection suggests this increase occurred between plateaus of more constant values (Fig. 1-S3), from -16.6 ± 0.1‰ (-2680 to -2300 CE, n=49), to -16.3 ± 0.1‰ (-2290 to -2080 CE, n=41), before reaching a third plateau of -15.8 ± 0.1‰ (-1940 to -1630 CE, n=64). Isotopic data can be found in appendix

3.6 Coupling vs. Decoupling of Nitrogen and Carbon Isotope Records

The combined isotope records show several distinct periods of coupling where $\delta^{13}C$ and $\delta^{15}N$ values trend similarly, corresponding closely to what has been observed in records from this region in the last millennium. However, equally common in the longer Holocene records are periods where $\delta^{13}C$ and $\delta^{15}N$ variability

is decoupled, with little change in $\delta^{15}N$ while $\delta^{13}C$ changes dramatically. Unlike the most recent ~1400 years with coupled $\delta^{13}C$ and $\delta^{15}N$, for more than a thousand years (-580 to 670 CE) $\delta^{13}C$ and $\delta^{15}N$ values are generally decoupled, suggesting a different regime than modern (Fig. 1-4, "DC1", representing L2 and part of L1). As noted previously, the $\delta^{15}N$ values throughout this period (-580 to 670 CE, including the gap between L1 and L2 records) remained relatively constant (mean of 9.3 ± 0.3‰), while in contrast the $\delta^{13}C$ values increased in L1 and L2 corals (from -430 to -70 CE and 250 to 670 CE), with an additional large decline in $\delta^{13}C$ values (~1‰) required to connect values between these two records. Further back in the ~1000 year period between L3 and L2 (Fig. 1-4, "??"), the offset between coral records suggests an overall shift in both $\delta^{15}N$ and $\delta^{13}C$ to much lower values from past to present. The Mid-Holocene trends in $\delta^{13}C$ and $\delta^{15}N$ values are decoupled once again from -2550 to -1650 CE, with $\delta^{15}N$ values averaging 10.9 ± 0.3‰, while $\delta^{13}C$ values increase by ~1.5‰. Finally, in the earliest part of this L3 records (-2950 to -2550 CE), both $\delta^{15}N$ and $\delta^{13}C$ values again trend in the same direction.

4. Discussion

4.1 Nitrogen Isotopic Records

The records exhibit a surprisingly wide range in $\delta^{15}N$ values of about 3.5‰, marked by several distinct regimes, with the most positive $\delta^{15}N$ values seen in the Mid-Holocene and lowest in the present day (Fig. 1-2). Using this new 5000 year $\delta^{15}N$ dataset for context, it is clear that the rate of the post-1850 decline (1.5‰ in 150

yrs) is unique. More common in the coral data are long periods of relative stability, with millennial-scale plateaus of similar $\delta^{15}N$ values in three intervals (from approximately -2960 to -1650 CE, -580 to 660 CE, and from 660 to the 1800s; Fig. 1-2). While there are no direct coral data for the millennial-scale gap from -1530 to -580, the offset between L2 and L3 indicates that a ~1.5‰ shift in $\delta^{15}N$ must have occurred in this period. However without more data it is not possible to determine if the shift in the $\delta^{15}N$ value of export production occurred rapidly, like the change in the last 150 years, or was more drawn out or variable over ~1000 years (Fig. 1-2A).

Since nitrate is fully utilized on an annual scale in the NPSG, isotope mass balance requires that the overall $\delta^{15}N$ value of autotrophs represents an integrated signal of the $\delta^{15}N$ value of their nitrogen sources. Thus, gyre-based paleo-$\delta^{15}N$ records can be interpreted in terms of the relative balance of isotopically distinct nutrient sources supporting export production (e.g., Altabet, 2006; Dore et al. 2002; Sherwood et al 2014). The large ~3.5‰ variability in $\delta^{15}N$ values recorded in these corals could therefore be driven by either changing phytoplankton communities (i.e., relative importance of diazotroph N_2-fixation), and/or shifts in the source $\delta^{15}N$ value of advected nitrate. This latter aspect includes both the water mass being entrained during mixing due to changes in stratification as well as changing $\delta^{15}N_{NO3}$ values sourced from the margins. Both situations could have been influenced by changes in water column stability and ocean-biogeochemistry dynamics.

In the NPSG near the Hawai'ian islands nitrogen fixation leads to characteristically low $\delta^{15}N$ values (~0‰) in the upper euphotic zone, while

mesopelagic nitrate sources have much higher values (Dore et al., 2002; Casciotti et al., 2008). By assuming mass balance based on a two-component mixing model, with $\delta^{15}N_{N2\text{-}fix}$ = 0‰ and $\delta^{15}N_{NO3}$ = 6.5‰, and a sinking particulate bulk $\delta^{15}N$ value of 3.5 ± 0.2‰ at 300 m (Casciotti et al., 2008; Dore et al., 2002; Karl et al., 1997), around half (~46%) of present-day exported production is supported by N_2 fixation. The amino acid phenylalanine $\delta^{15}N_{phe}$ values in Hawai'ian proteinaceous corals have been used as a proxy for baseline nitrate and average 2.5 ± 0.3‰ over the late 20th and early 21st century (n=7; Sherwood et al., 2014; McMahon et al., 2017), which implies a similar, albeit slightly higher (~60%) fraction of export production supported by nitrogen fixation. As documented by Sherwood et al. (2014), there is a very strong 1:1 relationship (R^2= 0.77) between bulk skeleton $\delta^{15}N$ and $\delta^{15}N_{phe}$ in *K. haumeaae.* Assuming that this 1:1 covariance is maintained in the Lanikai specimens, it is possible to directly transform (interpret) changes in bulk coral $\delta^{15}N$ variability into baseline variability.

Water column denitrification discriminates strongly against the heavier ^{15}N isotope, leaving seawater nitrate more positive in $\delta^{15}N$, and ocean circulation patterns can transport this isotopic signal from the Eastern Tropical Pacific throughout the Pacific (Altabet, 2006; Sigman et al., 2009). Analysis of North Pacific sediment records (n=30) indicates an overall decline of ~0.5‰ in bulk sediment $\delta^{15}N$ values since the Mid-Holocene (Fig. 1-S4, 1-S5). The decline in sedimentary $\delta^{15}N$ is assumed to reflect changes in source nitrate values and has been attributed to a decline in water column denitrification through the Holocene (Jia and Li, 2011 and

references therein). However, a gradual ~0.5‰ decline in North Pacific Ocean $\delta^{15}N_{NO3}$ values clearly cannot be the primary driver of $\delta^{15}N$ values in our coral records, which exhibit significant variability in $\delta^{15}N$ values rather than a monotonic change. There is also little variability in sedimentary $\delta^{15}N$ values from source regions of the Eastern Pacific that intersect water-masses (isopycnals) ventilating the NPSG interior (Fig. 1-2C), which corresponds to variability in $\delta^{15}N$ export production as reconstructed by coral data. We are thus left with two potential mechanisms that drive the variability we observe. The first is a change in plankton community structure with variable importance of nitrogen fixing diazotrophs and the second is a change in the source of water being entrained into the mixed layer that provides nitrate to the NPSG. It is likely that the physical forcing for these two aspects is related: a more stratified ocean has diminished input from deeper water masses and could provide an expanded niche for diazotrophs (Karl et al., 2001; McMahon et al., 2015).

Mid-Holocene $\delta^{15}N$ values from the L3 specimen average 10.8‰ with sustained positive values in excess of 11‰. Within the context of the modern endmember model previously discussed, a value of 11‰ implies that ~80% of the export production is supported by subsurface nitrate (i.e., only ~20% supported by nitrogen fixation). By -580 CE, the NPSG contribution of N_2-fixation to export production is close to equal with the contribution of subsurface nitrate. By the beginning of the Little Ice Age (~1450 CE), a return to production supported more by nitrate (~70%) than nitrogen fixation (~30%) appears likely. The value of entrained nitrate could be altered if there were 1) simply a higher concentration of NO_3^- sourced

from similar present-day depth, 2) more positive $\delta^{15}N_{NO3}$ entrained from deeper isopycnals, or 3) a different source origin. Deepening of the mixed-layer due to cooling and/or more frequent storm events (windiness) is an obvious mechanism to reduce stratification and increase the vertical flux of NO_3^- into the mixed-layer. In the modern NPSG, stratification is the most common underlying driver associated with shifts in diazotroph communities and rates of nitrogen fixation (Karl et al., 2001). Increased rates of N_2-fixation with abundant populations of *Trichodesmium* have been found to occur during the El Niño warm phase of El Niño Southern Oscillation (ENSO; Karl et al., 1995; Corno et al., 2007) when persistent subsidence leads to decreases in cloud cover, rainfall, and storminess in the Hawai'ian Islands (Diaz and Giambelluca, 2012 and references within). A coupling of warm sea surface temperatures and increased stratification is likely associated with less cloudiness and reduced storminess, which should correspond to lower $\delta^{15}N$ values. Thus, on millennial timescales, the balance of nitrogen supporting export production likely reflects the large-scale circulation patterns associated with coupled ocean-atmosphere dynamics which follows summer insolation (Fig. 1-2B) affecting the descending limb of the Hadley Cell, which can impact ENSO and the migration of the Intertropical Convergence Zone (ITCZ, Clement et al., 2000; Schneider et al., 2014; Lu et al., 2018).

Solar forcing influences the position of the ITCZ by modulating its latitudinal extent (Clement et al., 2000; Schneider et al., 2014; Lu et al., 2018), which can influence NPSG surface ocean currents. Sediment $\delta^{15}N$ varies by latitude, with values

~2.5‰ more positive offshore of Mexico in comparison to the equator (Fig. 1-2C). A southward ITCZ is expected to enhance equatorial upwelling (Schneider et al., 2014) and may impact the $\delta^{15}N$ of gyre waters by changing the source region of nitrate. When the ITCZ is located more southward such as during the Late-Holocene, water advects from lower latitudes in the Eastern Tropical Pacific which have comparatively more negative $\delta^{15}N$ values than higher latitudes (Fig. 1-2C). During the Mid-Holocene, a northward ITCZ may transport waters from latitudes with more positive nitrate $\delta^{15}N$ values. Future work modeling nitrate advection may help determine the contribution of nitrogen fixation versus a change in the source water impacting these coral isotopes.

4.2 Carbon Isotopic Records

The ~2‰ range in coral $\delta^{13}C$ values across our 5000 yr record also appear to occur within a number of discrete cycles, with low $\delta^{13}C$ values similar to present day having occurred multiple times since the Mid-Holocene (in L1 ~ 200 CE; in L2 ~ -800 CE; in L3 ~ -2800 CE, Fig. 1-3A). Bulk coral $\delta^{13}C$ values have a strong, positive relationship with essential amino acid $\delta^{13}C$ values in *K. haumeaae,* particularly the $\delta^{13}C$ value of phenylalanine (R^2= 0.69, McMahon et al. 2015), which indicates that most bulk $\delta^{13}C$ variability can be tied to changes in the source carbon at the base of the food web. However, it should be noted that variations in bulk $\delta^{13}C$ values are typically muted in magnitude compared to the $\delta^{13}C$ signal from essential amino acids (Schiff et al. 2014; McMahon et al., 2015), thus suggesting bulk coral $\delta^{13}C$ records may underestimate the full extent of variability in baseline export changes.

There are multiple factors influencing planktonic $\delta^{13}C$ values in the marine environment, but on long timescales the dominant controls include SST, ambient CO_2 (aq.) concentrations, the $\delta^{13}C$ of dissolved organic carbon (DIC), and taxon-specific fractionation values (ε_f) (Rau et al., 1996; Young et al., 2013; McMahon et al., 2015, Table 1-3). Given that these factors can be inter-linked, definitively assigning causes to past changes in export production $\delta^{13}C$ values is challenging. Increased CO_2 availability, whether through increased atmospheric CO_2 concentrations or increases in [DIC], generally results in decreased phytoplankton $\delta^{13}C$ values and a greater isotopic discrimination between the phytoplankton and source CO_2 (Rau et al., 1989; Young et al., 2013). However, from the Mid-Holocene to the Little Ice Age, the concentration of CO_2 in the atmosphere has increased by only ~10 ppm, with little to no change in atmospheric $\delta^{13}C$ (Fig. 1-3C; Monnin et al., 2004), suggesting that the signal being recorded in these corals is not mainly due to pCO_2 change. The low sensitivity of plankton $\delta^{13}C$ to changes in pCO_2 (0.0003‰ ppm^{-1}; Young et al. 2013) would further indicate that atmospheric $\delta^{13}C$ value is not a main driving mechanism for the large changes in our coral records. Baseline changes in the $\delta^{13}C$ of DIC are also likely to be too small to be driving the trends in coral $\delta^{13}C$ (Quay and Stutsman, 2003; Monnin et al., 2004).

Laboratory and field experiments document that temperature exerts an important control on phytoplankton and exported organic matter $\delta^{13}C$ values (Table 1-3, and associated references). In general, warmer conditions contribute to more positive exported organic $\delta^{13}C$ values. Multiple approaches have attempted to

quantify the effects of temperature on the $\delta^{13}C$ values of primary production, including: estimates of the effect of temperature on fractionation factors in culture (ε_p; +0.12‰ / °C), on natural phytoplankton $\delta^{13}C$ (+0.11-0.23‰ / °C), and suspended particulate organic carbon $\delta^{13}C$ (+0.41‰ / °C) in natural ocean systems (Table 1-3). Mid- to Late-Holocene SST estimates using both the Modern Analog Technique and alkenone-SST relationships in sediment cores near Oahu indicate temperatures within 1°C of early 20th century data (Fig. 1-3B, Lee et al., 2001). These estimates are similar to higher resolution Northern Hemisphere reconstructions (e.g., Pei et al., 2017). A ≤1°C SST change would only account for ~0.4‰ or less of the 2‰ $\delta^{13}C$ variability, suggesting temperature alone is only partially responsible for the trends in coral $\delta^{13}C$.

Shifting plankton community composition, implicitly including size/morphology and growth rate, is the most likely explanation for the large changes in $\delta^{13}C$ values of our coral records over the last 5000 yrs. Different phytoplankton species have unique carbon isotope fractionations during photosynthesis (Laws et al., 1995; Rau et al., 1996), and thus a shifting phytoplankton community composition can be a major driver behind changes in $\delta^{13}C$ of export production over time (McMahon et al., 2015). Prokaryotic cyanobacteria (e.g., *Prochlorococcus*, *Synechoccocus*) and picoeukaryotes are typically the dominant phytoplankton groups in open ocean regions like the NPSG (e.g., Karl et al., 2001), and of these, *Synechoccocus* and picoeukaryotes are most strongly associated with carbon export in oligotrophic regions (Guidi et al. 2016). Picoeukaryotes are also larger than

prokaryotes (cell diameters of 2.0 and 0.5 μm respectively) and this contributes to differences in their ecological performance as well as the extent of carbon fixation and export (Massana and Logares 2013). Based on distinct isotopic fractionations associated with enzymatic, intracellular carbon fixation (ε_f; Laws et al., 1995; Scott et al., 2007), the differences between prokaryotic and eukaryotic contributions to exported organic matter manifest as differences in $\delta^{13}C$ values: where ~0.6‰ of $\delta^{13}C$ variability can be explained by a 1‰ shift in community fractionation ε_f (Table 1-3). More positive $\delta^{13}C$ values indicate higher relative contributions of eukaryotic phytoplankton, consistent with the well-known general trend that larger phytoplankton cells (e.g. diatoms) express more positive $\delta^{13}C$ values than small-celled nanoplankton (e.g., Laws et al., 1995; Popp et al. 1998).

Coral $\delta^{13}C$ values suggest centennial- to millennial-scale trends towards increasing eukaryotic contributions in exported production followed by hypothesized events (e.g. between L3 and L2) that reset the NPSG to be more prokaryotic-dominated. Picoeukaryotes are metabolically less flexible than prokaryotic organisms, perhaps causing them to be less resilient to environmental changes (Massana and Logares, 2013). Prokaryotic CO_2 fixers also outgrow and outperform eukaryotes in oligotrophic gyre ecosystems (Zubkov 2013), which suggests that during periods of stratified, nutrient-limited conditions, prokaryotic organisms may dominate primary production and thus export production in the NPSG. The stability of the water column due to the frequency of ENSO events may influence community structure, with periods of low ENSO activity (e.g., ~3.5-5 kyrs ago) allowing for a long term

community increase of eukaryotic organisms. This would result in the observed steadily increasing $\delta^{13}C$ values of coral L3), while periods of high ENSO activity (e.g. 1-2 kyrs ago and 3-4 kyrs ago; Moy et al. 2002, Fig. 1-3D) would correspond to a community consistently dominated by prokaryotes and low, stable $\delta^{13}C$ values (averaging -16.9 ± 0.2‰ from 200 to 1000 CE, Fig. 1-3). Shifts between smaller celled prokaryotes and larger picoeukaryotes can modulate the amount of organic matter exported to depth and may cause cascading effects on pelagic and benthic food webs (Finkel et al. 2010).

4.3 Coupling vs. Decoupling of export production $\delta^{15}N$ and $\delta^{13}C$ values

Existing records from deep-sea corals from the NPSG in the last 1000 yrs have uniformly documented coupled changes in $\delta^{15}N$ and $\delta^{13}C$ values at the base of the food web, with authors hypothesizing that such shifts are linked to recent shifts in local/regional temperature and the ecosystem response derived from the dynamical oceanographic setting coincident with warmer surface temperatures (e.g., Sherwood et al., 2014; McMahon et al., 2015). Therefore the observation that in the longer Holocene record that relative changes in $\delta^{15}N$ and $\delta^{13}C$ values of export production are often not coupled and trend in *opposite* directions was unexpected. The $\delta^{15}N$ and $\delta^{13}C$ data from these coral specimens clearly indicate two periods in which changes in $\delta^{15}N$ and $\delta^{13}C$ values are largely synchronous (moving in the same direction, with generally similar slopes), and two periods in which values appear decoupled (Fig. 1-4; *Results* 3.5). This suggests a more complex set of biogeochemical forcings on the longer time scales of these records.

In all coral records for the last millennium, the direct coupling between $\delta^{15}N$ and $\delta^{13}C$ shifts is one of the most striking overall features (Fig. 1-4). This observation supports the conclusion that regional plankton community changes are the underlying driver for changes observed in isotope records, primarily reflecting shifts between a more stable water column promoting oligotrophic and N_2-fixation conditions versus cooler periods with increased vertical mixing and entrainment (Sherwood et al., 2014; McMahon et al., 2015). Specifically, more recent warmer periods are characterized by more stratified and nutrient-poor conditions with enhanced nutrient recycling and fewer large eukaryotic cells (e.g., Chavez et al., 2011). Such conditions favor microbial-loop dominated systems characterized by lower $\delta^{13}C$ values. The enhanced N_2-fixation and nutrient recycling in such systems also leads to lower $\delta^{15}N$ values, accounting for linked $\delta^{15}N$ and $\delta^{13}C$ changes. Conversely, higher nutrient environments are typified by faster growing, larger eukaryotic autotrophs supported by upwelled nitrate, leading to concurrent increases in both $\delta^{15}N$ and $\delta^{13}C$ primary production values.

The decoupling of $\delta^{15}N$ and $\delta^{13}C$ changes in earlier periods of this ~5000 yr record suggest distinctly different local to basin-scale drivers for $\delta^{15}N$ and $\delta^{13}C$ values. While earlier data indicate several periods of coupled $\delta^{15}N$ and $\delta^{13}C$ change in the NPSG that appear to be analogues to the recent millennium, the distinct periods of coupling and decoupling must indicate different mechanisms are driving changes in primary production N and C cycles. The two periods of *decoupled* isotopic behavior (Fig. 1-4, DC1, DC2) occur when hemispheric temperatures may have been ~0.5°

cooler than present (Pei et al., 2017) and proxy records suggest reduced ENSO climate variability (Lu et al. 2018; Moy et al. 2002). In contrast, the coupled period C1 includes the warmer Industrial Revolution and Medieval Climate Anomaly where proxy records agree on enhanced ENSO conditions (Lu et al. 2018 and references therein), and C2 occurs during enhanced ENSO activity periods as characterized by some proxy records (e.g. Moy et al. 2002, Fig 3). One hypothesis for this apparently contrasted behavior is that coupling versus decoupling may be related to relative regional sea surface temperatures and stratification. Cooler periods of reduced ENSO variability are decoupled in $\delta^{15}N$ and $\delta^{13}C$ values, while warmer, enhanced ENSO periods are more consistently coupled. While speculative, this could be due to changing nutrient regimes. Generally warmer SSTs correspond to enhanced ocean stratification, shallower mixed layer depths, and a slowdown in gyre circulation. Under such oligotrophic conditions, phytoplankton communities may rely more heavily on the supply of N_2-fixed nitrate from localized diazotroph production, and community composition may shift towards prokaryotic, N_2-fixing organisms, perhaps causing a coupling in $\delta^{13}C$ and $\delta^{15}N$ values of export production. In contrast, there is both more mixing from depth and/or enhanced lateral advection of water from ocean margins during cooler, often windier, climatic periods (Sigman et al. 2009). The result is lower rates of N_2-fixation (Galbraith et al., 2004) and more nitrate with more positive $\delta^{15}N$ values possibly advected from higher latitudes of the Eastern Pacific (Fig. 1-2C). Thus, community composition changes may serve to shift $\delta^{13}C$ values, while the signal of advected $\delta^{15}N_{NO3}$ and not N_2-fixation drives the $\delta^{15}N$ value of

exported organic matter during periods of cooler SSTs, thus decoupling the $\delta^{13}C$ and $\delta^{15}N$ values. McMahon and coauthors (2015) support this idea, suggesting nitrate utilizing cyanobacteria dominate community composition over some periods while N_2-fixating cyanobacteria dominate over others during the most recent millennium. While this idea cannot be directly tested using bulk isotope analysis, further work could address it.

Lastly, spectral and wavelet analysis did not reveal consistent multi-decadal to centennial scale power and while the detected regimes did not often overlap in timing between $\delta^{15}N$ and $\delta^{13}C$ records most regimes (~60%) lasted between 30 and 90 years in duration (Fig. 1-S3). We posit that the regime analysis confirms multi-decadal variability, but that there is more than one mechanistic forcing and ecosystem response influencing the $\delta^{13}C$ and $\delta^{15}N$ of export production, that are not always in sync with each other.

5. Conclusions

This study documents variability in export production $\delta^{15}N$ and $\delta^{13}C$ values for the Holocene NPSG, extending previously published records by approximately ~4000 years deeper into the Mid-Holocene. These new data reveal a dynamic biogeochemical system, in which substantial changes in $\delta^{15}N$ and $\delta^{13}C$ values of export production have been common on millennial time scales. Our records indicate that the natural isotopic range of production in the NPSG has varied by up to 3.5‰ for $\delta^{15}N$ values and 2‰ for $\delta^{13}C$ values over the last 5000 yrs. In particular, Mid-

Holocene export production $\delta^{15}N$ values appear to have been substantially higher (by ~1.5 to 2‰) than in the Late-Holocene, and these longer records confirm that present day $\delta^{15}N$ values recorded in corals (~8‰) are the lowest in ~5000 years. In contrast, low $\delta^{13}C$ values similar to those recorded in modern corals (~ -17‰) were reached during at least two other periods since the Mid-Holocene.

While these data clearly show periods of major change in both $\delta^{15}N$ and $\delta^{13}C$ values over the last 5000 years similar in magnitude to changes in the Anthropocene, past changes appear to have occurred over much longer (~millennial) timescales. In addition, these new records also indicate that distinct periods of coupled and decoupled $\delta^{15}N$ and $\delta^{13}C$ dynamics occurred in different periods throughout the Holocene. This in turn suggests a number of independent biogeochemical regimes over the last 5000 years. We hypothesize that these regimes are most likely linked to shifts in plankton community structure, possibly coupled with independently varying $\delta^{15}N$ values of nitrate in this region. The coupled $\delta^{15}N$ and $\delta^{13}C$ periods are similar to shifts observed in both NPSG instrumental records and also in more recent coral chronologies, likely explained by relative importance of nitrogen fixation and upper water stratification (McMahon et al., 2015; Sherwood et al., 2014). Periods in which δ13C values change with no major shifts in $\delta^{15}N$ values imply changes in phytoplankton community structure without clear linkage to shifts in nutrient supply, potentially explained by relative abundance of non-nitrogen fixing prokaryotic autotrophs in this region (McMahon et al. 2015). However, to test these ideas more

work will be necessary to identify the relative influence of baseline nutrient supply versus changes in autotrophic community structure.

Overall, the dynamism of Holocene biogeochemical systems revealed by this study strongly emphasizes the need to develop new proxies that can be used to determine past climate and environmental conditions at high resolution in the NPSG. Future work should include compound specific analysis of amino acids within coral archives to further constrain these hypotheses. Such information would allow researchers to directly examine if present microbial-loop dominated system of the NPSG has been constant or if variation in community structure has been responsible for isotopic variability of our records earlier in the Holocene. Further, this approach would allow for testing of the underlying assumption that average trophic structure of NPSG planktonic systems, which strongly influences the $\delta^{15}N$ value of export production, has remained constant through time. While data from Sherwood et al. (2014) indicated that average planktonic ecosystem trophic position has remained constant over the most recent millennium, it is not known if this also would hold true for earlier parts of this record, specifically during periods of $\delta^{13}C$ and $\delta^{15}N$ decoupling. Regardless, we show that while NPSG plankton and nutrient dynamics are highly variable over the last 5000 yrs, the modern Anthropocene regime remains unique in the magnitude and timing of changes in ecosystem dynamics in the context of Holocene variability.

Acknowledgements:

None of this work would have been possible without the captain and crew of the RV *Ka'imikai-o-Kanaloa* and the pilots and engineers of the Hawai'i Undersea Research Lab's Pisces IV and V. Sample collection was funded by NOAA/NURP and the National Geographic Society (7717-04). A portion of this work was performed under the auspices of the U.S. Department of Energy (DE-AC52-07NA27344). The majority of the work presented here was funded by the NSF (OCE 1061689). D.S. Glynn was supported by a Cota Robles and NSF GRFP Fellowship. Further thanks go to D. Andreasen, C. Carney, R. Franks, and J. Schiff for laboratory assistance and training. We thank two anonymous reviewers for critical and constructive comments on the initial manuscript submission.

Chapter 2

Investigating Preservation of Stable Isotope Ratios in Subfossil Deep-Sea Proteinaceous Coral Skeletons as Paleo-Recorders of Biogeochemical Information over Multi millennial Timescales

The results presented in this chapter are published in Geochimica et Cosmochimica Acta as an article by Danielle S. Glynn and co-authors as follows:

Glynn, D. S., McMahon, K. W., Sherwood, O. A., Guilderson, T. P., & McCarthy, M. D. (2022). Investigating preservation of stable isotope ratios in subfossil deep-sea proteinaceous coral skeletons as paleo-recorders of biogeochemical information over multimillennial timescales. *Geochimica et Cosmochimica Acta*, **338**, 264-277.

Abstract

Paleoproxy records in deep-sea proteinaceous coral skeletons can reconstruct past ocean conditions on centennial to millennial time scales. Commonly recovered subfossil specimens could potentially extend these archives through the Holocene. However, protein matrix stability and integrity of stable isotope proxies over multi-millennial timescales in such specimens have never been examined. Here we compare amino acid (AA) composition together with bulk and AA compound-specific carbon ($\delta^{13}C$) and nitrogen ($\delta^{15}N$) isotopes in live-collected and subfossil (~9.6–11.6 kyrs BP) *Kulamanamana haumeaae* deep-sea coral specimens from the central Pacific to understand the effects of long-duration benthic oxic exposure on primary coral chemistry. We find large coupled shifts in bulk $\delta^{15}N$ (~7‰) and $\delta^{13}C$ (~2‰) in the outermost portion (0–10 mm) of the subfossil coral, coincident with extensive alteration of the protein matrix. Microstructural changes in skeletal texture coincide with higher C/N ratios (+0.8) and isotope-based amino acid degradation parameters (e.g. $\Sigma V \geq 3$), indicating extensive degradation of seawater-exposed gorgonin.

However, interior gorgonin (>10 mm) retained amino acid molecular compositions (with exception of major Glycine loss) and bulk and amino acid-specific isotopic values that were similar to live-collected specimens. These results indicate that compound-specific isotope analysis of amino acids can reconstruct paleo-oceanographic biogeochemical and ecosystem information in subfossil corals beyond a clear diagenetic horizon, which is easily identifiable from an evaluation of C/N ratios together with the ΣV degradation proxy.

1. Introduction

Deep-sea proteinaceous corals are ideal recorders of sub-decadal resolution surface biogeochemistry, due to their ubiquitous distribution, long lifespans, and near continuous deposition of skeletal material (reviewed in Williams 2020). These corals consume organic matter exported from the surface ocean and incorporate the isotopic values of exported production into concentric growth layers in their proteinaceous skeletons (Druffel et al., 1995; Roark et al., 2006). In recent years, deep-sea proteinaceous coral skeletons have been used to reconstruct the history of exported organic matter over centennial to millennial timescales globally, including the North Pacific Gyre (Sherwood et al., 2014; McMahon et al., 2015; Glynn et al., 2019), North Atlantic (Sherwood et al. 2009a, 2011), southern Australia (Sherwood et al., 2009b), the Equatorial Pacific (Williams and Grottoli, 2010), and the California Margin (Hill et al., 2014; Schiff et al., 2014). Deep-sea proteinaceous coral studies have been particularly useful in understanding the most recent millennia of ocean

history, a period characterized by rapid oceanographic and climatic change, but one in which detailed sedimentary records in many locations are severely limited by slow sedimentation rates or significant bioturbation. In many regions, proteinaceous corals also represent the only archive capable of decadal or finer temporal scale reconstructions, making them especially useful to understand multi-decadal variability of biogeochemical cycling and phytoplankton community dynamics recorded in the signal of export production (Sherwood et al., 2011; 2014, McMahon et al., 2015).

To properly evaluate paleo-environmental interpretations from organic proxies, the preservation of chemical and isotopic information must be carefully considered. Proteinaceous deep-sea coral skeletons are composed of a cross-linked, fibrillar protein that is among the most diagenetically resistant proteinaceous materials known (Goldberg, 1974, 1976; Ehrlich, 2010; Strzepek et al., 2014). For example, skeletons of black corals are predominantly composed of protein (~50-70%) and contain lipids, diphenols, and chitin (Holl et al. 1992). However, far less is known for gold corals besides being composed of primarily amino acids (AAs) (Goodfriend 1997, Sherwood et al. 2006, 2014). At the molecular level, the AA composition of modern *K. haumeaae* shows little variability over the duration of the coral skeleton's growth (Goodfriend, 1997; Sherwood et al., 2006), and AA composition is also similar in live-collected versus 1000-2000 year old specimens (Sherwood et al., 2006), suggesting that coral skeleton protein is stable over at least millennial time frames.

The abundance of non-living coral skeletons encountered on the seafloor in many locations suggests the possibility to go far beyond the time horizon constrained by living corals. For example, Guilderson and coauthors (2013) describe a range of ^{14}C dated specimens from both the Hawaiian and Line Islands that collectively spanned the entire Holocene. Edinger and Sherwood (2012) conducted year-long decay experiments on deep-sea corals of different skeletal compositions and documented a range of physical changes such as pitting, corrosion, hydration, and disintegration of the organic gorgonin. Noé and Dullo (2006) and Noé et al. (2007) noted the presence of micritized borings in subfossil gorgonian corals. To date, there have been no detailed studies of $\delta^{15}N$ and $\delta^{13}C$ preservation of subfossil deep-sea proteinaceous coral specimens collected in-situ on the seafloor. Thus, the susceptibility of the gorgonin protein matrix to degradation and the integrity of archived geochemical information on multi-millennial timescales are not well known. A detailed understanding of skeletal preservation over long timescales will substantially improve confidence in the use of subfossil corals for paleoceanographic study, since degradative effects could easily be confused with signatures of past environmental variation.

The goal of this study was to assess the integrity of the $\delta^{15}N$ and $\delta^{13}C$ values and AA profiles recorded in deep-sea proteinaceous corals over extensive time and degradation potential. We compared the structural, chemical, and isotopic data in a subfossil (~9.6-11.6 kyr BP) coral with the same properties in a live-collected specimen from the same location at Cross Seamount, Hawaii. We used a multi-metric

approach to examine central aspects of physical, chemical, and isotopic change as a function of preservation along a gradient from inner protected layers to outer seawater exposed regions. Scanning electron microscopy (SEM) was used to investigate physical structural change in the skeleton matrix. Chemical composition changes were examined using bulk tissue carbon to nitrogen (C/N) elemental ratios and molecular-level AA composition (mol%). Patterns in bulk tissue $\delta^{15}N$ and $\delta^{13}C$ values as well as carbon and nitrogen compound-specific isotope analysis of AAs (CSIA-AA) were compared to examine potential impacts of degradation on geochemical fidelity. These comparisons allowed us to directly determine how ~10 kyrs of oxic seawater exposure altered the chemistry and the paleo-archival potential of the proteinaceous skeleton. We used these data to propose metrics for evaluating the integrity of proteinaceous corals and the geochemical data they archive.

2. Materials and Methods

2.1 Study site and sample collection

Living and subfossil deep-sea proteinaceous corals (*Kulamanamana haumeaae*) were collected from 447 and 415 m respectively from Cross Seamount (19°N, 158°W), southwest of the Big Island of Hawaii, in 2004. Cross Seamount waters at 400 m have average in situ temperatures of ~9 °C and dissolved oxygen concentration of ~100-120 μmol/kg (Boyer et al., 2018). The polyps of live-collected corals were removed and all skeletons were rinsed first with seawater, followed by freshwater, before being air dried on deck. In the lab, ~0.7 cm thick cross-sectional

disks were sectioned from near the base of each skeleton, then polished and mounted to glass slides, following standard procedures (Sherwood et al., 2014). A detailed sample processing flow chart and description can be found in the supplemental file (Fig. 2-S1A).

2.2 Scanning electron microscopy (SEM)

For scanning electron microscope images, sections of the same coral disks were coated with ~20 nm of gold using a Technics Hummer VI sputter coater (3 minutes @ 80 mtorr, 17 mA current) and then imaged on a FEI Quanta 3D dual beam microscope (electron beam operating at 5 kV and 6.7 pA) in the W.M. Keck Center for Nanoscale Optofluidics at the University of California – Santa Cruz. SEM images (300 µm and 30-40 µm resolution) were visually compared to examine structural changes in the skeletal matrix between the live-collected and subfossil corals.

2.3 Radiocarbon dating and age models

Radiocarbon dating was performed on nine sample aliquots (~1 mg total material) each spread ~5 mm apart along the skeleton cross section transect. Samples were first fumed with concentrated HCl and subsequently dried before being transferred with methanol into 6 mm short quartz tubes and dried. The 6 mm tubes were then placed inside larger 9 mm quartz tubes with an appropriate amount of CuO, prior to pumping off excess atmosphere, sealing, and combusting to produce CO_2. The CO_2 after cryogenic purification was converted to graphite and analyzed at the Lawrence Livermore National Laboratory. Results were corrected for $\delta^{13}C$ and

background ^{14}C using similarly handled ^{14}C-free coal. Radiocarbon results were transformed into calibrated years before present (yr BP). These ages and subsequent age models were generated with Calib 8.2 (Stuiver et al. 2021) using a local reservoir (ΔR) correction of -177 ± 16, (Druffel et al., 2001; Guilderson et al., 2021) and the Marine20 database (Heaton et al. 2020) and linearly interpreted to provide a continuous age-model.

2.4 Bulk stable isotope analysis

A computerized Merchanteck micromill was used to drill a radial transect from the outside to the inner layers of the coral skeleton cross section at 0.1 mm resolution, yielding 2-3 mg of powdered skeletal material per sample interval. All 168 samples from the live-collected coral were analyzed (155 samples in duplicate); while of the 455 subfossil samples drilled, 193 were analyzed, with a greater sample density analyzed from the outermost 10 mm. Bulk powdered coral material (~0.4 mg) was enclosed in tin capsules for bulk $\delta^{13}C$ and $\delta^{15}N$ analyses via continuous-flow isotope-ratio mass spectrometry (IRMS) using a Carlo-Erba elemental analyzer connected to an Optima Isotope Ratio Mass Spectrometer (IRMS). C/N ratios were simultaneously determined. The analytical error for these measurements, as determined from analysis of standards of known composition (pugel and acetanilide), was ±0.2‰ for both $\delta^{13}C$ and $\delta^{15}N$ values and ±0.1 for C/N ratios. To test for the impact of secondary authigenic carbonate in the sample matrix, a subset of the same samples from the subfossil coral (1–2 mg each, n = 7) were acidified using 1 N HCl for 20 h under refrigerated conditions, followed by filtration onto a 0.22 μm glass fiber filter. The

filter was dried overnight at 45°C before material was transferred into a tin capsule and analyzed following the same procedure as described above.

2.5 Amino Acid Molar Percent

Adjacent growth bands were combined to obtain ~10-11 mg of total material which, after homogenization, was used for each analysis (typically used 8-10 samples of ~1 mg from each adjacent 0.1 mm layers). Of these composite samples, approximately 0.5-1 mg of coral material was needed for measurement of AA molar concentrations, with the rest being used for CSIA-AA described in Section 2.6. Wet chemical protocols for AA measurements in proteinaceous corals followed established protocols (detailed in McMahon et al, 2018). Briefly, individual AAs were liberated using standard acid hydrolysis conditions (1 ml of 6 N HCl at 110°C for 20 h), then spiked with a norleucine internal standard and derivitized, followed by purification with cation-exchange chromatography and a salt-removal step (p-buffer = KH_2PO_4 + Na_2HPO_4 in Milli-Q water, pH 7), and finally rinsed with chloroform three times with centrifugation before final conversion to trifluoroacetyl/isopropyl ester (TFAA) derivatives. The AA mole percent (mol%) compositions were quantified using a GC–MS (Agilent 7890 GC coupled to a 5975 MSD) based on single ion monitoring data of the major ion relative to authentic AA external standard calibration curves. Commercial AA standards (Pierce Biochemicals) were used to create concentration series, and response factors from these external standards were used to calculate relative molar concentrations. Reproducibility, as measured by the standard deviation of GC-MS replicates analyses, typically averaged <5 mol%.

2.6 Compound Specific Stable Isotope Analysis of Amino Acids (CSIA-AA)

CSIA-AA for both carbon and nitrogen was performed on aliquots of the same TFAA derivatives prepared as described in Section 2.5, using ~4 mg for $\delta^{13}C$ and ~6 mg $\delta^{15}N$ CSIA-AA measurements. Derivatized samples were injected in triplicate on a coupled Gas Chromatography- IRMS (Thermo Trace GC, coupled to a Delta + IRMS), as described in McMahon et al. (2018). Isotopic ratios were measured for 13 of the common protein AAs (see supplementary material, Fig. 2-S1): alanine (Ala), glycine (Gly), serine (Ser), valine (Val), threonine (Thr), leucine (Leu), isoleucine (Ile), proline (Pro), phenylalanine (Phe), tyrosine (Tyr), lysine (Lys), glutamine + glutamic acid (Glx), and asparagine + aspartic acid (Asx). Cystine (Cys) and histidine (His) break down during acid hydrolysis and were not measured.

For $\delta^{13}C_{AA}$ higher sensitivity coupled with good chromatographic separation permitted all AA $\delta^{13}C$ values to be measured in single chromatographic run (Fig. 2-S1). However for $\delta^{15}N_{AA}$, the much larger on-column AA amounts required by much lower intrinsic IRMS sensitivity for N made it impossible to obtain both adequate chromatography and peaks sizes simultaneously for all AAs in a single run. We therefore performed independent GC-IRMS $\delta^{15}N$ run series for high verses low mol% AAs (Fig. 2-S1). The early eluting AA peaks (Ala, Gly, Ser, Thr, and Val) were all large and well separated (Fig. 2-S1) and necessitated only duplicate injections. GC-IRMS error was therefore reported for these peaks as mean deviations. Subsequent independent runs at higher concentrations then employed a cut-off method to remove early peaks (directed to back-flush), so that lower mol% peaks could be quantified

(Asx, Glx, Ile, Leu, Lys, Phe, Pro, Tyr). These injections were made in triplicate, with concentrations adjusted to produce at least 80 mV IRMS N_2 signal intensity for the smallest peaks (typically Phe and Ile).

Overall reproducibility for individual AA isotopes values among sample injections was, in general, <1‰ for both $\delta^{13}C$ and $\delta^{15}N$ CSIA-AA, based on internal lab working standards. Accuracy of $\delta^{13}C$ and $\delta^{15}N$ CSIA-AA data was verified following protocols described in McCarthy et al., 2013. Briefly, three independent, overlapping approaches were used to assess accuracy: first a Nor-Leu internal standard added to every sample, second an external (L-amino acid) AA standard mix injected repeatedly after every third sample, and finally a natural cyanobacteria long term (> 10 yr) in-house working standard, run as an unknown with every sample batch. The Nor-Leu internal standard was used to verify that each specific injection for each sample gave expected values. The external bracketed standards were used in different ways for $\delta^{13}C$ and $\delta^{15}N$ values based on the need to correct for added derivatization moieties for $\delta^{13}C$ only. For $\delta^{13}C$, the measured IRMS values are not actual AA $\delta^{13}C$ values but must corrected for added derivative C; this was done following the method of Silfer (1991). For $\delta^{15}N$ values the measured IRMS values directly represent the $\delta^{15}N$ value of each AA and therefore external standard values can be used to directly assess accuracy and make corrections. For $\delta^{13}C$, the average measured $\delta^{13}C$ value of each external standard AA across the entire run was therefore compared against its authentic value, and any systematic bias/offset used to correct sample AA values, following the approach described by McCarthy et al., 2013

(supplementary information, Fig. 2-S2). Finally, both $\delta^{13}C$ and $\delta^{15}N$ AA results from the McCarthy lab internal laboratory reference material (dried/homogenized cyanobacteria) standard run with each sample batch were evaluated for accuracy against a long term (>10 yr) internal control chart. The supplemental file contains more information on the order of sample processing, including specific protocols for CSIA-AA corrections, representative chromatograms, and minimum mV peak information (Fig. 2-S1A, 2-S1B).

2.7 Nomenclature, AA groupings, and CSIA-AA parameters

We report and discuss AA isotope data in terms of commonly used CSIA-AA groupings for both $\delta^{13}C$ and $\delta^{15}N$, which in turn are based on metabolic pathways and observed differences in isotope fractionation during trophic transfer (reviewed by McMahon and McCarthy, 2016, Ohkouchi et al., 2017). For $\delta^{15}N$ data, we treat Phe, Tyr, and Lys as Source AAs (those with minimal isotope fractionation during trophic transfer); Asx, Glx, Ile, Leu, Pro, Val as Trophic AAs (close linkage to central glutamate pool, with correspondingly large isotope fractionation during trophic transfer), and Gly and Ser as Intermediate AAs, based on recent literature that shows they display variable behavior, very often falling between the two customary groupings (McMahon and McCarthy, 2016). Lastly, Thr was plotted alone, as it displays a unique inverse isotope fractionation behavior with trophic transfer (McMahon and McCarthy, 2016).

For $\delta^{13}C$, we used common essential and non-essential AAs categories. There is minimal isotope fractionation for essential AAs with trophic transfer, while there

can be highly variable fractionation in the nonessential AAs due to resynthesis (McMahon et al. 2010). The essential AAs (Thr, Ile, Val, Phe, and Leu) can be synthesized by both phytoplankton and microbes, however most metazoans cannot synthesize them and must incorporate the essential AA from their diet (Larsen et al. 2013). While we note that it is possible that some coral species, or more likely microbes associated with them, could also potentially synthesize essential AA, prior work has indicated that essential AA $\delta^{13}C$ CSIA-AA in proteinaceous corals correspond to expected primary production patterns and local endmember values and thus directly track export production (Schiff et al., 2014, McMahon et al., 2018, Shen et al., 2021).

We quantified possible microbial reworking of skeletal protein using AA $\delta^{15}N$ values using the CSIA-AA metric ∑V, which is a proxy for total heterotrophic microbial AA resynthesis of proteinaceous material (McCarthy et al., 2007, Ohkouchi et al, 2017). ∑V was calculated using the average deviation of $\delta^{15}N$ values of the trophic AAs Ala, Val, Leu, Ile, Pro, Asx, Glx:

$$\sum V = \frac{1}{n}\sum |X_i|$$

where X_i is the offset in $\delta^{15}N$ of each individual AA from the average ($X_i = \delta^{15}N_i$ – AVG $\delta^{15}N_i$), and n is the number of AAs used in the calculation.

The CSIA-AA-based trophic position ($TP_{CSIA\text{-}AA\ Skeleton}$) of deep-sea corals is a proxy for trophic structure of both the coral and the overlying planktonic food web contributing to export production. This parameter was calculated using the difference

in Phe (source) and Glx (trophic) $\delta^{15}N$ values according to a proteinaceous coral – specific formula:

$$TP_{CSIA-AA\ Skeleton} = 1 + \left(\frac{\delta^{15}N_{Glx} + \partial - \delta^{15}N_{Phe} - \beta}{TDF_{Glx-Phe}}\right)$$

recently determined by McMahon et al. (2018). This formula incorporates an additional correction factor (∂) for Glx of 3.4 ± 0.1‰ to account for the consistent offsets observed between polyp and skeletal Glx $\delta^{15}N$ values across multiple deep-sea coral species (McMahon et al., 2018). The β value (3.4‰; empirical difference between the $\delta^{15}N_{Glx}$ and $\delta^{15}N_{Phe}$ of non-vascular autotrophs) and the TDF value (7.6‰; trophic discrimination factor of $\delta^{15}N_{Glx}$ relative to $\delta^{15}N_{Phe}$ per trophic transfer; Chikaraishi et al., 2009). We note that alternate β (3.3 ± 1.8‰; Ramirez et al. 2021) and TDF (6.6 ± 1.7‰; Nielson et al. 2015) values have recently been proposed to represent better averages over many ecosystems. We present alternate TP value using these values in the supplemental material, however because the lower TDF value in particular gives unrealistically high TP values for corals, we have here elected to use the same β and TDF values used for deep sea proteinaceous corals in McMahon et al. (2018).

2.8 Statistics and interpretational framework

We discuss coral data in the context of different regions of degradation, described by ranges of radial distance along the skeletal disc. The subfossil coral is discussed mainly in terms of three separate zones for bulk isotopic and C/N data: 1) outer diagenetic horizon (0-10 mm), as defined by very rapid changes in both C/N

and isotope values, 2) inner, intermediate zone (10-36 mm) defined by only minor offsets from expected values, and 3) the innermost most protected zone (>36 mm), with C/N values within expected ranges for live-collected specimens. However, for the mol% and CSIA-AA data these changes are only observed in the outermost layer. We therefore discuss these results only for the two distinct zones: 1) the outer diagenetic horizon (0-5 mm) and 2) the inner layers from 10 mm to the skeleton's center. For data from a live-collected coral there are no analogous degradation zones, however, here we group results to separate pre-industrial samples from the Industrial Revolution, using 1900 CE based on coral-specific age models as a comparison of data more comparable to the subfossil coral.

For CSIA-AA comparisons between live and subfossil specimens and within the subfossil coral (0-5 mm versus >10 mm), the AA isotope data were normalized by taking each individual AA isotope value and subtracting the average value of all total hydrolysable AAs (THAA) in that sample, to allow direct examination of biosynthetic patterns (after McCarthy et al., 2007) without the confounding variable of differential $\delta^{15}N$ baseline. The normalized data include propagation of errors in quadrature. We note that for THAA normalized values the errors become larger because of the spread in AA values from which the average THAA value is calculated and the process of data normalization. This is important information for understanding that the uncertainty in these types of calculations is not unduly biased by small n in this case. To test for significant differences across zones, measured parameters were compared using two-sample group t-tests, assuming unequal variances with 95% confidence

intervals. Statistics were calculated using Real Statistics Resource Pack software (Release 6.2; Zaiontz, 2019).

3. Results

The live-collected specimen had a radius of 17 mm and radiocarbon analyses (n = 11) indicated an age of ~710 years (research data 1). The subfossil specimen had a radius of 46 mm and radiocarbon analyses (n = 9) indicated an age of 1,890 yrs (~9,670 to 11,560 years BP; Fig. 2-S2, research data table 2-2).

3.1 Scanning Electron Microscopy

Under 125x magnification, the live-collected coral skeleton exhibited concentric growth layers, exaggerated by the presence of desiccation cracks generated during sample drying, aligned parallel to the growth layers (Fig. 2-1A). Under 1250x magnification, the live-collected coral growth layers were imaged as <1 μm thick sheets of tightly woven fibers (Fig. 2-1B). For the subfossil coral, the outer skeleton appeared less dense (Fig. 2-1C) and exhibited a flakey microstructure with an absence of the tightly woven fibers (Fig. 2-1D). The inner section of the same subfossil coral appeared less altered compared to the outer skeleton and retained a concentrically layered appearance (Fig. 2-1E) along with some of the woven fibrous character, despite the presence of flakey microstructure (Fig. 2-1F).

3.2 C/N ratios

The C/N values from all subsamples of the live-collected modern coral averaged 2.75 ± 0.11 and were invariant within the analytical error. C/N values were

higher in the subfossil specimen, increasing from 3.12 ± 0.05 (n = 18) in the innermost skeleton, to 3.28 ± 0.12 (n = 88) in the middle 10-36 mm zone of the skeleton, to 3.36 ± 0.16 (n = 88) in the outer 10 mm of the skeleton. Acidification resulted in small decreases of 0.09-0.14 in C/N ratios compared to non-acidified samples for the intermediate and innermost layers, which was within instrumental error of the non-acidified sample C/N ratios, and more substantial decreases of 0.32–0.68 in C/N ratios compared to non-acidified samples in the outer 10 mm (n = 3, research data 3 and 4).

The mean elemental weight percent of subfossil samples for the outermost layer (0-10 mm) was 4.7 ± 0.9 wt% C and 15.7 ± 2.6 wt% N (n = 88), with a low value of 2.9 wt% C and 10.7 wt% N observed in the outermost 0.1 mm. The inner intermediate zone (10-36 mm, n = 88) mean elemental weight percent was 5.4 ± 0.8 wt% C and 17.6 ± 2.4 wt% N with no clear trend. The innermost zone (>36 mm, n = 18) mean was 7.0 ± 0.7 wt% C and 21.8 ± 2.1 wt% N (research data 4), falling within the range of modern specimens.

3.3 AA Molar Distribution

The modern coral AA mol% values (Fig. 2-3, research data table 2-5) for all AAs recovered were consistent with previous results for AA composition of *K. haumeaae* gorgonin (Druffel et al. 1995; Goodfriend, 1997; Sherwood et al. 2014). However, for the subfossil coral the mol% value of Gly alone was much lower (29.0 ± 3.8%) than observed in the modern coral (52.4 ± 2.4%; Fig. 2-3B). When Gly was removed from the relative mol% calculation then the mol% distribution of remaining

AA was essentially identical between subfossil and modern corals (research data 7.3) with only the mol% values for Ser, Val, Pro, and Thr showing small, but significantly different values between the subfossil (>10 mm) and live-collected coral ($p = <0.002$, research data 7).

Within the subfossil coral zones there were no significant differences in relative mol% for Ala, Thr, Ser, Val, Leu, Ile, Pro, and Phe between the inner (>10 mm) and outer (0-5 mm) layers (research data 7). Five other AAs did have small but statistically significant changes in mol% from the inner (>10 mm) to outer (0-5 mm) layers (Fig. 2-3A): decreases in Tyr (-3.2%, $p = 0.023$), Lys (-3.9%, $p = 0.001$), and increases in Asp (+1.9%, $p = 0.008$), Gly (+3.7%, $p = 0.02$), and Glu (+0.9%, $p = 0.06$).

3.4 Bulk $\delta^{15}N$ and $\delta^{13}C$ Results

Bulk $\delta^{15}N$ values in the Cross Seamount live-collected coral were 11.2 ± 0.5‰ (n = 290) before the Industrial Revolution (1270-1900 C.E.) with a high of 12.5‰ in ~1410 C.E. During the 1900's Industrial Revolution the $\delta^{15}N$ values declined steadily to a low value of ~8.8‰ in the outermost layers (research data 3). Mean bulk $\delta^{13}C$ values in the live-collected coral skeleton from the preindustrial era (prior to 1900 C.E.) were -16.3 ± 0.3‰ (n = 290), reaching a high of -15.5‰ during the 1620-1650s C.E. Similar to bulk $\delta^{15}N$ values, $\delta^{13}C$ values also declined after the 1900s to the lowest observed value of -17.2‰ in the outermost layers (research data 2-3).

Subfossil coral skeleton $\delta^{15}N$ values were overall more positive than the live-collected coral, ranging from 12 to 20‰ (research data 2-4). Within the subfossil coral the outermost $\delta^{15}N$ values (0-10 mm) increased by ~7‰ relative to the mean to a high of ~20.1‰ in the outer ~1 mm, while the intermediate region (10-36 mm) mean value was 13.7 ± 0.5‰ with no temporal trend (n = 88; Fig. 2-2B). The innermost zone (>36 mm) mean $\delta^{15}N$ value was (12.6 ± 0.6‰; n = 18) and was slightly lower relative to the intermediate zone (Fig. 2B).

The bulk $\delta^{13}C$ values in the subfossil coral ranged from -17.3 to -14.6‰ over the entire record (Fig. 2-2C), very similar to the modern coral from this site as well as to other coral records reported from the North Pacific Subtropical Gyre region (McMahon et al., 2015). Similar to the $\delta^{15}N$ data, there was a large (~2‰) and nearly monotonic increase in $\delta^{13}C$ values in the outer layers (0-10 mm) of the skeleton. The intermediate region (10-36 mm) mean value was -16.5 ± 0.4‰ (n = 88) and the innermost (>36 mm) mean value was -17.0 ± 0.3‰ (n = 18). Similar to C/N results discussed in Section 3.2, acidification prior to EA analysis reduced $\delta^{13}C$ values primarily in the outer 0-10 mm layers (0.6-1.4‰ lower relative to unacidified skeleton; n = 3) and to a lesser extent in intermediate region (10-36 mm; 0.4-0.9‰ lower relative to unacidified skeleton; n = 3). There were no significant differences in $\delta^{13}C$ values due to acidification observed in the innermost zone (>36 mm) (Fig. 2-2C, research data 4.2). While these results suggest progressive influence of authigenic calcite, under a microscope there were no visible formation of bubbles when raw coral material was subjected to 1 N HCl at room temperature.

3.5 CSIA-AA $\delta^{13}C$ data

The normalized $\delta^{13}C$ CSIA-AA values ($\delta^{13}C_{norm\text{-}AA}$) showed very similar biosynthetic patterns between the modern specimen and the inner subfossil coral layers (>10 mm, Fig. 2-4). Within the subfossil coral, $\delta^{13}C_{norm\text{-}AA}$ values also remained similar between the subfossil's inner (>10 mm) and outer (0-5 mm) regions (Fig. 2-4), in contrast to the large changes observed in $\delta^{15}N_{norm\text{-}AA}$ values in the outermost horizon (Fig. 2-5). Comparing the normalized patterns of the pre-industrial live-collected (n = 3) and subfossil (inner >10 mm, n = 6) corals only two non-essential AAs had statistically different $\delta^{13}C_{norm\text{-}AA}$ values (Asp -2.3‰, p = 0.01, Pro +1.4‰, p = 0.03). The mean essential AA $\delta^{13}C_{EAA}$ values (Phe, Thr, Ile, Leu, Val, Lys) of deep-sea corals have been shown to directly reflect $\delta^{13}C$ baseline of export production (Schiff et al., 2014, Shen et al. 2021). The live-collected Cross Seamount coral (excluding the rapidly shifting regions after the Industrial Revolution) had a mean essential $\delta^{13}C_{EAA}$ value of -18.6 ± 0.3‰ (n = 3, research data 2-S11). The subfossil Cross Seamount inner layers $\delta^{13}C_{EAA}$ values (-16.0 ± 1.5‰; n = 6, research data 12) were +2.6‰ more positive than the modern specimen from the same location (Fig. 2-6). The subfossil coral's outer layers (0-5 mm) had a mean $\delta^{13}C_{EAA}$ value of -17.1 ± 0.7‰ (n = 2, research data 12), and there were no significant differences in $\delta^{13}C_{EAA}$ values between the normalized outer (0-5 mm, n = 2) and inner (>10 mm, n = 6) subfossil coral zones (Fig. 2-4, research data table 2-13).

3.6 CSIA-AA $\delta^{15}N$ data

Normalized CSIA-AA $\delta^{15}N$ patterns ($\delta^{15}N_{norm\text{-}AA}$) were very similar between the subfossil coral inner (>10 mm) layers and modern coral (Fig. 5, research data 8 and 9), consistent with the similarity observed in AA molar composition (with the sole exception of Gly). Comparing $\delta^{15}N_{norm\text{-}AA}$ values between the subfossil inner layers (>10 mm, n = 6; Fig. 2-5; blue filled circles) and the pre-industrial live-collected (n = 3; Fig. 2-5; yellow filled circles) coral, all $\delta^{15}N_{norm\text{-}AA}$ values except for Glx and Ile fell within one standard deviation of modern coral data. Gly and Ile had clear offsets from modern coral $\delta^{15}N_{norm\text{-}AA}$ patterns (Glx +3.4‰, p = 4.6E-5 and Ile -7.2‰, p = 0.002). Four additional AAs also had smaller offsets between modern and subfossil (>10 mm) coral $\delta^{15}N_{norm\text{-}AA}$ values, which while statistically significant for these runs, were also not notably different from typical analytical variation for GC-IRMS analyses (Asx +1.7‰, p = 0.02, Ser +2.1‰, p = 0.02, Lys +2.5‰, p = 0.004, and Phe +1.5‰, p = 0.02; research data 2-S10). A sample CSIA-AA chromatograph showing peak separation for both modern and subfossil coral hydrolysate is in the supplemental material (Fig. 2-S1B). Mean THAA $\delta^{15}N_{norm\text{-}AA}$ values were 17.7 ± 1.0‰ (n = 5) for the outer diagenetic horizon (0-5 mm), while the inner layers (>10 mm) mean THAA $\delta^{15}N_{norm\text{-}AA}$ values were 19.2 ± 0.8‰ (n = 6). This offset in THAA $\delta^{15}N_{norm\text{-}AA}$ values was in the opposite direction of the bulk $\delta^{15}N$ trend (Fig. 2-6).

In contrast to the similar and very consistent CSIA-AA patterns observed in the inner >10 mm layers described above, the $\delta^{15}N_{norm\text{-}AA}$ values in the outer seawater exposed layers were highly variable, with some more positive (Asx, Lys, Gly, Ala,

Val, Ser, Leu; Fig. 2-S3), others more negative (Ile, Thr, Glx, Pro; Fig. 2-S4), and some varying with no consistency across subsamples analyzed (Phe, Tyr; Fig. 2-S5). After normalization to THAA (proxy for average protein $\delta^{15}N$ value) there were also significant differences in $\delta^{15}N_{norm\text{-}AA}$ patterns between the outer diagenetic horizon (0-5 mm, n = 5) and inner layers (>10 mm, n = 6) (Fig. 2-5; red vs. yellow filled circles). These normalized values, reflecting the relative biosynthetic offset from average protein, were substantially different for most AAs: Asx (+2.3‰, p = 0.01), Gly (+2.1‰, p = 0.006), Lys (+1.8‰, p = 0.02), Ala (+2.8‰, p = 0.03), Val (+3.0‰, p = 0.03), Pro (+2.4‰, p = 0.03), and Thr (-14.5‰, p = 0.01; Fig. 2-5, data table 2-10).

3.7 Trophic and Degradation Proxies

Consistent with the individual AA isotope differences presented in Section 3.5, there were very large differences in the ∑V parameter for microbial degradation and protein resynthesis between modern and subfossil corals, in particular between the inner verses outer zones of the subfossil specimen. Due to the uniquely large $\delta^{15}N$ offset of Ile (-7.2‰) between live-collected and subfossil specimens, ∑V was calculated both with and without Ile. The modern specimen had very consistent standard ∑V values, mean 2.7 ± 0.1 (3.0 ± 0.2 when Ile was excluded, n = 4, Fig. 2-6C). The subfossil inner (>10 mm) layers, where most $\delta^{15}N_{AA}$ data were consistent with live-collected coral, also had a consistent but elevated standard ∑V value of 4.0 ± 0.3 using all AA (n=6). However, this result was very strongly driven by Ile $\delta^{15}N$ values alone. Recalculating ∑V without Ile, the inner subfossil coral average ∑V was

3.4 ± 0.2 (n = 6), comparable to data for the modern coral. Finally, the diagenetic horizon (0-5 mm) subfossil coral layers had very high ∑V values, reaching among the highest values (range 5-6, Fig. 2-6C, research data 2-S9).

$TP_{CSIA\text{-}AA\ Skeleton}$ values also varied substantially within the subfossil coral but were again similar between the inner subfossil layers (>10 mm) and the modern coral. Subfossil inner layers (>10 mm) had $TP_{CSIA\text{-}AA\ Skeleton}$ values with a mean of 3.1 ± 0.1 (n = 5), very close to modern coral values (3.3 ± 0.5, n = 4), while the subfossil outer layers reached a low $TP_{CSIA\text{-}AA\ Skeleton}$ of 1.2 (at 2.8 mm) in the same region with highest ∑V (Fig. 2-6D). Alternative calculations for trophic position were also examined, all indicating similar trends within and among zones (Fig. 2-S6).

4. Discussion

Understanding the long-term preservation of deep-sea proteinaceous coral skeletons is critical to extending the time horizon of paleo-applications using these valuable bioarchives. Comparisons of subfossil (~9.6-11.6 kyr BP) and modern *K. haumeaae* skeletons across a wide range of physical features, bulk chemical composition based on C/N, bulk $\delta^{13}C$ and $\delta^{15}N$ values, molecular level AA molar percentages and isotope compositions, and CSIA-AA parameters for degradation (ΣV) and trophic position (TP_{CSIA}) show excellent preservation of physical and geochemical composition in the inner subfossil coral skeleton. These findings lend confidence to the paleo-application of geochemical proxies in deep-sea proteinaceous coral skeletons to reconstruct biogeochemical cycling, plankton community trophic dynamics, and export production back through the Holocene. At the same time, we

also clearly identified a very distinct seawater exposed, outer diagenetic horizon of the skeleton with both abiotic alteration (e.g., loss of glycine, potential carbonate addition) and biotic degradation (e.g., increased variability in AA isotope values, ΣV, $TP_{CSIA\text{-}AA\ Skeleton}$) accompanied by physical changes in the skeleton matrix (SEM images). Identification of this region will help to avoid potential misinterpretation of geochemical data in degraded regions of these archives.

4.1 Physical structure: matrix changes in subfossil coral

Skeletons of *K. haumeaae* exhibit concentric growth layers composed of a tightly bound fibrillar protein, similar to other proteinaceous corals (Goldberg, 1976; Noé and Dullo 2006; Sherwood et al. 2006). Visually there was little difference in skeletons between the live-collected and subfossil specimens without magnification. While the subfossil disk was lighter in color, with a drier, flaky outer crust, there was no visual indication of the physical or chemical degradation zonation. Specifically, the diagenetic horizon (outer 10 mm) discussed extensively in subsequent subsections, could not be visually identified.

Under higher magnification (SEM) structural differences between the live-collected and subfossil specimens were readily apparent (Fig. 2-1). For the live-collected specimen the regular banded fibrous layers were clearly visible in SEM images (Fig. 2-1A, 2-1B). This suggests while the modern skeleton itself is not living, it was physically very well protected from the influence of ocean water by the living outer polyp colony and intact outer skeleton. It has been hypothesized that the tightly woven fibrous structure of proteinaceous coral skeletons contributes to degradation

resistance by preventing seawater penetration (Druffel et al., 1995), with the implication being that physical protection slows down biological as well as abiotic compositional changes. Similar physical protection of organic matter is well known in a range of matrixes including as eggshell/bone (e.g., Hendy, 2021) and soil organic matter (e.g., Krull et al., 2003). In shallow water carbonate corals it is only after the polyps die that the skeleton is exposed and significant colonization by bacteria, borers, and physical grazing occurs (Le Campion-Alsumard et al. 1995). The protection of the inner coral skeleton is therefore likely applicable to other genera of corals as well as skeletons of different ages but further research is necessary to confirm this.

The subfossil coral skeleton showed hallmarks of matrix degradation at both a macro and microscale level, particularly in the outer most, seawater exposed zone of the skeleton (Fig. 2-1). Visually, a more brittle and paper-like apparent character in SEM images of the very outermost layers (<0.1 mm) suggest possible structural changes in the protein matrix. Furthermore, SEM imaging showed clear loss of tightly woven fibers and a flakey microstructure (Fig. 2-1C, 2-1D). Overall, the loss of microfiber banding and less dense sheeting in the subfossil coral suggests intensive structural degradation in the outermost, most seawater impacted region (Fig. 2-1C, 2-1D), likely due to a combination of degradation with time and seawater exposure/infiltration. We hypothesize that these physical changes could provide more surface area for microbial activity in outer layers (Ingalls et al. 2003), in contrast to the denser, better protected inner layers. Finally, we note that the physical transition

from the outer layers' distinctive plate-like structure to more dense layers in the inner layers appears gradual, and we could not clearly identify the distinct chemical diagenetic horizon in SEM images which appeared quite sharp in the geochemical proxies.

4.2 Elemental Composition Changes

The C/N ratio of unaltered gorgonin can be used as a reference to evaluate changes in skeletal composition associated with degradation, since it should be both fixed and predictable within any coral species. A similar C/N ratio approach has commonly been taken to assess both diagenesis and exogenous organic contamination impacting the integrity of collagen, which has structural similarities to gorgonin (e.g., Ambrose and Norr, 1992).

The C/N ratio of proteinaceous skeleton material from live-collected *K. haumeaae* in this study (2.8 ± 0.1) agrees with a number of previous studies on live-collected *K. haumeaae* from the Hawaii Islands (2.7-3.0 Sherwood et al., 2014, McMahon et al., 2015) and the Atlantic (2.8-3.0 Druffel et al., 1995, Goodfriend 1997). It should be noted that most previous studies used acidification prior to EA analysis to ensure no influence of inorganic carbonates on C/N ratios. Prior published data using acidified samples (e.g., Guilderson et al., 2013, Glynn et al., 2019) has shown indistinguishable C/N values from those we observed in our live-collected non-acidified specimens, all suggesting that a C/N ratio of 2.7-3.0 would be expected for intact / non-degraded *K. haumeaae* skeletons, which is similar to the expected

C/N of pure protein (~3), and that acidification does not change greatly these values for the intact organic matrix after any carbonate is removed.

However, in our non-acidified subfossil skeleton samples, we observed elevated C/N values (+0.1-0.8 C/N units higher versus the live-collected *K. haumeaae* skeleton; *results 3.2*; Fig. 2-2). These findings corroborate a recent study showing that *non*-acidified subfossil coral C/N values can deviate well above 3.0, particularly in outer exposed layers (Glynn et al. 2019). These deviations suggest either carbonate precipitation or selective organic N loss with degradation in exposed specimens. We also observed an essentially linear shift in C/N ratios in the subfossil coral outer diagenetic horizon (0-10 mm), culminating in the highest C/N ratios at the seawater interface (C/N = 3.7, Fig. 2-2A). Further, while acidification did reduce C/N ratios across the entire coral transect, acidification did not "restore" C/N values in the outer diagenetic horizon to the reference value. This strongly suggests that both carbonate formation and organic degradation are simultaneously occurring. Finally, the fact that the inner skeleton layers of the subfossil coral had C/N ratios within instrumental error to fresh gorgonin, regardless of acidification (average offset +0.1 C/N units in >10 mm layers, research data 4), strongly indicates that inner skeleton layers remain well protected from degradation even in a ~10 kyr specimen. Overall, we propose C/N ratios *after* acidification can be used a simple metric to assess degradation state in non-living coral sea floor specimens: C/N ratios >3 indicate appreciable degradation of the gorgonin organic matrix, suggesting great caution in interpreting bulk $\delta^{13}C$ and $\delta^{15}N$ values (as discussed in Sections 4.3-4.4). We recommend that

future subfossil coral studies analyze C/N to test degradation state prior to interpretation of environmental signatures.

4.3 Mechanisms of elemental C/N and bulk $\delta^{13}C$ changes

4.3.1. Glycine loss

The acidification tests described in Section 4.2 suggest that elevated C/N values are at least in part due to the presence of secondary authigenic carbonate. However, a change in organic gorgonin molecular composition is an additional possibility. While molecular AA data indicate a relatively similar composition for most AAs between subfossil and live-collected coral skeleton (Fig. 2-3B, data table 2-3.3), glycine (Gly) was the major exception. The ~50% lower Gly contribution in all layers of the subfossil specimen compared with modern gorgonin suggests a major organic structural change. At the same time, Gly also has the lowest C/N value of any AA (2.0). Therefore, the large loss of glycine must contribute at least in part to higher C/N values observed throughout the subfossil skeleton. A mass balance calculation based on the modern coral mol% values can broadly constrain this effect: our observed change in Gly from 52% in live-collected skeleton to 23% in subfossil skeleton would be expected to increase C/N by 0.35-0.41, assuming that all other organic composition remains constant. We note that while acidification results show this cannot be the only process at work, at the same time this result is quite similar to the actual C/N offsets observed between the subfossil inner layers (>10 mm) and the average of modern corals (research data 3). One caveat to this estimate is that our acid hydrolysis-based analytical method cannot measure Histidine. Histidine is an N-rich

(low C/N) AA that is very abundant in many gorgonin-based proteins (18-30%; Druffel et al., 1995, Goodfriend, 1997) such that any major "hidden" changes in this AA could have substantial C/N impacts. However, the fact that our simple calculation based on Gly loss alone is consistent with both observed C/N and molar data suggests that loss of glycine is likely the dominant organic process driving the C/N offset between modern and subfossil corals over millennial timescales.

The mechanism leading to large glycine losses from coral skeleton over millennia is uncertain. However, the fact Gly appears to be lost and not gained in subfossil corals compared with modern corals, coupled with only minor changes in other AA molar composition (results 3.3), strongly suggests an abiotic mechanism. Gly mol% increases are a widely used AA indicator for microbial degradation (e.g., Dauwe et al., 1999; Yamashita and Tanoue, 2003; Kaiser and Benner, 2009), making a nearly 50% Gly reduction inconsistent with typical biologically-mediated changes. Further the widely used Degradation Index (DI; based on AA mol% shifts observed with marine organic matter degradation; Dauwe et al., 1999) yields DI values close to "fresh" plankton in the inner coral (Fig. 2-S8). In fact, most of the subfossil coral DI values *elevated* (indicating *less* degradation) versus the values of the modern coral specimen. As discussed further below (chapter 2, section 4.5) this is likely due in part to the unique AA composition of the gorgonin skeleton, rather than microbial degradation of subfossil coral skeleton.

We hypothesize that abiotic glycine decarboxylation may be the main mechanism for subfossil coral Gly loss. The spontaneous aqueous decarboxylation of

free glycine is well known, whereby water molecules assist with proton transfer cleaving the Gly C-N bond, resulting in degradation of Gly (e.g., Catão and López-Castillo, 2018 and references within). As structurally the simplest of all AAs, glycine ($C_2H_5NO_2$) is thermodynamically favored to remove the amide group to form bicarbonate and also requires the least water ($4H_2O$) to do so (LaRowe and Van Cappellen, 2011). We note that this process may also contribute to authigenic carbonate formation, potentially accounting for some of the C/N offset between the acidified and non-acidified data. While this reaction has not been previously reported for glycine bound in a proteinaceous structure, it would provide a potential mechanism for Gly degradation in the seawater exposed outer diagenetic horizon of coral skeletons over ~10 kyrs.

Gly loss would also be consistent with physical structure changes, as Gly plays an important role in holding adjacent layers together in *K. haumeaae* skeletons (Druffel et al. 1995). We therefore further hypothesize that selective abiotic Gly loss contributes to the altered physical matrix observed in subfossil coral SEM images (Fig. 2-1). Finally, we note that while the dramatic Gly molar depletion (~50%) is clear in all subfossil coral samples, the more minor Gly changes observed from inner vs. outer subfossil skeleton (~5 mol%; Fig. 2-3) are in the opposite direction. While these more minor offsets are approaching the analytical variation of chromatography methods, this result at least suggests that some addition biotic degradation of the protein matrix is occurring, superimposed on the earlier rapid and far larger abiotic decarboxylation. Investigation into whether AA degradation in protein-bound AAs

follows the same hydrolysis-based degradation pathways as free AAs is necessary to validate this hypothesis. Such work would shed additional light on other unknown compounds besides the dominant proteinaceous material in these types of deep-sea corals that may also be altered during this degradation process.

4.3.2 Secondary authigenic carbonate

Higher C/N ratios and $\delta^{13}C$ values observed after acidification must in part be due to carbonate precipitation, particularly in the outermost coral layers (0-10 mm) most subjected to seawater infiltration. Though of note, even if the inner layers (>10 mm) are protected from direct seawater influence, if our hypothesis regarding Gly decarboxylation is correct then inorganic carbonate could also accumulate here (Catão and López-Castillo, 2018). While seawater carbonate precipitation is therefore never mutually exclusive from an abiotic decarboxylation mechanism, one major difference is that carbonate precipitation should lead to a contemporaneous increase in bulk $\delta^{13}C$ values. Glycine loss is more difficult to constrain, however it would most likely work in the opposite direction (i.e., *decreasing* bulk $\delta^{13}C$ values), because Gly is typically ~3‰ higher in $\delta^{13}C$ value compared to the average of all proteinaceous AAs (Shen et al. 2021, McCarthy et al., 2013).

As carbonate $\delta^{13}C$ endmembers can be estimated, the potential quantitative influence of authigenic carbonate on bulk $\delta^{13}C$ values can be constrained using isotope mass balance. If we assume a $\delta^{13}C$ value of 1‰ for dissolved inorganic carbon (DIC) and a fractionation (ε) from DIC to calcite of 1‰, then authigenic

calcite should have a $\delta^{13}C$ value of ~2‰ (Romanek et al., 1992; Quay et al., 2003). This means that the maximum observed offset of ~1.4‰ between the acidified and non-acidified samples in the outermost 1 mm (Fig. 2-2C) would require ~7-8% of total C to be present as calcite precipitate. Returning to our C/N data, if the "fresh" gorgonin C/N is ~2.8, then 8% carbonate accumulation (as a fraction of total C) would cause C/N to increase to ~3.0. This shift of ~0.2 C/N would therefore represent approximately half of the ~0.4 C/N shift we calculated above from loss of glycine.

Currently no studies have focused on carbonate precipitation in deep-sea proteinaceous coral skeletons. Estimates of sedimentary secondary authigenic carbonate formation can reach as high as 10% in high depositional regions (Sun and Turchyn, 2014). While the mechanism for sedimentary authigenic carbonate formation is clearly different than in deep-sea corals, and in particular is likely much more dependent on pH and degrading organic matter, nevertheless we note that the similar magnitudes of maximum carbonate in our outer coral layers and in sediments at least suggest that this mass balance estimate of possible secondary authigenic carbonate formation is not unreasonable. Some additional carbonate precipitation could also be related to respiration of the skeletal organic matter should seawater intrusion supply enough oxygen that pH does not facilitate dissolution. Particularly in the outer diagenetic horizon, both processes are likely contributing to observed isotope shifts. For sediments, locations with enhanced microbial respiration tend to have the largest amount of authigenic carbonate formation, because microbes affect pore water chemistry by converting organic matter to CO_2, which then precipitates as

carbonate (e.g., Sun and Turchyn, 2014). Further analysis to discover whether unique microbial populations facilitate deep-sea coral degradation and how the deposition and degradation of sediments upon dead skeletons impact water chemistry should be conducted.

4.4 Biological degradation in seawater exposed gorgonin: impact on bulk $\delta^{15}N$ values and CSIA-AA parameters

In contrast to the protected inner layers, the outer diagenetic horizon (0-10 mm) layers show clear evidence of microbial degradation, discernible at the molecular level. While carbonate precipitation and abiotic Gly loss described in Section 4.3.1 can account for some of the C/N and isotope ratios changes (Fig. 2-2), the $\delta^{15}N_{AA}$ values in the outer layers bear the signature of microbial resynthesis with highly elevated ΣV values in comparison to both the modern coral specimen and the subfossil coral interior (McCarthy et al., 2007: Fig. 2-6C). The ΣV parameter quantifies variability in $\delta^{15}N_{AA}$ patterns as a measure of progressive degradation and reflects the selective microbial resynthesis of individual AAs (McCarthy et al., 2007, Batista et al., 2014, Sauthoff et al., 2016, Ohkouchi et al, 2017). Together with strongly elevated bulk $\delta^{15}N$ values, ecologically unrealistic CSIA-AA trophic position values (Fig. 2-6D; discussed in Section 4.4.1), and dramatic outer layer structural changes seen in SEM imaging (Fig. 2-1), this data suggest significant biological degradation of the outer gorgonin matrix after direct contact with seawater.

We propose that the coupled large changes in bulk $\delta^{15}N$ and $\delta^{13}C$ values observed in the diagenetic horizon likely reflect combined abiotic and biological effects of oxic seawater exposure. Multiple lines of evidence support this conclusion. First, the large and almost linear increase in $\delta^{15}N$ values of ~7‰ in the outer layers is consistent with expected impact of microbial degradation on organic matter, typically imparting a strong increase in the $\delta^{15}N$ values of the residual or substrate organic matter, with changes in $\delta^{15}N$ values up to 6‰ observed in sediments and suspended particles (Saino and Hattori, 1980; Saino and Hattori, 1987; Altabet, 1988; Lehmann et al., 2002). While some baseline $\delta^{15}N$ shift cannot be ruled out, the unidirectional change in $\delta^{15}N$ values in the outer coral is substantially greater than any documented change in comparable corals since at least the last 5 kyrs (Williams and Grottoli, 2010, Sherwood et al., 2014, Glynn et al. 2019). This suggests $\delta^{15}N$ baseline changes are exceedingly unlikely to be the main driver of the $\delta^{15}N$ change in the outer diagenetic horizon. Second, some part of the $\delta^{13}C$ value increases may also be due to microbial degradation removing the lighter ^{12}C from the skeleton, in addition to respiration contributing to carbonate formation discussed in Section 4.3.2. Given that our isotope mass balance exercise above suggests ~1‰ of the observed $\delta^{13}C$ change could be due to carbonate formation, this would theoretically leave another ~1‰ of the total shift observed in the outer layers due to a mechanism like microbial degradation.

Finally, we also evaluated the degradation index (DI) because is one of the most widely used degradation proxies in organic geochemistry, commonly applied in

sediments, ocean particles, and other detrital organics (Dauwe et al., 1999). The underlying assumption of the DI index is that AAs have different and predictable relative lability to bacterial degradation of proteinaceous materials. However, the standard DI formulation does not appear to indicate lability in gorgonin as DI indicated more "degraded" values in the most protected inner coral layers, becoming "fresher" with progressive structural deterioration and alteration of other degradation metrics (Fig. 2-S8). In particular in the outer diagenetic horizon where evidence of degradation seems unambiguous, DI does not change in a uniform manner. We hypothesize that either the very different AA composition of gorgonin (a very specific, single structural protein), or different mechanisms by which bacteria are able to degrade this material, underlie these observations. We conclude that standard DI is not a useful metric to evaluate relative degradation state/integrity of gorgonin structural protein but by utilizing skeletons spanning a variety of ages it should be possible to create a coral specific DI.

4.4.1 Preservation and likely fidelity of CSIA-AA parameters

Degradation in the outer diagenetic horizon had major impacts on two important CSIA-AA proxies of environmental biogeochemistry and trophic dynamics. $TP_{CSIA\text{-}AA}$ is commonly applied in deep sea corals and sediments to indicate relative changes in planktonic food web structure (Batista et al. 2014, Sherwood et al. 2014, Sauthoff et al., 2016). It appears that microbial degradation in the outer subfossil coral material also strongly impacts $TP_{CSIA\text{-}AA\ Skeleton}$, consistent

with elevated ΣV data in this zone. Specifically, the lowest $TP_{CSIA\text{-}AA\ Skeleton}$ value of 1.7 in the outer subfossil coral layers is more than a full trophic step lower than the inner (>10 mm) layers ($TP_{CSIA\text{-}AA\ Skeleton}$ = 3.1 ± 0.1), with swings of ~1.5 trophic levels between adjacent samples (Fig. 2-6D). It seems very unlikely that large and rapid shifts in overlying plankton ecology and unrealistically low TP values occur only at the end of this coral colony's millennial lifespan. We note that the mean trophic–source $\delta^{15}N_{AA}$ offsets, often used as proxy for relative TP change that avoids issues of TDF and β selection, (McCarthy et al. 2007, Sherwood et al. 2011, Batista et al. 2014), show similar patterns. Together, these data indicate that TP_{CSIA} values are viable in the intermediate (transition) and inner most protected coral regions, but should not be trusted in the outer diagenetic horizon without corroborating evidence of minimal degradation (i.e., ΣV value and/or C/N ratio).

The significantly higher ΣV values in the outer zone of the subfossil coral skeleton (maximum 5.8, Fig. 2-6C) were clearly distinct from both the inner zone and modern corals and were consistent with strong microbial resynthesis. The ΣV values (3-4) observed throughout the inner subfossil coral are high relative to the range typically found in plankton or non-degraded proteinaceous materials (<2.0; McCarthy et al, 2007), and slightly elevated compared to modern coral specimens (~3.0; Sherwood et al., 2014; this study, Fig. 2-6). In the modern coral, the difference in ΣV value from fresh material has been attributed to the unique AA composition of the gorgonin structural protein (Sherwood et al., 2014). However, note that the ~1 ΣV value offset between modern and inner subfossil coral layers is almost exclusively

driven by changes in isoleucine. Without isoleucine, both modern and subfossil ΣV values are very similar (0.4 ΣV offset), which is consistent with the very similar CSIA-AA biosynthetic patterns (Fig. 2-5, 2-6B). This apparently singular $\delta^{15}N$ shift in isoleucine in the subfossil coral is puzzling. A unique isoleucine shift of this kind has never been observed in CSIA-AA $\delta^{15}N$ patterns for degrading OM; in fact here it might not be biological at all, given that it is observed even in the innermost, protected coral layers. Further research into this loss could shed more light on the mechanisms underlying multi-millennial gorgonin alteration. Overall, bulk $\delta^{15}N$ values and $\delta^{15}N_{AA}$ patterns for all other AAs indicates that CSIA-AA proxies were well preserved in the inner coral layers with the only exception being the trophic AA Ile. Similarly, with the exception of Ile and the metabolic AA Thr, the scatter of the individual non-normalized as well as THAA-normalized values in the ≥10 mm interior of the sub-fossil specimen were similar to the scatter in not only the modern Cross Seamount specimen, but a larger data-set in near-modern specimens from off Oahu (Sherwood et al., 2014) (Fig. 2-S3 to 2-S6).

4.5 Inner coral preservation of CSIA-AA parameter integrity

The excellent preservation of expected molecular geochemistry parameters (e.g., mol%, ΣV, TP_{CSIA}) in the inner coral (>10 mm) strongly suggests that beyond the outer diagenetic horizon, subfossil deep-sea proteinaceous skeletons remain viable as paleoenvironmental bioarchives. As baseline $\delta^{13}C$ or $\delta^{15}N$ values of primary production from ~9.6-11.6 kyr BP cannot be known, it is not possible to directly

confirm this hypothesis. However, there are ways to evaluate the integrity of CSIA-AA values by examining CSIA-AA patterns and source AA values in order to reconstruct paleo-export production values.

The first way is specifically evaluating relative CSIA-AA *patterns* with those from marine primary production and sinking particles (Fig. 2-S9). The observation of expected *patterns* in normalized CSIA-AA data provides strong evidence for the preservation of individual AA isotope *values* since degradation processes scrambles CSIA-AA patterns and degradation is unlikely to alter values of every AA in exactly the same way (e.g. McCarthy et al., 2007, Okhouchi et al., 2017). The essentially identical $\delta^{15}N_{norm\text{-}AA}$ patterns observed for almost all AAs (Fig. 2-5; Results section 3.5) in the inner (>10 mm) zone of the subfossil coral match those CSIA-AA biosynthetic patterns expected for live-collected deep sea corals, which consume photosynthetic marine algae and sinking particles (Fig. 2-S9; Shen et al., 2021, McCarthy et al., 2013, this study). Average source and trophic AA group values can represent an additional check on the influence of any possibly anomalous individual AA isotope changes with degradation (McCarthy et al., 2007). Both these metrics also show stable plateaus for the inner (>10 mm) layers of the subfossil coral (Fig. 2-6), consistent with the relatively low and stable ΣV values described earlier, and again supporting good preservation of CSIA-AA $\delta^{15}N$ values in the protected interior coral skeleton.

A second way to evaluate if AA values have been well preserved is to ask if shifts in predicted 'baseline" correspond with records from other archives in this

region. The shift in "baseline" $\delta^{15}N$ values indicated by CSIA-AA (e.g., Source AA's Lys, Phe, Tyr; non-normalized) are in fact consistent with expected changes in this Pacific region. The shift in average source AA values indicates a change in the source nitrate $\delta^{15}N$ value of ~3‰ between the subfossil inner layers (10-11.6 kyrs BP; $\delta^{15}N_{source}$= 9.4 ± 0.5‰) and the modern coral ($\delta^{15}N_{source}$= 6.3 ± 1.3‰, research data 8 and 9). Based on the molecular changes found in this study, such as the shift in Gly from 52-26%, these composition changes may account for a ~1‰ increase in bulk $\delta^{15}N$ over this timeframe. This would account for a third of the ~3‰ change between modern and inner subfossil, leaving ~2‰ attributed to environmental change, which is still within range suggested by sedimentary margin records (~1-5‰; Tesdal et al. 2013). The CSIA-AA $\delta^{13}C$ (mol% weighted THAA; a proxy for baseline) also supports a baseline shift between the modern coral (-9.9 ± 0.7‰; n = 3) and the subfossil coral (-11.9 ± 0.2‰; n = 6), again consistent with the export production $\delta^{13}C$ values that have increased by ~2‰ from the Younger Dryas (~12 kyrs ago) to the late Holocene in Pacific Margin sedimentary $\delta^{13}C$ records (references within Tesdal et al. 2013). Together these results also suggest that $\delta^{13}C_{AA}$ plankton community fingerprinting approaches recently demonstrated in ~1000 yr old gold corals (McMahon et al., 2015) may also be able to reconstruct plankton community structure of exported production from subfossil corals, assuming that proper phytoplankton end-members are used for a given time period.

5. Summary and Conclusions

By comparing a subfossil (~9.6-11.6 kyr BP) *K. haumeaae* coral skeleton with a live-collected specimen from the same seamount in Hawaii, this study documented microstructural, molecular, and geochemical changes accompanying degradation of the proteinaceous coral gorgonin matrix. These changes occurred primarily in the outermost skeleton, which we hypothesize are due to a combination of abiotic and biotic degradation as a function of contact with oxic seawater for ~10 kyr. The physical structure of the outer subfossil coral showed pronounced loss of banding, shifting to a randomized plate-like and presumably less dense structure. We hypothesize that these structural changes contributed to seawater penetration and subsequent microbial activity that altered skeleton molecular and geochemical values in this outer diagenetic horizon. At the molecular level, all layers of the subfossil coral had only about half the expected molar glycine content of live-collected coral skeleton, while the effects of acidification on skeleton $\delta^{13}C$ values indicated significant authigenic carbonate formation, particularly in the outer zone. We hypothesize that this carbonate formation was enhanced by the abiotic degradation of glycine and associated production of bicarbonate. However, despite all these changes, molar compositions for all other AAs were similar to the live-collected counterpart for all but the outermost (0-10 mm) layers.

The outermost ~10 mm of the subfossil coral was distinct in every molecular parameter, with extensive changes consistent with both microbial degradation and substantial carbonate precipitation, both likely linked to seawater exposure. Large

linear increases in bulk $\delta^{13}C$ and $\delta^{15}N$ values, coupled with high values of the degradation parameter ΣV and anomalous CSIA-AA trophic position values indicated extensive, progressive, and easily identifiable microbial degradation. Together, these shifts are consistent with progressive organic degradation with seawater infiltration and attendant gorgonin physical structure breakdown, occurring in this coral at approximately 1 mm per 1000 yrs.

In contrast to the outer diagenetic horizon, all the same proxies within the intermediate and innermost coral layers indicated excellent preservation of the gorgonin protein, in particular molecular level AA isotope values. We propose C/N ratio as a basic metric to evaluate skeleton integrity, where C/N values above 3 for this species indicate degradation extensive enough to confound bulk isotope data interpretations. This should be supplemented by acid tests (or direct $\%CaCO_3$ determination) to evaluate carbonate contamination. Further, we suggest that while the DI index appears to not function reliably in the gorgonin matrix, the CSIA-AA based ΣV metric beyond the typical gorgonin baseline value of 3.0 can provide clear information about microbial influence.

While gorgonin bulk isotope and elemental values can be strongly altered in the outer zone of subfossil specimens, CSIA-AA values and associated proxies appear to be far more robust to these degradation processes. In particular CSIA-AA proxies for isotopic baseline (Phe, mean source AA $\delta^{15}N$ values, and mean essential AA $\delta^{13}C$ values) appeared to be well preserved beyond the outer diagenetic horizon, with biosynthetic patterns very similar to both primary production and modern coral

gorgonin for both $\delta^{13}C$ and $\delta^{15}N$ values. Even Gly, despite its very large molar loss, had normalized CSIA-AA patterns that matched those expected from modern corals for both $\delta^{13}C$ and $\delta^{15}N$. The $\delta^{15}N$ values of Ile were one notable exception, with substantially elevated $\delta^{15}N$ values in all zones of the subfossil coral. To our knowledge, such shifts in Ile $\delta^{15}N$ values have not been previously observed, and based on these observations, we suggest that ΣV in protein corals should in the future be calculated without Ile.

Overall, the excellent CSIA-AA pattern preservation in the inner deep-sea proteinaceous coral skeletons on multi-millennial time scales indicates that source and essential AAs can be used to determine environmental information about export production and degradative processes in subfossil coral skeletons when C/N and ΣV values fall within expected ranges. We propose that a combination of elemental and CSIA-AA metrics can be used to readily gauge gorgonin integrity and screen subfossil samples for more reliable geochemical interpretations. This work opens wide potential to the use of CSIA-AA proxies for reconstructing baseline biogeochemical cycling, export production dynamics, and algal trophic structure and community composition, at least back through the Holocene using the wealth of available subfossil specimens.

Acknowledgements

None of this work would have been possible without the captain and crew of the RV Ka‘imikai-o-Kanaloa and the pilots and engineers of the Hawai’i Undersea Research Lab. Sample collection was funded by NOAA/NURP and the National Geographic Society (7717-04). A portion of this work was performed under the auspices of the U.S. Department of Energy (DE-AC52-07NA27344). The majority of the work presented here was funded by the National Science Foundation (OCE 1061689). D.S. Glynn was supported by a Eugene Cota-Robles Fellowship and a National Science Foundation Graduate Research Fellowship (NSF-GRFP; 1339067). We acknowledge Dr. T. Yuzvinsky for assistance with sample preparation and electron microscopy and the W.M. Keck Center for Nanoscale Optofluidics for use of the FEI Quanta 3D Dualbeam microscope. Further thanks go to D. Andreasen, C. Carney, R. Franks and a team of undergrad interns (S. Kaplan, A. Jalali-Sohi, K. Miles, L. Gomez, Z. Wright) for laboratory assistance. Thanks to the assisting editors and anonymous reviewers for their feedback.

Chapter 3

Equatorial Pacific corals show 2000 years of $\delta^{15}N$ and $\delta^{13}C$ variability linked to source water mass shifts and phytoplankton community change

Abstract

Within the equatorial waveguide, the central tropical Pacific is one of the most productive open-ocean regions, greatly influenced by basin boundary water-mass sources and their properties which are transported to the central Pacific by the North and South Equatorial Current (NEC and SEC) and North Equatorial Counter Current (NECC). On interannual (e.g., El Niño Southern Oscillation) timescales, water mass and nutrient variability is mainly driven by changes in recently upwelled waters from the Eastern Equatorial Pacific. This upwelled water is characterized by high [NO_3] and more positive $\delta^{15}NO_3$ values, versus waters from the Western Equatorial Pacific which are characterized by low [NO_3], in situ nitrogen fixation, and low $\delta^{15}NO_3$ values. To document decadal to centennial scale variability in the mixing or replacement of these waters in the Central Equatorial Pacific, we developed nitrogen ($\delta^{15}N$) and carbon ($\delta^{13}C$) bulk isotope records along with compound specific analysis of amino acid $\delta^{15}N$ values in a pair of Kingman Reef (6°N, 162°W) proteinaceous deep-sea *Kulamanamana spp* skeletons. These records provide novel insight into nitrate nutrient variability and phytoplankton community shifts over the most recent 2000 years.

We found that the $\delta^{15}N$ and $\delta^{13}C$ bulk coral isotope values were typically coupled, with a long-term positive trend in both isotopes from 100-800 CE of 2‰ and 1.5‰ respectively, with 30-60 year ~0.5‰ fluctuations superimposed on top of the

long term trend for $\delta^{15}N$ values only. A decoupled period between the isotopes begins in ~1400 CE, where $\delta^{15}N$ values drop by 1‰ while $\delta^{13}C$ values stay approximately constant. This is followed by a period of relatively stable $\delta^{15}N$ and $\delta^{13}C$ values during the Little Ice Age (1500-1800 CE), prior to the most rapid drop in the record (>1‰) in the most recent two centuries for both $\delta^{15}N$ and $\delta^{13}C$ values.

Together, these data indicate major long term fluctuations in algal ecosystems and biogeochemical systems, marked by several distinct regimes over the last 2000 years in the central Pacific, during which $\delta^{13}C$ and $\delta^{15}N$ of primary production are typically linked, driven by similar shifts in source nutrient changes, related to trade wind dynamics and ocean current shifts. We interpret higher coral $\delta^{15}N$ values as primarily due to enhanced transport of waters upwelled in the Eastern Equatorial Pacific, while lower $\delta^{15}N$ values are interpreted as a stronger influence of Western Equatorial Pacific waters, advected eastward within the NECC. We propose that the coral $\delta^{13}C$ are likely tracking changes in extant plankton assemblages, in particular variations between diatom and eukaryotic populations (higher $\delta^{13}C$; Fry and Wainright, 1991, McMahon et al. 2015) versus prokaryotic and/or N_2 fixing organisms (lower $\delta^{13}C$; McMahon et al. 2015, Schmittner and Somes, 2016).

To broadly interpret observed shifts, we use ENSO inter-annual changes in current intensity and relative position of the major currents as an interpretative framework to understand long term variability. Specifically, during warm, wet periods (El Niño-like conditions) the NECC impacting our study site is shifted south with a strengthened west to east flow, likely contributing to the lower $\delta^{15}N$ values and

smaller cell-dominated communities. Conversely during cool, dry periods (La Niña-like conditions) the east to west NEC carries higher nutrient water which is also impacted by signatures of denitrification, contributing to enriched $\delta^{15}N$ values, while also promoting larger celled eukaryotic (diatom) algal communities. Results from this research provide the first high fidelity records of biogeochemical changes for this region over decadal to century timescales, together with a new framework for their interpretation, over a time period and resolution typically unavailable in sedimentary records, demonstrating the potential of deep sea corals for examining equatorial Pacific ecosystem dynamics.

1. Introduction

The tropical Pacific Ocean is one of the most productive open-ocean regions in the world, due to both equatorial upwelling as well as upwelling focused in the eastern Pacific. In addition to being a large contributor to global new production (Chavez and Toggweiler, 1995, Chavez et al. 1996), the tropical Pacific Ocean is the largest natural source of carbon dioxide to the atmosphere (Tans et al. 1990, Feeley et al. 1987). However, ocean-atmosphere interactions also strongly influence surface productivity and C uptake, through climate patterns such as El Niño and La Niña cycles (ENSO, Turk et al., 2001; Wang and Fiedler, 2006; Park et al., 2011, Costa et al. 2017), and through the positioning and seasonality of the Intertropical Convergence Zone (ITCZ; Dandonneau et al., 2004; Koutavas and Lynch-Stieglitz, 2004) which impacts the supply of key nutrients e.g., nitrate, iron, and silica (Costa et al. 2017, Coale et al., 1996; Moore et al., 2001; Baines et al., 2011; Brzezinski et al.,

2011, Altabet 2001). As the ITCZ is the dominant control over precipitation in the region, ENSO variability essentially tracks the swings in precipitation and SSTs (warm/wet for El Niño, cool/dry for La Niña).

The coupled physical oceanography and biogeochemistry of this region are also particularly complex on a variety of timescales, due to the intimate coupling of the trade winds, ocean currents, sea surface temperatures, nutrient dynamics and ecosystem productivity (Johnson et al. 2002, Pennington et al. 2006, McPhaden and Zhang 2002). Currently there are two main environmental states of the central equatorial Pacific related to the strength of trade winds: 1) stronger east to west flow (i.e. La Niña-like conditions) versus 2) weaker or reversed trade winds (i.e. El Niño-like conditions). There are also two basic types of El Niño events, one related to maximum SST anomalies in the tropical eastern Pacific (EP-ENSO) with another related to a broad SST anomaly center in the central Pacific (CP-ENSO, Kao and Yu, 2009, Trenberth and Smith, 2006). This second CP-ENSO (Modoki variant) has a SST anomaly pattern closer to the so-called Pacific Decadal Oscillation (Mantua et al. 1997; Zhang et al. 1997; Zhang et al. 1998, Kao and Yu, 2009), which may be resolved within high-resolution proxies collected from the central equatorial Pacific. Regardless of the type of El Niño condition, these contrasting trade wind patterns impact current dynamics, with a weaker trade wind regime (El Niño) causing the North Equatorial Counter Current (NECC) to increase in flow from west to east, while during stronger trade wind periods (La Niña) the North and South Equatorial Currents (NEC and SEC) advect more water east to west, diluting the signature of

NECC waters and entraining more nitrate from the equatorial upwelling region and the eastern Pacific denitrification zone.

The relative strength, duration, and oscillation between these contrasting regimes have important implications for both productivity and regional carbon flux. Nitrate is the most common limiting nutrient for primary productivity in the open ocean, and the nutrient supply in the central equatorial Pacific is tightly linked with upwelling and current conditions, which in turn is strongly impacted by trade winds on a variety of timescales (seasonal, inter-annual, multidecadal, millennial). When the NECC advects water from the West Pacific, there is both lower nitrate content and an oligotrophic $\delta^{15}N$ signature strongly influenced by Western Pacific nitrogen fixation, leading to lower $\delta^{15}N$ values of production and exported POM. Conversely, the east to west flowing NEC and SEC have both higher nitrate concentrations and more enriched $\delta^{15}N$ values, due to advection of waters impacted by eastern Pacific denitrification signatures, as well as the fact that residual nitrate has typically undergone progressive Rayleigh fractionation away from the equatorial upwelling zone, associated with incomplete nitrate utilization (Rafter and Sigman, 2015). As a consequence, $\delta^{15}N$-nitrate values at the equator surface are typically relatively high in the modern ocean ($\delta^{15}N$ values of 13-18‰ between 155°W and 170°W; Rafter and Sigman, 2015) and $\delta^{15}N$ values of exported particulate organic matter (POM) of 7-13‰ between 4-8°N near our study site (140°W; Altabet 2001) before values decline northward into the subtropical gyres (0-5‰, 180°W; Horri et al. 2018).

Our study site of Kingman Reef (6°N, 162°W) lies within the Line Islands, and is situated within the eastward flowing NECC and impacted by the ITCZ which influences stratification, current strength, precipitation, and SSTs which primarily varies due to La Niña – El Niño cycles (Brainard et al. 2019). Nutrient levels in the NECC are generally low and comparable to subtropical gyres (Fiedler and Talley, 2006) which suggests near-complete utilization of nitrate, while positive values of N* suggests the region near the Line Islands could at times be a site of local N_2 fixation based on C/N/P data from Martiny et al, (2014, Fig. 3-S1), consistent with N_2 fixation estimates inferred from surface nutrients through an inverse modeling approach (Deutsch et al 2007, Gruber 2016). Thus coral isotope proxies for export production from Kingman Reef ought to reveal both shifts in relative source waters, as well as potential shifts in local nitrogen fixation. Finally, as this site lies at the mixing boundary between low nitrate waters (NECC) and higher nitrate eastern Pacific waters, it represents a key region to study how fluctuations in $\delta^{15}N$ values are related to changing current and temperature variations.

Similarly, oscillations in nutrient abundance also influence phytoplankton community structure, which in turn can be traced via organic $\delta^{13}C$ values. Different phytoplankton groups have unique characteristic carbon isotope fractionations during photosynthesis, based largely on cell size and dissolved inorganic carbon uptake mechanism (Laws et al., 1995; Rau et al., 1996), and thus shifting phytoplankton community composition represents one major driver behind changes in $\delta^{13}C$ of export production over time (McMahon et al., 2015). Small celled organisms, like

prokaryotic cyanobacteria are more dominant during weak winds and stratified conditions, with characteristically lower $\delta^{13}C$ values (Horri et al. 2018, McMahon et al. 2015, Rau et al. 1996). Larger cells, such as eukaryotes and diatoms, are more reliant on higher nutrient conditions and are characterized by more positive $\delta^{13}C$ values (McMahon et al. 2015, Fry and Wainright, 1991, Bidigare et al. 1999, Laws et al., 1995; Popp et al., 1998). Therefore, organic $\delta^{13}C$ values of export production represent a second dimension that can be used to assess changes in biogeochemical cycling and upper ocean ecology with climate change.

Paleo-archives which can directly record (or reflect) $\delta^{15}N$ and $\delta^{13}C$ of export production therefore represent a powerful repository of information for reconstructing multiple aspects of climate driven shifts in biogeochemistry of both C and N. In particular, the linkage of $\delta^{13}C$ values to nitrate concentration means that both $\delta^{15}N$ and $\delta^{13}C$ values are often expected to shift synoptically in response to nutrient supply, however sometimes they are decoupled from each other, which can provide unique insight into changes in a system, such as changes in nutrient source values without corresponding shifts in phytoplankton composition (Glynn et al., 2019). Proxy records derived from sediment cores or corals can thus reveal the history of both relative nutrients and phytoplankton community changes, through an examination of individual variability in carbon and nitrogen stable isotopes. Deep-sea proteinaceous corals are among the most reliable archives for such reconstructions in the open ocean, because they record within their organic skeletons the isotopic signatures of exported particulate organic matter, typically at annual to decadal resolution given the

high resolution of radiocarbon dating. Deep-sea corals such Hawaiian gold corals (*Kulamanamana haumeaae*) have radial growth rates of 36 ± 20 μm per year and extreme longevities (Roark et al. 2009), yielding a reliable preservation of organic skeletal material on millennial timescales (Glynn et al. 2022), and not subject to bioturbation as observed in sediment cores. These unique features particularly important in low sedimentation rate areas with oxic bottom waters, such as the oligotrophic open ocean, for which sedimentary records are low in resolution and often lacking coverage for the Late Holocene time period.

Here we present new high fidelity $\delta^{15}N$ and $\delta^{13}C$ records of two *K. haumeaae* specimens collected from Kingman Reef (6°N, 162°W) in the Line Islands. We evaluate bulk $\delta^{15}N$ and $\delta^{13}C$ values, as well as $\delta^{15}N$ amino acid data from selected samples, over the last 2000 years, using these records to infer climate-state driven changes in biogeochemical cycling in the Line Islands region of the Central Pacific Ocean. Our broad goal is to interpret how deep sea coral inferred export POM isotope signatures, which reflect together nutrients and phytoplankton communities, have shifted through time, related to trade wind dynamics impacting the marine ecosystem. To do this, we use characteristic environmental changes observed during El Niño Southern Oscillation (ENSO) as a model for the dynamic and far longer lasting periods which may have occurred over centennial to millennial timescales. For example, Kingman Reef is most strongly influenced by the ITCZ (Brainard et al. 2019), where warmer and wetter periods (El Niño-like) are inversely related to chlorophyll producing lower levels of biomass (Park et al. 2011), likely due to

enhanced stratification. At the same time, the main current patterns noted above also shift depending on trade wind conditions, with the North Equatorial Counter Current strengthened during warmer/wetter periods with reduced trade winds (Johnson et al. 2002), bringing with it more source water flow from the west Pacific. Thus, while our coral records do not resolve individual ENSO events, we will use modern ENSO dynamics as a framework for analyzing past changes in trade winds over longer timescales, and coupled shifts in equatorial current strength and positioning to interpret the variability in Kingman Reef coral $\delta^{15}N$ and $\delta^{13}C$ records. Our ultimate goal is to use these interpretations of our new coral records to infer nutrient and phytoplankton assemblage changes driven by Late Holocene climate shifts linked to large basin scale changes in central Pacific oceanography.

2. Methods

2.1 Collection, drilling, and age model

Specimens of *K. haumeaae* were collected using DSRV Pisces IV and V from ~400 m depth offshore Kingman Reef (6°23′N, 162°25′W) in 2005. Skeletons were washed first with seawater and then fresh water before being air-dried on deck. For this study, a live-collected (Kingman 1 – K1) and one sub-fossil (Kingman 2 – K2) specimen were used. Cross section disks ~0.7 cm thick were cut from close to the basal attachment, polished, and mounted onto glass plates before being drilled by a Merchanteck micromill. Approximately 2–3 mg of proteinaceous coral skeleton was collected at 0.1 mm resolution along radial transects from the outer edge to the center. The direct center was avoided due to concerns over the host coral parasitized by the

K. haumeaae organisms. Radiocarbon analyses were performed on ~1 mg acid-pretreated sub-samples (n=6 for K1, n=7 for K2) based on previously described methods (Glynn et al. 2019, 2022). Calibrated ages were generated using Bacon, a Bayesian modeling approach (Blaauw and Christensen 2011), using a local reservoir (ΔR) correction of -134 ± 65 years derived from data presented in Zaunbracher et al., (2010) and the Marine20 database (Heaton et al. 2020) and linearly interpreted to provide continuous age-models (see supplemental materials).

2.2 Bulk isotope analysis

Bulk $\delta^{15}N$, $\delta^{13}C$, and C/N analyses were performed synchronously on ~0.3 mg raw material using a Carlo Erba 1108 elemental analyzer coupled to a ThermoFinningan Delta Plus XP isotope ratio mass spectrometer. Results are reported in conventional per mil (‰) notation relative to air and VPDB standards for $\delta^{15}N$ and $\delta^{13}C$, respectively. Reproducibility was ~0.2‰ for both $\delta^{15}N$ and $\delta^{13}C$, with duplicate coral analyses suggesting an average reproducibility of also ~ 0.2‰ (n=21) and 0.1‰ (n=70) for $\delta^{15}N$ and $\delta^{13}C$ respectively, while the acetanilide standard (n=9) indicated <0.1‰ for both isotopes. Duplicates of C/N values indicate a reproducibility of 0.2.

To determine the degradative state and any impact of authigenic calcite, and following Glynn et al., (2019), a subset of coral powdered samples (1–2 mg each, n= 20) were acidified in 1 N HCl for 20 hours at room temperature, filtered onto a 0.22 μM GFF, the filter was dried overnight at 45°C before being scraped off into a tin capsule for EA analysis. Utilizing C/N values and a comparison of acidified versus

non-acidified isotope results, the outermost 2.5 mm of the subfossil specimen was determined to be likely impacted by calcite contamination, and so was excluded from our interpretations. Data for these samples are included in the supplement for completeness.

2.3 CSIA-AA analysis and TP calculation

Compound specific analyses were performed utilizing skeletal material from combining adjacent layers to have enough material (~6-10 mg) for CSIA-AA $\delta^{15}N$ measurements. Analysis involves established wet chemistry protocols for coral materials (e.g. McMahon et al. 2018) where AAs were liberated using standard acid hydrolysis conditions (1 ml of 6 N HCl at 110°C for 20 hours), then spiked with a norleucine internal standard and derivatized (based on Silfer, 1991), followed by purification with cation-exchange chromatography and a salt-removal step (p-buffer = KH_2PO_4 + Na_2HPO_4 in Milli-Q water, ph 7) before a 3x chloroform rinse and centrifugation before the final conversion to trifluoroacetyl/isopropyl ester (TFAA) derivatives. Derivatized samples were injected in triplicate on a coupled Gas Chromatography-IRMS (ThermoTrace GC, coupled to a Delta + IRMS), as described in McMahon et al. (2018). Injections were made utilizing concentrations adjusted to produce at least 80 mV IRMS N_2 signal intensity for the smallest peaks (typically phenylalanine and isoleucine).

Using these protocols, isotopic ratios could be reliably measured on 13 AAs: alanine (Ala), glycine (Gly), serine (Ser), valine (Val), threonine (Thr), leucine (Leu), isoleucine (Ile), proline (Pro), phenylalanine (Phe), tyrosine (Tyr), lysine (Lys),

glutamine + glutamic acid (Glx), and asparagine + aspartic acid (Asx). A range of verification approaches were employed simultaneously to ensure accurate CSIA-AA data. The Nor-Leu internal standard was used to verify that injections gave expected results. Bracketed standards of L-amino acids were repeatedly analyzed after every triplicate coral skeleton injection, and the average measured value of each external standard AA across the entire run was compared against its authentic value, and any systematic bias/offset used to correct sample AA values, following the approach described by McCarthy et al. (2013). Lastly we utilized a McCarthy lab internal laboratory reference material (dried/homogenized cyanobacteria) which was run with each sample batch to evaluate accuracy against a long term (>10 yr) internal control, ensuring long-term reproducibility for individual AA isotope values. Analytical reproducibility from triplicate sample injections was, in general, <1‰ for $\delta^{15}N$ CSIA-AA, based on these internal lab working standards.

2.3.1: CSIA-AA nomenclature and Proxies

Amino acid (AA) $\delta^{15}N$ isotopes fractionate differently based on metabolic pathways and observed differences in isotope fractionation during trophic transfer (McMahon and McCarthy, 2016, Ohkouchi et al., 2017). Phe, Tyr, and Lys are considered Source AAs with minimal isotope fractionation during trophic transfer, while Asx, Glx, Ile, Leu, Pro, Val are Trophic AAs with a linkage to the glutamate pool causing larger fractionations, and Gly and Ser are Intermediate AAs with more

variable behavior, and lastly Thr with an inverse isotopic behavior with trophic transfer (McMahon and McCarthy, 2016).

Using these differences in individual AA fractionation, the CSIA-AA trophic position (TP_{CSIA}) can be calculated, revealing information about both coral trophic structure and the overlying food web. TP_{CSIA} was determined using the difference in Phe (source) and Glx (trophic) $\delta^{15}N$ values according to a proteinaceous coral–specific formula from McMahon et al. (2018):

$$TP_{CSIA-AA\ Skeleton} = 1 + \left(\frac{\delta^{15}N_{Glx} + \partial - \delta^{15}N_{Phe} - \beta}{TDF_{Glx-Phe}}\right)$$

Corrections include: (∂) for Glx of 3.4 ± 0.1‰ (due to offsets observed between polyp and skeletal $\delta^{15}N_{Glx}$ values across multiple deep-sea coral taxons; McMahon et al., 2018), a β value of 3.4‰ (empirical difference between the $\delta^{15}N_{Glx}$ and $\delta^{15}N_{Phe}$ of non-vascular autotrophs) and a TDF value of 7.6‰ (trophic discrimination factor of $\delta^{15}N_{Glx}$ relative to $\delta^{15}N_{Phe}$ per trophic transfer; Chikaraishi et al., 2009).

Finally, we estimated the relative influence of heterotrophic microbial resynthesis on bulk isotope values using a combination of C/N values and ∑V (McCarthy et al., 2007, Ohkouchi et al., 2017). ∑V was calculated using the average deviation of $\delta^{15}N$ values of the trophic AAs (Ala, Val, Leu, Ile, Pro, Asx, Glx) using the equation $\sum V = (1/n) \sum|Xi|$ where Xi is the offset in $\delta^{15}N$ of each individual AA from the average ($Xi = \delta^{15}N_i - AVG\ \delta^{15}N_i$), and n is the number of AAs used in the calculation.

2.4 Spectral analysis

To determine spectral characteristics of the individual records, we utilized the ARAND Time-Series Analysis Software (Howell et al., 2006), a Blackman-Tukey method for spectral estimation, an approach which is well-suited for identifying broad-band cycles. Data were first interpolated to a constant (mean average) time step for each coral. Linear trends were removed by calculating residuals from a linear regression and the mean subtracted, i.e., the mean of each series was zero. Spectral character was determined at the 95% confidence interval, and the number of lags set at ⅓ the time series length.

2.5 Regime shift detection

Isotopic regime shifts were detected using the methodology of Rodionov (2004), with a significance level of 0.1, cut off length of 10, and a Huber's weight parameter of 1. The regime shift program uses a sequential t-test to determine regimes and can detect shifts in both the mean level of fluctuations and the variance (Rodionov 2004).

3. Results

The Kingman 2 coral grew from ~0-930 CE, with the outer layers from ~825-930 CE being excluded from environmental analysis due to concerns of degradation. This represents a growth rate of ~22 μm / yr with each data point representing on average 4.5±0.5 years. The Kingman 1 coral grew from 1240-2007 CE with a growth rate of ~14 μm / yr with each data point representing on average 7.0±2.4 years.

3.1 Bulk isotope and CSIA-AA results

3.1.1 $\delta^{15}N$ Bulk coral records

Based on our ^{14}C-age models, the older K2 coral grew from -5-932 CE, and by excluding the outer growth layers due to authigenic calcite (see methods) this coral produced a record spanning ~0-820 CE (Fig. 3-S2). For $\delta^{15}N$ bulk K2 record, $\delta^{15}N$ values increase over the entire record, shifting from 16.2‰ to 18.3‰ at a rate of 0.17‰ per hundred years ($\delta^{15}N = 0.0017*age +16.1$, $R^2=0.71$, p= <0.001) (Fig. 3-2A). Within this long term increase, the $\delta^{15}N$ values also express a cyclic behavior with swings of ~0.5-1.2‰ on ~40-60 year timescales (see spectral analysis and regime shift results below).

The younger live-collected K1 coral grew from 1240 to 2007 CE (Fig. 3-S3). Coral $\delta^{15}N$ value trends over this time period had a more complex behavior; with large swings in values during the first several hundred years, then an approximate plateau spanning approximately ~1500-1800 CE, followed by a large decrease in values into the present. Specifically, the $\delta^{15}N$ values increased from ~17‰ in 1220 to ~18‰ in 1310 CE, before declining from 1310 to 1400 CE to a minimum of 16.6‰, then rising by ~1‰ from ~1460-1500 CE. From 1500 to 1800 CE values remained approximately stable, averaging 17.6±0.2‰ (n=51). From the 1800s to 1950s there is an overall strong declining $\delta^{15}N$ trend at a rate of 0.04‰ per decade ($R^2= 0.72$, p= <0.001), punctuated by oscillations of ~0.6‰ (see spectral analysis results). Finally, from the 1950s to when this coral was collected in 2007, $\delta^{15}N$ values decline from 17.4‰ to a low of 15.4‰ at an average rate of 0.2‰ per decade (data table 3-2, 3-3).

3.1.2 $\delta^{13}C$ Bulk coral records.

The $\delta^{13}C$ record overall shows very similar long term trends to the $\delta^{15}N$ values, with values from both corals correlating well (K1 R^2 = 0.55, p = <0.001 and K2 R^2 = 0.65, p = <0.001, Fig. 3-S4). However, the $\delta^{13}C$ record has fewer complex features. From the start of the Kingman 2 record (~0 CE) the $\delta^{13}C$ values increased steadily from -16.4‰ at an average rate of 0.02‰ per decade, reaching average high value of -15.2‰ at 770 CE. We note there were increased $\delta^{13}C$ values in the most recent layers of K2 which are likely due to incorporation of carbonate and were thus excluded from environmental reconstruction. As noted above, acidification results suggest the outermost layers of K2 may be impacted by calcite contamination causing a $\delta^{13}C$ increase of ~1‰, so the outermost 2.5 cm have been excluded from plots (Fig. 3-S7).

The gap between K1 and K2 then suggests an overall decline must have occurred in $\delta^{13}C$ values from ~ -15.6‰ in 820 CE to an average value of -16.1±0.1‰ (n=17) from 1240-1430 CE. During this period, the records therefore suggest that $\delta^{13}C$ and $\delta^{15}N$ records were decoupled to a larger degree due to the oscillations in the K1 $\delta^{15}N$ record as described above. From ~1450 to 1800's the longer term average $\delta^{13}C$ values remained fairly stable, however punctuated by several small oscillations of up to 0.5‰ around an average value of -15.8±0.1‰ (n=54). As noted below, however, these oscillations are not significant according to spectral analysis. Finally, from the 1800s to the present (~2007 CE) the $\delta^{13}C$ values declined rapidly at a rate of 0.07‰ per decade, from the higher average value of -15.6‰ to a low of -17.4‰.

3.1.3 $\delta^{15}N$ CSIA-AA coral data

Phe $\delta^{15}N$ values ($\delta^{15}N_{Phe}$; n=9) range from 7.0-11.1‰ over the entirety of the record in both K1 and K2 corals (Fig. 3-2). Due to the low sampling density it is challenging to identify correlations or trends; however these nine data plots seem to have two different groupings when compared with bulk $\delta^{15}N$ values. Five $\delta^{15}N_{Phe}$ values (3 from K1, 2 from K2) aligned with bulk $\delta^{15}N$ values >17‰, and have a significant positive correlation (R^2= 0.65, p= 0.098; Fig. 3-S5). In contrast, four $\delta^{15}N_{Phe}$ values (2 from each coral) aligned with bulk $\delta^{15}N$ values <17‰ have a weak negative correlation (R^2= 0.34, p= 0.41, Fig. 3-S5). A positive correlation between bulk and Phe $\delta^{15}N$ values has been previously noted for Hawaiian corals of the same species (Sherwood et al. 2014). $\delta^{15}N_{Phe}$ values shifted from 10.1‰ at 160 CE to lower values averaging 8.2±0.3‰ (n=5) over 400-1420 CE before reaching a peak of 11.8‰ at 1820 CE before slightly declining 8.5‰ in the 1990s (Fig. 3-2). Source AAs (Phe, Tyr, Lys; n=9) have a more positive value, ranging from 9.9-12.3‰ and are not correlated with bulk $\delta^{15}N$ values.

3.1.4 Trophic Position

TP_{CSIA} is low at 160 CE at 3.6 before increasing to 3.9 from 400-1700 CE, and then declining to 3.5-3.6 from 1800-2000 CE (Fig. 3-2), which overall agrees with data from previous coral studies from the Hawaiian islands (Sherwood et al. 2014). There is a similar low sampling density for trophic position, with $\delta^{15}N_{Phe}$ values significantly inversely related with trophic position (R^2 = 0.77, p=0.005, Fig. 3-S6). Such an inverse correlation been noted in sedimentary records (Batista et al.

2014) and deep-sea corals (Pugsley et al. in prep). Similarly source $\delta^{15}N_{Phe, Tyr, Lys}$ are also inversely correlated to trophic position (K1 $R^2 = 0.46$, $p = 0.21$; K2 $R^2 = 0.86$, $p = 0.07$).

3.2 Proxies testing organic preservation

C/N values for both inner coral regions (>2.5 mm from outer edge) were highly consistent, averaging 2.7±0.1 (n=115) for K1, while K2 averages were 2.8±0.1 (n=221; Fig. 3-S7); for both corals these C/N values were within range expected for modern coral samples, indicating excellent gorgonian preservation, and the integrity of bulk isotope data (Glynn et al. 2022). In contrast, the outer layers from 2.5-0 mm of K2 increase in C/N from 2.9 to 3.3 (Fig. 3-S7), corresponding to the ~1‰ increase in $\delta^{13}C$ between acidified and non-acidified samples in the same region (noted above). Thus the outermost 2.5 mm are excluded from environmental interpretation based on higher C/N values and results from the acidification tests (Fig. 3-S7).

The degradation proxy ∑V also indicates good preservation, with an average value of 3.5±0.3 (n=5) for K1 and slightly higher at 3.4±0.4 (n=4) for the subfossil K2 (Fig. 3-S7). While higher than many modern materials, these values are still within the range found for modern and well-preserved subfossil gorgonin for this same species (Glynn et al. 2022). No ∑V exists for the outermost layers of K2 but the bulk C/N and acidification results indicate degradation in the outer 2.5 mm warranting exclusion from environmental analysis.

3.3 Spectral analysis and regime shift detection

Spectral analysis for the K2 subfossil coral $\delta^{15}N$ values shows significant peaks for both 40 and 60 year cycles within the 95% confidence interval (Fig. 3-S8). The K1 modern coral also resulted in peaks for 40-50 years cycles for $\delta^{15}N$ values (Fig. 3-S9), however is below the 95% confidence level so may not be significant. There were no significant oscillations detected by spectral analysis for $\delta^{13}C$ values in either coral.

For regime shift detection analysis, the K2 subfossil $\delta^{15}N$ record expressed ten regime shifts, four of 30-50 years, four of 50-70 years, and two of 80-90 years. The K2 $\delta^{13}C$ record expressed eight regime shifts, three for 20-40 years, two for 50-60 years, two for 100-120 years, and one for 157 years (Fig. 3-S10). The K1 modern $\delta^{15}N$ record expressed seven regime shifts, four within 25-50 years, one at 90 years, one at ~130 years, and one at ~340 years (during the 1500-1800 CE period). The K1 $\delta^{13}C$ record expressed nine regime shifts, four of 30-60 years, three of 80-100 years, and two of 120-140 years (Fig. 3-S10). The regime shift detection agrees with spectral analysis and also denotes $\delta^{15}N$ regimes do not necessarily occur during regime shifts in $\delta^{13}C$ values.

4. Discussion

Together, our isotope analyses on these coral skeletons provide the first sub-decadal resolution records of $\delta^{15}N$ and $\delta^{13}C$ variability for the open ocean central Pacific region over the last 2000 years of the Holocene. Given their high resolution, they are therefore nearly unique for the region, offering the possibility to deconvolve

the scale and major periods of biochemical change, and potential links to climate fluctuations, at a new level of detail.

In the discussion below we interpret both $\delta^{15}N$ and $\delta^{13}C$ coral records in terms of climate-influenced biogeochemical and physical drivers. However, in order to make these interpretations it is necessary to first discuss basic nitrogen isotope systematics and processes most likely linked to variable export production $\delta^{15}N$ values, and to also draw links to likely planktonic community composition changes which typically drive $\delta^{13}C$ values (of organic matter). We therefore first consider basic $\delta^{15}N$ fractionation processes, and how these may or may not be applicable to the Line Islands region of our coral records.

These considerations then allow us to interpret the coral $\delta^{15}N$ values primarily in terms of climate-driven changes in source water that alternate the relative influence of source waters containing very different nutrient levels and isotopic source signatures. As noted above (*introduction*), throughout the discussion we use ENSO as a broad model providing a specific example of the impact that changing trade wind dynamics and subsequent shifts in strength and latitude of major equatorial currents can have on oceanic nutrient concentrations and phytoplankton communities, and in turn on $\delta^{15}N$ and $\delta^{13}C$ values of export production.

4.1 Assessing $\delta^{15}N$ fractionation processes which may drive Line Island coral $\delta^{15}N$ changes: denitrification, assimilation, and N_2-fixation

The distribution of nitrogen isotopes in the ocean is driven by multiple interwoven biogeochemical processes, including nitrate concentrations and relative

fractional algal NO_3^- uptake, nitrogen fixation, and water column denitrification, in addition to large scale transport of these signals by oceanic currents (Somes et al. 2010). Chemical and biological processes break or form N bonds with predictable fractionations, resulting in characteristic differences in $\delta^{15}N$ values of primary production in different oceanic areas. Bulk isotope records are an amalgamation of the falling organic matter isotope signatures, so in order to interpret our coral records we need to tease apart which processes are most important in influencing export production $\delta^{15}N$ values in our study region.

There are three basic possibilities which we can evaluate in terms of either occurring locally in the Kingman reef region or else being important only for their influence on $\delta^{15}N$ signatures of source water current systems. The first is the possibility of substantial differences in surface nitrate concentrations, leading to changes in the degree of nitrate utilization (i.e., the fraction of the gross nitrate supply to the euphotic zone that is consumed by assimilation; Rafter and Sigman 2015). During algal NO_3^- assimilation there is a preferential discrimination against ^{15}N relative to ^{14}N which results in net enrichment of ^{15}N in the residual NO_3^- and net depletion of ^{15}N in phytoplankton and detrital organic matter. However, even over the course of transitioning between El Niño and La Niña conditions as nitrate concentrations change from relatively low to high, the relative NO_3^- utilization in this region does not change substantially (Altabet 2001). This leads to the assumption of a constant value for nitrate assimilation isotope effects, as has been assumed for sedimentary paleooceanographic studies (e.g. Altabet 2001). Second, diazotrophic

nitrogen fixation occurs commonly in subtropical oligotrophic tropical gyres (>25°C, such as the Kingman Reef region), and leads to a depleted $\delta^{15}N$ signatures of fixed dissolved nitrogen which is then reflected in the organic matter(Karl et al. 2002, Carpenter et al., 1997). Finally, as a sink of nitrogen denitrification occurs in suboxic zones such as the Eastern Pacific, where microbes preferentially utilize $^{14}N\text{-}NO_3^-$ during respiration which converts nitrogen to gaseous forms, leaving residual nitrate more enriched in ^{15}N (up to ~20-30‰; Voss et al. 2001). Together, these three processes are the primary factors shaping nitrate signatures and subsequent particulate organic $\delta^{15}N$ values.

In terms of which of these processes that could be important in our corals, at least two of these three can be essentially ruled out as major drivers for coral $\delta^{15}N$ values at Kingman Reef. First, this site is not suboxic, so localized denitrification can be ruled out as a major driver of $\delta^{15}N$ variability. Second, with utilization fractionation relatively unchanging on annual cycles (Altabet 2001) and across the equatorial Pacific (ε ~5-6‰; Rafter and Sigman 2015), possible changes in utilization has a minor impact on $\delta^{15}N$ values (~2‰, Somes et al. 2010). Furthermore, waters in this region, while not fully in the gyre, are still relatively oligotrophic with annual values of <1 μM NO_3^- at all times (Altabet et al. 2001, Rafter et al. 2017). This suggests essentially complete NO_3^- utilization at this study site such that sinking organic matter should represent the source water NO_3^- isotopic values and thus the coral $\delta^{15}N$ values likely track the alteration between source currents coming from the east and west Pacific regions.

Finally, N_2 fixation is the only major process that cannot be fully ruled out as having importance in the Kingman Reef region. Since this ocean region is largely oligotrophic, and with SSTs ranging from 25-30°C (Brainard et al. 2019), some contribution of local N_2 fixation influence is possible. However, we note that it is difficult to deconvolve local N_2 fixation shifts from advected source waters of the west Pacific, which are similarly impacted by diazotrophy (*see discussion below, section 4.2.7*). Overall, consideration of these processes therefore suggests that while some local N_2 fixation cannot be fully ruled out, Kingman $\delta^{15}N$ records are primarily driven by source water variations, with climate driven changes in current mass transport carrying water with distinctly different nitrate $\delta^{15}N$ values.

4.2 Source water mass shifts as main driver of trends in coral $\delta^{15}N$ values

Within the framework developed above, major features of the combined coral record can most likely be interpreted in terms of major source water mass shifts, driven by climate condition alteration. Specifically, the long term coral isotope trends (e.g., increasing trend in K2, stability during 1500-1800 CE in K1) are likely broadly related to shifts in temperature, rainfall, stratification and currents controlled by changes in ITCZ strength and latitudinal positioning and is the predominant climatic influence for Kingman Reef (Brainard et al. 2019). In addition to the long term trends, there are distinct shifts of ~1‰ between the end of the Medieval Warm Period and onset of the Little Ice Age (1300-1500 CE). There are also clear multidecadal variability (fluctuations of ~1‰ every ~60 years in K2), likely related to shifts between warmer/wetter/stratified and cooler/drier/mixing conditions (i.e.

multidecadal ENSO fluctuations, Fig. 3-3E), which has similarly been noted as a driver of west Pacific sediment $\delta^{15}N$ records (Fig. 3-3B, Langton et al. 2008). We next discuss these features moving forward through our records, to interpret changes in bulk $\delta^{15}N$ values in the context of changing source water mixtures (section 4.2.1 to 4.2.5); we then delve into the CSIA-AA $\delta^{15}N_{Phe}$ and trophic position results, assessing how these can constrain bulk isotope data (section 4.2.6), and finally present a caveat detailing possible influence of localized signatures of N_2-fixation (section 4.2.7).

4.2.1: Increasing $\delta^{15}N$ values within K2 coral

The first feature of note is the distinct long term increasing $\delta^{15}N$ trend from 16 to 18‰ from ~200 to 800 CE in the older K2 coral, which implies a long term shift from primarily NECC source waters to a greater contribution from eastern Pacific waters. This interpretation is supported by an 8.8 to 10‰ increase in $\delta^{15}N$ values noted in a Hawaiian deep sea coral record (Glynn et al. 2019), suggesting enhanced flow of denitrified waters from the east Pacific into the oligotrophic oceans. Similarly, while not synchronous, a west Pacific Indonesian sediment record also increases from ~2.5 to 4‰ over this period, attributed to a decline in N_2 fixation and an enhanced mixing environment at this island found within the west Pacific NECC (Fig. 3-3, Langton et al. 2008).

Within our modern ENSO interpretation framework, the shift to higher $\delta^{15}N$ values implies strengthened trade winds and a La Niña-like state for the central Pacific with weakened NECC flow (Fig. 3-1). This assessment is consistent with ancillary records available for this time period, such as a proxy-based cross equatorial

precipitation reconstruction of the Pacific Southern Oscillation Index (SOI; made possible due to the correlation between precipitation and sea level pressure), which suggests a shift from 300-800 CE towards drier, cooler conditions in the central and eastern Pacific (Fig. 3-3, Yan et al. 2011). A South American lake sediment record also expresses fewer El Niño events in the Eastern Pacific over this 0-900 CE period in respect to 900-1300 CE, despite some deviations of intense El Niño behavior during ~275-410 CE and 575-675 CE (Moy et al. 2002). At the same time, the $\delta^{15}N$ sedimentary record from the Eastern Pacific from within the South Equatorial Current (Fig. 3-3, Sauthoff 2016) does not express this increasing trend, nor does a compilation of other marginal sedimentary records over this period (Tesdal et al. 2013, Glynn et al. 2019), which suggests that this was not due to an overall shift in source $\delta^{15}N$-nitrate of the whole Pacific (Ch. 1, Fig. 1-S5), though the low resolution of most sedimentary records (not including the Langton et al. 2008 record) makes this harder to verify. Instead, strengthening trade winds and a shift to drier conditions over the 200-800 CE period (SOI, Fig. 3-3), should have sourced more waters from the eastern Pacific denitrification region into the oligotrophic central Pacific to produce the trend seen in the K2 coral (Fig. 3-1, Fig. 3-3).

4.2.2: Medieval Warm Period and transition to Little Ice Age cause swings in K1 $\delta^{15}N$ values

For the younger K1 coral, there is a distinct increase in $\delta^{15}N$ values from 17-18‰ starting from ~1200-1300 CE during the end of the Medieval Warm Period (MWP) before declining from ~1330-1420 CE to a low of 16.6‰ and increasing once

more by ~1‰ from ~1460-1520 CE during the start of the Little Ice Age (LIA). There is significant variability in the reported date ranges of the MWP (~900–1450 CE) and LIA (~1450–1850 CE) as well as contested ENSO states for the central Pacific during these climate intervals. Records of western Pacific hydroclimate based on speleothem records suggest that during the MWP the western Pacific was generally drier while the central and eastern Pacific experienced wetter conditions, which can be equated to a weakening Pacific Walker Circulation and a more 'El Niño-like' mean state (Griffith et al. 2016). Conversely, some earlier published ENSO reconstructions agree to there being wetter conditions in the central Pacific (Sachs et al. 2009), but suggest 'La Niña-like' conditions during the MWP (Cobb et al. 2003; Oppo et al. 2009).

The K1 coral record has relatively low $\delta^{15}N$ values of 17‰ during ~1200 CE and ~1420-1460 CE which we interpret to be due to more persistent 'El Niño-like' conditions and a higher contribution of west Pacific source waters in the NECC. Based on the fact that both east and west sedimentary records similarly have a drop in $\delta^{15}N$ values of ~1‰ during ~1300-1400 CE (Fig. 3-3, Langton et al. 2008, Sauthoff 2016) suggests this 'El Niño-like' state may be occurring throughout the entirety of the equatorial Pacific. However the high values of ~18‰ from ~1300-1330 CE in the K1 coral would be more indicative of 'La Niña-like' conditions, indicating that at least at the end of the MWP there are signs of both states of ENSO occurring on 40-60 year timescales, similar to the multidecadal swings seen in the K2 record, which

could help explain the variable proposed states of tropical Pacific ENSO during this time period.

4.2.3: Stable $\delta^{15}N$ values during the Little Ice Age

During the LIA, the K1 coral from the 1500 to 1800s appeared to return to a relatively stable regime (average $\delta^{15}N$ value of ~17.5‰), similar to that at the end of the K2 record, before entering the period of marked decline to the present day (Fig. 3-2). Based on the relatively high $\delta^{15}N$ coral values during the LIA, this would indicate a long period of stronger trade winds and a greater contribution of source waters from the eastern Pacific denitrification region. This agrees with climatic records which indicate that the western Pacific was generally wetter during the LIA, while the central and eastern Pacific experienced drier conditions, similar to modern La Niña events, consistent with an overall strengthening of the Pacific Walker Circulation (Griffiths et al. 2016; Thompson et al. 2013; Yan et al. 2011).

The LIA is also a period where western warm pool waters cooled by ~1°C, while eastern Pacific SSTs increased by ~1°C (Oppo et al. 2009, Rustic et al. 2015), which can alter subsurface dynamics (extent of mixed layer and oxygenated waters) coupled with changes in productivity. A decline in western Pacific SSTs could have led to lower contribution of N_2 fixation signatures within the NECC source waters (Karl et al., 2002), while the warmer eastern Pacific waters could have contributed to increased rates of denitrification (Yang et al. 2017) which may account for the higher $\delta^{15}N$ values seen in the eastern Pacific sediment record (Sauthoff 2016) as well as the K1 coral record.

4.2.4: Multidecadal oscillations in $\delta^{15}N$ coral records

The multidecadal oscillations of ~1‰ in the multiple parts of the deep sea coral $\delta^{15}N$ records are also suggestive of an additional climatic driver impacting ocean nutrient conditions. We hypothesize that this is most likely related to CP-ENSO variability. Particularly in the older K2 coral obvious 1‰ oscillations of ~30-60 years (Fig. 3-2, spectral analysis and regime shift detection, Fig. 3-S8, 3-S9), are suggestive of shifts in the advective strength and latitudinal position of the equatorial currents (Fig. 3-1). While the coral $\delta^{15}N$ for K2 does not directly correlate with the precipitation SOI, possibly due to differences in age models, there are also similar ~30 year oscillations in the associated equatorial precipitation record (Yan et al. 2011, Fig. 3-3E). As the CP-ENSO (Modoki variant) has an SST anomaly pattern more similar to the Pacific Decadal Oscillation (Mantua et al. 1997; Zhang et al. 1997; Zhang et al. 1998, Kao and Yu, 2009), we propose that the K2 coral record is tracking the multidecadal changes in trade winds and currents to produce the observed oscillations in $\delta^{15}N$ values.

However, during the LIA, these oscillations no longer appear (Fig. 3-2, spectral analysis results, Fig. 3-S9), coincident with weakened/stronger trade winds as implied by a reconstruction of the SOI across the 1500-1800 CE time period (Fig. 3-3). Over the LIA, the Eastern Pacific experienced more EP-ENSO events from 1500-1850 CE as the ITCZ shifted southward with a weaker cold-tongue development (Rustic et al. 2015). We hypothesize that the higher frequency swings of this variation of EP-ENSO (2-7 yrs) may have created an averaging effect on coral $\delta^{15}N$ values,

contributing to the lack of multidecadal oscillations. Finally, our results support a "Mid-Millennial Shift" during the transition into the LIA, however unlike the eastern Pacific which may have had a more El Niño-like state (Rustic et al. 2015), the central Pacific appears to have experienced stronger trade winds, as indicated by the relatively high $\delta^{15}N$ values, in agreement with the precipitation SOI (Fig. 3-3, Yan et al. 2011) and other climate reconstructions (Griffith et al. 2019).

4.2.5: Declining $\delta^{15}N$ values during the Industrial Revolution

Lastly, after the LIA as SSTs began warming by ~1°C during the Industrial Revolution, coral $\delta^{15}N$ values declined almost 2‰ to ~15.5‰ over 1800-2007 CE (*results* 3.1.1; Fig. 3-2). Such a decline has also been recorded in west Pacific sediment records (Fig. 3-3, Langton et al. 2008), in multiple Hawaiian corals (Sherwood et al. 2014, Glynn et al. 2019), as well as in other equatorial Pacific *Muricella* corals (Williams et al. 2010). This has been attributed to an expansion of oligotrophic conditions and enhanced contribution of N inputs by N_2 fixation due to the warmer, more stratified oceanic environment (Sherwood et al. 2014). In addition to the increase in N_2 fixation (*discussed in 4.2.3*), there may have also been changes in the source waters of the denitrification zone as eastern Pacific sediment records tracking the oxygen minimum zone show a similar decline in $\delta^{15}N$ values of ~2‰ from the 1850-2000 CE, attributed to weakened trade winds (Deutsch et al. 2014). The decline in Kingman coral $\delta^{15}N$ values agrees with a slowdown of trade winds and a strengthening of the NECC, in agreement with a slowdown in meridional east-west Pacific circulation and weakened equatorial upwelling (McPhaden and Zhang, 2002).

4.2.6: CSIA-AA isotope baseline data: additional constraints on N source and trophic position

CSIA-AA data can help further examine our hypotheses in two ways. The first is to examine the idea that bulk isotope shifts are mainly driven by changes in "baseline" nitrogen sources, linked to shifting current systems with characteristically different nitrate $\delta^{15}N$ values. If this is the case, we would generally expect the $\delta^{15}N_{Phe}$ to track bulk isotope values (Sherwood et al., 2014), while at the same time having specific $\delta^{15}N_{Phe}$ values which correspond to known nitrate $\delta^{15}N$ values in source waters. The second is to examine the TP_{CSIA} values, which can allow us to evaluate hypotheses about periods in which Line Islands ocean region was more nutrient rich vs oligotrophic (McMahon et al. 2018), which as noted above should also be linked to shifts in source waters.

While our CSIA-AA data is limited, overall the $\delta^{15}N_{Phe}$ conforms generally well with bulk $\delta^{15}N$ in both coral records (Fig. 3-2, results). A majority of the $\delta^{15}N_{Phe}$ data are correlated with bulk values, similar to the results found in pervious deep sea coral studies, which suggests $\delta^{15}N_{Phe}$ values track source nitrate in the ecosystem (Sherwood et al. 2014). Furthermore the $\delta^{15}N_{Phe}$ values also approximate our expectations for shifting current sources as they match with nitrate values expected for the region. Western Pacific waters influencing the NECC have nitrate values of 4-8‰ while eastern Pacific waters have higher values of 10-14‰ (Fig. 3-1, Somes et al. 2010), bracketing the range of values seen in the coral $\delta^{15}N_{Phe}$ values of 6.6-11.8‰ (Fig. 3-2). A majority of the record has lower $\delta^{15}N_{Phe}$ values of 8.2±0.3 (n=5) from

400-1450 CE, supporting a depleted nitrogen source likely advected from the oligotrophic west Pacific, which also corresponds to some of the dips to lower values seen in the bulk $\delta^{15}N$ record (Fig. 3-2). The highest $\delta^{15}N_{Phe}$ values of 9.5-11.8‰ are seen during a more positive oscillation ~100 CE and during the 1600-1900s peak of the LIA (Fig. 3-2), likely due to advected source waters from the east Pacific with characteristically higher nitrate $\delta^{15}N$ values noted above (Fig. 3-1, Voss et al. 2001, Somes et al. 2010). Overall, while not extensive, we conclude that $\delta^{15}N_{Phe}$ values corroborate with the hypotheses laid out for the bulk $\delta^{15}N$ record, supporting the idea of source water mass changes as the main influence on exported particulate organic matter recorded in these corals.

We should note that again notwithstanding the relatively limited CSIA-AA data, it also appears that source AAs have an overall inverse relationship with trophic position (e.g. $\delta^{15}N_{Phe}$ $R^2 = 0.77$, Fig. 3-2, 3-S6). Such an inverse relationship has been observed previously in both sediment and coral records (Batista et al., 2014; Pugsley et al., in prep), and arises from a mass balance linkage between N pools (Batista et al., 2014). This linkage results in $\delta^{15}N_{Phe}$ and TP_{CSIA} values which are no longer fully independent, as is typically assumed in most modern ecological applications (e.g., Ohkouchi et al. 2017). The direct mechanism for this coupling is increased recycling during oligotrophic conditions where nitrate is fully utilized, such that the ^{15}N and ^{14}N brought into a system as new N (Dugdale and Goering, 1967) must be fully partitioned into source vs. trophic AA, while at the same time longer food chains, increased recycling also characterize low nutrient conditions (Chavez et al. 1996).

This results in a shift in nutrient sources toward recycled ammonia and nitrate (Montoya and McCarthy, 1995). Since the heavy ^{15}N isotope preferentially partitions into zooplankton, under mass balance constraints (assuming complete nutrient utilization) an increase in TP_{CSIA} must result in isotopic depletion of phytoplankton (Pugsley, in prep). Overall, however, while this observation would support recent CSI-AA observations in sediments and corals noted above, it also would have no real impact for most of our Line Islands record, simply because TP_{CSIA} is similar and apparently not changing in most of our data (Fig 2; ~400-1600 CE). As noted by Batista and co-authors (2014), in regions where planktonic TP_{CSIA} remains relatively constant, even though this coupling may exist it does not impact CSIA-AA baseline estimates, such that $\delta^{15}N_{Phe}$ can still accurately reflect baseline changes.

However, there are two periods in the records where TP does appear to have changed, at beginning of K2 (~100 CE) and the end of K1 (1600-2000 CE). This suggests there may have been substantially different phytoplankton community structure during these times of higher nutrient conditions (*see also next section*), in contrast to the more stratified conditions (higher TP_{CSIA}) which typify most of the data record. One implication is that despite the fact TP_{CSIA} was not changing, and so could not influence any observed changes in bulk or $\delta^{15}N_{Phe}$, we also cannot rule out that $\delta^{15}N_{Phe}$ in periods of likely low nutrients may be somewhat lower than actual baseline source values, due to increased recycling and/ or potential N fixation (discussed in 4.2.7). Therein the periods where TP_{CSIA} seems have become much lower (beginning of K1, end of K2 records); this would imply $\delta^{15}N_{Phe}$ may be the

closest to fully reflecting baseline nutrient $\delta^{15}N$ values. However, in either scenario, both TP_{CSIA} and $\delta^{15}N_{Phe}$ remain consistent with our central interpretation of $\delta^{15}N$ value trends being mainly linked to variations in source waters.

4.2.7: Possible contribution of localized N_2 fixation

Finally, one caveat to our main interpretations is that as noted above it is not possible to fully rule out nitrogen fixation occurring locally in the Kingman Reef region, therefore contributing to the lower $\delta^{15}N$ values in at least some periods in the coral record. Positive values of N* (>3 in upper 100 meters) suggest the region near the modern Line Islands may be a site of local N_2 fixation (C:N:P data from Martiny et al., 2014, Fig. 3-S1), as do N_2 fixation estimates inferred from surface nutrients through an inverse modeling approach (Deutsch et al 2007, Gruber 2016). As noted in the last section, CSIA-AA trophic position data is relatively high for most of the coral record where we have data (~3.3-3.5 from 400-1600 CE, Fig. 3-2), consistent with oligotrophic, N recycling conditions in the equatorial Pacific. With high TP_{CSIA} remaining constant through much of the record, we therefore hypothesize that while N_2 fixation is occurring, it represents a similar influence on $\delta^{15}N$ values though most of record (~400-1600 CE). This is supported by similar TP_{CSIA} values across these periods, and suggests that N fixation cannot be the main cause of the trends as TP_{CSIA} does not change substantially. Therefore, we hypothesize that in addition to increased recycling discussed above; localized N_2 fixation may be lowering the observed values only slightly from impact of variation in current sources alone.

4.3 Changing phytoplankton communities as driver of $\delta^{13}C$ values

As noted above, coral $\delta^{13}C$ values have fewer features than the $\delta^{15}N$ records, however at the same time they also follow the same general trends, with major periods of increase and decrease mostly coupled (i.e., changing in similar direction) with those in the $\delta^{15}N$ records (*results 2.2;* Fig. 3-2). The main long-term $\delta^{13}C$ value changes (increase between ~0-800 CE and 1300-1500 CE during the MWP, approximate plateau from ~1500-1820 CE during the LIA; sharp decline in Anthropocene), have also been previously observed in Hawaiian coral $\delta^{13}C$ values over the last 2 millennia (Glynn et al. 2019, McMahon et al. 2015), as well as an ensemble of 22 different surface coral $\delta^{13}C$ records over the most recent millennia from the west and central Pacific (Wu et al. 2018). These previous studies have attributed pre-Anthropocene $\delta^{13}C$ shifts as primarily due to changing surface wind strength and zonal advection impacting stratification (Wu et al. 2018, Linsley et al. 2019), and in turn impacting the phytoplankton communities (McMahon et al. 2015). Overall, this interpretation also is consistent with our idea of source water mass changes driving coral $\delta^{15}N$ trends. In contrast in the Anthropocene, the decline since the mid-1800s the Suess Effect, resulting from the emission of ^{13}C-depleted fossil carbon, has a major impact, due to decrease in $\delta^{13}C$ values of dissolved inorganic carbon (DIC) in the surface ocean (Quay et al., 2003). Similar to previous studies, we estimate roughly half of the decline since the 1800s is due to the change in atmospheric $\delta^{13}C$ values while the rest is due to environmental factors, such as changing phytoplankton communities (McMahon et al. 2015, Glynn et al. 2019).

For the majority of the record, however, we interpret the pre-Seuss effect coral $\delta^{13}C$ changes primarily based on shifting phytoplankton communities, as has previously been done for deep sea corals (e.g., McMahon et al. 2015, Glynn et al., 2019), and so will first lay out some of the background necessary to understand community shifts impacts on $\delta^{13}C$ values. As different phytoplankton groups have unique $\delta^{13}C$ fractionations during photosynthesis (Laws et al., 1995; Rau et al., 1996), a shift in phytoplankton community composition can be a major driver behind changes in $\delta^{13}C$ of export production over time in deep sea corals (McMahon et al., 2015). Within the equatorial Pacific the major groups are Prochlorococcus, Synechococcus, nano-eukaryotes and diatoms; the relative abundance of these species leads to more positive $\delta^{13}C$ primary production values near the equator and more negative values in the oligotrophic gyres (Masotti et al. 2011). Picoplankton typically have depleted $\delta^{13}C$ values compared to microphytoplankton species (Rau et al., 1996, Horri et al. 2018). Diatoms in particular are a source of ^{13}C-rich organic carbon in marine food webs (Fry and Wainright, 1991, Bidigare et al. 1999, Laws et al., 1995; Popp et al., 1998). Previous studies have suggested that broadly speaking, more positive $\delta^{13}C$ coral values indicate export production having greater relative contributions of eukaryotic phytoplankton, while more negative $\delta^{13}C$ values correspond with more small-celled prokaryotic organisms (McMahon et al. 2015, Glynn et al. 2019).

This framework can not only explain most $\delta^{13}C$ shifts, but also ties together coupled $\delta^{13}C$ and $\delta^{15}N$ changes. As noted above, coral $\delta^{15}N$ values are generally

coupled with $\delta^{13}C$ values in both records (K1 R^2 = 0.55, K2 R^2 = 0.65), consistent with the expectation that changes in nutrient conditions influences changes to community composition between prokaryotes (lower values) and eukaryotes (higher values) (McMahon et al. 2015). Specifically, the periods of lower $\delta^{13}C$ values (during 100-400 CE, 1200-1400 CE, and in the 1900's) suggest greater abundance smaller celled prokaryotes, coincident with weakened trade winds, stronger NECC, and thus an advected signature of oligotrophic waters (Fig. 3-3). As noted above, all these things would also correspond with periods of depleted $\delta^{15}N$ values, as observed in the record. Periods of higher $\delta^{13}C$ (during the 500-800 CE and 1500-1800 CE), in contrast, represent enhanced larger cell (especially diatom) contributions, which would be expected to be facilitated by increased nutrient transport from the east Pacific (Fig. 3-3). Higher $\delta^{15}N$ values would be expected in such periods, and area also observed in the record. Our interpretations regarding phytoplankton community structure shifts as forcing $\delta^{13}C$ values therefore directly support our hypotheses regarding climate and physical current regime as being the ultimate forcings behind our isotope records.

Finally, however, there are also some exceptions to the typical coupling of $\delta^{13}C$ and $\delta^{15}N$ value trends in the record. The clearest are the ~1‰ oscillations in $\delta^{15}N$ values found in the K2 record and start of the K1 record, which are not expressed in the $\delta^{13}C$ record. We hypothesize that oscillation events observable in $\delta^{15}N$ may be tracking changes in source water $\delta^{15}N$ signatures, rather than localized changes in stratification and nutrient concentration which would be expected to

influence the overall phytoplankton community, and so $\delta^{13}C$ values. We note that similar "decoupling" behavior between $\delta^{13}C$ and $\delta^{15}N$ trends has also been documented in previous coral records over the last 5000 years (Glynn et al. 2019). One idea propose has been a shift in phytoplankton community composition between nitrate utilizing cyanobacteria and versus N_2 fixing cyanobacteria with a lower $\delta^{15}N$ signature, which would be expected to alter $\delta^{15}N$ without substantially changing $\delta^{13}C$ values as the phytoplankton composition remains prokaryotic (Glynn et al. 2019, McMahon et al. 2015). While we do not have ancillary data that would be required to evaluate this idea for our region, if this mechanism operated here, it would offer support for a possible additive effect of localized N_2 fixation, as discussed in section 4.2.7.

Overall, the coupled $\delta^{13}C$ and $\delta^{15}N$ isotope records we observe through most of our coral records can provide synergistic information about water mass shifts and changing phytoplankton communities, where higher $\delta^{13}C$ values suggest more diatoms and enhanced export, while lower values indicate more stratified, recycling conditions and lower export. Coupling $\delta^{13}C$ and $\delta^{15}N$ therefore produces a record that may be linked to millennial cycles of relative carbon export ultimately driven by changing climate and current systems, which in turn impacts multiple ecosystem properties, including production, mesopelagic particle flux, and trophic structure (e.g. fish populations and recruitment which also vary due to ENSO, Lambrides et al. 2018).

5.0 Synthesis: Shifting $\delta^{15}N$ and $\delta^{13}C$ linked to ITCZ position

Taken together, we propose that these new coral records provide a unique high resolution proxy for the influence of relative shifts in equatorial Pacific current biogeochemistry through much of the late Holocene, likely linked to long term shifts in the ITCZ. We draw this conclusion from the likelihood that both source water mass changes and localized shifts in N_2 fixation influence the overall coupled $\delta^{15}N$ and $\delta^{13}C$ coral records we observe. However, neither baseline shift nor N fixation mechanisms are mutually exclusive, and as discussed above they are in fact likely additive for this system, as both are likely related to the SOI and positioning of the ITCZ which impacts the strength of the NECC. This is because the ITCZ is the primary control on temperatures and precipitation for the central equatorial Pacific, and subsequently controls stratification and upwelling and current strength (Broccoli et al., 2006; Kang et al., 2008, Johnson et al. 2002). During southward ITCZ shifts with a strengthened NECC, the strong easterlies that normally drive upwelling in the eastern equatorial Pacific are suppressed, leading to higher SSTs, more El Niño-like conditions, reduced nutrient delivery / utilization, and reduced surface productivity (Dubois et al., 2014, Clement et al., 1999, Koutavas and Lynch-Stieglitz, 2004, Costa et al. 2017, Rafter and Charles, 2012, Johnson et al. 2002).

Such conditions appear to correspond well with lower $\delta^{15}N$ and $\delta^{13}C$ values in our coral records, consistent with both smaller cell sizes (shift in relative production to cyanobacteria), and possibly increases in local N_2 fixation. Conversely with a more northward ITCZ there are cooler, drier conditions with enhanced upwelling, and a more La Niña-like state, leading to greater nutrient delivery and utilization from the

east Pacific source waters (Beaufort et al., 2001; Koutavas et al., 2002; Pena et al., 2008, Rafter and Charles, 2012, Costa et al. 2017, Johnson et al. 2002). This state would correspond to increased $\delta^{15}N$ and $\delta^{13}C$ values in our corals record, consistent with delivery of more and more enriched $\delta^{15}N$ nitrate to the overall system, larger cells (e.g. diatoms), and less potential for N_2 fixation.

6.0 Conclusions

These first high resolution data set represents spanning the most recent ~2000 yrs of the late Holocene for the central equatorial Pacific indicate both consistent large scale physical trends on millennial scales, as well as rapid short term fluctuations, in a range of interlinked processes. Specifically, our records show multiple and distinct long term regimes (e.g. the multi-centennial slow shift from ~100 to 800 CE, consistent conditions from ~1500 to 1800 CE, and then the rapid multi-centennial ongoing change into the Anthropocene), presumably indicative of long term average ITCZ position trends reflected in current sources and local oceanographic conditions at our study site, ultimately linked to the larger climatic state. This suggests that from ~100-800 CE the ITCZ may have shifted from south to north where it remained through the LIA, which is contrary to a documented southward shift through the last millennia seen in eastern Pacific and South American records (Haug et al. 2001, Rustic et al. 2015). However, at the same time our coral records are consistent with other climatic records which suggest stronger trade winds, drier, La Niña-like conditions in the central Pacific western Pacific during the LIA

(Griffiths et al. 2016; Thompson et al. 2013; Yan et al. 2011), which in turn should indicate a more northward ITCZ. If additional coral skeletons from different regions across the Pacific were studied, together these records might provide finer scale data regarding which of these climatic dynamics is prevalent in the different regions of the equatorial Pacific.

Most broadly, this new work further demonstrates the potential of deep sea protein coral records to understand high resolution variations in tropical climate and oceanography. Our high resolution records showing long term trends can both complement and vastly increase the resolution available from Pacific sedimentary records, for which there very few in the equatorial Pacific, and which all lack resolution in the Late Holocene (e.g., Altabet 2001). At the same time, higher resolution coral records can reveal aspects of climate state and rapid shifts that likely would be invisible or difficult to detect using any other means: for example, specific timing and magnitude around the sharp $\delta^{15}N$ shift and decoupling from $\delta^{13}C$ near the LIA, and relative presence/ absence as well as timing of spectral oscillations during different periods, would be very unlikely to be available from bioturbated low accumulation sediments which characterize this area. To our knowledge, this data set documents these features for the first time. Finally, deep sea protein corals can also greatly extend geographic coverage of such reconstructions, and as noted above are not influenced by bioturbation like many sediment cores. Coral records across the Pacific may therefore be used to more accurately establish links of export production

composition, isotope values, and food web dynamics in the equatorial ocean to climatological changes.

Based on all these aspects, we suggest that deep sea corals may represent the best archives available to examine open ocean changes over the most recent millennia in nutrient and phytoplankton dynamics. Our new work shows that such records can provide highly detailed new chronologies of the water mass dynamics, while improving knowledge of historical climate impacts on ecology and biogeochemistry. By examining corals in multiple locations spanning the equatorial Pacific, it may also be possible that the different variations of ENSO can also be studied on millennial timescales, to better determine how changes in central pacific ENSO versus east Pacific ENSO impact ecosystems on longer timescales.

Figures

The following pages represent all of the main figures as discussed in the chapters above, followed by the appendix compiled during this dissertation that includes supplementary and artistic figures. The figures are presented in same order as the chapters they appeared within.

Chapter 1 Figures

Figure 1-1. Study Location. **A)** SeaWIFS ocean color globe of chlorophyll during boreal summer with Hawai'ian Islands squared in red. **B)** An annual SST (°C) map of Hawaii using World Ocean Atlas 1955-2015 annual data, with arrows pointing to the two coral collection locations on the eastern side of Oahu Island; L for Lanikai (this study), M for Makapu'u (Sherwood et al., 2014), and two sediment core locations P17 and P20 from Lee et al. 2001. Also shown is Station ALOHA from the HOTS program (open circle).

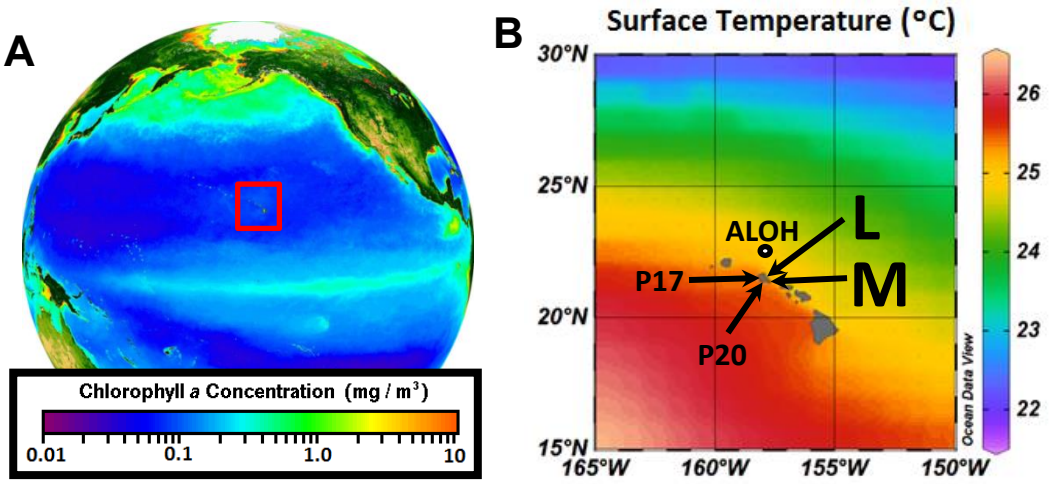

Figure 1-2. Late Holocene bulk coral $\delta^{15}N$ records compared with selected climactic and sedimentary $\delta^{15}N$ records. **A)** Three new bulk coral $\delta^{15}N$ records from Lanikai (colors indicate coral; *see legend*); blue shading indicates previously published records (Makapu'u) from the same region. **B)** Mid-month insolation 15°N for July which is primarily driven by changes in solar precession cycles (Berger and Loutre, 1991). Also shaded are major ENSO periods where most proxy records agree (Lu et al. 2018). **C)** Data from bulk $\delta^{15}N$ sediment records from the North East Pacific binned by 250 yr time steps from 3 records from offshore Mexico (22 to 23°N), 5 off Central America (7 to 16°N), and 4 in the Eastern Tropical Pacific (ETP, 0 to 1°N). Data from the NICOPP database from Tesdal et al. 2013; see supplemental file for more information. Error bars indicate standard deviation.

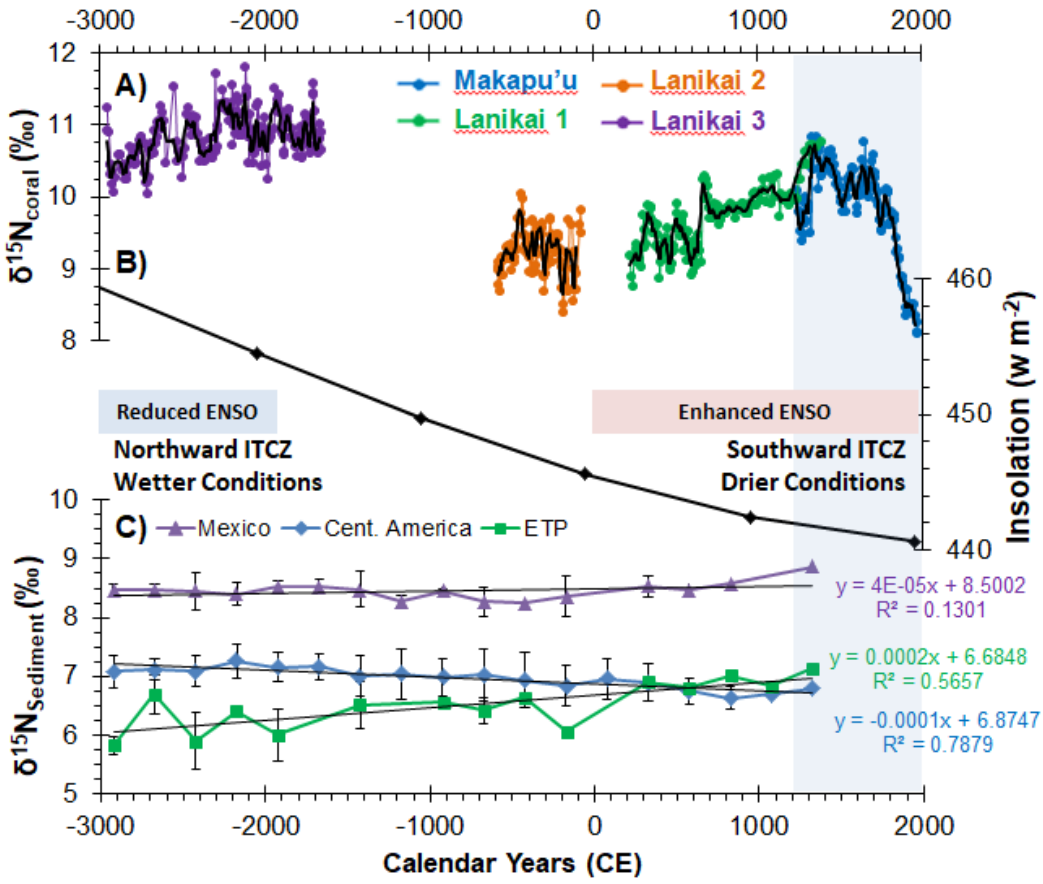

Figure 1-3. Late Holocene bulk coral $\delta^{13}C$ records compared with selected climactic data, sedimentary and atmospheric $\delta^{13}C$ records. A) Bulk coral carbon isotope record, with blue shading depicting extent of previous coral records from the region, black lines representing a 5 point moving average. **B)** Alkenone SST records for the 2 sediment cores (P17, P20) collected near Oahu, Hawaii (Lee et al. 2001) believed to be representative of wintertime SST conditions in the NPSG. **C)** Atmospheric CO_2 concentration from Antarctic ice core records (Monnin et al. 2004). **D)** Red sediment color intensity record (grey), interpreted to be driven by El Nino Southern Oscillation with the black line designating a 20 year moving average (Moy et al. 2002).

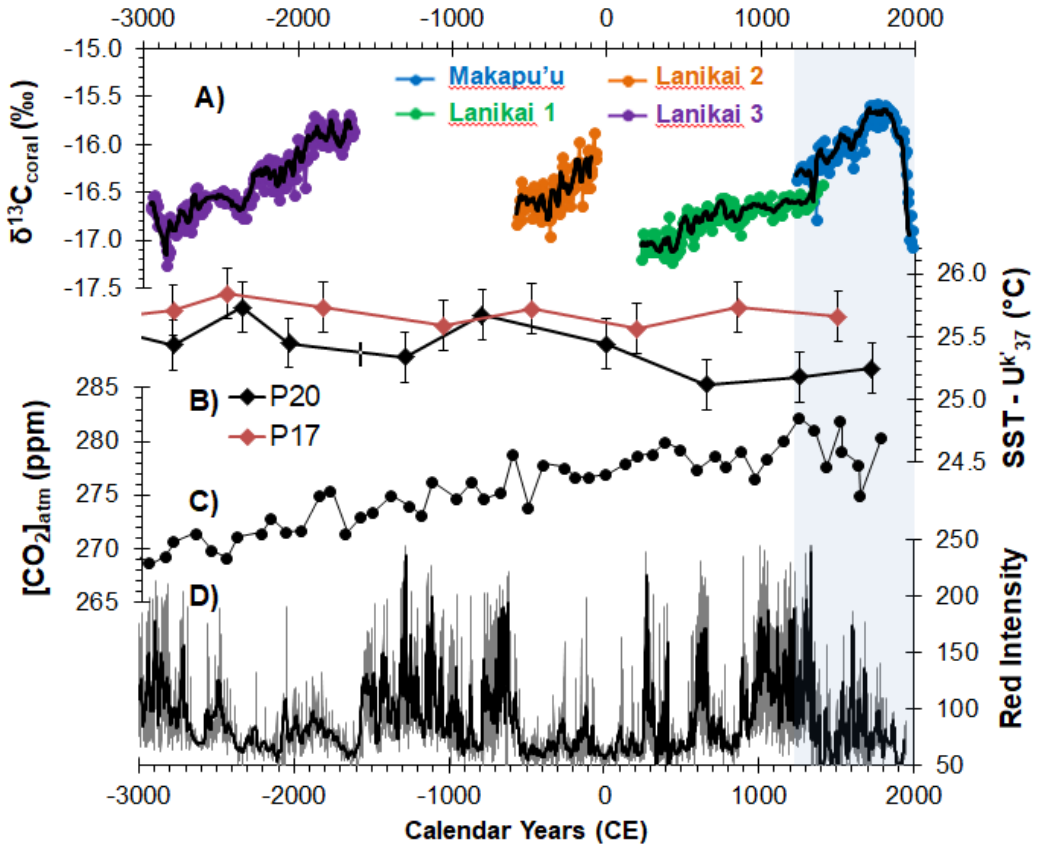

Figure 1-4. Coupled vs. decoupled changes in $\delta^{15}N$ and $\delta^{13}C$ bulk isotope values of export production in NPSG through the Late-Holocene. Bulk nitrogen and carbon isotopic records from *K. haumeaae* (A and B; as presented in prior figures) are overlain to indicate distinct periods of coupling vs. decoupling in isotopic change. Unshaded periods indicates where $\delta^{15}N$ and $\delta^{13}C$ are decoupled (DC1, DC2), while red shading indicates coupling as the isotope systems trend in the same direction (C1, C2), and blue shading is unknown (??). Grey dashed arrows indicate the hypothesized trend in isotope values during discontinuities in our current records while black lines designate the 5 point moving average.

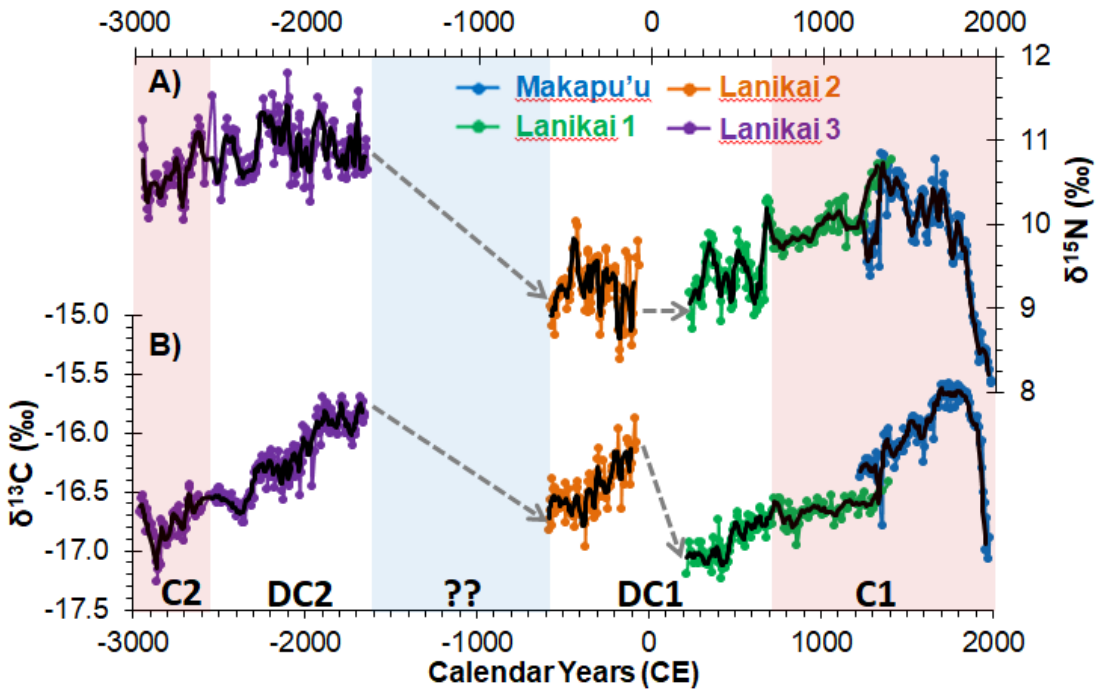

Chapter 2 Figures

Figure 2-1. Scanning electron microscope (SEM) images live-collected *Kulumanamana haumeaae* and subfossil gold coral skeletons collected from the same Cross Seamount location. For all figures, the growth axis progresses from right to left (outer layers left, inner layers right). Images on the top are magnified by 125x while the bottom are higher magnifications and representing the area inside the red squares on top images; scale bars are white arrows and also on lower right of each image. **A and B)** Live-collected coral skeletons showing the layered fibrous nature of living skeletons from ~14 mm from edge. Panel B is a 1250x (30 µm) magnified image of the modern of area in the white square; ~600 yr CE). **C and D)** Outer subfossil coral material, ~3 mm from the outer edge (~9.6 kyrs BP), which shows extreme structural alteration at 1000x (40 µm) magnification. **E and F)** Inner subfossil coral material imaged ~25 mm from the edge (~10.7 kyr BP), with similar magnifications to the outer layers.

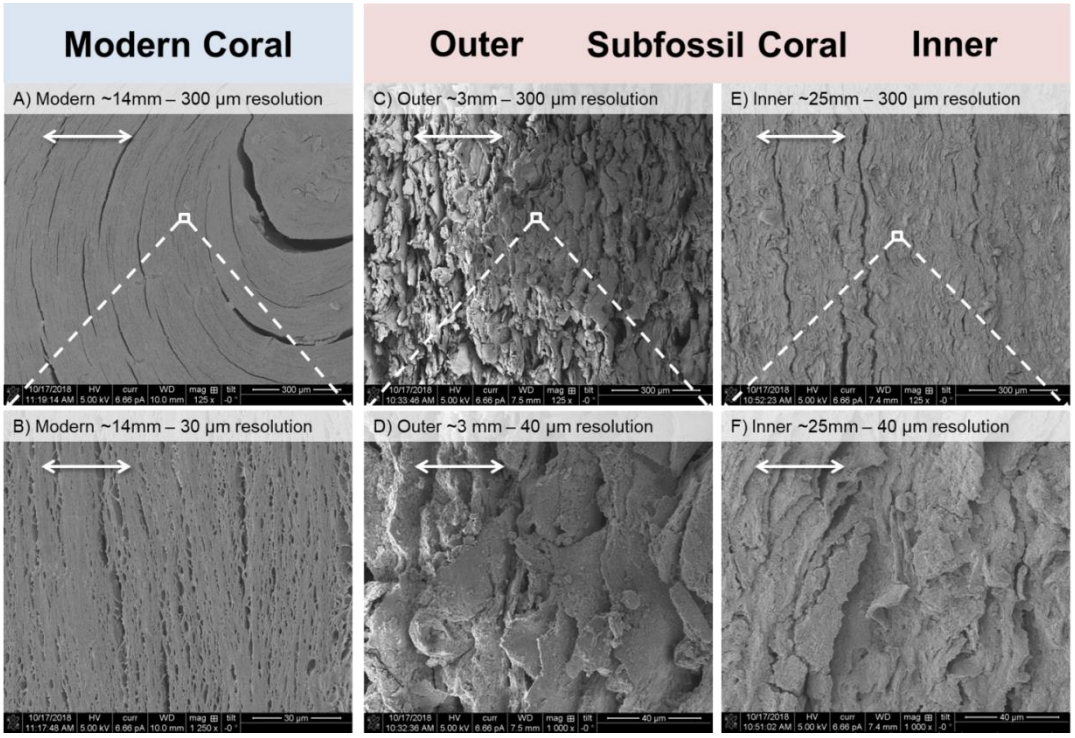

Figure 2-2. C/N and bulk isotope values. **A)** C/N ratios for *K. haumeaae* coral skeletons. From left to right, a live-collected Cross Seamount coral C/N average and standard deviation (blue, this study), literature range for live-collected corals (dark green; Druffel et al., 1995, Goodfriend 1997; Sherwood et al., 2014; McMahon et al., 2015), range of previous dead-collected, subfossil coral values (light green; 1-5 kyrs BP, Glynn et al., 2019), and this study's results for a subfossil Cross Seamount skeleton (red). **B)** Bulk nitrogen and **C)** bulk carbon isotope values of live-collected (blue boxes) and subfossil *K. haumeaae* (red) gorgonin skeletal material, collected from the same Cross Seamount site. Due to the rapid change in isotopic values during the Industrial Revolution, live-collected coral values are plotted as separate averages and standard deviations for recent time (dark blue, since 1950 CE) versus the pre-Industrial Revolution (before 1900 CE, ~600 yrs). The subfossil coral data represents a 46 mm transect from the outer layers to the inner layers, with each point representing 0.1 mm resolution (~5-7 yrs). Black squares are for selected acidified samples. Pink shading represents the outer 10 mm diagenetic horizon discussed in the text.

(Figure on next page)

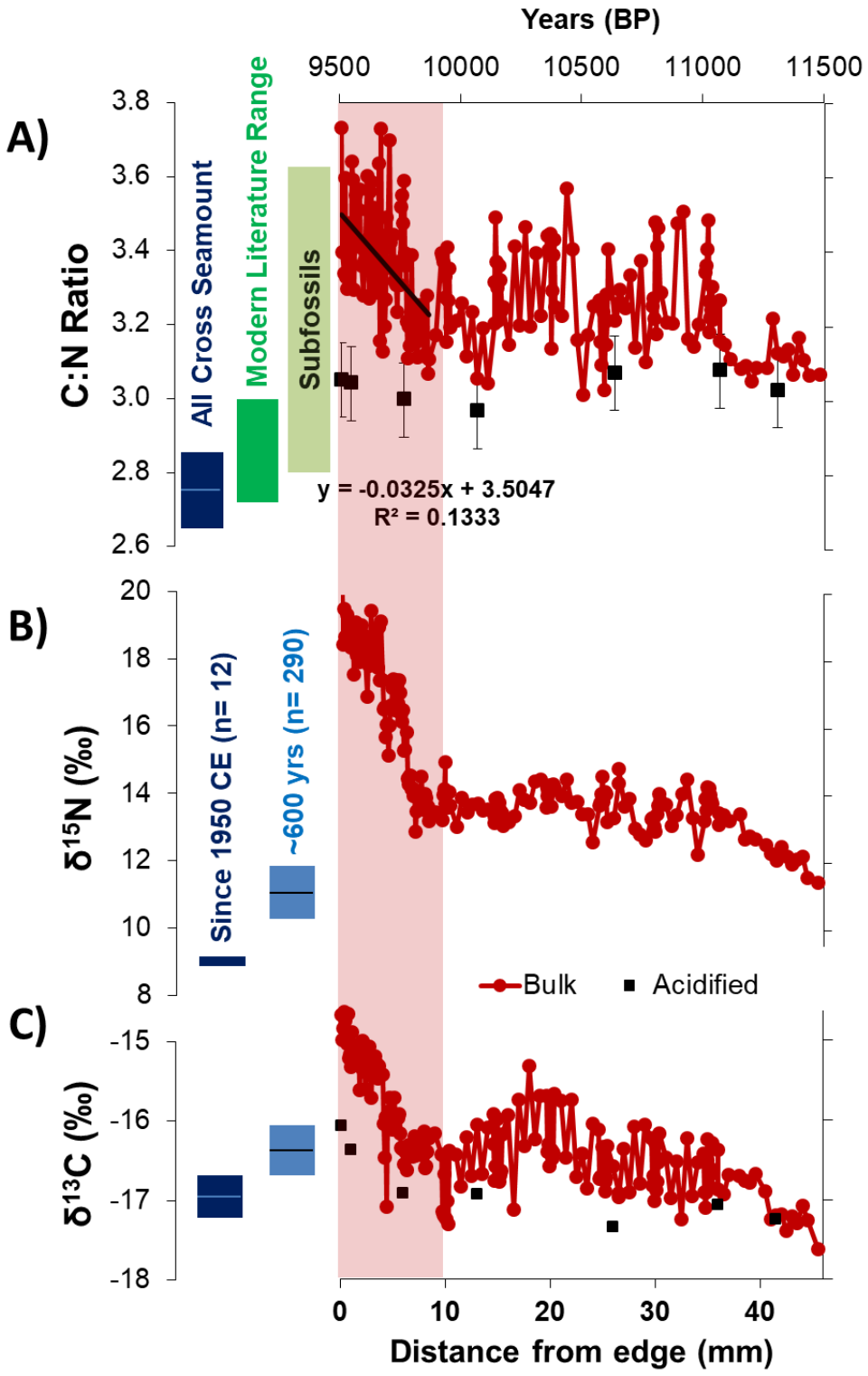
Years (BP)
9500
10000
10500
11000
11500
A)
C:N Ratio
3.8
3.6
3.4
3.2
3.0
2.8
2.6
All Cross Seamount
Modern Literature Range
Subfossils
y = -0.0325x + 3.5047
R² = 0.1333
B)
δ15N (‰)
20
18
16
14
12
10
8
Since 1950 CE (n= 12)
~600 yrs (n= 290)
Bulk
Acidified
C)
δ13C (‰)
-15
-16
-17
-18
0
10
20
30
40
Distance from edge (mm)

Figure 2-3. Molar percentage (mol%$_{AA}$) of AAs for ancient and modern *K. haumaeea* skeletons. **A)** Subfossil vs. Modern *K. haumeaae* mol%$_{AA}$ comparison. Average molar distribution in modern specimen (n=9; blue bars) versus average of only subfossil coral inner layers (>10 mm, n=10, red bars). There were significant mol%$_{AA}$ differences between all AAs (P <0.02) except Tyr (P <0.12) and Ile (P <0.09; t-test assuming unequal variances, alpha = 0.05). AA's denoted with a star (*) indicate AA's which retain significantly different mol%$_{AA}$ values if Gly values are set to be equal, as described in the text. **B)** Inter-coral subfossil skeleton mol%$_{AA}$ data (n=19) from Cross Seamount, HI. Data are binned by skeletal depth highlighting AA composition changes between degraded outer layers vs. protected inner layers.

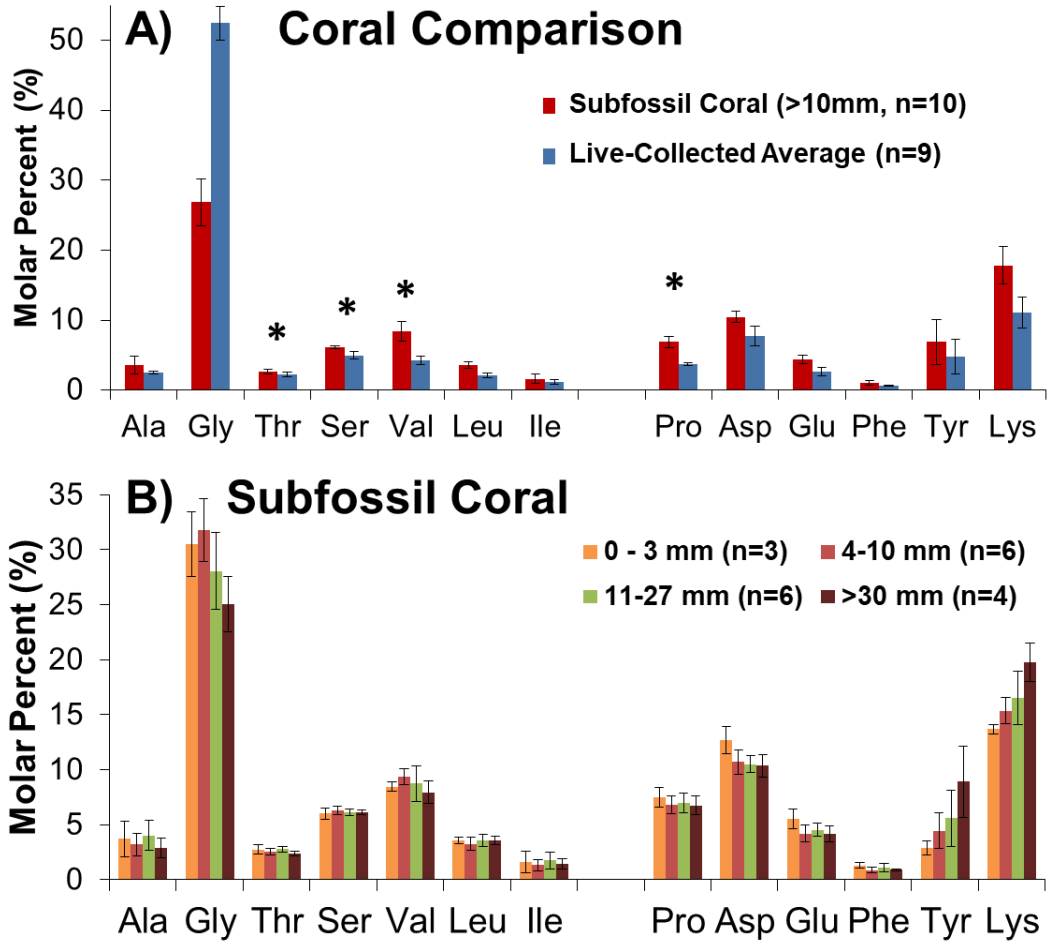

Figure 2-4. Normalized $\delta^{13}C$ AA values in live-collected (blue) and subfossil *K. haumeaae* skeletons (red and yellow). AA $\delta^{13}C$ values normalized by subtraction of average THAA ($\delta^{13}C_{THAA}$). AAs are grouped as described in the text and error bars indicate the standard deviation of the average binned $\delta^{13}C$ values.

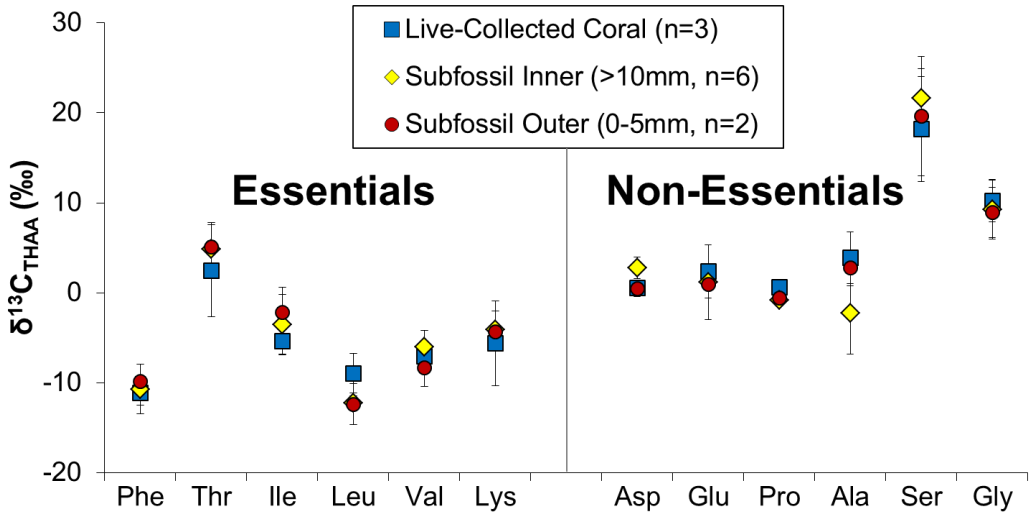

Figure 2-5. Normalized $\delta^{15}N$ isotope values for AAs of the live-collected (blue) and subfossil *K. haumeaae* skeletons (red and yellow). AA $\delta^{15}N$ values normalized by subtraction to average $\delta^{15}N$ of hydrolysable protein (THAA parameter; see methods). Note that Thr is plotted on a separate secondary axis. AAs are grouped as described in the text and error bars indicate the standard deviation of the binned coral values.

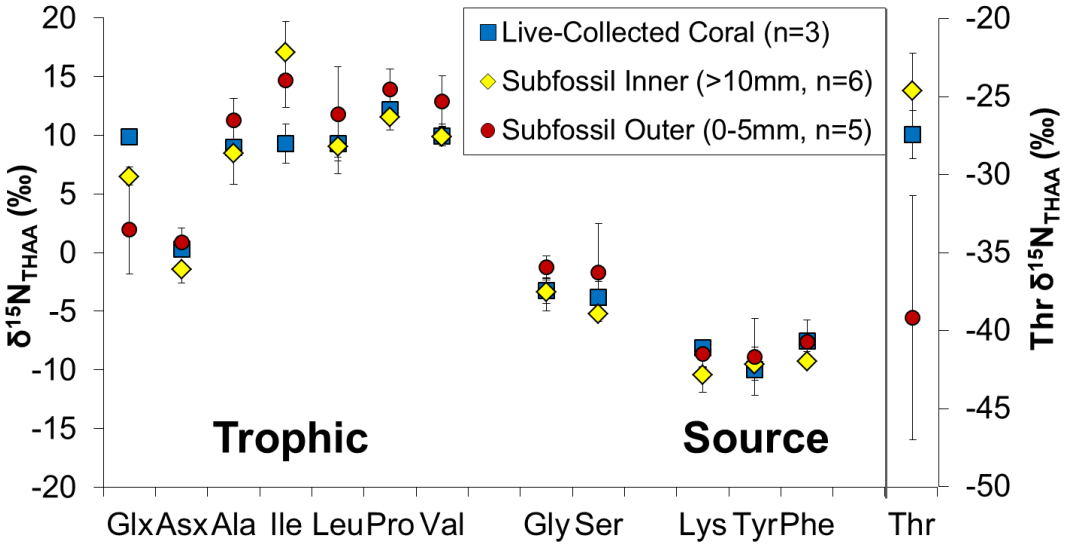

Fig. 2-6. Modern coral ranges compared to subfossil coral $\delta^{15}N_{AA}$ proxies. Ranges of values found for the modern specimen on the left and the subfossil coral on the right. **A)** Bulk $\delta^{15}N$ values plotted along with average total hydrolysable AAs (THAA) $\delta^{15}N$ average values (black), average $\delta^{15}N$ value of the trophic AAs (Glx, Asx, Ala, Ile, Leu, Pro, Val), and average $\delta^{15}N$ values source AA values (Phe, Lys, Tyr). **B)** Average of measured $\delta^{13}C$ values for essential AA (Phe, Thr, Ile, Leu, Val, Lys) plotted along with the bulk $\delta^{13}C$ values. **C)** $\sum V$ values, calculated using all trophic AAs (blue) and excluding Ile values (red). **D)** Trophic position after McMahon et al. 2018 (see methods).

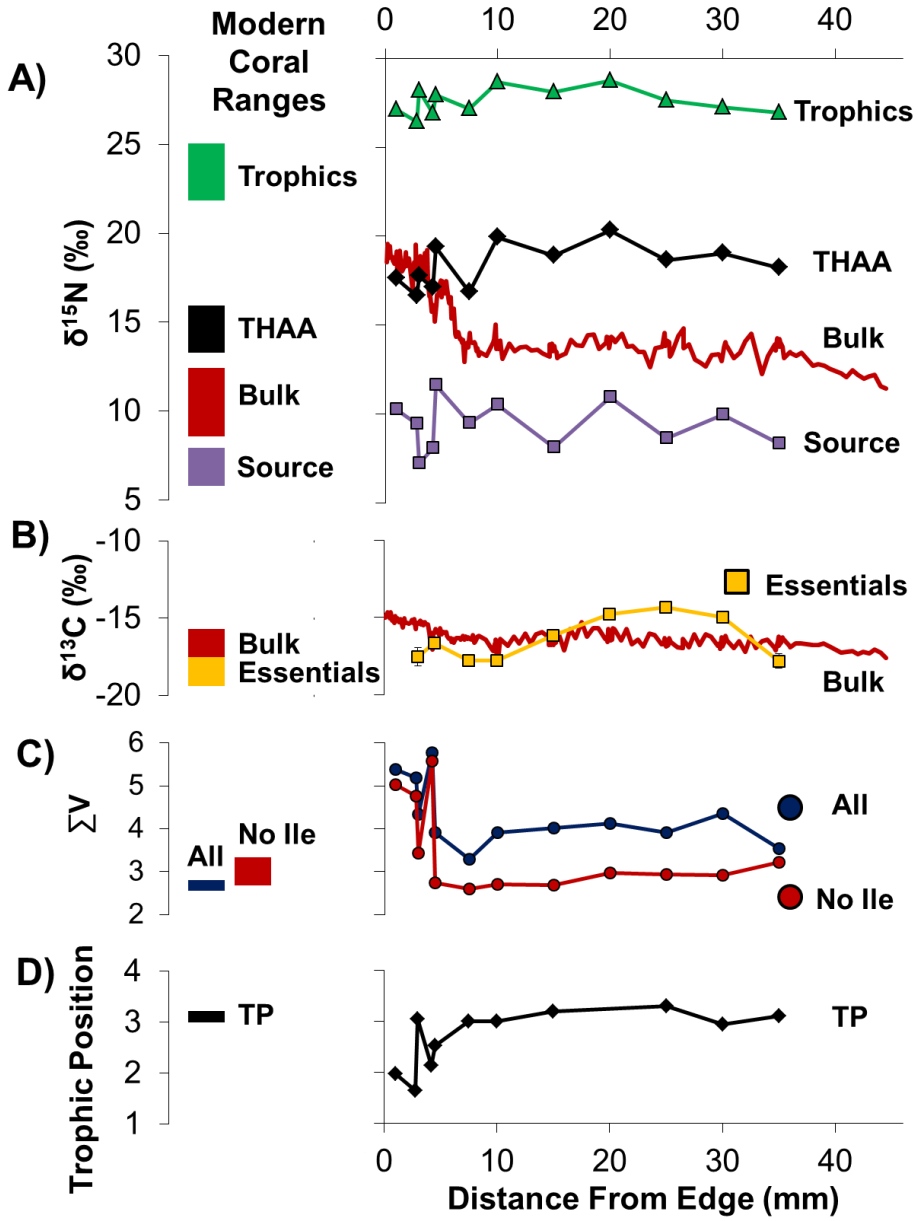

Chapter 3 Figures

Figure 3-1. Map of $\delta^{15}N$: A) Depiction of $\delta^{15}N$ of nitrate from 150 m the central tropical Pacific based on modeled and observational data from Somes et al (2010) and Rafter and Charles (2016). Black open star indicates the coral collection site of Kingman Reef. White squares indicate the two sedimentary records compared in this study from the west Pacific (Langton et al. 2008) and the east Pacific (Sauthoff 2016). Black arrows designate the strength and latitude of the west to east NECC and east to west NEC during weakened trade winds (El Niño-like conditions; solid arrows) and strengthened trade winds (La Niña-like conditions; dashed arrows).

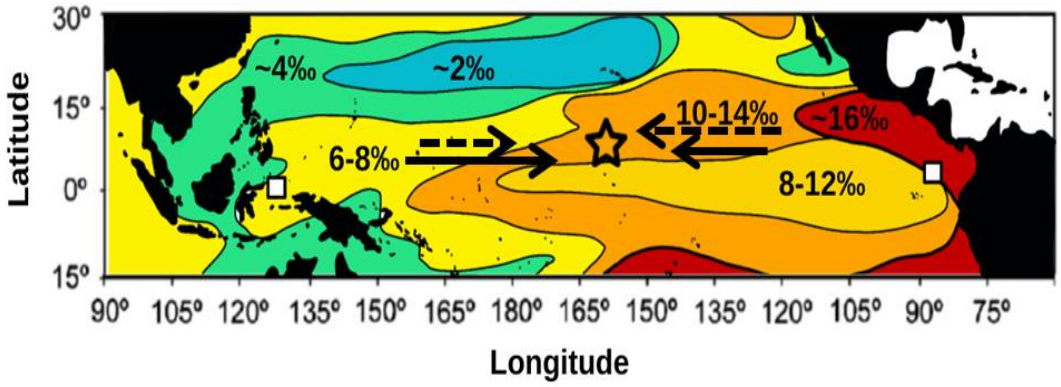

Figure 3-2. Coral proxy information: **A)** $\delta^{15}N$ bulk values of *K. Haumeaae* corals from Kingman Reef (6°23′N, 162°25′W) and **B)** values for the source amino acids Phe, Tyr, Lys (black squares) and the individual amino acid Phe values (grey squares). **C)** Trophic position (yellow triangles) calculated using coral specific TP equation = ((Glu + 3.4) - Phe - 3.4) / 7.6 + 1 (McMahon et al. 2018). **D)** $\delta^{13}C$ bulk values of *K. Haumeaae* corals along with acidified bulk samples (yellow diamonds) test for presence of calcite ($CaCO_3$) which occurs during in-situ degradation on the sea floor, showing that the outermost layers only are likely impacted by calcite (grey, open circles). Note that the degraded outer layers of K2 coral based on C/N and acidification tests were excluded from this plot (see fig. S7).

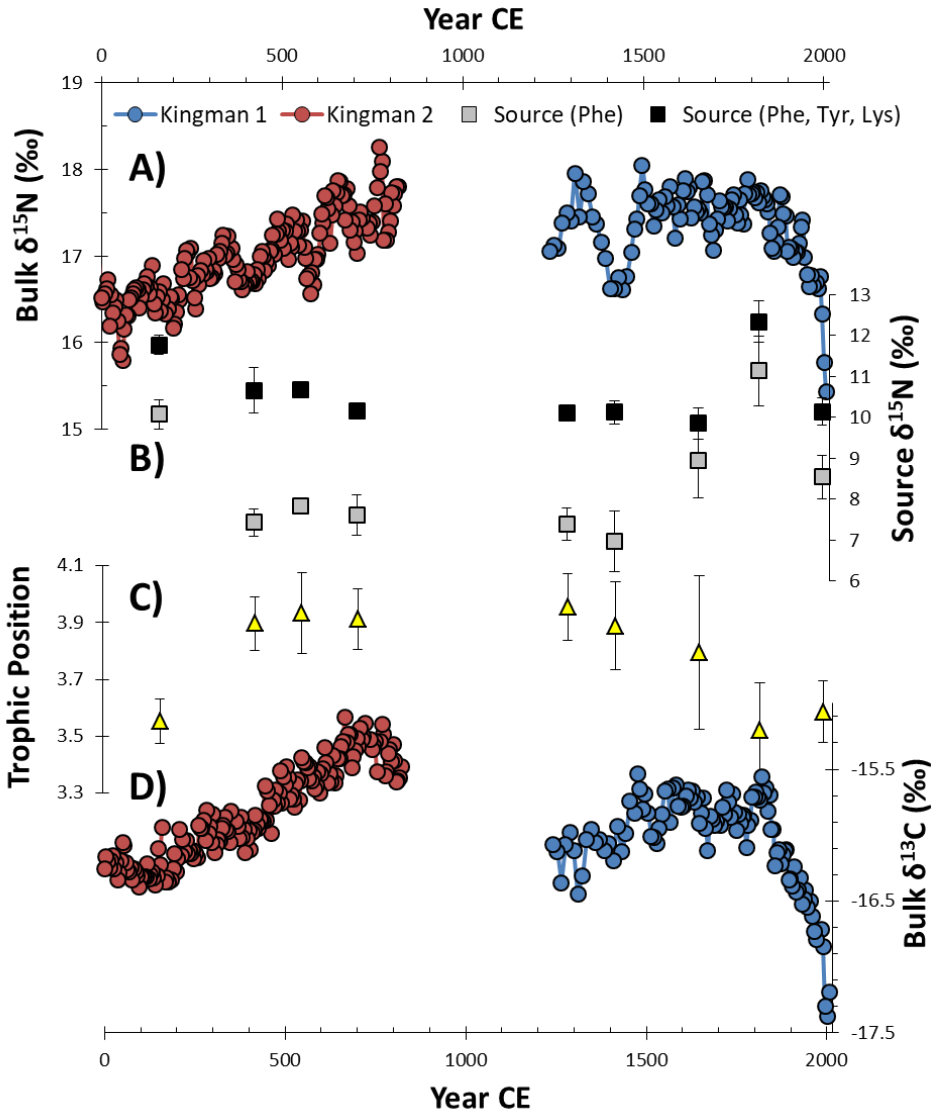

Figure 3-3. Sediments & SOI compared with corals Fig 3) Coral, sedimentary, and climate records and suspected drivers behind proxy variability. A) $\delta^{15}N$ of coral record. B) West Pacific $\delta^{15}N$ record from Langton et al. (2008) based on an Indonesian sediment core. C) East Pacific $\delta^{15}N$ sediment record from Sauthoff (2016). D) $\delta^{13}C$ of coral record. E) Precipitation based proxy of the Southern Oscillation Index record based on rainfall proxies spanning the equatorial Pacific (Yan et al. 2011).

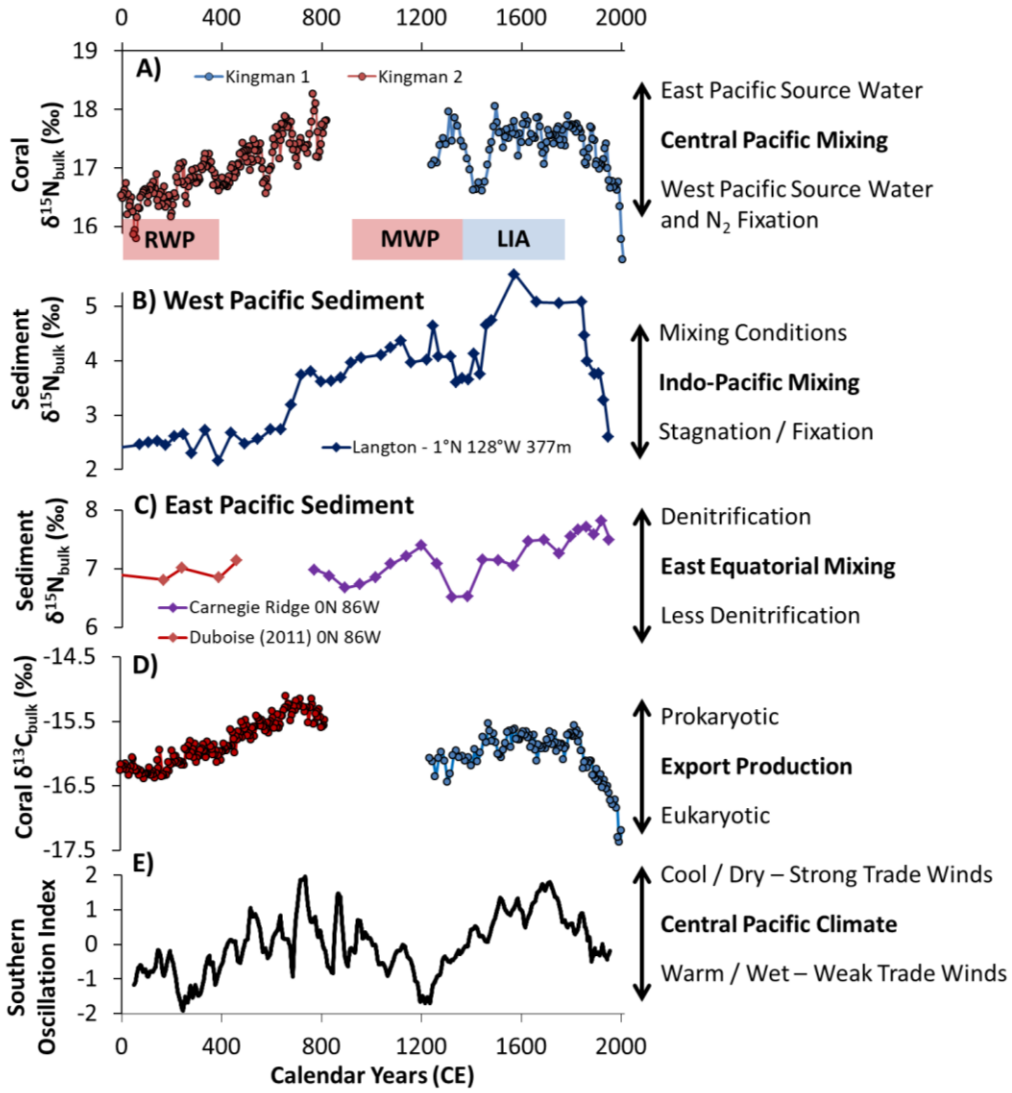

Appendix

The following pages represent all of the supplemental figures and supplementary text presented and discussed in the chapters above, followed by the data tables compiled during this dissertation.

Chapter 1 Supplemental Figures

Appendix Figure 1-S1. Radiocarbon age models. Age-models were determined for each specimen using a Bayesian modeling approach, Bacon (Blaauw and Christensen 2011) using Marine13 (Reimer et al., 2013) and a reservoir age correction (expressed as ΔR) of -28 ± 4 (Druffel et al., 2001). Blue-shaded areas represent the conventional calibrated ^{14}C age distributions. Dark grey lines represent all iterations (n=10,000) of the model, while the fine red line is based on the weighted mean age for each depth which was used in this study. Lanikai 1 age model was calculated using an accumulation rate of 10 yrs/0.1 mm while Lanikai 2 and 3 used an accumulation rate of 5 yrs/0.1 mm. All corals used an accumulation shape of 1.5, memory strength 4, and a mean memory of 0.7. The grey stippled lines show the 95% confidence intervals which averaged 98 ±15 years. The shape of the curves reflects variable growth rates in the four coral samples illustrated. **A, B, C)** Lanikai corals used in this study with original collection names also listed.

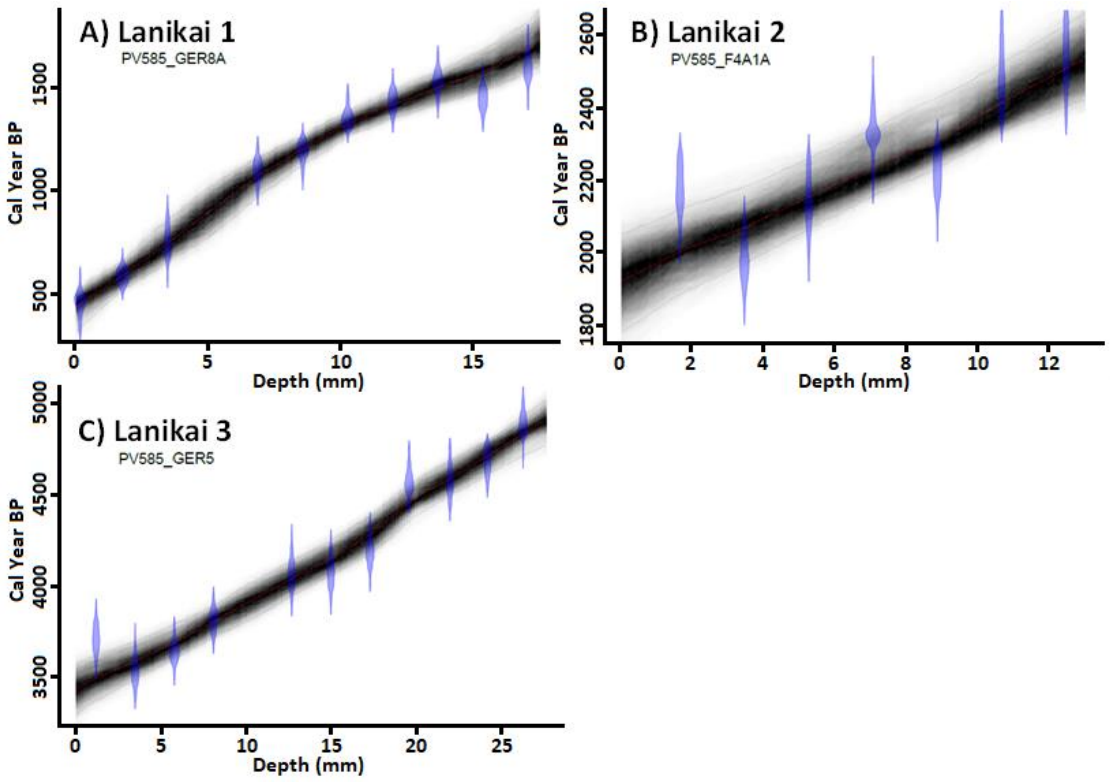

Appendix Figure 1-S2. Comparison of acidified vs. non-acidified $\delta^{13}C$ and C:N ratio values for Lanikai coral skeleton samples. Bulk non-acidified sample values (blue diamonds) are compared with acidified samples of the same coral skeletal material (red squares) for our three coral specimens, showing consistent offsets in both C:N and $\delta^{13}C$ values consistent with carbonate formation in the outer coral skeletal layers. Highlighted in red are the portions of the skeletons where C:N values exceeded the values expected for fresh/ living coral specimens, and therefore were excluded from data sets analyzed in the main paper (see section 3.3 for more information). "Duplicate" indicates samples which were not acidified, however analyzed on the same EA-IRMS run as the acidified samples, while the "Acid Dup" (L3 11.0 mm) indicates a duplicate acidified sample. Error bars indicate standard laboratory error of ±0.2‰for $\delta^{13}C$ and ±0.1 for C:N values. The increase in C:N and $\delta^{13}C$ in non-acidified samples could be due to precipitation of inorganic carbonate or selective loss and remineralization of certain compound classes. A $\delta^{13}C$-DIC of ~1‰ (eg., Quay et al., 2004; 2017) and an ε-ΣDIC-calcite of ~1‰ (Romanek et al., 1992) would yield authigenic calcite with a $\delta^{13}C$ value of ~2‰. To shift $\delta^{13}C$ values that otherwise would be -16‰ by +0.8‰ would require ~4% carbonate (C/C). Note that due to consistently documented chemical loss/fractionation of $\delta^{15}N$ values in proteinaceous corals skeletons, sediments, and other materials associated with acidification (Kim et al., 2016; Mateo et al., 2008), we did not analyze analogous $\delta^{15}N$ results. Selective remineralization and loss of compound classes should most likely influence N-containing compounds, too. For these conservative reasons, ie., whether addition of trace amounts of calcite or loss of certain compound classes from the bulk skeletal matrix, we exclude all data in the red shaded zones from analysis and discussion in the main text.

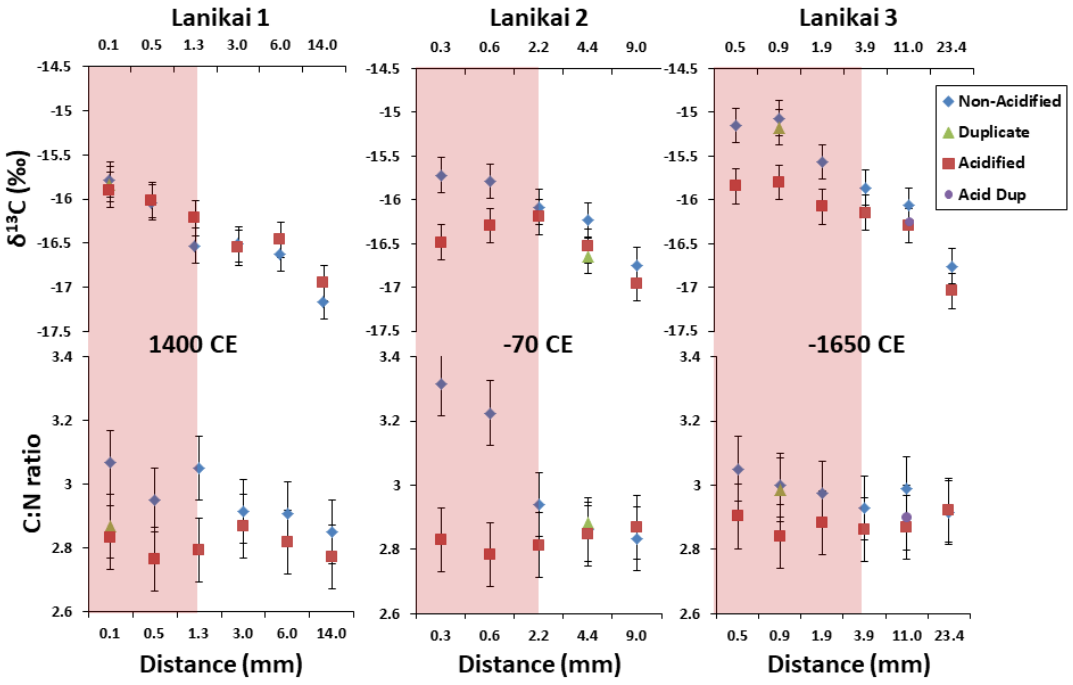

Appendix Figure 1-S3. Regime shift detection. **A&D)** Bulk coral $\delta^{15}N$ and $\delta^{13}C$ records from Lanikai (colors same as previous figures). Black lines signify regimes detected by software designed to automatically detect statistically significant shifts in the mean level and the magnitude of fluctuations in time series using sequential t-tests (Rodionov 2004). **B&E)** $\delta^{15}N$ and $\delta^{13}C$ residuals after the stepwise regime function is removed. **C&F)** Weight attributed to outliers (using Huber's weight function, weight = min(1, parameter/(|anomaly|)), where the anomaly is the deviation from the expected mean value of the new regime normalized by the standard deviation averaged for all consecutive sections of the cut-off length in the series (http://www.beringclimate.noaa.gov/regimes/help.html). If anomalies are less than or equal to the value of the parameter then their weights are equal to one. Otherwise, the weights are inversely proportional to the distance from the expected mean value of the new regime.

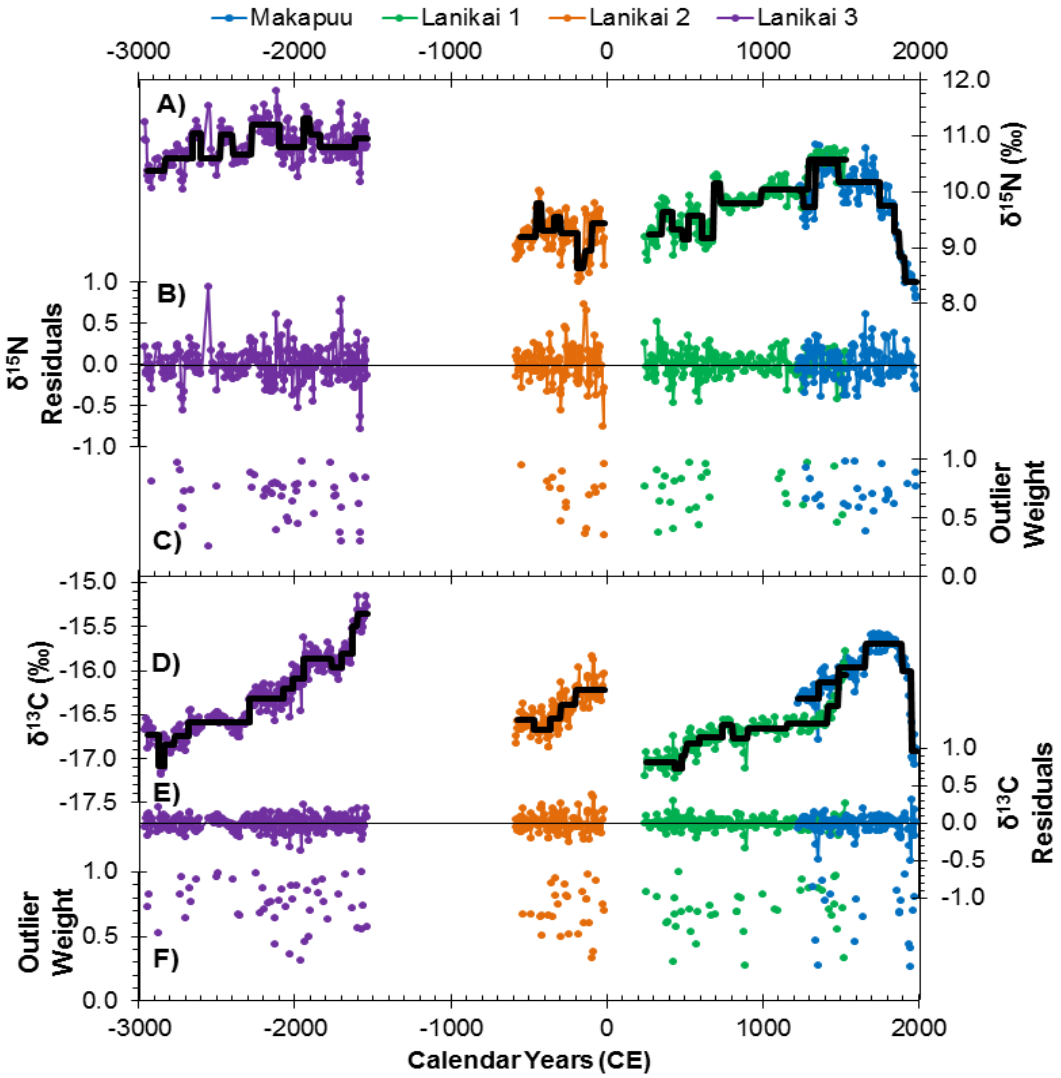

Appendix Figure 1-S4. Map of sediment core locations and regional sections. West Pacific (yellow) includes seven sediment $\delta^{15}N$ records published in Kienast et al. (2008), Jia and Li (2011), Langton et al. (2008)*, Rafter and Charles (2012). North West Pacific (red) includes four records published in Kao et al. (2008)*, Kienast (2000). North East Pacific (blue) includes nine records published in Hendy et al (2004)*, McKay et al (2004)*, Chang et al. (2008)*, Emmer and Thunell (2000)*, Kienast et al. (2002), Ganeshram et al. (1995*, 2000*), Arellano-Torres (2010)*. East Pacific (green) includes ten records published in Dubois et al. (2011), Pichevin et al. (2009, 2010), Thunell and Kepple (2004)*, Hendy and Pedersen (2006)*, and Robinson et al. (2009). References marked with a * indicates records using updated age-models. Sedimentary age models were updated using the CALIB program (Stuiver et al. 2017) and Marine13 (Reimer et al., 2013), while retaining reservoir age corrections from the original studies before applying a piecewise linear regression to form an updated age model.

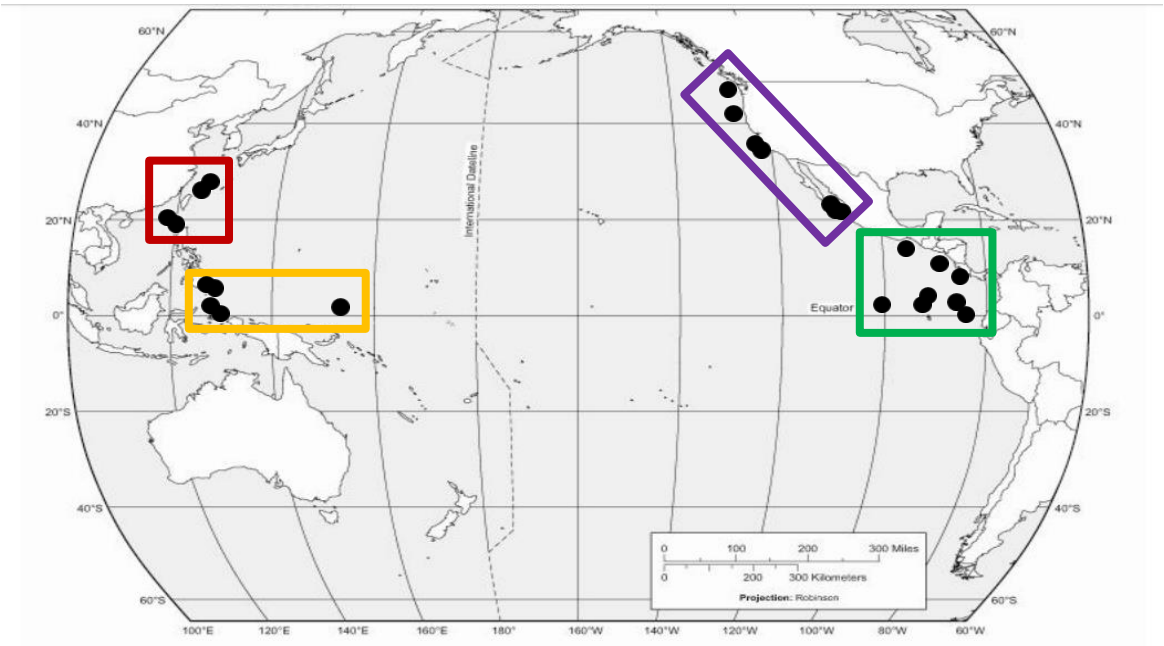

Appendix Figure 1-S5. Linear regressions of sedimentary $\delta^{15}N$ records. Sediment data limited to the last 6000 years (-4000 to 2000 CE) and records with >2 points within this period (n=30; see methods). Regions correspond to Fig. S3. Data was standardized to a mean of zero for the 6000 years in order to remove site specific variability in absolute values (e.g. depth differences). What this means is that for each record, the mean $\delta^{15}N$ value of the last 6000 years for that record was subtracted out to create a record of anomalies. This was done in order compare records with each other, irrespective of differences in absolute $\delta^{15}N$ values which are largely driven by differences in water depth during sediment core collection. Black line designates the overall linear trend of North Pacific sediment $\delta^{15}N$ over 6000 years.

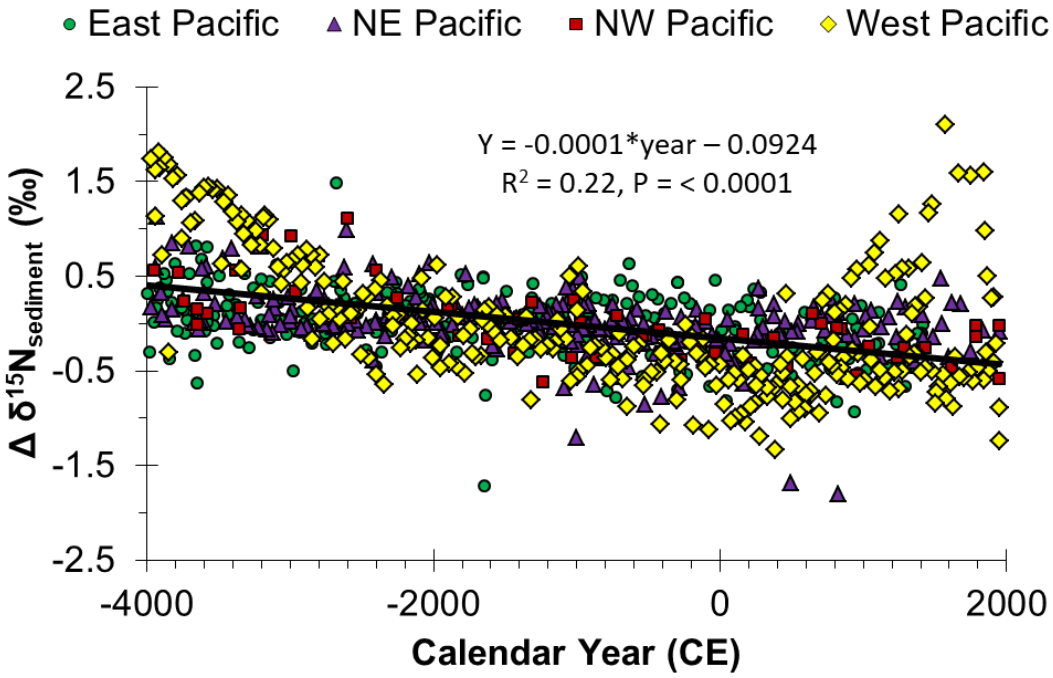

Chapter 2 Supplemental Figures and Text

Appendix Figure 2-S1A. Flow Chart of detailed sampling and analytical process.

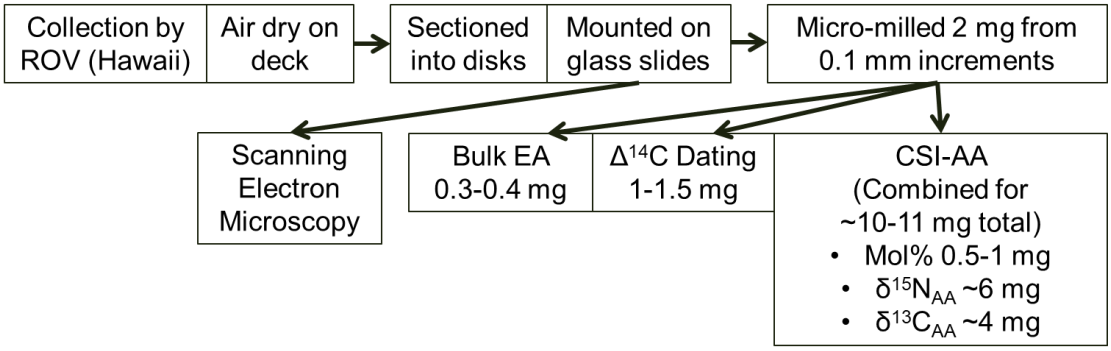

Collection and sampling: Coral skeletons were collected via submersible from Cross Seamount, Hawaii at 447 m (live-collected) and 415 m (subfossil). Skeletons were rinsed and air dried on deck. Cross sectioned disks were prepared using a water-cooled diamond blade tile saw at Stanford University. Subfossil coral disks (~0.7 cm in height) were cut and mounted onto glass slides using a thermoplastic glue. Mounted disks were micromilled in 0.1 mm increments to a depth of ~2.5 mm and length of ~7 mm (this length shortens when approaching the disk center due to the smaller circumference of the growth layers).

Sample Processing: Coral skeleton micromilling yielded ~2 mg per sample, which was transferred to glass vials using a scalpel. Target sample amounts varied by analysis: ~0.3-0.4 mg was used for bulk analysis at the Stable Isotope Lab at University of California Santa Cruz; ~1 mg was used for radiocarbon dating at Livermore National Laboratory. Because CSIA-AA analyses were far more sample intensive, samples from nearby drilled layers (typically ~8-10 samples) were combined into ~10 mg composite samples (~1 mg per layer). This breaks down to ~4 mg for C-CSIA-AA, ~6 mg for N-CSIA-AA, ~0.5-1 mg for mol%. Mol% and CSIA-AA analyses were performed at University of California Santa Cruz - McCarthy Lab as described in the main text. Derivatized AA samples used for CSIA-AA were reconstituted in ethyl acetate (~100 µL volume for smaller peaks and ~200 µL total volume for the larger peak samples) before being run for CSIA-AA. Exact dilutions aimed to be above minimum chromatographic thresholds of 80 mV for N and 150 mV for C CSIA-AA analyses (further discussion on peak heights under Fig. S1B).

SEM requires sputtering with gold, which occurred after drilling the transect and all other sample analysis. SEM performed at the W.M. Keck Center for Nanoscale Optofluidics at University of California Santa Cruz.

Appendix Figure 2-S1B. Chromatograms from the GC-IRMS for nitrogen (upper) and carbon (lower) for the individual amino acids for a selected subfossil coral sample (sample distance 15.0 mm).

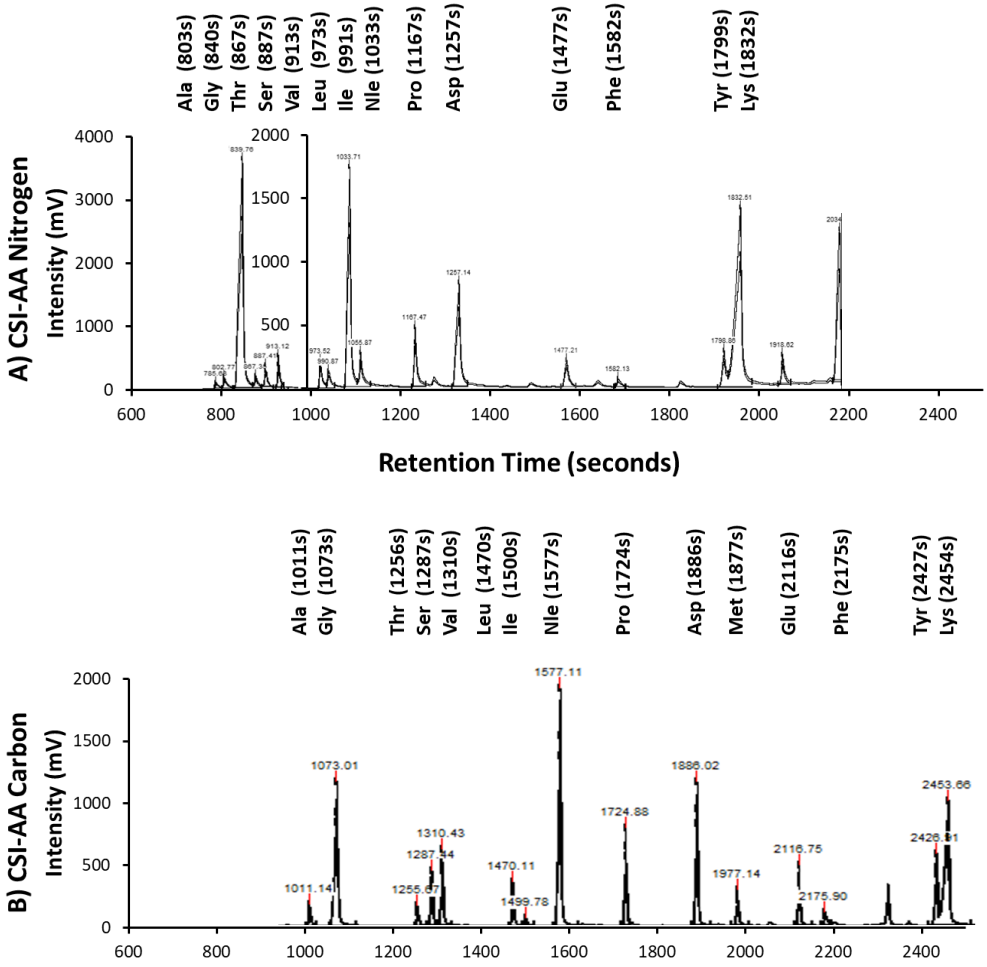

A) Nitrogen AA chromatogram. There were two methods used for the GC-IRMS (see methods), where the first eluting peaks were run as duplicate analyses at a lower concentration to examine the high glycine values (839s) and then AAs which elute after 1000 seconds (Leu onwards) using a cutoff program which would vent that high peak (note separate intensity scale bars) in order to protect the instrument source components from the high concentrations of glycine.

B) Carbon AA chromatogram. See methods section for details. Standard runs showed that Met was problematic and could not be reliably used for calculating isotopic values.

CSIA-AA data verification and corrections: Additional information.

Accuracy of $\delta^{13}C$ and $\delta^{15}N$ CSIA-AA data was verified following McCarthy et al., 2013. Value accuracy verification used three independent and overlapping approaches: first comparing values for a nor-Leu internal standard, second by using a bracketed external (L-amino acid) AA standard mix injected repeatedly after every third sample, and finally by comparison to a natural cyanobacteria long term (> 10 yr) in-house working standard.

The nor-Leu internal standard was used to verify that for each individual sample and injection a known compound gave expected values. If the measured Nor-Leu value was within one standard deviation of the known off-line value, then the data were considered acceptable. For $\delta^{15}N_{AA}$ measurements, external AA standard mix $\delta^{15}N$ AA values from the same run sequence were also used to evaluate the overall run performance, and in some cases make corrections. If an average external standard AA value for the entire run was within one standard deviation of the authentic AA $\delta^{15}N_{AA}$ value, then the overall accuracy was considered acceptable and no corrections were made. However, if any external standard AA had an average value over the entire run outside one standard deviation of the authentic value, this AA was considered to have a systematic bias, under that day's run-specific conditions. $\delta^{15}N_{AA}$ values for any such AA were then adjusted by an offset "correction factor", representing the difference between the know standard value and its average measure value in the run, following the approach described by McCarthy et al., 2013 (*described n supplement)*. We note that such corrections of $\delta^{15}N_{AA}$ values were rare, and in no case was an AA value corrected or considered acceptable if standard values were beyond 2 standard deviations of the known value.

For $\delta^{13}C$ CSIA-AA, directly measured $\delta^{13}C$ values of derivatized AAs must corrected for added derivative C, as well as fractionation, during derivatization reactions. This was done using average external AA standard $\delta^{13}C$ values for an entire run, following the method of Silfer and coauthors (1991). Because this derivatization correction will also intrinsically correct for any offset from the known standard values, no process analogous to $\delta^{13}C$ value correction can be used.

Finally, both $\delta^{13}C$ and $\delta^{15}N$ AA results from an internal cyanobacteria laboratory reference material, run from hydrolysis through the entire sample protocol with each batch, were examined. Individual AA isotope values were compared against a long term (>10 yr) control chart. Essentially this process checks for long term entire protocol reproducibility, and so the integrity of the full hydrolysis to GC-IRMS analytical sequence. Batch data were considered acceptable if average value fell within one standard deviation of long term average values.

Sample amounts and CSIA-AA chromatograph peak heights:

When running CSIA-AA samples, each aliquot of derivatized coral sample was individually reconstituted with ethyl acetate in order to meet at least the minimum peak intensities for isotope accuracy on our IRMS system. The exact dilution and peak height, therefore, varied among samples due to the amount of skeleton material used for derivatization. For N-CSIA-AA, we aimed for ~ 200 mV peaks with ~80 mV on our system as the lower limit to produce a maximum precision of about ±1‰. Thus samples peak heights range from 80 mV to ~2000 mV for most amino acids, while Lys and Gly were ~3000 and ~4000 mV, respectively. For C-CSIA-AA, the lower limit peak height is ~150 mV (for ±1‰ precision), however typical peak heights used were >250 mV to ~1500 mV. We note, however, that exact peak intensities needed to procure target precision are IMRS specific and must be determined for each instrument.

Appendix Figure 2-S2. Age model based on radiocarbon dating for the modern and fossil coral skeleton. Calibrated years before present (ybp) ages and subsequent age models were generated with Calib8.1 (Stuiver et al. 2021), a local reservoir (ΔR) correction of -177 ± 16 (Druffel et al., 2001; Guilderson et al., 2021) and the Marine20 (Heaton et al., 2020) database.

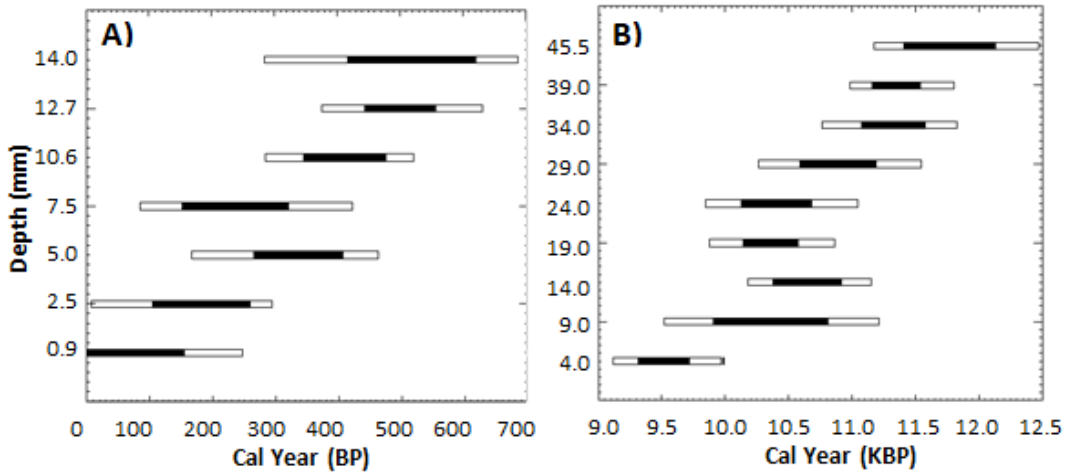

A) For the modern coral an age model was constructed using linear interpretation from the radiocarbon dates using formula Years (BP) = 30.7 x depth (mm) + 87.9 which had an $R^2 = 0.89$ and P = 0.01. The modern coral had an age of 711 years and a radius of 16.9 mm, suggesting a growth rate of 24 µm-yr^{-1}.

B) For the fossil coral an age model was constructed using linear interpretation from the radiocarbon dates using formula Years (BP) = 45.5 x depth (mm) + 9642.1 which had an $R^2 = 0.87$ and P = 0.001. The fossil coral total of 1893 years old and 45.5 mm radius suggesting the same growth rate of 24 µm-yr^{-1} as the modern specimen. Handling and chemical pre-treatment of the sub-fossil samples ended up yielding 70-180 µgC targets, which contributes to relatively large radiocarbon age uncertainty. Guilderson et al. 2013 also radiocarbon dated this coral and found similar ^{14}C ages.

Appendix Figures S3 to S6: individual AA $\delta^{15}N$ variation

The following **Figures S3, S4, S5, S6** present the CSIA-AA nitrogen isotopic values (blue points, blue line) along with the mol% AA for each individual amino acid measured in this study plotted using the distance from the coral's edge as the x-axis. The figures are separated into different supplemental figures based on the behavior of the $\delta^{15}N$ values particularly in the outermost 0-10 mm, with increased values in the outer edge (S2 – Asp, Lys, Gly), more variable amino acids yet still positive values (S3 – Ala, Val), variable but more negative values (S4 – Ile, Thr, Glx, Pro), and those that are variable about the mean from the inner >10 mm (S5 – Tyr, Phe). We also calculated the $\delta^{15}N$ average standard deviations for the error of each amino acid and the $\delta^{15}N$ propagated error calculated for the whole subfossil coral (n=12) from the standard deviations from each individual sample using $\sqrt{((AA_{1mm})^2+(AA_{2.8mm})^2+\ldots+(AA_{35mm})^2)}$. We note that while on the individual AA level there is greater variation, greater analytical variation is expected for more degraded or complex matrixes, and variation observed between values in similar coral regions is within propagated error. Because it is difficult to interpret a single AA isotope value taken in isolation with confidence, the averaged values for general regions presented in the main text are the best reflection of values of any given AA in a given coral region.

Appendix Figure 2-S3. Increasing $\delta^{15}N$ and mol% AA from inner to outer layers for **A)** Asp ($\delta^{15}N$ average standard deviation ±0.23‰, propagated error ±0.96‰), **B)** Lys ($\delta^{15}N$ average standard deviation ±0.43‰, propagated error ±1.98‰), and **C)** Gly ($\delta^{15}N$ average standard deviation ±0.15‰, propagated error ±0.71‰). All three amino acids had a significant $\delta^{15}N$ and mol% AA trend towards increasing values from inner to outer layers. Error bars indicate standard deviation of the individual sample runs (analytical error).

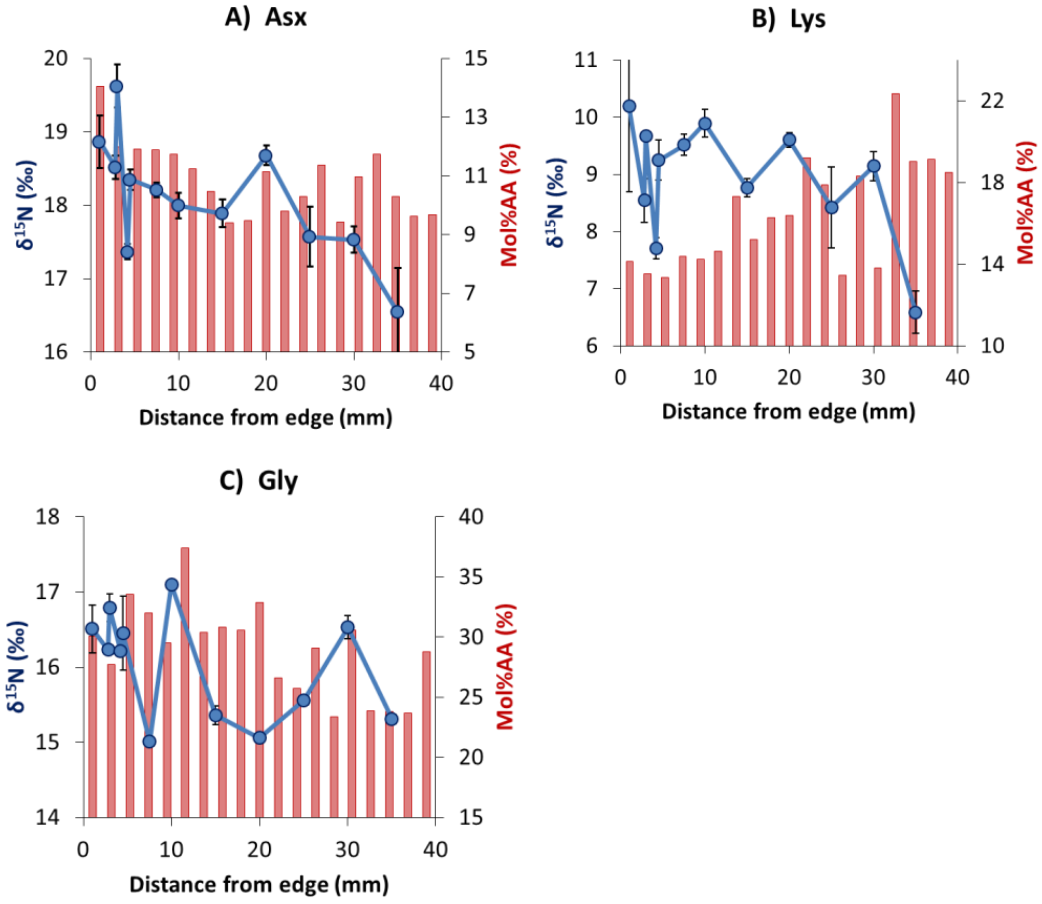

Appendix Figure 2-S4. Variable AAs in outer 10 mm with more positive $\delta^{15}N$ values compared to inner >10 mm for amino acids **A)** Ala ($\delta^{15}N$ average standard deviation ±1.04‰, propagated error ±4.09‰), **B)** Val ($\delta^{15}N$ average standard deviation ±0.30‰, propagated error ±1.13‰), **C)** Ser ($\delta^{15}N$ average standard deviation ±0.68‰, propagated error ±3.22‰), **D)** Leu ($\delta^{15}N$ average standard deviation ±1.00‰, propagated error ±5.43‰). When binned between the 0-10 mm and >10 mm sampling depths, the outermost 0-10 mm was statistically elevated in $\delta^{15}N$ compared to the inner most layers. Error bars indicate standard deviation of the individual sample runs (analytical error).

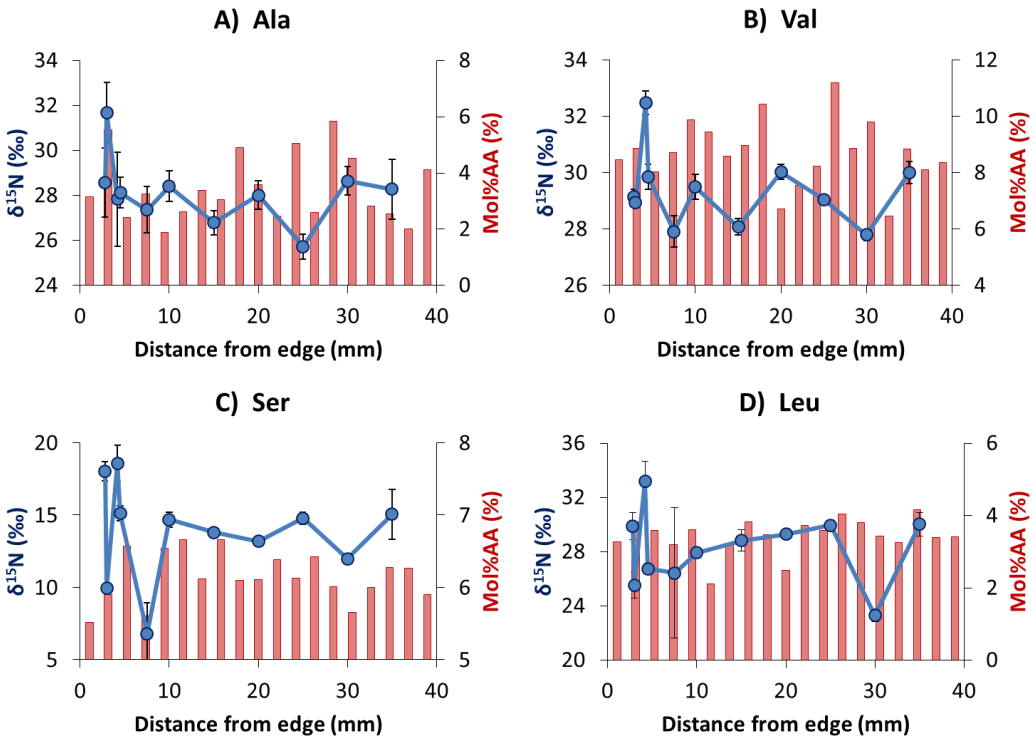

Appendix Figure 2-S5. Variable AAs in outer 10 mm with more negative $\delta^{15}N$ values compared to inner >10 mm. **A)** Ile ($\delta^{15}N$ average standard deviation ±1.50‰, propagated error ±6.88‰), **B)** Thr ($\delta^{15}N$ average standard deviation ±0.80‰, propagated error ±3.29‰), **C)** Glx ($\delta^{15}N$ average standard deviation ±0.42‰, propagated error ±1.60‰), **D)** Pro ($\delta^{15}N$ average standard deviation ±0.57‰, propagated error ±2.34‰). When comparing between the 0-10 mm and >10 mm sampling depths, the outermost 0-10 mm was statistically elevated in $\delta^{15}N$ compared to the inner most layers. Error bars indicate standard deviation of the individual sample runs (analytical error).

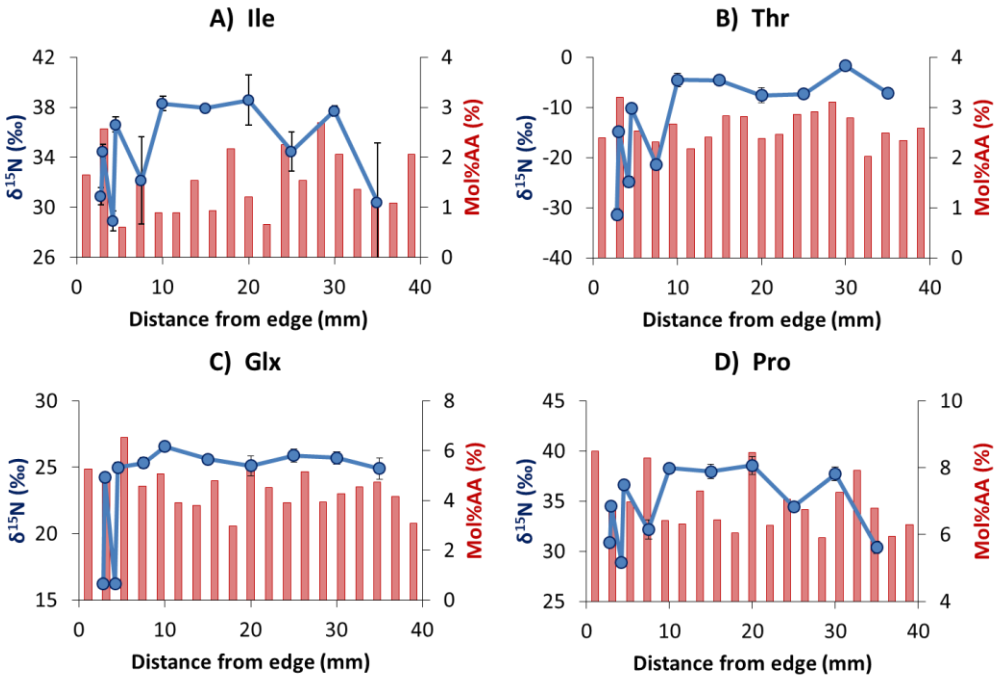

Appendix Figure 2-S6. Variable AAs in outer 10 mm hovering around the average $\delta^{15}N$ of the inner layers (>10mm) includes the amino acids **A)** Tyr ($\delta^{15}N$ average standard deviation ±0.80‰, propagated error ±3.29‰) and **B)** Phe ($\delta^{15}N$ average standard deviation ±0.88‰, propagated error ±3.29‰). No statistically significant trends in $\delta^{15}N$ values for Tyr or Phe, however Tyr does show a significant trend in molar % values declining from the inner to outer layers.

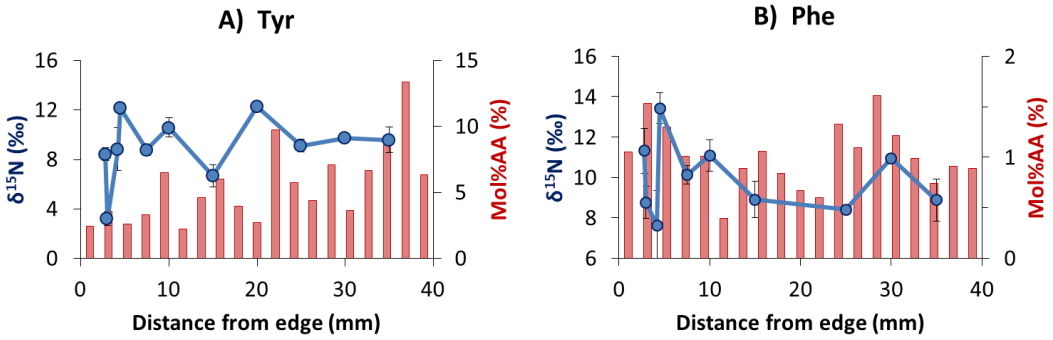

Appendix Figure 2-S7: Comparison of alternative methods to calculate trophic position using different correction factors as well as the amino acids Glu and Phe. The

"Coral Specific" formulation is presented in the main manuscript.

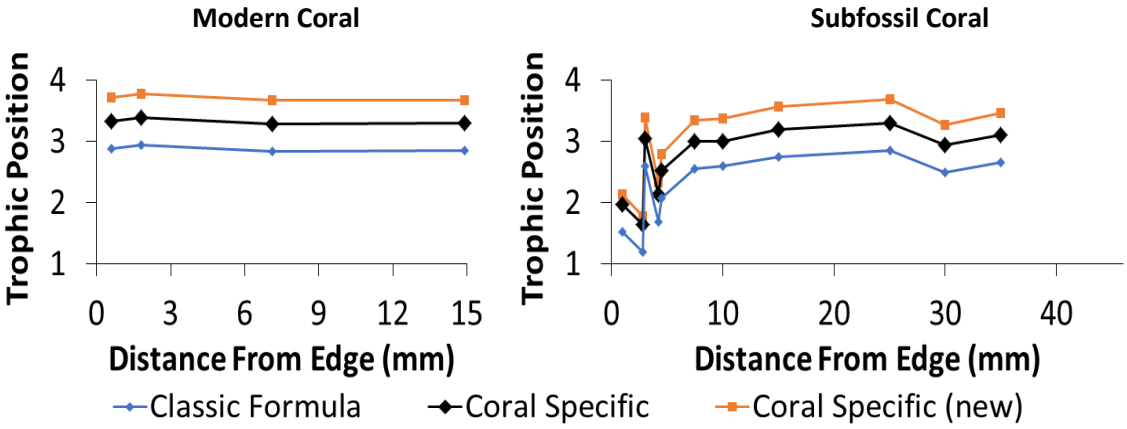

"Classic Formula": TP = 1+(($\delta^{15}N_{Glu}$-$\delta^{15}N_{Phe}$-Beta)/$TDF_{Glu-Phe}$), after Chikaraishi et al., 2009; where δ^{15}N(Glu-Phe) = measured offset between Glu and Phe δ^{15}N; 3.4‰ is the Beta value (Glu-Phe) expected for phytoplankton at base of food web; 7.6‰ is the Trophic Discrimination Factor (TDF) between Glu and Phe for a single trophic transfer, and 1 is added to account for the base of the food web. Therefore this formulation would indicate phytoplankton as TP = 1, a primary consumer would be TP = 2, and so on.

"Coral Specific": Equation from McMahon et al. 2018 which examined Hawaiian Gold Corals (*K. Haumeaae*) where TP = 1+((($\delta^{15}N_{Glu}$+δ_coral)-$\delta^{15}N_{Phe}$-Beta))/$TDF_{Glu-Phe}$, using a correction value for Glu (∂_coral) of 3.4‰, and the beta (3.4) and TDF (7.6) is the same as the "Classic" calculation.

"Coral Specific – New": Utilizing the equation from McMahon et al. 2018, TP = 1+((($\delta^{15}N_{Glu}$+δ_coral)-$\delta^{15}N_{Phe}$-Beta))/$TDF_{Glu-Phe}$, but with a beta value of 3.3±1.8‰ (Ramirez et al. 2021), and a trophic discrimination factor of 6.6±1.7‰ (Nielsen et al. 2015).

There are a variety of ways to calculate trophic position using Glu and Phe amino acids and different correction factors. Regardless of which calculation used, the pattern remains the same while the value changes. When compared to Chikarashi's classical formulation, the coral specific calculations which take into account an extra skeletal fractionation of Glu during assimilation have higher estimates for trophic position. We note that Shen et al., (2021) independently estimated the TDF of *Isididae*, a taxon of octocorals which produce a similar proteinaceous skeletal matrix, as 7.9. Finally, we note that the trophic position using the meta-analysis of Rameriz et al., 2021, and the TDF of Nielsen overlap within uncertainty of the specific formulation proposed by McMahon et al., 2018.

Appendix Figure 2-S8. Degradation proxies plotted alongside the sedimentary degradation index (bottom) for the modern coral (blue) and the fossil coral (red).

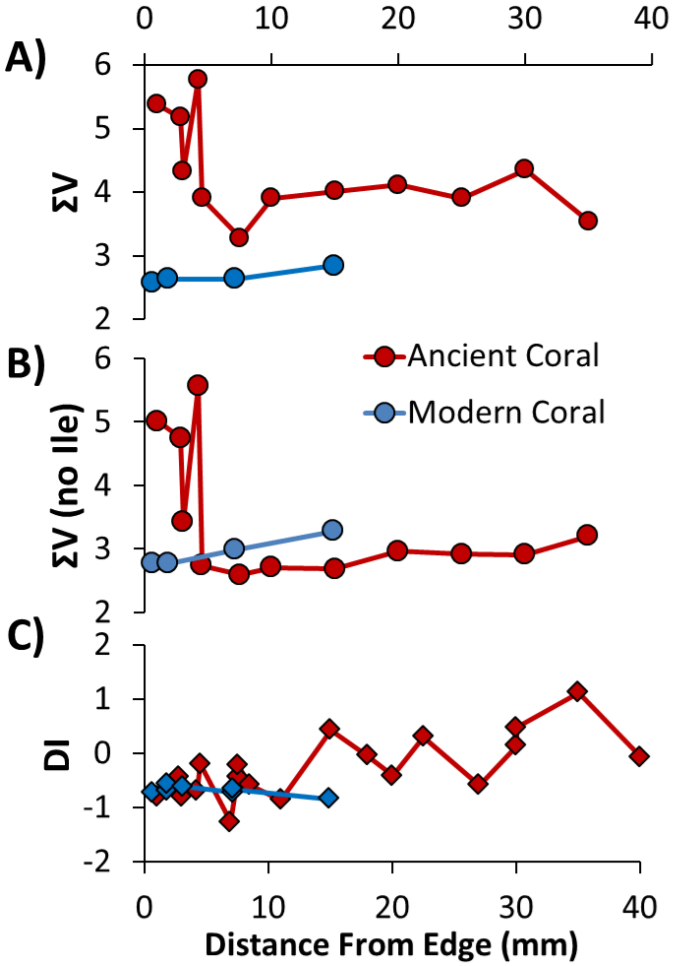

A) The ∑V parameter is a proxy for total heterotrophic amino acid resynthesis of proteinaceous material (McCarthy et al., 2007), and was calculated using the most common formula, bashed on the average deviation of $\delta^{15}N$ values of the trophic amino acids Ala, Val, Leu, Ile, Pro, Asx, Glx: $\sum V = 1/n \sum |X\_i|$ where X_i is the offset in δ15N of each individual amino acid from the average ($X_i = \delta^{15}N_i - AVG\ \delta^{15}N_i$), and n is the number of amino acids used in the calculation. Fossil coral plotted in red, modern coral plotted in blue.

B) ∑V values when Ile is excluded from the calculation.

C) Sedimentary Degradation Index (DI) after Dauwe et al. 1999. According to Dauwe (1999), fresh phytoplankton and/or bacteria from sediment traps have a value of 1-1.5, Margin sediment values of -0.3 to 1, Pelagic deep sea sediment values of < -1. Thr/Asp/Gly has a negative effect on the degradation index while Phe/Ile/Leu/Tyr has a more positive effect.

As detailed in the main manuscript, ∑V parameter does appear to show the outer layers of the fossil coral being more degraded. The amino acid Ile seems to distinctly show a difference between the modern and fossil skeletons, impacting the ∑V parameter. Without Ile in the calculation, the inner layers of the fossil coral (>10mm) appear to have a ∑V value similar to the modern skeleton, signaling preservation of the amino acid signatures and not microbial fractionation.

We also plot the sedimentary degradation index as it is a commonly used degradation proxy, which does show higher values for the fossil coral in the inner layers, which would indicate a 'fresher' and better preserved signature compared to the outermost layers. We note there is no offset between the modern and fossil coral. The degradation index, being created for sedimentary organic matter, as currently constructed, is likely not appropriate for the proteinaceous coral matrix. Future research exploring a proteinaceous deep-sea coral matrix specific index is warranted.

Appendix Figure 2-S9. CSIA-AA values of the different corals used in this study compared to live-collected bamboo corals and phytoplankton particulate organic matter (POM) collected from deep sea sediment traps from Monterey Bay, California (Shen et al. 2021) as well as phytoplankton species more representative of the North Pacific Subtropical Gyre which were grown in 1 L cultures (average of Synechococcus, Prochlorococcus, Trichodesmium; McCarthy et al. 2013). A) Normalized $\delta^{15}N$ CSIA-AA values for corals and plankton. Note that there are no published values for Tyr for phytoplankton so coral normalized values have been recalculated without Tyr. This study finds similar patterns as the offset between bamboo corals and particulate organic matter where trophic AAs are higher, while source AAs and Thr are lower than POM (Shen et al. 2021). Due to the trophic fractionation within corals, offsets between corals and plankton are expected and similar offsets have been found for primary consumers in feeding studies (McMahon and McCarthy, 2016). B) Measured $\delta^{15}N$ CSIA-AA values for source amino acids comparing this study with bamboo corals and POM collected from Monterey Bay (Shen et al. 2021). Planktonic source values are incorporated into the skeletons of corals with little to no trophic fractionation and are thus the best amino acids to track changing nitrate sources when using measured values rather than normalized values. The offset between live collected bamboo and gold corals fits with expectations based on different oceanic regions (margin vs oligotrophic gyre). C) Normalized $\delta^{13}C$ CSIA-AA values. Essential amino acids are those that have little to no fractionation through food webs and have been used to track primary productivity (Shen et al. 2021).

(Figure on the next page)

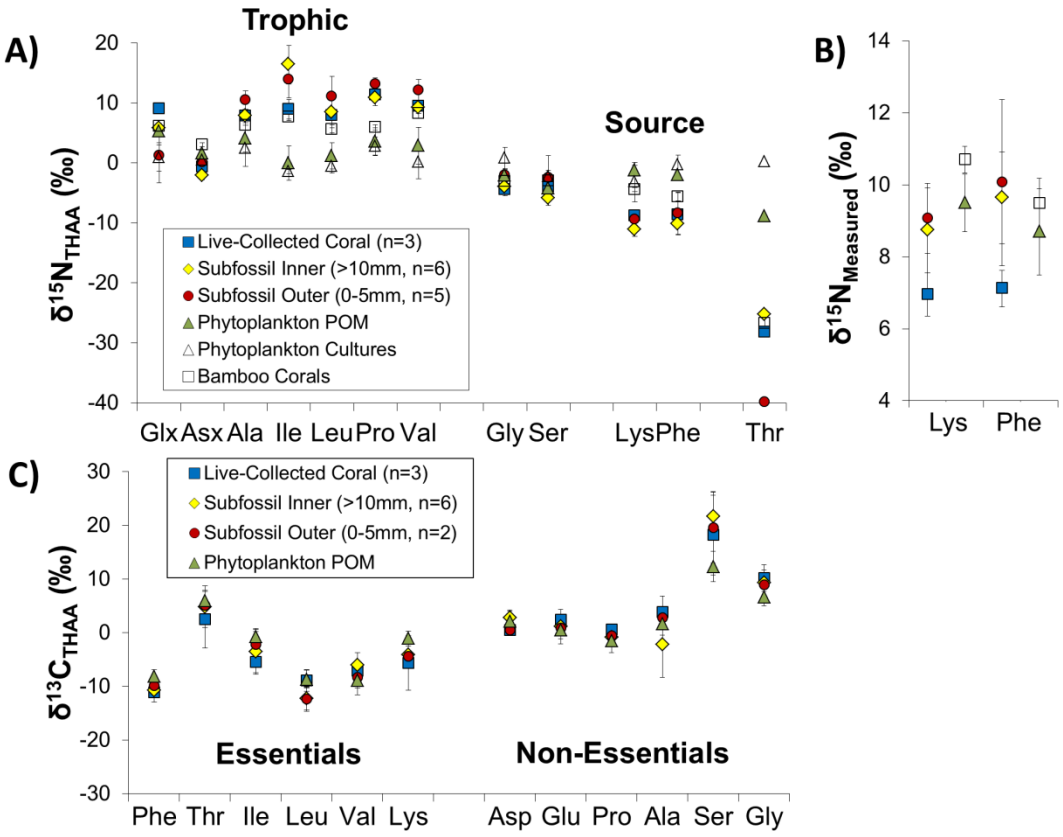
A)
Trophic
Source
δ15NTHAA (‰)
Live-Collected Coral (n=3)
Subfossil Inner (>10mm, n=6)
Subfossil Outer (0-5mm, n=5)
Phytoplankton POM
Phytoplankton Cultures
Bamboo Corals
Glx Asx Ala Ile Leu Pro Val Gly Ser Lys Phe Thr
B)
δ15NMeasured (‰)
Lys Phe
C)
δ13CTHAA (‰)
Live-Collected Coral (n=3)
Subfossil Inner (>10mm, n=6)
Subfossil Outer (0-5mm, n=2)
Phytoplankton POM
Essentials
Non-Essentials
Phe Thr Ile Leu Val Lys Asp Glu Pro Ala Ser Gly

Chapter 3 Supplemental Figures:

Appendix Figure 3-S1. Calculations of N* based on C:N:P data from Martiny et al. (2014). N* is calculated from the equation PON – 16*POP + 2.9 utilizing data from 50 m (left) and 100 m (right). Higher values (>3) are more indicative of regions where N_2-fixation may occur.

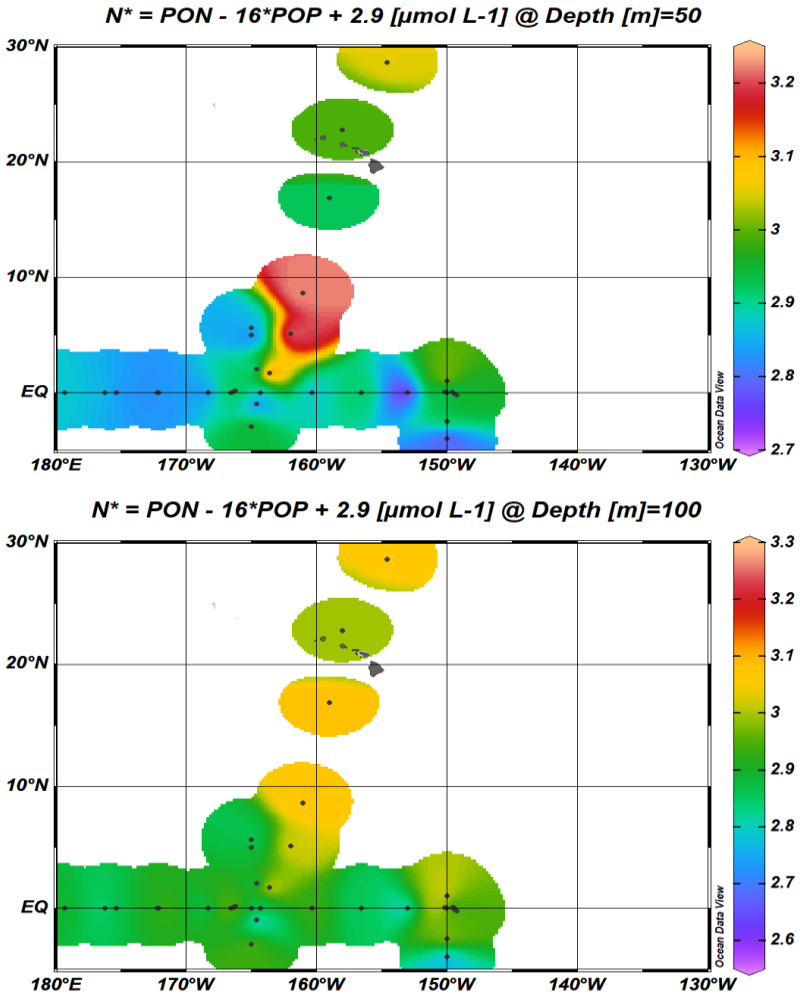

Appendix Figure 3-S2. Calibrated ages (Cal yr BP) based on radiocarbon data with the x-axis being depth in cm from the coral's outer edge for the subfossil Kingman 2 coral.

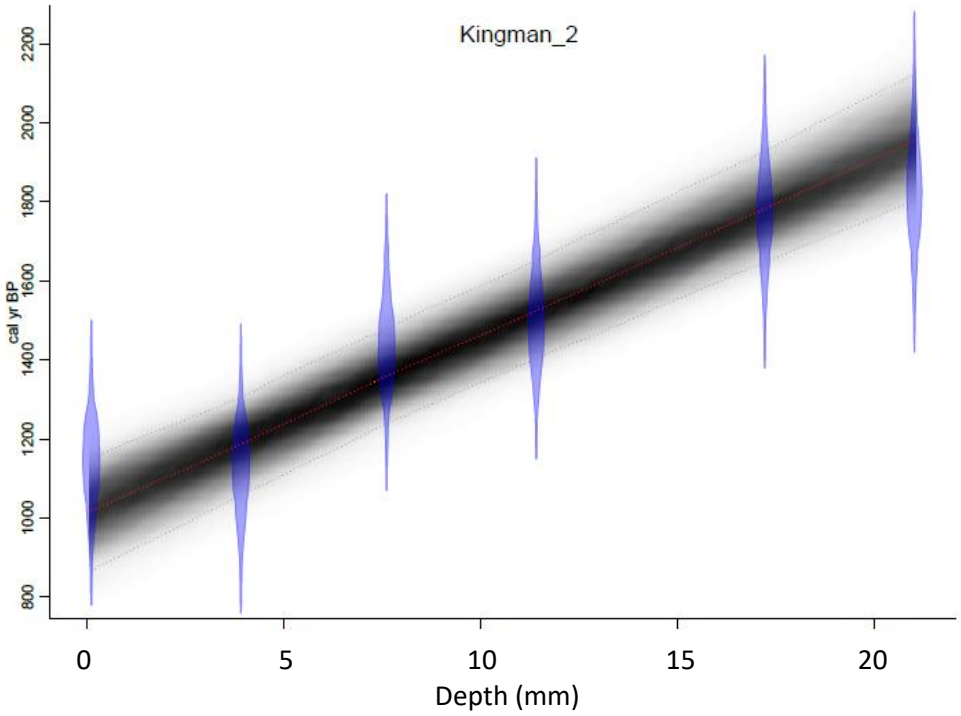

Appendix Figure 3-S3. Calibrated ages (Cal yr BP) based on radiocarbon data with the x-axis being depth in cm from the coral's outer edge for the live-collected Kingman 1 coral. The collection date of 2007 was assumed for 0 mm and set as the intercept for creating a linear age model.

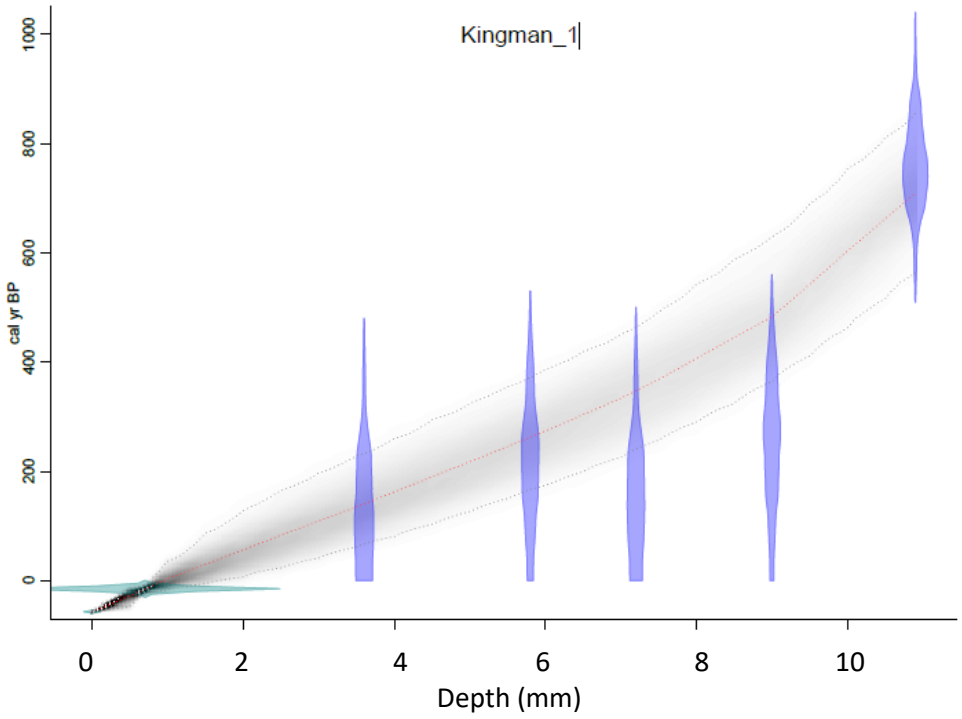

Appendix Figure 3-S4. Correlation between $\delta^{15}N$ and $\delta^{13}C$ bulk values for the two coral specimens, which are both significant for K1 (p = 4.18E-20) and K2 (p = 5.91E-43).

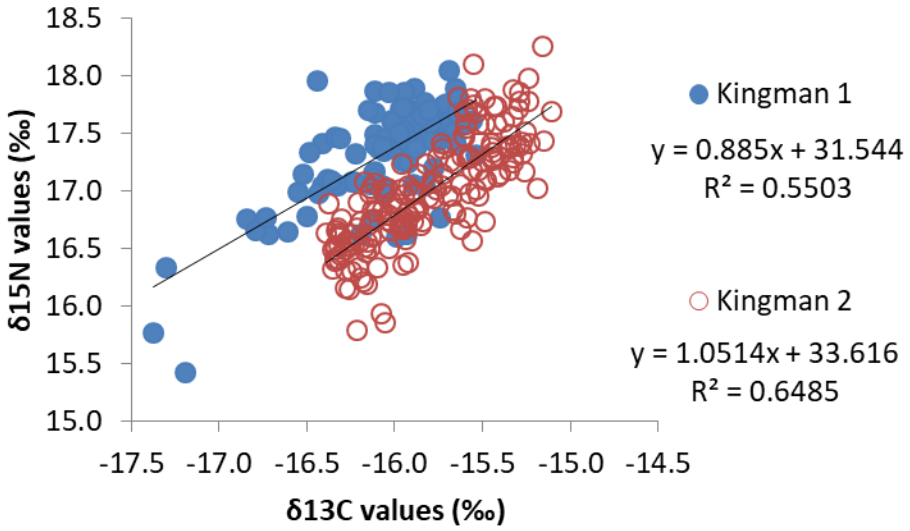

Appendix Figure 3-S5. Correlations between bulk $\delta^{15}N$ and $\delta^{15}N_{Phe}$ values, examined in multiple ways. Kingman 1 all indicates all five data points for the K1 coral, which are not significantly correlated. Utilizing only three data points of K1 appear to hold a positive correlation (p = 0.024). Kingman 2 all indicates the four data points have a similar non-significant correlation. The data points seem to plot with five data points above a bulk $\delta^{15}N$ value of 17‰ (labeled Kingman (5pts)) which are positively correlated (p = 0.169) and four data points below 17‰ (labeled Kingman (4pts)) which are negatively correlated (p = 0.089). Open and closed symbols designate different machines.

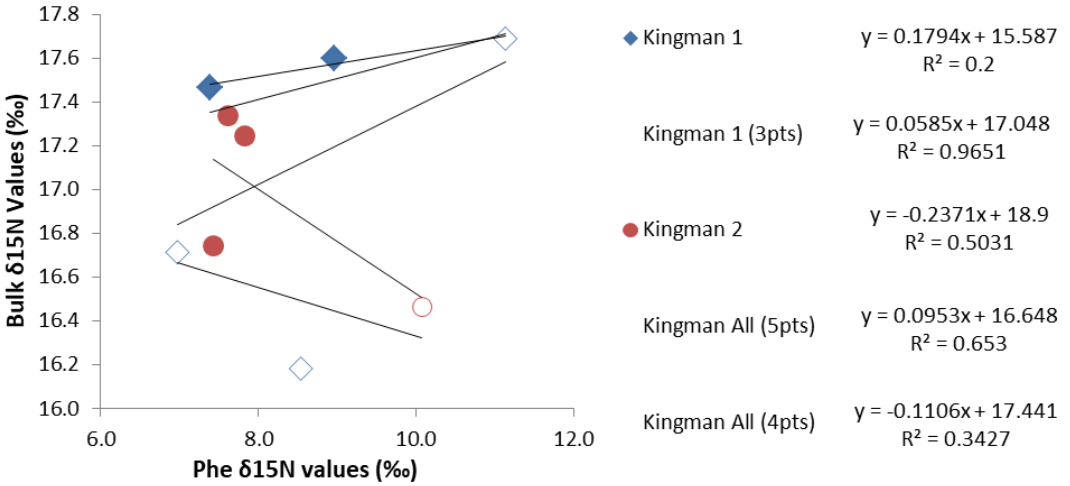

Appendix Figure 3-S6. Trophic position and $\delta^{15}N_{Phe}$ correlations examined overall and in individual corals. These trends are significant for all coral (n=9, p = 0.002), K1 (n= 4, p= 0.023), and K1 (n= 5, p= 0.079).

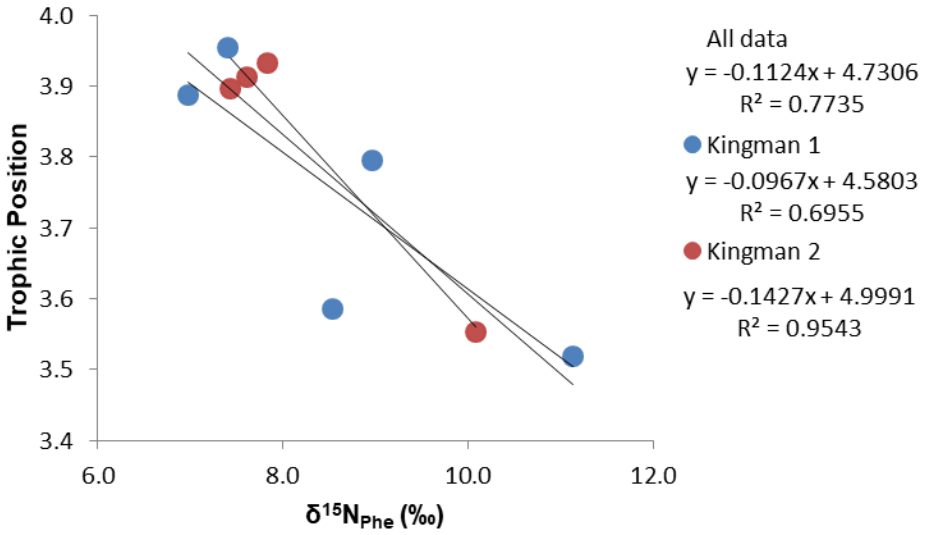

Appendix Figure 3-S7. Degradation tests to exclude the outermost 2.5 mm layers of K2. A) C/N ratio where the outermost layer of K2 reaches a high of 3.3, above the typical threshold for gold corals (2.8-3.0; Glynn et al. 2022). B) Coral bulk $\delta^{13}C$ values and acidified results (yellow diamonds), similar in magnitude to other subfossil corals and suggestive of ~7-8% calcite in the outermost layer of K2. C) The degradation proxy ∑V, with values of 3.2-3.7, consistent with range found previously for well-preserved Hawaiian specimens (Sherwood et al. 2014).

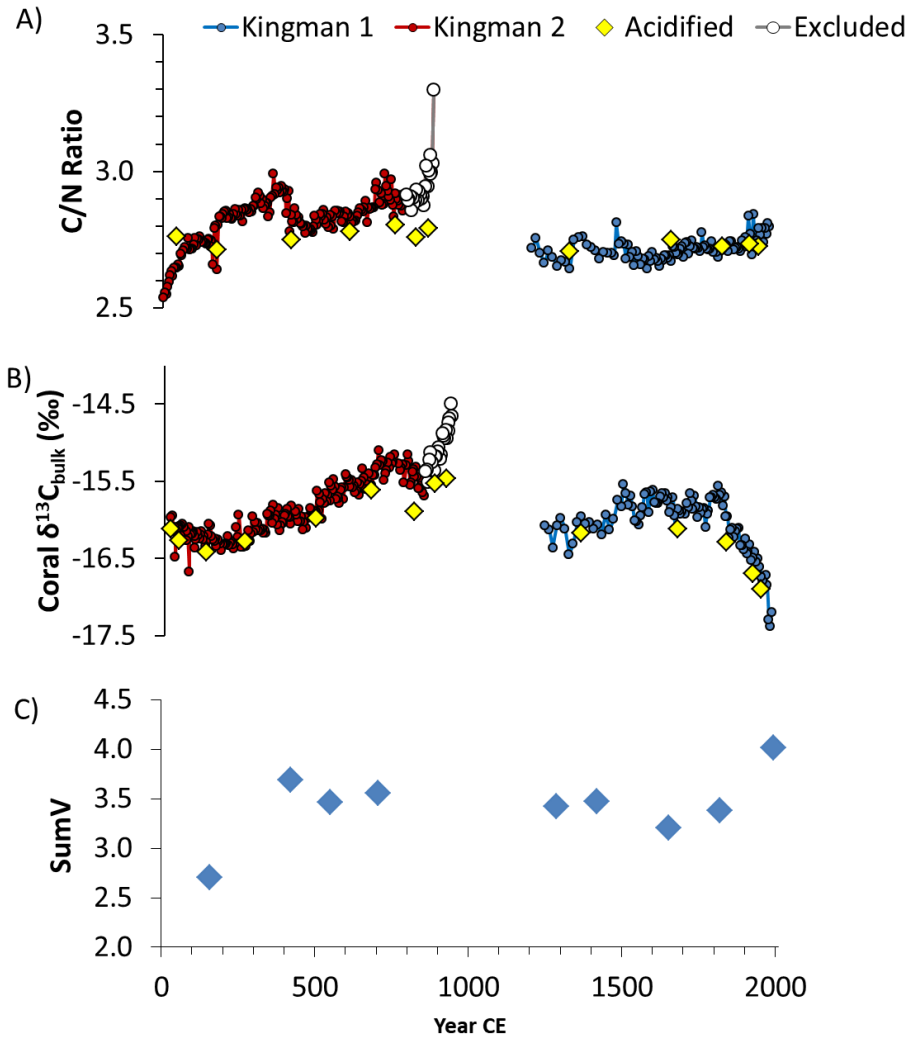

Appendix Figure 3-S8. Spectral analysis for the Kingman 2 - older subfossil coral $\delta^{15}N$ values. The 95% confidence level is seen in the upper right corner, indicating the peak at ~40-60 year is significant.

Appendix Figure 3-S9. Spectral analysis of the Kingman 1 – modern coral $\delta^{15}N$ values. The 95% confidence level is seen in the upper right corner, indicating the peak ~40-60 year does not reach the 95% confidence level.

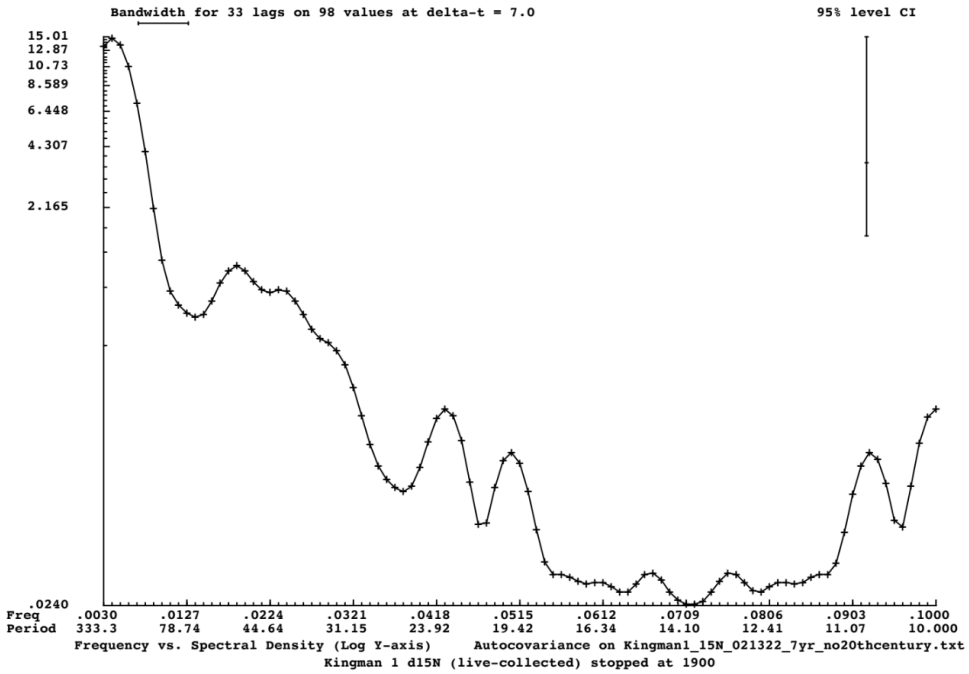

Appendix Figure 3-S10. Regime shift detection detected using the methodology of Rodionov (2004) which uses a sequential t-test to determine regimes and can detect shifts in both the mean level of fluctuations and the variance (see methods section). A) Coral $\delta^{15}N$ values with black lines indicating regime shifts. B) Coral $\delta^{13}C$ values and black lines indicating regime shifts.

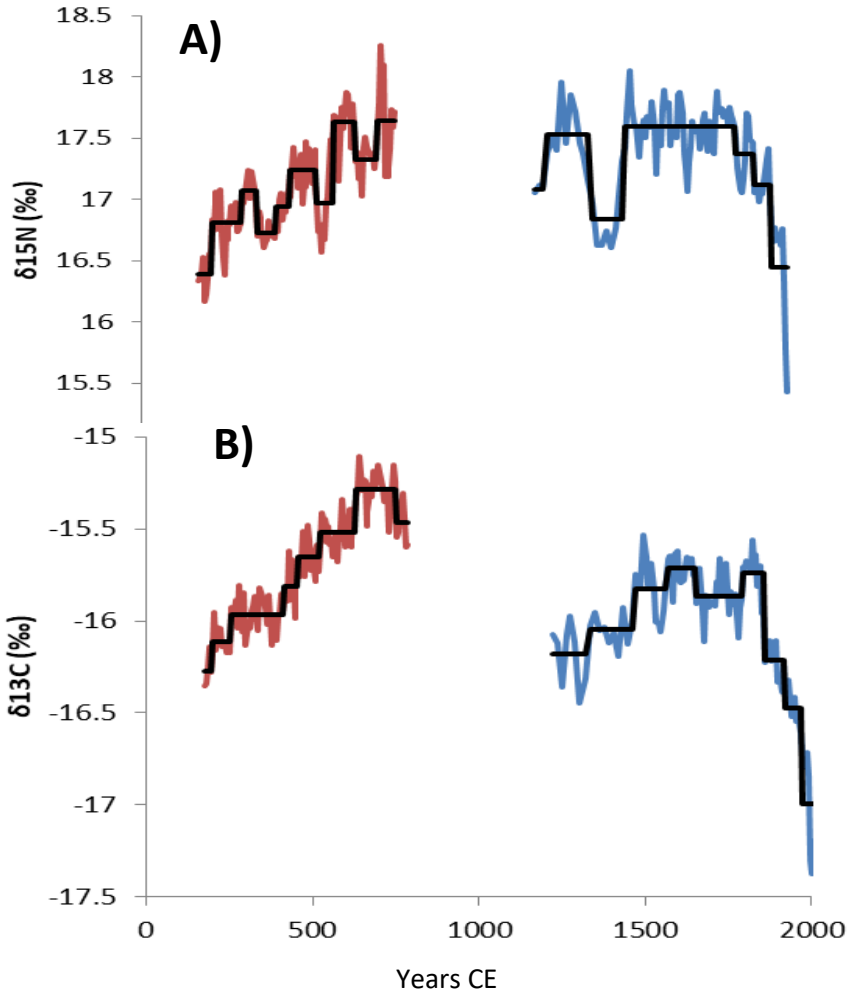

Figure X-1. Artistic representation of how phytoplankton in the surface ocean are eventually exported into the deep sea where the living polyps on corals consume the organic matter. The signature of the organic matter is then routed into the skeleton matrix where the chemical signatures can then be utilized to reconstruct changes in the marine environment. Artwork by Danielle S. Glynn in 2018.

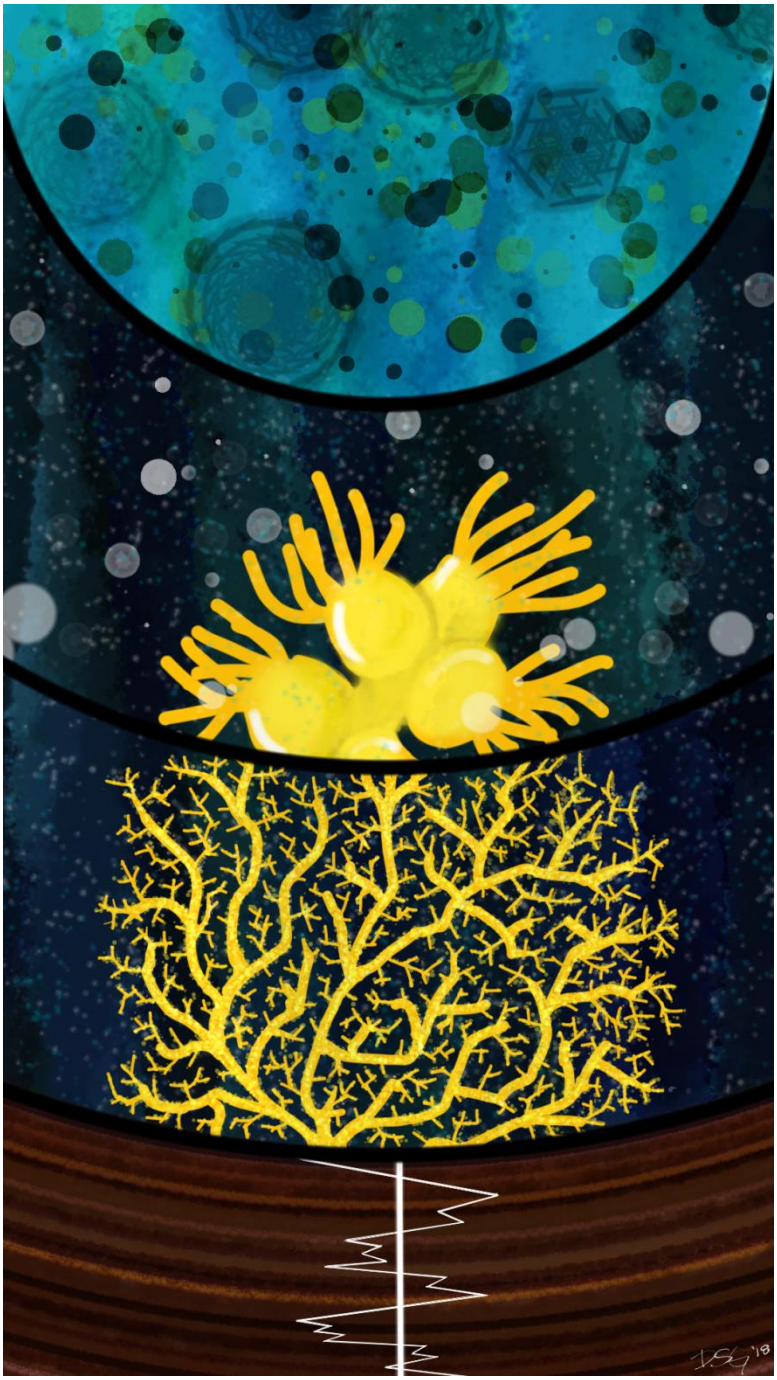

Figure X-2. Artistic representation of how deep sea corals are relatively similar to sediment traps as both can be used in the study of export production in the oceans. As climate has warmed (note the yellow to red transition at the top of the image, indicative of cooler to warmer temperatures), there have been changes in food web dynamics as a transition from larger (left) to smaller celled organisms (right) as more stratified conditions in the open ocean environment became prevalent (like in the North Pacific Subtropical Gyre). This can impact food web dynamics, such as contributing to a transition from fish to jellyfish. Artwork by Danielle S. Glynn in 2018.

Chapter 1 Tables

Appendix Table 1-1. *K. haumeaae* radiocarbon data. All analysis performed at Lawrence Livermore National Laboratory, following previously established radiocarbon methods for proteinaceous deep-sea corals (Roark et al., 2009, Guilderson et al. 2013). Briefly, this involves converting acid-pretreated coral samples to CO_2 via sealed tube combustion before being reduced to graphite in the presence of an iron catalyst and hydrogen gas (Vogel et al., 1987). Results are reported as Fraction Modern, including both a background and $\delta^{13}C$ correction (cf. Reimer et al., 2004), and as conventional radiocarbon years as per Stuiver and Polach, 1977. A constant ΔR of -28±4 (Druffel et al., 2001) was used for age modeling.

Coral	CAMS ID	ID #	Distance (mm)	$\delta^{13}C$ (‰)	Fraction Modern	error	^{14}C age	error	Model Age (yr BP)	95% Confidence interval	Model Age (yr CE)
Lanikai 1	166951	2	0.2	-15.92	0.9046	0.006	805	50	451	97	1499
	166952	18	1.8	-16.49	0.8859	0.004	975	40	589	69	1361
(PV585	166953	35	3.5	-16.6	0.8647	0.007	1170	70	747	100	1203
Ger8)	166955	69	6.9	-16.77	0.8278	0.003	1520	35	1072	90	878
	166956	86	8.6	-16.6	0.8191	0.004	1605	35	1203	72	747
	166957	103	10.3	-16.73	0.8006	0.003	1785	30	1325	59	625
	166958	120	12	-16.92	0.7932	0.003	1860	30	1419	69	531
	166959	137	13.7	-17.15	0.7846	0.003	1950	30	1503	79	447
	166960	154	15.4	-17	0.7918	0.003	1875	35	1582	98	368
	166961	171	17.1	-17.11	0.7793	0.004	2005	40	1691	123	259
Lanikai 2	166962	17	1.7	-16.22	0.7347	0.003	2475	35	2001	117	-51
	166963	35	3.5	-16.09	0.7488	0.003	2325	35	2069	106	-119
(PV585	166964	53	5.3	-16.34	0.737	0.003	2450	40	2152	97	-202
F4A1)	166965	71	7.1	-16.32	0.722	0.002	2615	30	2239	93	-289
	166966	89	8.9	-16.64	0.7304	0.003	2525	35	2312	96	-362
	166967	107	10.7	-16.63	0.7122	0.003	2725	35	2413	94	-463
	166968	125	12.5	-16.68	0.709	0.003	2765	40	2507	112	-557
Lanikai 3	168323	12	1.2	-15.16	0.6276	0.003	3740	45	3489	124	-1539
	168324	35	3.5	-15.65	0.6392	0.004	3595	50	3581	104	-1631
(PV585	168325	58	5.8	-16.03	0.6322	0.002	3685	30	3682	94	-1732
GER5)	168326	81	8.1	-16.01	0.6212	0.002	3825	30	3801	89	-1851
	168327	127	12.7	-16.45	0.6068	0.003	4015	45	4036	96	-2086
	168328	150	15	-16.38	0.6067	0.003	4015	40	4147	97	-2197
	168329	173	17.3	-16.59	0.6005	0.002	4095	35	4280	102	-2330
	168330	196	19.6	-16.58	0.5798	0.002	4380	30	4455	100	-2505
	168331	220	22	-16.67	0.5796	0.003	4380	45	4589	96	-2639
	168332	242	24.2	-16.68	0.5739	0.002	4460	35	4713	95	-2763
	168333	263	26.3	-16.77	0.5621	0.003	4630	45	4837	109	-2887
	168333	263		0.5621	0.0029	-437.9	2.9	4630	45	4220.7	101

Appendix Table 1-2. *K. haumeaae* $\delta^{13}C$ and $\delta^{15}N$ bulk data and C:N ratios. All analysis performed at the Stable Isotope Lab of the University of California Santa Cruz using VPDB and N_2 air as standards for $\delta^{13}C$ and $\delta^{15}N$ respectively. Any samples with an identification ending in "D" are duplicate analyses and those ending with "A" are acidified samples (see Fig. S3). Samples with a * symbol in ID were excluded from analysis due to an abnormal C:N ratio (below 2.72 or above 3.00), an estimated mass of under 20 μg N (which approaches the limit of detection for $\delta^{15}N$ on an EA-IRMS), or over concerns of calcite contamination as per the results of the acidification test. Samples labled L1 stand for Lanikai 1 (youngest subfossil), L2 for Lanikai 2 (intermediate age), and L3 for Lanikai 3 (oldest subfossil).

ID	depth (mm)	Year (CE)	95% CI (yrs)	$\delta^{13}C$ (‰)	$\delta^{15}N$ (‰)	C:N Ratio
L1_1*	0.1	1508	101	-15.78	10.72	3.07
L1_1D*	0.1	1508	101	-15.83	11.36	2.87
L1_2*	0.2	1499	97	-15.92	10.57	3.03
L1_3*	0.3	1490	93	-16.09	10.20	3.14
L1_4*	0.4	1481	91	-16.12	10.58	3.00
L1_5*	0.5	1473	92	-16.04	10.67	2.95
L1_6*	0.6	1464	95	-16.21	10.44	3.02
L1_7*	0.7	1456	91	-16.31	10.15	3.11
L1_8*	0.8	1447	87	-16.31	10.46	2.98
L1_9*	0.9	1439	84	-16.28	10.78	2.96
L1_10*	1	1430	85	-16.43	10.56	3.08
L1_10D*	1	1430	85	-16.47	10.66	2.88
L1_11*	1.1	1421	87	-16.54	10.54	3.10
L1_12*	1.2	1413	81	-16.37	10.75	2.94
L1_13*	1.3	1404	77	-16.53	10.52	3.05
L1_14	1.4	1396	74	-16.42	10.76	2.97
L1_15*	1.5	1388	73	-16.57	10.57	3.03
L1_16*	1.6	1379	74	-16.62	10.49	3.03
L1_17*	1.7	1370	71	-16.62	10.52	3.04
L1_18	1.8	1361	69	-16.49	10.69	3.00
L1_19*	1.9	1351	70	-16.53	10.56	3.03
L1_20	2	1342	74	-16.50	10.71	2.95
L1_21*	2.1	1332	80	-16.63	10.68	3.04
L1_22	2.2	1323	80	-16.59	10.71	2.96
L1_23	2.3	1314	81	-16.56	10.61	2.94
L1_24	2.4	1305	84	-16.64	10.44	2.99
L1_25*	2.5	1295	90	-16.68	10.46	3.08
L1_25D	2.5	1295	90	-16.56	10.47	2.88
L1_26	2.6	1287	96	-16.68	10.61	2.93
L1_27*	2.7	1278	94	-16.70	10.50	3.02

ID	depth (mm)	Year (CE)	95% CI (yrs)	$\delta^{13}C$ (‰)	$\delta^{15}N$ (‰)	C:N Ratio
L1_28	2.8	1268	94	-16.62	10.43	2.97
L1_29	2.9	1259	95	-16.62	10.24	2.97
L1_30	3	1250	99	-16.51	10.23	2.91
L1_31	3.1	1241	103	-16.56	9.98	2.94
L1_32*	3.2	1232	100	-16.69	9.71	3.08
L1_33	3.3	1222	98	-16.70	9.97	2.96
L1_34	3.4	1213	98	-16.61	9.93	2.98
L1_35	3.5	1203	100	-16.60	10.04	2.94
L1_36	3.6	1194	104	-16.59	9.90	2.94
L1_37	3.7	1184	102	-16.53	9.95	2.95
L1_38	3.8	1174	102	-16.55	9.99	2.94
L1_39	3.9	1165	104	-16.58	9.95	2.90
L1_40	4	1155	107	-16.64	9.98	2.93
L1_41	4.1	1145	113	-16.62	10.03	2.92
L1_42	4.2	1136	111	-16.54	9.72	2.96
L1_43	4.3	1126	110	-16.73	10.31	2.95
L1_44*	4.4	1116	112	-16.69	10.08	3.01
L1_45	4.5	1106	115	-16.70	10.29	2.92
L1_45D	4.5	1106	115	-16.65	10.00	2.85
L1_46	4.6	1097	120	-16.68	10.26	2.88
L1_47	4.7	1088	117	-16.69	9.91	2.91
L1_48	4.8	1078	115	-16.79	10.27	2.97
L1_49*	4.9	1068	116	-16.68	9.99	3.01
L1_50	5	1058	118	-16.53	9.93	2.92
L1_51	5.1	1049	121	-16.66	10.09	2.94
L1_52	5.2	1039	118	-16.67	10.23	2.91
L1_53	5.3	1030	116	-16.68	10.12	2.88
L1_54	5.4	1020	116	-16.59	9.96	2.94
L1_55	5.5	1010	117	-16.69	10.05	2.89
L1_56	5.6	1000	120	-16.63	9.90	2.88
L1_57	5.7	991	115	-16.63	10.06	2.93
L1_58	5.8	981	112	-16.55	10.04	2.91
L1_59	5.9	972	111	-16.66	9.94	2.93
L1_60	6	962	111	-16.62	9.87	2.91
L1_61	6.1	953	112	-16.63	9.77	2.96
L1_62	6.2	943	107	-16.67	9.77	2.99
L1_63	6.3	933	103	-16.72	9.80	2.98

ID	depth (mm)	Year (CE)	95% CI (yrs)	$\delta^{13}C$ (‰)	$\delta^{15}N$ (‰)	C:N Ratio
L1_64	6.4	924	101	-16.58	9.76	2.96
L1_65	6.5	914	100	-16.66	9.92	2.93
L1_66	6.6	904	101	-16.70	9.91	2.92
L1_67	6.7	896	96	-16.66	9.87	2.94
L1_68	6.8	887	92	-16.68	9.80	2.94
L1_69	6.9	878	90	-16.77	9.85	2.88
L1_70*	7	869	90	-17.11	9.70	3.05
L1_71	7.1	860	92	-16.95	9.70	2.98
L1_72	7.2	852	89	-16.83	9.81	2.97
L1_73	7.3	845	87	-16.67	9.90	2.87
L1_74	7.4	837	86	-16.79	9.92	2.90
L1_75	7.5	830	88	-16.78	9.83	2.90
L1_76	7.6	823	90	-16.67	9.83	2.84
L1_77	7.7	815	86	-16.71	9.77	2.86
L1_77D	7.7	815	86	-16.59	9.77	2.83
L1_78	7.8	807	83	-16.84	9.83	2.88
L1_79	7.9	800	81	-16.80	9.78	2.85
L1_80	8	792	81	-16.81	9.76	2.85
L1_81	8.1	785	83	-16.70	9.81	2.86
L1_82	8.2	777	77	-16.68	9.66	2.88
L1_83	8.3	770	74	-16.58	9.61	2.86
L1_84	8.4	762	72	-16.56	9.72	2.83
L1_85	8.5	755	71	-16.56	9.89	2.86
L1_86	8.6	747	72	-16.60	9.72	2.86
L1_87	8.7	740	69	-16.64	9.91	2.83
L1_88	8.8	732	68	-16.56	9.70	2.86
L1_89	8.9	725	68	-16.65	9.86	2.88
L1_90D	9	717	70	-16.77	9.71	2.93
L1_90	9	717	70	-16.66	9.84	2.86
L1_91	9.1	710	74	-16.71	9.82	2.87
L1_92	9.2	703	71	-16.79	10.00	2.84
L1_93	9.3	695	69	-16.71	10.15	2.81
L1_94	9.4	688	69	-16.76	10.26	2.81
L1_95	9.5	681	70	-16.89	10.30	2.84
L1_96	9.6	674	73	-16.80	9.98	2.86
L1_97	9.7	667	68	-16.69	10.26	2.85
L1_98	9.8	659	65	-16.76	9.10	2.84
L1_99	9.9	652	63	-16.63	9.25	2.78

ID	depth (mm)	Year (CE)	95% CI (yrs)	$\delta^{13}C$ (‰)	$\delta^{15}N$ (‰)	C:N Ratio
L1_100	10	645	63	-16.64	9.35	2.78
L1_101	10.1	638	65	-16.80	9.46	2.78
L1_102	10.2	632	61	-16.82	9.04	2.81
L1_103	10.3	625	59	-16.73	9.21	2.79
L1_104	10.4	619	59	-16.83	9.39	2.81
L1_105	10.5	613	60	-16.83	8.97	2.83
L1_106	10.6	606	63	-16.76	9.08	2.87
L1_107	10.7	601	62	-16.72	9.12	2.83
L1_108D	10.8	596	62	-16.89	8.92	2.81
L1_108	10.8	596	62	-16.71	9.24	2.78
L1_109	10.9	590	63	-16.82	9.23	2.83
L1_110	11	585	65	-16.77	9.34	2.78
L1_111	11.1	579	68	-16.70	9.52	2.77
L1_112	11.2	574	67	-16.77	9.51	2.80
L1_113	11.3	569	66	-16.84	9.12	2.97
L1_114	11.4	564	66	-16.96	9.52	2.78
L1_115	11.5	558	68	-16.89	9.75	2.81
L1_116	11.6	553	70	-17.04	9.24	-
L1_117	11.7	548	68	-16.91	9.64	2.74
L1_118	11.8	542	67	-16.78	9.68	2.79
L1_119	11.9	537	67	-16.85	9.45	2.88
L1_120	12	531	69	-16.92	9.63	2.81
L1_121	12.1	526	71	-16.76	9.57	2.85
L1_122	12.2	521	70	-16.67	9.64	2.82
L1_123	12.3	516	70	-16.71	9.56	2.81
L1_124	12.4	511	71	-16.79	9.77	2.80
L1_125	12.5	506	73	-16.85	9.92	2.78
L1_126	12.6	501	75	-16.79	9.56	2.80
L1_127	12.7	496	74	-16.78	9.33	2.79
L1_128	12.8	491	74	-16.82	9.25	2.85
L1_129*	12.9	486	75	-17.79	9.13	3.21
L1_130D	13	481	76	-16.90	9.22	2.86
L1_130	13	481	76	-16.91	9.07	2.80
L1_131	13.1	476	78	-16.95	9.03	2.84
L1_132	13.2	471	77	-17.01	8.99	2.82
L1_133	13.3	466	76	-16.98	9.12	2.84

ID	depth (mm)	Year (CE)	95% CI (yrs)	$\delta^{13}C$ (‰)	$\delta^{15}N$ (‰)	C:N Ratio
L1_134	13.4	461	77	-17.10	9.18	2.86
L1_135	13.5	457	78	-17.10	9.56	2.84
L1_136	13.6	452	80	-17.11	9.40	2.86
L1_137	13.7	447	79	-17.15	9.33	2.85
L1_138	13.8	442	80	-17.03	9.41	2.80
L1_139	13.9	437	81	-17.11	9.43	2.73
L1_140	14	432	83	-17.16	9.37	2.87
L1_141	14.1	428	85	-17.14	9.34	2.85
L1_142	14.2	423	85	-16.96	9.24	2.87
L1_143	14.3	419	86	-17.23	9.20	2.79
L1_144	14.4	414	87	-16.91	9.33	2.88
L1_145	14.5	410	89	-17.11	9.08	2.81
L1_146	14.6	405	92	-16.74	8.85	2.94
L1_147	14.7	401	91	-17.10	9.26	2.86
L1_148	14.8	396	92	-16.98	9.46	2.84
L1_149	14.9	392	93	-17.08	9.61	2.81
L1_150D	15	387	95	-17.00	9.61	2.88
L1_150*	15	387	95	-17.02	9.39	2.71
L1_151	15.1	383	97	-17.04	9.32	2.88
L1_152	15.2	378	96	-17.05	9.52	2.88
L1_153	15.3	373	96	-16.89	9.63	2.89
L1_154	15.4	368	98	-17.00	9.65	2.85
L1_155	15.5	364	99	-17.19	9.51	2.89
L1_156	15.6	359	102	-17.06	9.82	2.77
L1_157	15.7	352	102	-17.12	9.86	2.81
L1_158	15.8	346	103	-17.12	9.70	2.75
L1_159	15.9	339	105	-17.05	9.67	2.80
L1_160	16	333	108	-17.11	9.88	2.87
L1_161	16.1	326	112	-17.11	9.34	2.86
L1_162	16.2	319	111	-17.00	9.54	2.79
L1_163	16.3	313	112	-17.06	9.30	2.86

ID	depth (mm)	Year (CE)	95% CI (yrs)	$\delta^{13}C$ (‰)	$\delta^{15}N$ (‰)	C:N Ratio
L1_164	16.4	306	113	-16.93	9.75	2.75
L1_165	16.5	299	116	-17.06	9.02	2.93
L1_166	16.6	292	119	-17.11	9.06	2.91
L1_166D	16.6	292	119	-16.93	9.15	2.91
L1_167	16.7	286	118	-17.04	9.26	2.83
L1_168	16.8	279	118	-17.04	9.10	2.82
L1_169	16.9	272	118	-17.05	9.09	2.82
L1_170	17	266	120	-17.03	9.34	2.81
L1_171	17.1	259	123	-17.11	9.27	2.74
L1_172	17.2	250	123	-17.03	9.19	2.78
L1_173	17.3	241	126	-17.01	8.76	2.88
L1_174	17.4	232	131	-16.93	8.90	2.81
L1_175	17.5	222	137	-17.20	9.18	2.82

ID	depth (mm)	Year (CE)	95% CI (yrs)	$\delta^{13}C$ (‰)	$\delta^{15}N$ (‰)	C:N Ratio
L2_1*	0.1	27	135	-16.32	9.85	3.53
L2_2*	0.2	22	133	-17.01	9.18	3.80
L2_3*	0.3	18	132	-15.72	9.01	3.32
L2_4*	0.4	13	131	-15.53	9.32	3.17
L2_5*	0.5	8	131	-15.65	9.54	3.02
L2_6*	0.6	3	130	-15.79	8.94	3.23
L2_7*	0.7	-2	128	-15.94	8.97	3.16
L2_8*	0.8	-7	126	-15.60	8.84	3.06
L2_9*	0.9	-12	125	-15.94	8.86	3.10
L2_10*	1	-17	123	-16.04	9.16	3.04
L2_11*	1.1	-22	123	-16.05	8.68	3.13
L2_12*	1.2	-27	121	-16.18	9.10	3.19
L2_13*	1.3	-32	119	-16.35	9.43	3.05
L2_14*	1.4	-37	118	-16.25	9.33	3.07
L2_15*	1.5	-42	118	-16.29	9.66	3.00
L2_16*	1.6	-47	118	-16.29	9.67	3.01
L2_17*	1.7	-51	117	-16.22	9.59	2.93
L2_18*	1.8	-55	116	-16.36	9.41	3.00
L2_18D*	1.8	-55	116	-16.22	9.56	2.90
L2_19*	1.9	-59	115	-16.34	9.31	3.01
L2_20*	2	-63	115	-16.23	9.47	2.92
L2_21*	2.1	-67	115	-16.21	9.07	3.08
L2_22	2.2	-71	114	-16.08	9.51	2.94
L2_23*	2.3	-75	113	-16.26	9.55	3.02
L2_24	2.4	-78	112	-16.15	9.80	2.92
L2_25	2.5	-82	112	-15.88	9.60	2.96
L2_26*	2.6	-86	112	-15.63	9.56	3.02
L2_27*	2.7	-89	110	-15.83	9.38	3.02
L2_28*	2.8	-93	109	-15.46	9.48	3.03
L2_29	2.9	-97	109	-	-	-
L2_30	3	-100	109	-16.26	8.94	2.99
L2_31	3.1	-104	108	-16.31	8.71	2.98
L2_32	3.2	-108	107	-16.44	9.01	2.93
L2_33	3.3	-112	106	-16.32	8.69	2.92
L2_34	3.4	-115	106	-16.32	8.55	3.00

ID	depth (mm)	Year (CE)	95% CI (yrs)	$\delta^{13}C$ (‰)	$\delta^{15}N$ (‰)	C:N Ratio
L2_35	3.5	-119	106	-16.09	8.72	2.85
L2_36	3.6	-123	105	-16.05	9.00	2.91
L2_36D	3.6	-123	105	-16.06	9.22	2.84
L2_37	3.7	-128	104	-16.24	9.60	2.90
L2_38	3.8	-132	103	-	-	-
L2_39	3.9	-137	102	-	-	-
L2_40	4	-142	103	-16.44	9.67	2.88
L2_41	4.1	-146	103	-	-	-
L2_42	4.2	-151	102	-	-	-
L2_43	4.3	-156	101	-16.38	8.68	2.85
L2_44D	4.4	-160	101	-16.64	9.20	2.88
L2_44	4.4	-160	101	-16.23	8.73	2.86
L2_45*	4.5	-165	101	-16.28	8.46	3.01
L2_46	4.6	-170	102	-16.24	8.77	2.84
L2_47	4.7	-174	100	-16.23	8.83	2.82
L2_48	4.8	-179	99	-15.97	8.39	2.89
L2_49	4.9	-184	98	-16.17	8.50	2.85
L2_50	5	-188	99	-16.18	8.74	2.93
L2_51	5.1	-193	99	-16.28	9.03	2.88
L2_52	5.2	-198	98	-16.19	9.12	2.87
L2_53	5.3	-202	97	-16.34	9.27	2.86
L2_54	5.4	-207	96	-16.38	9.42	2.88
L2_54D	5.4	-207	96	-16.28	9.48	2.81
L2_55	5.5	-212	97	-16.33	9.49	2.82
L2_56	5.6	-217	97	-16.45	9.26	2.94
L2_57	5.7	-222	96	-16.44	9.41	2.92
L2_58	5.8	-226	95	-16.44	9.23	2.97
L2_59	5.9	-231	95	-16.42	9.39	2.87
L2_60	6	-236	96	-16.48	9.40	2.88
L2_61	6.1	-240	97	-16.65	9.26	2.93
L2_62	6.2	-245	95	-16.42	9.41	2.89
L2_63	6.3	-250	95	-16.56	9.11	2.87
L2_64	6.4	-255	94	-16.44	9.47	2.83
L2_65	6.5	-260	94	-16.24	9.68	2.87

ID	depth (mm)	Year (CE)	95% CI (yrs)	$\delta^{13}C$ (‰)	$\delta^{15}N$ (‰)	C:N Ratio
L2_66	6.6	-264	95	-16.44	9.71	2.85
L2_67	6.7	-269	93	-16.54	9.14	3.00
L2_68	6.8	-274	93	-16.41	9.17	2.84
L2_69	6.9	-279	92	-16.40	9.05	2.88
L2_70	7	-284	92	-16.43	9.14	2.89
L2_71	7.1	-289	93	-16.32	8.95	2.86
L2_72	7.2	-293	92	-16.13	8.68	2.86
L2_73D	7.3	-297	92	-16.22	8.87	2.91
L2_73	7.3	-297	92	-16.34	8.91	2.90
L2_74	7.4	-301	93	-16.68	9.62	2.93
L2_75	7.5	-305	94	-16.58	9.57	2.86
L2_76	7.6	-309	96	-16.53	9.49	2.88
L2_77	7.7	-313	95	-16.72	9.58	2.86
L2_78	7.8	-317	95	-16.67	9.57	2.77
L2_79	7.9	-321	95	-16.59	9.59	2.81
L2_80	8	-325	96	-16.42	9.47	2.88
L2_81	8.1	-329	97	-16.39	9.50	2.88
L2_82	8.2	-333	96	-16.45	9.57	2.84
L2_83	8.3	-337	96	-16.66	9.45	2.84
L2_84	8.4	-341	97	-16.54	9.20	2.85
L2_85	8.5	-345	97	-16.35	9.05	2.83
L2_86	8.6	-349	97	-16.41	8.97	2.86
L2_87	8.7	-353	97	-16.50	9.31	2.79
L2_88	8.8	-358	96	-16.63	9.44	2.83
L2_89	8.9	-362	96	-16.64	9.47	2.91
L2_90	9	-366	96	-16.74	9.65	2.83
L2_91	9.1	-370	97	-16.96	9.69	2.92
L2_91D	9.1	-370	97	-16.77	8.95	2.83
L2_92	9.2	-376	96	-16.71	9.35	2.83
L2_93	9.3	-382	95	-16.77	8.96	2.91
L2_94	9.4	-388	95	-16.70	9.17	2.86
L2_95	9.5	-393	95	-16.55	9.25	2.84
L2_96	9.6	-399	96	-16.67	9.34	2.82
L2_97	9.7	-405	95	-16.60	9.22	2.87

ID	depth (mm)	Year (CE)	95% CI (yrs)	$\delta^{13}C$ (‰)	$\delta^{15}N$ (‰)	C:N Ratio
L2_98	9.8	-411	94	-16.47	9.42	2.84
L2_99	9.9	-417	94	-16.41	9.46	2.83
L2_100	10	-423	95	-16.47	9.63	2.82
L2_101	10.1	-429	97	-16.80	9.97	2.81
L2_102	10.2	-434	95	-16.71	10.03	2.80
L2_103	10.3	-440	94	-16.71	9.76	2.81
L2_104	10.4	-446	94	-16.62	9.70	2.81
L2_105	10.5	-452	95	-16.62	9.70	2.79
L2_106	10.6	-458	96	-16.68	9.28	2.85
L2_107	10.7	-463	94	-16.63	9.45	2.77
L2_108	10.8	-469	94	-16.48	9.16	2.76
L2_109	10.9	-474	95	-16.58	9.10	2.77
L2_110	11	-479	96	-16.43	9.18	2.75
L2_111	11.1	-485	98	-16.76	9.21	2.82
L2_112	11.2	-490	98	-16.63	8.99	2.83
L2_113	11.3	-495	98	-16.54	9.29	2.73
L2_114	11.4	-501	99	-16.52	9.34	2.73
L2_115	11.5	-506	101	-	-	-
L2_116	11.6	-511	104	-	-	-
L2_117	11.7	-516	103	-16.65	9.32	2.81
L2_118	11.8	-521	103	-16.52	9.14	2.75
L2_119	11.9	-527	105	-16.50	9.30	2.72
L2_120*	12	-532	106	-16.57	9.27	2.70
L2_121*	12.1	-537	109	-16.37	9.18	2.70
L2_122	12.2	-542	108	-16.68	9.12	2.77
L2_123	12.3	-547	109	-16.47	8.92	2.78
L2_124	12.4	-552	110	-16.48	9.17	2.74
L2_125	12.5	-557	112	-16.68	9.13	2.80
L2_126	12.6	-562	114	-16.39	9.05	2.96
L2_126D	12.6	-562	114	-16.78	8.68	2.79
L2_127	12.7	-567	114	-16.57	9.10	2.74
L2_128	12.8	-572	116	-16.66	8.99	2.83
L2_129	12.9	-578	117	-16.74	8.78	2.79
L2_130	13	-583	119	-16.83	9.03	2.84

ID	depth (mm)	Year (CE)	95% CI (yrs)	$\delta^{13}C$ (‰)	$\delta^{15}N$ (‰)	C:N Ratio
L3_1*	0.1	-1483	139	-15.88	11.85	3.62
L3_2*	0.2	-1489	137	-15.13	12.19	3.26
L3_3*	0.3	-1494	135	-14.94	12.04	3.13
L3_4*	0.4	-1499	133	-15.05	12.08	3.06
L3_5*	0.5	-1504	132	-15.15	11.92	3.05
L3_6*	0.6	-1510	132	-14.86	11.25	3.03
L3_6D*	0.6	-1510	132	-16.39	10.57	2.86
L3_7*	0.7	-1515	130	-14.93	10.97	3.07
L3_8*	0.8	-1520	128	-15.02	11.22	3.07
L3_9*	0.9	-1525	127	-15.07	11.10	3.00
L3_9D*	0.9	-1525	127	-15.18	11.64	2.99
L3_10*	1	-1530	126	-15.13	10.80	3.03
L3_11*	1.1	-1535	125	-15.27	10.82	3.04
L3_12*	1.2	-1539	124	-15.16	11.01	3.02
L3_13*	1.3	-1543	123	-15.25	11.24	2.99
L3_14*	1.4	-1548	123	-15.40	10.77	3.01
L3_15*	1.5	-1552	122	-15.40	11.17	2.95
L3_16*	1.6	-1556	123	-15.31	11.12	3.00
L3_17*	1.7	-1560	121	-15.52	11.11	3.02
L3_18*	1.8	-1564	120	-15.42	10.91	2.96
L3_19*	1.9	-1568	119	-15.57	10.98	2.98
L3_20*	2	-1572	118	-15.48	10.78	2.95
L3_21*	2.1	-1576	118	-15.36	10.32	2.96
L3_22*	2.2	-1579	116	-15.35	10.17	2.96
L3_23*	2.3	-1584	115	-15.45	10.74	2.97
L3_24*	2.4	-1587	114	-15.32	10.86	2.95
L3_25*	2.5	-1591	113	-14.76	11.34	2.83
L3_26*	2.6	-1595	114	-15.16	10.87	3.00
L3_27*	2.7	-1599	111	-15.32	11.07	2.98
L3_28*	2.8	-1603	110	-15.47	11.18	2.98
L3_29*	2.9	-1607	109	-15.49	11.03	2.94
L3_30*	3	-1611	109	-15.48	10.92	2.97
L3_31*	3.1	-1615	109	-15.52	10.50	3.03
L3_32*	3.2	-1619	107	-15.57	10.83	2.98
L3_33*	3.3	-1623	106	-15.44	10.51	3.00

ID	depth (mm)	Year (CE)	95% CI (yrs)	$\delta^{13}C$ (‰)	$\delta^{15}N$ (‰)	C:N Ratio
L3_34*	3.4	-1627	105	-15.52	10.85	2.94
L3_35*	3.5	-1631	104	-15.65	10.80	2.96
L3_36*	3.6	-1635	104	-15.76	10.83	2.98
L3_37*	3.6	-1640	103	-15.92	10.92	2.94
L3_38*	3.8	-1644	102	-15.89	10.61	2.96
L3_39	3.9	-1648	101	-15.86	10.64	2.93
L3_40	4	-1653	102	-15.84	10.91	2.91
L3_41	4.1	-1657	102	-15.91	11.01	2.95
L3_42	4.2	-1661	101	-15.73	10.80	2.94
L3_43	4.3	-1666	100	-15.79	10.67	2.96
L3_44	4.4	-1670	100	-15.74	10.59	2.96
L3_45	4.5	-1674	100	-15.69	10.65	2.97
L3_46	4.6	-1679	100	-15.80	10.71	2.94
L3_47	4.7	-1683	99	-15.84	10.71	2.96
L3_48	4.8	-1687	98	-15.78	10.67	2.95
L3_49	4.9	-1692	97	-15.89	10.91	2.96
L3_50	5	-1696	98	-15.84	11.19	2.93
L3_51	5.1	-1701	98	-15.98	11.57	2.97
L3_52	5.2	-1705	97	-15.87	11.40	2.96
L3_52D	5.2	-1705	97	-16.02	11.44	2.94
L3_53	5.3	-1709	96	-15.85	10.70	2.97
L3_55	5.4	-1718	96	-16.10	10.59	2.96
L3_54	5.4	-1714	95	-15.92	10.68	2.92
L3_56	5.6	-1722	97	-16.01	10.71	2.97
L3_57	5.7	-1727	95	-16.04	10.82	2.93
L3_58	5.8	-1732	94	-16.03	10.85	2.94
L3_59	5.9	-1736	94	-15.89	11.13	2.94
L3_60	6	-1741	94	-16.02	11.10	2.94
L3_61	6.1	-1746	95	-15.86	11.14	2.94
L3_62	6.2	-1751	94	-15.85	11.01	2.95
L3_63	6.3	-1756	93	-15.97	10.78	2.94
L3_64	6.4	-1762	92	-16.01	10.70	2.92
L3_65	6.5	-1767	92	-15.76	10.55	2.93
L3_66	6.6	-1773	94	-15.77	10.54	2.92

ID	depth (mm)	Year (CE)	95% CI (yrs)	$\delta^{13}C$ (‰)	$\delta^{15}N$ (‰)	C:N Ratio
L3_67	6.7	-1778	92	-15.79	10.76	2.97
L3_68	6.8	-1783	91	-15.69	10.97	2.91
L3_69	6.9	-1788	90	-15.75	10.75	2.97
L3_69D	6.9	-1788	90	-15.87	10.86	2.95
L3_70	7	-1794	91	-15.86	10.74	2.93
L3_71	7.1	-1799	92	-15.94	10.56	2.93
L3_72	7.2	-1804	91	-15.92	10.72	2.94
L3_73	7.3	-1810	90	-16.02	10.70	2.95
L3_74	7.3	-1815	90	-15.89	10.78	2.91
L3_75	7.5	-1820	90	-15.99	10.83	2.89
L3_76	7.6	-1825	91	-15.89	10.80	2.91
L3_77	7.7	-1831	89	-15.85	10.95	2.91
L3_78	7.8	-1836	88	-15.94	10.82	2.89
L3_79	7.9	-1841	87	-15.95	11.21	2.94
L3_80	8	-1846	88	-15.80	11.21	2.90
L3_81	8.1	-1851	89	-16.01	11.12	2.93
L3_82	8.2	-1857	88	-15.92	11.09	2.91
L3_83	8.3	-1862	88	-15.87	11.07	2.87
L3_84	8.4	-1867	88	-15.75	10.97	2.88
L3_85	8.5	-1872	89	-15.77	11.00	2.91
L3_86	8.6	-1878	91	-15.80	10.57	2.89
L3_87	8.7	-1883	91	-15.87	10.82	2.88
L3_87D	8.7	-1883	91	-15.97	10.62	2.88
L3_88	8.8	-1888	91	-15.94	10.93	2.89
L3_89	8.9	-1893	91	-15.90	10.89	2.88
L3_90	9	-1898	93	-15.70	11.18	2.86
L3_92	9.1	-1908	94	-16.10	11.16	2.93
L3_91	9.1	-1903	95	-15.90	11.40	2.90
L3_93	9.3	-1913	94	-16.00	11.34	2.94
L3_94	9.4	-1918	95	-15.97	11.28	2.89
L3_95	9.5	-1923	96	-15.80	11.18	2.89
L3_96*	9.6	-1928	98	-15.81	11.50	3.04
L3_97	9.7	-1933	97	-15.86	11.50	2.90
L3_98*	9.8	-1938	96	-15.62	11.10	3.01
L3_99	9.9	-1944	97	-16.16	10.94	3.00
L3_100*	10	-1949	98	-16.00	10.55	3.01
L3_101*	10.1	-1954	100	-16.09	10.81	3.04
L3_102	10.2	-1959	99	-16.45	10.82	2.97
L3_103	10.3	-1964	99	-16.14	10.90	2.92
L3_104	10.4	-1969	99	-16.01	10.77	2.92
L3_105*	10.5	-1974	100	-16.19	10.49	3.03

ID	depth (mm)	Year (CE)	95% CI (yrs)	$\delta^{13}C$ (‰)	$\delta^{15}N$ (‰)	C:N Ratio
L3_106	10.6	-1979	101	-16.15	10.26	2.98
L3_107*	10.7	-1984	100	-15.93	10.48	3.02
L3_107D	10.7	-1984	100	-16.15	10.45	2.95
L3_108	10.8	-1989	99	-15.96	10.77	2.98
L3_109	10.9	-1994	99	-16.17	10.93	2.92
L3_110	11	-1999	100	-16.06	11.10	2.99
L3_111	11.1	-2004	101	-16.05	10.96	2.90
L3_112	11.2	-2009	100	-15.94	10.78	2.84
L3_113	11.3	-2014	98	-16.25	10.42	2.96
L3_114	11.4	-2019	98	-16.34	10.69	2.89
L3_115	11.5	-2024	99	-16.24	10.74	2.89
L3_116	11.6	-2029	100	-16.53	10.85	2.94
L3_117	11.7	-2035	98	-16.23	10.97	2.91
L3_118	11.8	-2040	97	-16.12	11.30	2.85
L3_119	11.9	-2045	98	-16.13	11.26	2.83
L3_120	12	-2050	98	-16.15	10.95	2.91
L3_121	12.1	-2055	99	-16.37	10.72	2.94
L3_122	12.2	-2060	98	-16.11	10.59	2.92
L3_123	12.3	-2065	96	-16.15	10.60	2.85
L3_124	12.4	-2071	96	-16.16	10.48	2.85
L3_125	12.5	-2076	96	-16.36	10.79	2.90
L3_127	12.6	-2086	96	-16.45	10.88	2.96
L3_126	12.6	-2081	97	-16.36	11.14	2.80
L3_128	12.8	-2091	95	-16.43	10.96	2.87
L3_129	12.9	-2096	95	-16.32	10.47	2.97
L3_129D	12.9	-2096	95	-16.27	10.84	2.93
L3_130	13	-2101	96	-16.17	11.39	2.89
L3_131	13.1	-2106	97	-16.24	11.50	2.84
L3_132	13.2	-2111	96	-16.23	11.44	2.84
L3_133	13.3	-2116	95	-16.29	11.80	2.85
L3_134	13.4	-2120	95	-16.42	10.96	2.93
L3_135	13.5	-2125	96	-16.57	10.90	2.94
L3_136	13.6	-2130	97	-16.49	11.15	2.88
L3_137	13.7	-2135	96	-16.39	11.15	2.82
L3_138	13.8	-2139	96	-16.29	10.86	2.88
L3_139	13.9	-2144	96	-16.35	10.90	2.83
L3_140	14	-2149	96	-16.31	10.99	2.88

ID	depth (mm)	Year (CE)	95% CI (yrs)	$\delta^{13}C$ (‰)	$\delta^{15}N$ (‰)	C:N Ratio
L3_141	14.1	-2154	97	-16.16	10.87	2.90
L3_142	14.2	-2159	96	-16.27	11.33	2.84
L3_143	14.3	-2163	95	-16.34	11.39	2.84
L3_144	14.4	-2168	96	-16.39	11.18	2.91
L3_145	14.5	-2173	96	-16.47	10.88	2.93
L3_146*	14.6	-2178	97	-17.10	11.18	3.10
L3_147	14.7	-2183	96	-16.29	10.99	2.86
L3_148D	14.8	-2188	96	-16.21	10.72	2.94
L3_148	14.8	-2188	96	-16.25	11.04	2.84
L3_149	14.9	-2192	96	-16.15	11.31	2.83
L3_150	15	-2197	97	-16.38	11.55	2.79
L3_151	15.1	-2202	98	-16.18	11.19	2.87
L3_152	15.2	-2207	97	-16.28	11.16	2.85
L3_153	15.3	-2213	97	-16.20	11.21	2.85
L3_154	15.4	-2218	97	-16.48	11.07	2.84
L3_155	15.5	-2224	98	-16.31	11.19	2.78
L3_156	15.6	-2229	100	-16.35	11.31	2.84
L3_157	15.7	-2235	98	-16.24	11.29	2.88
L3_158	15.8	-2241	99	-16.22	11.27	2.88
L3_159	15.9	-2247	99	-16.20	11.30	2.87
L3_160	16	-2253	101	-16.40	11.48	2.90
L3_161	16.1	-2259	103	-16.30	11.29	2.82
L3_162	16.2	-2265	102	-16.26	11.25	2.79
L3_163	16.3	-2271	101	-16.29	11.28	2.79
L3_164	16.4	-2277	101	-16.34	10.98	2.87
L3_165	16.5	-2282	102	-16.30	10.93	2.91
L3_166	16.6	-2288	104	-16.34	10.70	2.84
L3_167D	16.7	-2294	103	-16.41	10.65	2.91
L3_167	16.7	-2294	103	-16.55	10.61	2.88
L3_168*	16.8	-2300	102	-14.79	11.70	2.80
L3_169	16.9	-2306	102	-16.53	10.82	2.88
L3_170	17	-2312	103	-16.62	10.54	2.83
L3_171	17.1	-2318	105	-16.50	10.64	2.88
L3_172	17.2	-2324	103	-16.54	10.59	2.84

ID	depth (mm)	Year (CE)	95% CI (yrs)	$\delta^{13}C$ (‰)	$\delta^{15}N$ (‰)	C:N Ratio
L3_173	17.3	-2330	102	-16.59	10.66	2.89
L3_174	17.4	-2336	102	-16.61	10.79	2.84
L3_175	17.5	-2342	103	-16.58	10.57	2.89
L3_176	17.6	-2348	104	-16.76	10.52	2.83
L3_177	17.7	-2355	102	-16.65	10.61	2.85
L3_178	17.8	-2363	102	-16.76	10.50	2.92
L3_179	17.9	-2371	103	-16.62	10.60	2.84
L3_180	18	-2378	105	-16.65	10.75	2.89
L3_181	18.1	-2386	108	-16.60	10.72	2.84
L3_182	18.2	-2394	106	-16.71	10.49	2.90
L3_183	18.3	-2402	105	-16.58	10.88	2.87
L3_184	18.4	-2410	105	-16.62	11.11	2.84
L3_185	18.5	-2418	107	-16.64	10.89	2.92
L3_186	18.6	-2426	109	-16.63	11.09	2.94
L3_186D	18.6	-2426	109	-16.52	11.12	2.89
L3_187	18.7	-2434	106	-16.61	10.96	2.93
L3_188	18.8	-2442	104	-16.59	10.86	2.90
L3_189	18.9	-2450	103	-16.53	10.99	2.90
L3_190	19	-2458	104	-16.58	11.03	2.90
L3_191	19.1	-2466	107	-16.52	11.25	2.89
L3_192	19.2	-2474	103	-16.58	11.15	2.90
L3_193	19.3	-2481	99	-16.60	10.68	2.92
L3_194	19.4	-2489	99	-16.47	10.56	2.91
L3_195	19.5	-2497	99	-16.47	10.28	2.93
L3_196	19.6	-2505	100	-16.58	10.57	2.92
L3_197	19.7	-2512	97	-16.59	10.56	2.89
L3_198	19.8	-2519	96	-16.51	10.61	2.89
L3_199	19.9	-2526	95	-16.55	10.50	2.90
L3_200	20	-2533	96	-16.54	10.75	2.89
L3_201	20.1	-2540	98	-	-	-
L3_202	20.2	-2545	97	-	-	-
L3_203	20.3	-2551	96	-16.53	11.53	2.88
L3_204	20.4	-2556	97	-	-	-
L3_205	20.5	-2561	98	-	-	-

ID	depth (mm)	Year (CE)	95% CI (yrs)	$\delta^{13}C$ (‰)	$\delta^{15}N$ (‰)	C:N Ratio
L3_206	20.6	-2567	99	-	-	-
L3_207	20.7	-2572	98	-	-	-
L3_208	20.8	-2577	97	-	-	-
L3_209	20.9	-2582	97	-	-	-
L3_210	21	-2587	97	-	-	-
L3_211	21.1	-2592	98	-	-	-
L3_212	21.2	-2598	97	-16.65	10.48	2.92
L3_213	21.3	-2603	96	-	10.92	-
L3_214	21.4	-2608	96	-16.67	11.07	2.90
L3_215	21.5	-2613	97	-16.53	11.02	2.89
L3_216	21.6	-2619	98	-16.55	11.16	2.89
L3_217	21.7	-2624	96	-16.65	10.94	2.96
L3_218	21.8	-2629	96	-16.71	11.26	2.96
L3_219	21.9	-2634	96	-16.69	11.05	2.96
L3_220	22	-2639	96	-16.67	10.98	2.90
L3_221	22.1	-2644	98	-16.66	11.07	2.94
L3_222	22.2	-2650	96	-16.62	11.02	2.92
L3_223	22.3	-2655	95	-16.55	10.83	2.94
L3_224	22.4	-2661	95	-16.58	10.74	2.95
L3_225	22.5	-2667	95	-16.44	10.93	2.96
L3_226	22.6	-2672	97	-16.46	10.59	2.99
L3_227	22.7	-2678	96	-16.57	10.65	2.92
L3_227D	22.7	-2678	96	-16.62	10.72	2.91
L3_228	22.8	-2683	96	-16.74	10.73	2.90
L3_229	22.9	-2689	96	-16.81	10.58	2.92
L3_230	23	-2695	97	-16.70	10.68	2.95
L3_231	23.1	-2700	99	-16.92	10.66	2.92
L3_232	23.2	-2706	98	-16.84	10.27	2.93
L3_233	23.3	-2712	97	-16.78	10.19	2.94
L3_234	23.4	-2717	97	-16.76	10.04	2.92
L3_235	23.5	-2723	98	-16.72	10.20	2.90
L3_236	23.6	-2729	99	-16.62	10.34	2.92
L3_237	23.7	-2735	97	-16.88	10.76	2.95
L3_238	23.8	-2740	95	-16.67	10.73	2.91

ID	depth (mm)	Year (CE)	95% CI (yrs)	$\delta^{13}C$ (‰)	$\delta^{15}N$ (‰)	C:N Ratio
L3_239	23.9	-2746	95	-16.66	10.81	2.91
L3_240	24	-2752	95	-16.67	10.85	2.91
L3_241D*	24.1	-2758	96	-16.65	10.64	3.04
L3_241	24.1	-2758	96	-16.73	10.77	2.91
L3_242	24.2	-2763	95	-16.68	10.65	2.92
L3_243	24.3	-2769	93	-16.82	10.65	2.93
L3_244	24.4	-2774	93	-16.88	10.47	2.94
L3_245	24.5	-2780	93	-16.87	10.56	2.93
L3_246	24.6	-2785	94	-16.83	10.68	2.91
L3_247	24.7	-2792	93	-16.90	10.46	2.92
L3_248	24.8	-2797	93	-16.95	10.50	2.91
L3_249	24.9	-2803	94	-16.90	10.60	2.88
L3_250	25	-2809	96	-16.91	10.54	2.93
L3_251	25.1	-2815	98	-16.82	10.69	2.90
L3_252	25.2	-2821	98	-16.77	10.50	2.92
L3_253	25.3	-2827	99	-16.77	10.43	2.90
L3_254	25.4	-2833	100	-16.74	10.32	2.90
L3_255	25.5	-2839	102	-17.12	10.24	2.90
L3_256	25.6	-2845	105	-17.09	10.26	2.91
L3_257	25.7	-2851	105	-17.16	10.43	2.90
L3_258	25.8	-2857	105	-17.10	10.38	2.94
L3_258D	25.8	-2857	105	-17.26	10.36	2.89
L3_259	25.9	-2863	105	-17.02	10.38	2.93
L3_260	26	-2869	107	-16.87	10.58	2.93
L3_261	26.1	-2875	109	-16.84	10.57	2.92
L3_262	26.2	-2881	109	-	-	-
L3_263	26.3	-2887	109	-16.77	10.58	2.93
L3_264	26.4	-2893	109	-	-	-
L3_265	26.5	-2899	111	-	-	-
L3_266	26.6	-2905	113	-	-	-
L3_267	26.7	-2910	114	-16.65	10.28	2.91
L3_268	26.8	-2916	114	-16.74	10.07	2.91
L3_269	26.9	-2921	116	-16.84	10.36	2.93
L3_270	27	-2927	118	-16.65	10.18	2.93
L3_271	27.1	-2932	120	-16.59	10.46	2.92
L3_272D	27.2	-2937	121	-16.53	10.31	2.93
L3_272	27.2	-2937	121	-16.70	10.43	2.92
L3_273*	27.3	-2942	122	-16.89	10.29	3.03
L3_274	27.4	-2947	123	-16.55	10.90	2.92
L3_275	27.5	-2952	125	-16.64	10.93	2.90
L3_276	27.6	-2958	127	-16.67	11.24	2.90

Appendix Table 1-3. Sensitivity of $\delta^{13}C$ according to different environmental variables.

Variable	$\delta^{13}C$ sensitivity	Surface Seasonal Variable Range	Theoretical Seasonal $\Delta\delta^{13}C$	References
Temperature on εp	0.12‰ / °C	24-27 °C	0.36‰	Locarnini et al. 2010, Young et al. 2013
Temperature on δ13Cplankton	0.11‰ / °C *	24-27 °C	0.33‰	Rau et al. 1996
Temperature on δ13Cplankton	0.23‰ / °C	24-27 °C	0.69‰	Rau et al. 1989
Temperature on suspended POC	0.41‰ / °C	24-27 °C	1.23‰	Rau et al. 1992
pH	2.7‰ / 0.1 pH	8.085-8.115 pH	0.08‰	Hinga et al. 1994, Dore et al. 2009
Salinity on εp	0.003‰ / PSU	34.5 – 35.3 PSU	0.002‰	Antonov et al. 2010, Young et al. 2013
δ13C of DIC on εp	0.99‰ / ‰	1.25 – 1.45 ‰	0.20‰	Quay et al. 2003, Young et. al. 2013
pCO2 on εp	0.0003‰ / ppm	20 ppm	0.006‰	Takahashi et al. 2009, Young et al. 2013, Keeling et al. 2004
Species fractionation (εf)	0.55‰ / ‰ *	23.1-25.6‰ (Range for 0-200m)	1.37‰ (not seasonal value)	Rau et al. 1996, Hernes and Benner 2002 (upper 200m)

* Calculated based on equations and values found in Rau et al. 1996.

Chapter 2 Tables

Appendix Table 2-1. Modern (live-collected) coral radiocarbon data and age modeled dates calculated using Calib Calibration 8.1 - (Stuiver et al. 2021) and Marine20 Calibration curve (Heaton et al. 2020; doi: 10.1017/RDC.2020.68.) Sample Coral ID: PV590, from Cross Seamount, Hawaii.

CAMS #	Depth (mm)	$\delta^{13}C$	fraction Modern	±	^{14}C age	± yrs	Age Model Cal Yr BP	1σ error	Age Model (yr CE)	Age Model (yr BP)
157079	0.2	-17.04	1.074	0.004	>Modern				1978	-28
157080	0.3	-17.37	1.086	0.004	>Modern				1971	-21
157081	0.5	-16.74	0.971	0.003	235	25			1958	-8
157082	0.7	-16.70	0.959	0.003	335	25			1944	6
157083	0.9	-16.57	0.942	0.003	480	25	78	77	1931	19
157084	2.5	-16.48	0.935	0.003	540	25	180.5	78.5	1815	135
157085	5	-16.12	0.919	0.003	680	25	334.5	71.5	1698	252
157086	7.5	-15.54	0.926	0.004	615	35	235.5	85.5	1624	326
157087	10.6	-16.36	0.907	0.002	780	25	409.5	66.5	1505	445
157088	12.7	-16.33	0.896	0.003	885	25	496	57	1428	522
157843	14	-16.56	0.896	0.011	890	100	515	103	1383	567

* CAMS# 157843, PV 590 14.0mm was a 40µgC target. This is why the error is larger.

Appendix Table 2-2. Subfossil coral radiocarbon data and age modeled dates (using Stuiver et al. 2021 and Marine20 Calibration curve (Heaton et al. 2020; doi: 10.1017/RDC.2020.68.) Sample Coral ID: PV588 from Cross Seamount, Hawaii.

CAMS #	Depth	d13C	fraction	±	14C age	±	Age Model	1σ error
	mm	‰	Modern				Cal Yr BP	
178842	4	-15.43	0.334	0.006	8820	150	9519	206
178843	9	-16.17	0.308	0.012	9460	320	10364	457
178844	14	-16.10	0.300	0.007	9660	180	10654	277
178845	19	-15.70	0.308	0.006	9450	160	10363	222
178846	24	-16.05	0.307	0.008	9480	200	10412	283
178847	29	-16.07	0.293	0.008	9860	220	10897	307
178848	34	-16.53	0.283	0.006	10130	170	11332	257
178849	39	-16.30	0.282	0.004	10160	130	11356	197
178850	45.5	-16.30	0.272	0.008	10470	230	11777	365

Appendix Table 2-3.1. Modern Cross Seamount Bulk Data – Analyzed in 2011 by Owen Sherwood (Specimen ID: PV590).

depth (mm)	Age Yr CE	Wt % N (%)	wt% C (%)	C:N	δ15N (‰)	δ13C (‰)
0.1	1985	9.09	26.52	2.92	9.04	-17.27
0.2	1978	8.54	24.57	2.88	9.26	-17.04
0.3	1971	8.25	24.92	3.02	9.11	-17.37
0.4	1964	8.74	25.13	2.88	9.08	-16.81
0.5	1958	8.46	24.84	2.94	8.83	-16.74
0.6	1951	8.56	24.92	2.91	8.98	-16.58
0.7	1944	8.32	23.92	2.87	9.13	-16.70
0.8	1938	9.15	26.49	2.89	9.47	-16.78
0.9	1931	8.88	25.61	2.88	9.15	-16.57
1.0	1924	8.62	24.87	2.88	9.28	-16.63
1.1	1916	6.24	18.15	2.91	9.73	-16.57
1.2	1909	10.17	28.79	2.83	9.86	-16.39
1.3	1902	9.80	27.76	2.83	9.62	-16.44
1.4	1895	7.03	20.91	2.97	9.77	-16.74
1.5	1887	8.39	23.98	2.86	9.89	-16.26
1.6	1878	7.69	22.62	2.94	9.66	-16.47
1.7	1871	8.28	23.12	2.79	10.17	-16.26
1.8	1864	8.91	25.09	2.82	10.21	-16.23
1.9	1856	9.33	26.57	2.85	10.09	-16.45
2.0	1849	9.08	25.91	2.85	10.10	-16.40
2.1	1842	9.02	25.65	2.84	10.40	-16.41
2.2	1835	8.43	24.16	2.87	10.33	-16.45
2.3	1828	8.57	24.82	2.90	9.94	-16.54
2.4	1822	8.32	23.99	2.88	10.26	-16.53
2.5	1815	9.00	26.08	2.90	10.32	-16.48
2.6	1809	9.92	28.56	2.88	10.73	-16.50
2.7	1802	9.55	28.09	2.94	11.04	-16.67
2.8	1796	9.98	27.96	2.80	11.43	-16.49
2.9	1791	8.73	24.62	2.82	10.67	-16.50
3.0	1785	9.93	28.65	2.89	10.38	-16.56
3.1	1779	8.99	25.13	2.80	10.91	-16.39
3.2	1774	9.40	27.22	2.90	10.79	-16.81
3.3	1769	8.99	25.60	2.85	11.37	-16.57
3.4	1764	8.92	25.25	2.83	11.59	-16.49
3.5	1759	9.18	26.09	2.84	11.12	-16.48
3.6	1754	10.11	28.54	2.82	11.06	-16.59
3.7	1749	7.59	24.56	3.24	11.40	-16.72
3.8	1745	8.08	26.41	3.27	10.39	-16.74
3.9	1740	NA	NA	NA	NA	NA
4.0	1736	NA	NA	NA	NA	NA

depth (mm)	Age Yr CE	Wt % N (%)	wt% C (%)	C:N	δ15N (‰)	δ13C (‰)
4.1	1732	NA	NA	NA	NA	NA
4.2	1728	6.42	21.40	3.33	10.42	-16.70
4.3	1724	7.94	22.77	2.87	10.62	-16.15
4.4	1720	7.85	22.45	2.86	10.89	-16.00
4.5	1716	7.69	22.14	2.88	11.31	-16.03
4.6	1712	8.37	24.51	2.93	10.97	-16.08
4.7	1709	6.35	19.01	2.99	10.78	-16.06
4.8	1705	9.91	28.55	2.88	11.19	-16.35
4.9	1702	9.29	26.93	2.90	11.04	-16.12
5.0	1698	9.05	26.07	2.88	10.57	-16.12
5.1	1695	8.64	24.77	2.87	10.85	-16.07
5.2	1692	8.93	25.52	2.86	10.76	-16.08
5.3	1688	7.77	22.49	2.89	10.63	-16.02
5.4	1685	8.89	25.37	2.85	10.52	-16.04
5.5	1682	7.62	22.43	2.94	10.85	-16.14
5.6	1679	5.57	16.23	2.91	12.34	-16.77
5.7	1676	7.95	22.32	2.81	11.09	-16.03
5.8	1673	7.99	22.66	2.84	10.76	-15.87
5.9	1670	8.18	23.20	2.84	10.77	-15.82
6.0	1667	7.88	22.99	2.92	10.78	-15.83
6.1	1664	8.79	25.31	2.88	11.01	-15.78
6.2	1661	8.41	23.78	2.83	11.47	-15.91
6.3	1658	9.02	25.46	2.82	11.31	-15.99
6.4	1655	10.17	28.51	2.80	10.88	-15.80
6.5	1652	7.80	22.17	2.84	10.78	-15.68
6.6	1649	7.78	22.43	2.88	10.90	-15.69
6.7	1646	8.28	23.85	2.88	10.97	-15.53
6.8	1643	8.38	23.56	2.81	11.39	-15.71
6.9	1640	8.34	23.90	2.87	11.10	-15.55
7.0	1637	7.93	22.59	2.85	11.37	-15.64
7.1	1634	8.26	23.61	2.86	11.25	-15.63
7.2	1631	7.39	21.13	2.86	11.11	-15.74
7.3	1627	8.31	23.71	2.85	10.88	-15.60
7.4	1624	8.73	24.89	2.85	10.83	-15.53
7.5	1621	6.97	20.01	2.87	10.96	-15.54
7.6	1618	8.05	23.06	2.87	11.21	-15.62
7.7	1614	7.99	22.63	2.83	11.70	-15.69
7.8	1611	8.14	23.71	2.91	11.37	-16.21
7.9	1607	8.36	24.00	2.87	10.98	-15.67
8.0	1604	8.94	23.54	2.63	11.32	-15.97

depth (mm)	Age Yr CE	Wt % N (%)	wt% C (%)	C:N	δ15N (‰)	δ13C (‰)
8.1	1600	14.40	43.48	3.02	11.27	-16.13
8.2	1596	8.53	22.71	2.66	11.34	-15.93
8.3	1593	8.75	23.12	2.64	11.43	-15.98
8.4	1589	8.42	22.24	2.64	11.39	-15.91
8.5	1585	8.46	22.27	2.63	11.37	-16.02
8.6	1581	8.43	22.51	2.67	11.45	-16.15
8.7	1578	8.47	22.63	2.67	11.00	-16.07
8.8	1574	8.35	22.41	2.68	10.88	-16.04
8.9	1569	8.26	21.88	2.65	11.06	-15.98
9.0	1566	8.66	24.45	2.82	11.02	-16.02
9.1	1562	13.18	40.05	3.04	10.81	-16.43
9.2	1558	8.33	22.72	2.73	11.09	-16.02
9.3	1554	NA	NA	NA	NA	NA
9.4	1550	8.62	23.13	2.68	11.26	-16.19
9.5	1546	8.27	22.02	2.66	11.49	-16.33
9.6	1542	8.21	22.11	2.69	11.41	-16.32
9.8	1537	7.21	19.62	2.72	11.31	-16.46
9.9	1533	6.97	18.98	2.72	11.39	-16.30
10.0	1529	8.72	23.20	2.66	11.09	-16.25
10.1	1526	8.51	22.59	2.65	11.12	-16.23
10.2	1522	8.59	22.96	2.67	11.30	-16.23
10.3	1518	8.16	21.83	2.67	11.09	-16.15
10.4	1514	8.43	22.09	2.62	11.82	-16.02
10.5	1509	8.10	21.71	2.68	11.02	-16.11
10.6	1505	8.14	21.45	2.64	11.66	-16.24
10.7	1501	8.24	22.55	2.73	10.73	-16.36
10.8	1497	8.67	23.11	2.67	11.45	-16.26
10.9	1493	8.71	23.32	2.68	11.16	-16.39
11.0	1490	8.68	23.06	2.66	11.05	-16.16
11.1	1486	8.14	21.99	2.70	10.82	-16.20
11.2	1482	8.09	21.91	2.71	10.33	-16.01
11.3	1479	8.00	21.66	2.71	10.43	-16.07
11.4	1475	8.29	22.29	2.69	10.38	-16.13
11.5	1471	8.90	23.66	2.66	10.75	-16.20
11.6	1467	8.69	23.19	2.67	10.79	-16.30
11.7	1463	8.79	24.01	2.73	10.60	-16.33
11.8	1460	13.86	41.52	2.99	10.47	-16.34
11.9	1456	NA	NA	NA	NA	NA
12.0	1453	8.09	22.00	2.72	11.31	-16.30

depth (mm)	Age Yr CE	Wt % N (%)	wt% C (%)	C:N	δ15N (‰)	δ13C (‰)
12.1	1449	8.12	21.98	2.71	11.27	-16.21
12.2	1446	8.55	23.39	2.74	10.97	-16.28
12.3	1442	8.68	23.50	2.71	11.55	-16.43
12.4	1439	8.86	23.78	2.69	11.41	-16.35
12.5	1435	8.66	23.21	2.68	11.04	-16.17
12.6	1432	8.54	22.87	2.68	11.22	-16.32
12.7	1428	8.57	23.18	2.71	11.55	-16.30
12.8	1425	8.31	22.64	2.72	11.65	-16.33
12.9	1421	8.53	23.16	2.72	11.51	-16.34
13.0	1418	8.62	23.08	2.68	11.97	-16.44
13.1	1414	8.65	23.25	2.69	11.93	-16.52
13.2	1411	8.45	22.65	2.68	11.51	-16.52
13.3	1407	NA	NA	NA	NA	NA
13.4	1404	9.11	25.28	2.77	11.76	-16.54
13.5	1400	8.35	22.81	2.73	11.14	-16.69
13.6	1397	8.38	22.53	2.69	11.26	-16.59
13.7	1393	8.52	23.10	2.71	11.08	-16.62
13.8	1390	8.39	22.49	2.68	11.05	-16.58
13.9	1386	8.23	22.50	2.74	10.83	-16.73
14.0	1383	8.27	22.66	2.74	10.72	-16.67
14.1	1379	8.54	23.10	2.70	10.71	-16.56
14.2	1376	8.75	23.61	2.70	11.18	-16.77
14.3	1373	8.38	22.81	2.72	11.03	-17.00
14.4	1369	8.11	21.73	2.68	11.39	-16.69
14.5	1366	8.17	22.24	2.72	11.22	-16.75
14.6	1361	7.98	21.62	2.71	11.54	-16.69
14.7	1358	8.04	21.86	2.72	11.88	-16.76
14.8	1354	8.07	21.79	2.70	11.86	-16.62
14.9	1351	8.26	22.28	2.70	11.79	-16.74
15.0	1347	8.29	22.61	2.73	11.66	-16.70
15.1	1344	8.32	22.72	2.73	11.69	-16.74
15.2	1340	8.76	23.73	2.71	11.75	-16.75
15.3	1337	8.03	21.57	2.69	11.89	-16.72
15.4	1333	7.68	21.55	2.81	11.42	-16.65
15.5	1330	8.43	22.99	2.73	11.48	-16.80

Appendix Table 2-3.2. Modern Cross Seamount Bulk Data – Analyzed in 2013 by Kelton McMahon (Specimen ID: PV590) which includes some re-drilling to get at more layers close to the center of the coral.

depth (mm)	Age yr CE	Wt % N (%)	wt% C (%)	C:N	δ15N (‰)	δ13C (‰)
0.1	1985	8.53	24.14	2.83	8.92	-17.16
0.2	1978	7.60	21.44	2.82	8.93	-17.11
0.3	1971	8.81	25.48	2.89	8.80	-16.89
0.4	1964	7.78	21.71	2.79	9.00	-16.90
0.5	1958	9.91	27.91	2.82	9.05	-16.85
0.6	1951	9.14	25.99	2.84	9.17	-16.67
0.7	1944	7.18	20.31	2.83	9.24	-16.93
0.8	1938	7.58	21.37	2.82	9.04	-16.85
0.9	1931	7.89	22.30	2.83	9.19	-16.56
1.0	1924	10.13	28.37	2.80	9.37	-16.66
1.1	1916	7.31	21.03	2.88	9.42	-16.52
1.2	1909	8.65	24.14	2.79	9.49	-16.50
1.3	1902	8.14	22.97	2.82	9.80	-16.42
1.4	1895	7.38	20.92	2.84	9.58	-16.39
1.5	1887	7.62	21.08	2.77	10.02	-16.44
1.6	1878	8.29	23.55	2.84	9.86	-16.41
1.7	1871	8.02	22.51	2.81	10.04	-16.32
1.8	1864	8.02	21.70	2.71	9.95	-16.37
1.9	1856	7.86	22.03	2.80	9.95	-16.53
2.0	1849	8.37	23.53	2.81	10.23	-16.44
2.1	1842	6.10	17.74	2.91	10.34	-17.02
2.2	1835	9.75	27.29	2.80	10.05	-16.48
2.3	1828	8.03	22.70	2.83	10.38	-16.46
2.4	1822	9.25	26.49	2.86	10.41	-16.52
2.5	1815	7.11	19.89	2.80	10.85	-16.58
2.6	1809	8.46	24.09	2.85	11.11	-16.48
2.7	1802	9.12	25.76	2.83	11.06	-16.36
2.8	1796	8.10	22.55	2.79	11.10	-16.44
2.9	1791	6.90	19.33	2.80	10.73	-16.41
3.0	1785	5.73	16.18	2.83	10.53	-16.76
3.1	1779	9.52	26.24	2.76	10.82	-16.35
3.2	1774	7.99	22.69	2.84	10.58	-16.39
3.3	1769	7.47	20.67	2.77	10.76	-16.41
3.4	1764	7.88	21.62	2.74	10.67	-16.41
3.5	1759	6.30	17.63	2.80	11.20	-16.66
3.6	1754	6.74	19.53	2.90	11.66	-16.87
3.7	1749	7.05	18.96	2.69	11.67	-16.13
3.8	1745	7.82	21.95	2.81	11.39	-16.22
3.9	1740	8.24	21.91	2.66	11.51	-16.54
4.0	1736	7.92	21.42	2.70	11.20	-16.39

depth	Age	Wt % N	wt% C	C:N	δ15N	δ13C
(mm)	Yr CE	(%)	(%)		(‰)	(‰)
4.1	1732	7.87	21.64	2.75	11.37	-16.25
4.2	1728	8.22	23.11	2.81	11.17	-16.13
4.3	1724	8.12	22.63	2.79	11.70	-16.14
4.4	1720	8.12	23.03	2.84	11.34	-16.18
4.5	1716	10.75	29.95	2.79	11.24	-16.20
4.6	1712	9.26	25.99	2.81	11.10	-16.25
4.7	1709	8.69	24.53	2.82	10.85	-16.30
4.8	1705	7.74	21.32	2.75	10.78	-16.40
4.9	1702	9.50	25.86	2.72	10.97	-16.15
5.0	1698	8.37	22.80	2.72	11.02	-16.27
5.1	1695	8.09	21.84	2.70	10.92	-16.23
5.2	1692	9.20	24.91	2.71	10.92	-16.06
5.3	1688	7.35	20.02	2.72	11.21	-16.41
5.5	1685	7.05	19.50	2.76	10.89	-16.46
5.6	1682	7.35	19.87	2.70	10.90	-16.24
5.7	1679	7.58	20.17	2.66	11.42	-16.34
5.8	1676	6.89	18.39	2.67	11.36	-16.22
5.9	1673	7.74	20.76	2.68	11.60	-16.16
6.0	1670	8.03	21.73	2.71	11.53	-16.29
6.1	1667	8.11	21.61	2.66	11.66	-16.34
6.2	1664	7.62	20.18	2.65	11.04	-16.21
6.3	1661	7.32	19.38	2.65	11.34	-16.17
6.4	1658	7.13	18.75	2.63	11.28	-16.23
6.5	1655	7.92	20.96	2.65	11.35	-16.08
6.6	1652	8.75	22.92	2.62	11.39	-16.00
6.7	1649	8.09	21.32	2.64	11.52	-16.18
6.8	1646	10.44	27.81	2.66	11.40	-16.02
6.9	1643	7.89	21.26	2.69	11.18	-16.18
7.0	1640	8.28	21.86	2.64	11.42	-16.39
7.1	1637	6.73	17.54	2.61	11.68	-16.25
7.2	1634	7.82	20.65	2.64	11.04	-16.09
7.3	1631	7.79	20.39	2.62	11.57	-16.03
7.4	1627	7.83	20.71	2.65	11.59	-16.04
7.5	1624	7.96	20.81	2.62	11.76	-16.29
7.6	1621	7.23	19.18	2.65	11.63	-16.15
7.7	1618	7.82	20.60	2.63	11.52	-16.26
7.8	1614	7.80	19.89	2.55	11.17	-16.40
7.9	1611	6.82	17.75	2.60	11.14	-16.34
8.0	1607	7.68	20.38	2.66	11.31	-15.89

depth (mm)	Age Yr CE	Wt % N (%)	wt% C (%)	C:N	δ15N (‰)	δ13C (‰)
8.1	1604	8.07	21.44	2.66	11.72	-16.15
8.2	1600	8.46	22.51	2.66	11.74	-16.23
8.3	1596	7.59	19.93	2.63	11.76	-16.28
8.4	1593	7.08	19.09	2.70	11.84	-16.22
8.5	1589	7.20	19.30	2.68	11.52	-16.36
8.6	1585	7.59	20.08	2.64	11.50	-16.29
8.7	1581	7.76	20.57	2.65	11.51	-16.39
8.8	1578	8.07	21.23	2.63	11.40	-16.21
8.9	1574	8.38	23.23	2.77	11.18	-16.56
9.0	1569	7.65	20.40	2.66	11.35	-16.32
9.1	1566	7.60	20.36	2.68	11.55	-16.18
9.2	1562	7.48	19.79	2.64	11.58	-16.17
9.3	1558	8.09	21.58	2.67	11.63	-16.29
9.4	1554	8.98	23.94	2.67	11.53	-16.26
9.5	1550	7.18	18.88	2.63	11.06	-16.57
9.6	1546	7.39	19.10	2.58	11.35	-16.53
9.7	1542	7.34	19.15	2.61	11.33	-16.71
9.8	1537	7.44	19.47	2.62	11.51	-16.47
9.9	1533	7.45	20.11	2.70	11.34	-16.36
10.0	1529	7.26	19.37	2.67	11.40	-16.29
10.1	1526	7.86	20.95	2.67	11.32	-16.50
10.2	1522	6.57	17.23	2.62	11.48	-16.50
10.3	1518	6.33	16.57	2.62	11.37	-16.38
10.4	1514	8.38	22.06	2.63	11.44	-16.33
10.5	1509	7.44	19.63	2.64	11.46	-16.48
10.6	1505	8.74	23.44	2.68	11.39	-16.34
10.7	1501	6.92	18.26	2.64	11.74	-16.66
10.8	1497	6.89	18.12	2.63	11.43	-16.24
10.9	1493	8.18	21.50	2.63	11.41	-16.12
11.0	1490	7.88	20.69	2.63	11.41	-16.39
11.1	1486	8.49	22.53	2.65	10.99	-16.52
11.2	1482	7.58	20.42	2.69	11.36	-16.71
11.3	1479	7.60	20.10	2.64	11.03	-16.24
11.4	1475	6.98	18.34	2.63	10.84	-16.21
11.5	1471	6.65	17.34	2.61	10.62	-16.30
11.6	1467	7.24	19.22	2.66	10.76	-16.23
11.7	1463	8.37	22.25	2.66	10.31	-16.30
11.8	1460	12.26	33.11	2.70	10.44	-16.23
11.9	1456	7.91	20.99	2.65	10.87	-16.42
12.0	1453	7.96	22.40	2.81	11.04	-16.82

depth (mm)	Age Yr CE	Wt % N (%)	wt% C (%)	C:N	δ15N (‰)	δ13C (‰)
12.1	1449	8.83	23.91	2.71	10.99	-16.40
12.2	1446	7.38	19.90	2.69	11.34	-16.71
12.3	1442	7.25	19.33	2.67	11.72	-16.26
12.4	1439	7.33	19.47	2.66	11.45	-16.71
12.5	1435	7.22	19.59	2.71	11.63	-16.89
12.6	1432	8.06	21.70	2.69	11.82	-16.68
12.7	1428	7.59	20.25	2.67	11.90	-16.42
12.8	1425	7.73	20.75	2.68	11.88	-16.58
12.9	1421	7.83	20.95	2.68	11.60	-16.50
13.0	1418	8.38	22.48	2.68	11.76	-16.41
13.1	1414	7.95	21.69	2.73	11.48	-16.50
13.2	1411	7.80	21.05	2.70	11.62	-16.35
13.3	1407	8.02	21.89	2.73	12.45	-16.25
13.4	1404	8.53	23.07	2.70	12.19	-16.35
13.5	1400	6.69	18.01	2.69	12.18	-16.45
13.6	1397	7.22	19.37	2.68	12.29	-16.78
13.7	1393	8.06	21.68	2.69	11.90	-16.56
13.8	1390	7.14	19.31	2.70	11.55	-16.27
13.9	1386	7.08	18.89	2.67	11.89	-16.58
14.0	1383	7.46	20.22	2.71	11.98	-16.66
14.1	1379	9.63	26.11	2.71	11.95	-16.57
14.2	1376	7.27	19.06	2.62	11.80	-16.61
14.3	1373	8.10	21.97	2.71	11.50	-16.75
14.4	1369	7.99	21.56	2.70	11.81	-16.46
14.5	1366	8.27	22.02	2.66	11.57	-16.54
14.6	1361	7.87	21.16	2.69	11.66	-16.45
14.7	1358	8.62	23.42	2.72	10.97	-16.40
14.8	1354	8.96	24.37	2.72	11.36	-16.48
14.9	1351	8.16	22.16	2.71	11.21	-16.60
15.0	1347	9.74	26.80	2.75	11.15	-16.38
15.1	1344	8.08	21.91	2.71	11.30	-16.59
15.2	1340	7.32	19.77	2.70	11.37	-16.58
15.3	1337	8.57	22.94	2.68	11.90	-16.64
15.4	1333	6.58	17.37	2.64	12.05	-16.64
15.5	1330	8.42	22.67	2.69	11.89	-16.65
15.6	1326	7.12	18.77	2.64	11.28	-16.61
15.7	1322	6.44	16.93	2.63	11.97	-16.25
15.8	1318	8.97	24.13	2.69	11.90	-16.55
15.9	1314	7.04	19.00	2.70	12.05	-16.19
16.0	1310	7.40	19.73	2.67	12.05	-16.81

depth (mm)	Age Yr CE	Wt % N (%)	wt% C (%)	C:N	δ15N (‰)	δ13C (‰)
16.1	1306	7.52	20.15	2.68	11.78	-16.76
16.2	1302	7.37	19.58	2.66	12.05	-16.79
16.3	1298	7.62	20.16	2.65	11.99	-16.27
16.4	1294	7.65	20.21	2.64	11.88	-16.70
16.5	1290	6.95	18.25	2.63	12.24	-16.62
16.6	1286	8.56	22.73	2.65	12.17	-16.77
16.7	1282	8.43	22.15	2.63	11.80	-16.59
16.8	1278	8.69	22.79	2.62	12.28	-16.84
16.9	1274	8.06	21.62	2.68	12.30	-16.75

Appendix Table 2-4.1. Subfossil Cross Seamount Coral - Analyzed by Danielle Glynn (Specimin ID: PV588).

depth (mm)	Age yr BP	Wt % N (%)	wt% C (%)	C:N	δ15N (‰)	δ13C (‰)
0.1	9647	2.87	10.71	3.73	20.08	-14.68
0.2	9651	3.50	11.89	3.40	18.53	-15.00
0.3	9656	3.65	12.19	3.34	19.58	-14.85
0.4	9660	3.62	13.02	3.60	18.75	-14.64
0.5	9665	3.74	12.45	3.33	19.42	-14.76
0.6	9669	3.92	12.94	3.30	18.84	-15.05
0.7	9674	3.71	12.73	3.43	18.84	-14.67
0.8	9678	3.63	12.63	3.48	18.61	-15.22
0.9	9683	3.89	12.85	3.31	18.44	-15.18
1	9688	3.77	12.71	3.37	18.48	-15.34
1.1	9692	3.49	12.72	3.64	19.14	-14.90
1.2	9697	3.47	12.47	3.59	17.63	-15.08
1.3	9701	3.73	12.29	3.30	18.97	-15.06
1.4	9706	3.50	12.42	3.55	19.18	-15.31
1.5	9710	3.71	12.73	3.43	18.20	-15.29
1.6	9715	NA	NA	NA	NA	NA
1.7	9719	3.75	13.18	3.51	18.00	-15.10
1.8	9724	3.59	12.81	3.57	18.29	-15.62
1.9	9729	3.72	12.69	3.41	19.09	-15.04
2	9733	4.08	13.71	3.36	18.34	-15.35
2.1	9738	NA	NA	NA	NA	NA
2.2	9742	3.68	12.08	3.28	18.76	-15.35
2.3	9747	4.10	13.84	3.37	18.06	-15.40
2.4	9751	NA	NA	NA	NA	NA
2.5	9756	3.54	12.76	3.60	16.97	-15.28
2.6	9760	3.94	13.27	3.37	18.22	-15.13
2.6	9760	3.63	12.75	3.51	18.52	-15.37
2.7	9765	3.91	12.80	3.27	17.88	-15.40
2.8	9769	3.59	12.77	3.56	19.52	-15.08
2.9	9774	3.62	12.98	3.59	18.01	-15.72
3	9779	3.88	12.97	3.34	18.00	-15.35
3.1	9783	4.10	13.65	3.33	18.15	-15.36
3.2	9788	3.85	13.56	3.52	18.86	-15.41
3.3	9792	4.06	13.42	3.31	17.96	-15.20
3.4	9797	4.05	13.94	3.45	18.01	-15.45
3.5	9801	4.19	13.77	3.29	17.82	-15.30
3.6	9806	3.84	13.98	3.64	19.03	-15.48
3.7	9810	4.56	14.41	3.16	17.47	-15.32
3.8	9815	3.94	14.70	3.73	19.22	-15.41
3.9	9819	4.36	14.64	3.36	17.46	-15.43
4	9824	5.08	15.90	3.13	16.59	-15.43

depth (mm)	Age Yr CE	Wt % N (%)	wt% C (%)	C:N	δ15N (‰)	δ13C (‰)
4.1	9829	5.05	17.40	3.44	16.65	-16.05
4.2	9833	4.62	14.78	3.20	15.75	-16.48
4.3	9838	5.36	17.53	3.27	16.12	-15.97
4.4	9842	5.08	17.73	3.49	16.09	-17.09
4.5	9847	5.05	17.24	3.41	15.20	-15.98
4.6	9851	4.39	16.24	3.70	16.11	-15.97
4.6	9851	NA	NA	NA	NA	NA
4.7	9856	4.85	16.61	3.42	16.68	-15.73
4.8	9860	4.88	16.46	3.37	16.70	-15.88
4.9	9865	4.80	16.10	3.36	17.23	-15.92
5	9870	4.69	16.16	3.45	17.50	-16.12
5.1	9874	4.71	15.62	3.32	16.57	-15.72
5.2	9879	4.71	15.78	3.35	17.46	-16.10
5.3	9883	4.84	16.03	3.31	17.32	-15.96
5.4	9888	4.81	15.58	3.24	16.77	-15.96
5.5	9892	4.70	15.86	3.37	17.46	-15.97
5.6	9897	4.67	15.45	3.31	17.07	-15.93
5.7	9901	4.45	15.65	3.52	16.46	-16.17
5.8	9906	4.82	17.13	3.55	16.21	-16.35
5.9	9910	5.16	17.96	3.48	16.56	-16.37
6	9915	4.98	17.88	3.59	15.36	-16.36
6.1	9920	5.56	18.89	3.39	15.39	-16.56
6.2	9924	5.52	18.55	3.36	15.91	-16.41
6.3	9929	5.96	19.14	3.21	14.52	-16.62
6.4	9933	5.85	18.21	3.11	14.35	-16.43
6.5	9938	5.65	18.06	3.20	14.61	-16.31
6.6	9942	5.70	17.93	3.15	14.60	-16.34
6.7	9947	5.47	18.56	3.39	14.20	-16.31
6.8	9951	5.67	17.90	3.16	14.24	-16.35
6.9	9956	5.73	18.34	3.20	14.01	-16.46
7	9960	5.67	17.97	3.17	14.19	-16.29
7.1	9965	5.93	19.22	3.24	12.94	-16.21
7.2	9970	5.97	18.87	3.16	13.55	-16.45
7.3	9974	5.81	18.11	3.12	13.99	-16.22
7.4	9979	5.81	18.68	3.21	13.89	-16.25
7.5	9983	5.91	19.25	3.26	13.76	-16.39
7.6	9988	6.39	20.68	3.23	14.57	-16.26
7.7	9992	6.23	20.09	3.22	14.06	-16.37
7.8	9997	NA	NA	NA	NA	NA
7.9	10001	5.96	18.61	3.12	13.99	-16.44
8	10006	6.14	19.14	3.12	14.06	-16.14

depth (mm)	Age Yr CE	Wt % N (%)	wt% C (%)	C:N	δ15N (‰)	δ13C (‰)
8.1	10011	5.21	16.25	3.12	13.96	-16.61
8.2	10015	5.98	19.62	3.28	13.54	-16.59
8.3	10020	6.36	19.56	3.07	13.68	-16.40
8.4	10024	6.77	21.05	3.11	13.27	-16.23
9	10051	5.22	16.58	3.18	13.51	-16.17
9.6	10079	5.13	17.41	3.40	13.28	-16.44
9.7	10083	5.42	18.37	3.39	14.03	-17.15
9.8	10088	5.52	18.63	3.37	14.20	-17.19
9.9	10092	5.84	19.15	3.28	15.03	-16.68
9.9	10092	5.59	18.62	3.33	13.79	-17.21
10	10097	5.53	17.48	3.16	13.66	-16.44
10.1	10101	5.38	18.35	3.41	14.08	-17.24
10.2	10106	5.75	18.78	3.27	13.65	-17.02
10.3	10111	5.71	19.15	3.36	14.13	-17.31
10.4	10115	5.57	17.81	3.20	13.73	-16.39
11	10142	5.75	18.48	3.21	13.08	-16.44
11.5	10165	5.47	17.85	3.26	13.94	-16.83
12	10188	5.24	16.33	3.12	13.53	-16.22
12.5	10211	5.60	18.12	3.24	13.74	-16.70
13	10233	5.50	16.82	3.06	13.77	-16.06
13.5	10256	5.79	18.51	3.19	13.59	-16.68
14	10279	5.22	15.89	3.05	13.60	-16.10
14.6	10306	4.74	15.20	3.21	13.41	-15.93
14.6	10306	4.40	14.60	3.32	13.22	-16.30
14.7	10311	4.56	15.92	3.49	13.93	-16.77
14.8	10315	4.93	16.63	3.37	13.70	-16.59
14.9	10320	4.99	16.50	3.30	13.94	-16.76
15	10324	4.64	14.93	3.22	13.54	-15.99
15.1	10329	4.98	16.74	3.36	13.82	-16.78
15.2	10333	5.03	16.73	3.32	13.58	-16.69
15.3	10338	5.13	16.64	3.24	13.49	-16.64
15.4	10343	4.70	15.28	3.25	13.12	-16.19
16	10370	4.84	15.25	3.15	13.22	-15.94
16.5	10393	4.80	16.37	3.41	13.42	-17.13
17	10415	5.21	16.69	3.20	14.17	-15.75
17.5	10438	5.08	17.61	3.47	13.88	-16.33
18	10461	4.61	14.74	3.20	13.82	-15.32
18.5	10484	4.55	15.45	3.40	14.44	-16.24
19	10506	4.37	14.11	3.23	14.49	-15.70
19.6	10534	4.36	15.01	3.44	13.67	-15.70

depth (mm)	Age Yr CE	Wt % N (%)	wt% C (%)	C:N	δ15N (‰)	δ13C (‰)
19.7	10538	4.86	16.55	3.40	14.00	-16.40
19.8	10543	4.83	16.39	3.39	14.34	-16.30
19.9	10547	4.87	16.80	3.45	14.30	-16.58
20	10552	5.02	15.76	3.14	13.70	-15.73
20.1	10556	5.23	17.22	3.29	14.19	-16.38
20.2	10561	5.11	17.32	3.39	14.34	-16.49
20.3	10565	4.98	17.11	3.43	14.25	-16.42
20.4	10570	4.96	16.12	3.25	14.20	-15.68
21	10597	4.09	13.19	3.23	14.02	-15.76
21.5	10620	3.59	12.81	3.57	14.51	-16.47
22	10643	3.40	11.59	3.41	13.80	-15.75
22.5	10665	7.97	25.20	3.16	13.84	-16.72
23	10688	6.84	20.61	3.02	13.47	-16.43
23.5	10711	6.61	21.00	3.17	13.47	-16.86
24	10734	4.24	13.79	3.25	12.64	-16.05
24.6	10761	6.00	19.62	3.27	13.71	-16.13
24.7	10766	6.53	20.62	3.16	13.80	-16.73
24.8	10770	7.00	21.69	3.10	14.06	-16.72
24.9	10775	7.06	22.84	3.24	14.57	-16.73
25	10779	7.23	21.89	3.03	13.83	-16.34
25.2	10788	6.21	20.38	3.28	14.14	-16.89
25.2	10788	7.03	22.15	3.15	14.06	-16.77
25.3	10793	6.65	21.37	3.21	14.05	-16.73
25.4	10797	5.98	20.36	3.41	13.22	-16.33
26	10825	6.87	22.10	3.21	13.36	-16.58
26.5	10847	5.84	19.04	3.26	14.39	-16.92
26.5	10847	5.80	19.14	3.30	14.83	-16.96
27	10870	4.56	14.81	3.25	13.71	-16.37
27.5	10893	5.45	18.18	3.34	13.93	-16.90
28	10916	5.38	16.90	3.14	13.04	-16.09
28.5	10938	5.16	17.41	3.38	12.87	-16.80
29	10961	5.44	16.87	3.10	12.69	-16.07
29.6	10988	5.55	18.06	3.25	13.32	-16.23
29.7	10993	5.45	17.84	3.27	13.35	-16.82
29.8	10997	5.71	18.39	3.22	13.32	-16.70
29.9	11002	5.44	18.93	3.48	13.09	-17.02
30	11007	4.88	15.52	3.18	12.96	-16.29

depth (mm)	Age Yr CE	Wt % N (%)	wt% C (%)	C:N	δ15N (‰)	δ13C (‰)
30.1	11011	4.56	15.57	3.42	13.45	-16.88
30.2	11016	4.56	15.78	3.46	13.73	-16.78
30.3	11020	5.16	16.99	3.29	14.06	-16.53
30.4	11025	4.66	15.34	3.29	13.87	-16.17
31	11052	6.22	19.96	3.21	13.76	-16.48
31.5	11075	6.09	19.53	3.21	13.13	-16.98
32	11098	5.28	18.35	3.48	13.43	-16.53
32.5	11120	4.86	17.04	3.51	14.07	-17.25
33	11143	5.03	15.93	3.16	14.51	-16.23
33.5	11166	7.02	22.06	3.14	13.35	-16.95
34	11188	5.77	18.48	3.20	12.26	-16.53
34.6	11216	5.10	17.07	3.34	13.27	-16.43
34.7	11220	5.37	18.06	3.36	13.93	-16.91
34.8	11225	4.76	16.21	3.41	13.57	-17.10
34.9	11229	5.05	17.61	3.48	14.28	-16.91
35	11234	5.39	17.59	3.27	14.07	-16.51
35	11234	5.26	16.74	3.18	13.80	-16.24
35.1	11239	5.66	18.23	3.22	14.23	-16.83
35.2	11243	5.78	18.73	3.24	14.04	-16.69
35.3	11248	5.99	19.81	3.31	13.87	-16.62
35.4	11252	5.62	18.07	3.22	13.79	-16.29
36	11279	6.54	21.37	3.27	13.13	-16.38
36	11279	6.96	21.99	3.16	13.48	-16.88
36.5	11302	6.60	20.79	3.15	13.43	-16.94
37	11325	6.61	20.57	3.11	13.26	-16.69
38	11370	7.43	22.90	3.08	13.46	-16.70
38.5	11393	6.84	21.16	3.09	12.72	-16.76
39	11416	7.22	22.04	3.05	12.81	-16.78
39.5	11439	6.94	21.42	3.09	12.73	-16.68
40.5	11484	6.65	20.52	3.09	12.55	-16.89
41	11507	6.59	21.21	3.22	12.28	-17.25
41.5	11530	8.90	27.84	3.13	12.08	-17.20
42	11552	7.60	23.68	3.12	12.47	-17.18
42.5	11575	6.49	20.37	3.14	12.19	-17.39
43	11598	6.37	19.56	3.07	11.97	-17.21
43.5	11621	6.13	19.42	3.17	12.12	-17.30
44	11643	6.21	19.31	3.11	12.19	-17.08
44.5	11666	7.48	22.93	3.07	11.57	-17.26
45.5	11712	8.10	24.86	3.07	11.43	-17.63

Appendix Table 2-4.2. Acidified bulk data for the subfossil coral (PV588) and the difference in non-acidified samples minus the values of acidified samples.

depth (mm)	Age yr BP	Wt % N (%)	wt% C (%)	C:N	δ15N (‰)	δ13C (‰)	Difference C:N	Difference δ13C
0.1	9647	12.12	37.06	3.06	15.04	-16.07	0.68	1.39
1	9688	11.50	35.04	3.05	14.95	-16.38	0.32	1.04
6	9915	10.28	30.88	3.00	15.04	-16.92	0.59	0.56
13	10233	5.10	15.15	2.97	13.80	-16.94	0.09	0.88
26	10825	12.49	38.41	3.07	13.82	-17.35	0.14	0.77
36	11279	11.92	36.74	3.08	13.48	-17.07	0.08	0.19
41.5	11530	11.76	35.61	3.03	12.12	-17.25	0.10	0.05

Appendix Table 2-5. Modern Cross Seamount amino acid molecular percent (mol%) data – Analyzed by Danielle Glynn (Specimen ID: PV588)

.

distance (mm)	machine	runs	Ala (%)	stdev	Gly (%)	stdev	Thr (%)	stdev	Ser (%)	stdev	Val (%)	stdev
0.6	GC-MS	n=1	2.68		52.76		2.12		4.80		4.57	
0.6	GC-IRMS		2.34	0.06	56.68	0.14	2.97	0.00	5.69	0.11	4.94	0.08
1.8	GC-MS	n = 2	2.61	0.27	51.69	2.53	2.10	0.23	4.91	0.37	4.46	0.11
1.8	GC-IRMS		2.14	0.12	50.78	0.63	2.20	0.15	5.12	0.09	4.45	0.09
3.1	GC-MS	n = 4	2.63	0.24	51.77	1.22	2.02	0.10	4.27	0.08	4.77	0.13
7.1	GC-MS	n = 1	2.62		49.07		1.91		4.81		3.41	
7.1	GC-IRMS		2.14	0.03	51.53	0.09	2.12	0.02	4.63	0.01	3.41	0.00
14.9	GC-MS	n = 1	2.41		51.59		1.81		4.68		3.70	
14.9	GC-IRMS		2.44	0.08	55.79	0.21	2.56	0.03	5.90	0.10	4.22	0.08
Average of coral		**Count**										
0-15 mm		9	2.45	0.21	52.41	2.40	2.20	0.36	4.98	0.52	4.22	0.57

distance (mm)	machine	runs	Leu (%)	stdev	Ile (%)	stdev	Pro (%)	stdev	Asp (%)	stdev	Glu (%)	stdev
0.6	GC-MS	n=1	1.81		1.19		3.58		6.17		2.00	
0.6	GC-IRMS		2.55	0.01	0.90	0.01	3.95	0.01	6.98	0.02	3.24	0.03
1.8	GC-MS	n = 2	1.94	0.24	1.30	0.24	3.73	0.20	6.90	0.65	2.23	0.24
1.8	GC-IRMS		1.94	0.06	0.55	0.01	3.40	0.25	6.48	0.06	2.77	0.11
3.1	GC-MS	n = 4	1.87	0.10	1.39	0.13	3.49	0.04	6.62	0.03	2.04	0.03
7.1	GC-MS	n = 1	2.02		1.53		3.76		9.59		2.55	
7.1	GC-IRMS		2.13	0.04	0.90	0.02	3.46	0.01	8.29	0.03	3.00	0.03
14.9	GC-MS	n = 1	1.92		1.55		3.73		9.00		2.38	
14.9	GC-IRMS		2.59	0.02	1.34	0.01	4.01	0.02	9.61	0.03	3.74	0.01
Average of coral		**Count**										
0-15 mm		9	2.09	0.29	1.18	0.33	3.68	0.22	7.74	1.39	2.66	0.58

distance (mm)	machine	runs	Phe (%)	stdev	Tyr (%)	stdev	Lys (%)	stdev
0.6	GC-MS	n=1	0.67		6.01		11.64	
0.6	GC-IRMS		0.70	0.01	0.72	0.00	8.33	0.03
1.8	GC-MS	n = 2	0.66	0.09	5.90	0.55	12.97	1.32
1.8	GC-IRMS		0.57	0.08	7.30	0.59	12.29	0.11
3.1	GC-MS	n = 4	0.63	0.02	6.53	0.08	11.99	0.36
7.1	GC-MS	n = 1	0.73		5.11		12.89	
7.1	GC-IRMS		0.49	0.00	6.39	0.05	11.52	0.08
14.9	GC-MS	n = 1	0.69		4.70		11.86	
14.9	GC-IRMS		0.77	0.02	0.67	0.00	6.37	0.13
Average of coral		**Count**						
0-15 mm		9	0.66	0.09	4.81	2.46	11.09	2.24

Appendix Table 2-6. Subfossil Cross Seamount Coral Molar Percentage Data - Analyzed by Danielle Glynn (Specimin ID: PV588)

distance (mm)	machine	runs	Ala (%)	stdev	Gly (%)	stdev	Thr (%)	stdev	Ser (%)	stdev	Val (%)	stdev
1	GC-MS	n = 5	3.16	0.21	30.11	0.32	2.39	0.06	5.51	0.19	8.45	0.04
2.8	GC-MS	n = 3	5.54	1.05	27.75	1.54	3.20	0.37	5.90	0.12	8.86	0.11
3	GC-IRMS		2.43	0.03	33.58	0.44	2.53	0.05	6.57	0.13	8.03	0.10
4.2	GC-MS	n = 3	3.26	0.42	31.99	0.38	2.32	0.14	5.61	0.10	8.70	0.09
4.5	GC-IRMS		1.90	0.02	29.52	0.08	2.66	0.01	6.54	0.02	9.87	0.18
6.9	GC-MS	n = 1	2.61		37.40		2.18		6.66		9.44	
7.5	GC-MS	n = 2	3.37	0.02	30.39	0.18	2.40	0.02	6.11	0.04	8.58	0.07
7.5	GC-IRMS		3.06	0.06	30.81	0.08	2.83	0.05	6.66	0.01	8.95	0.07
8.5	GC-MS	n = 3	4.91	0.16	30.58	0.69	2.82	0.05	6.09	0.04	10.42	0.01
11	GC-MS	n = 3	3.57	0.37	32.88	0.43	2.38	0.12	6.11	0.20	6.70	0.15
15	GC-IRMS		2.46	0.01	26.59	0.08	2.47	0.00	6.38	0.02	7.55	0.07
18	GC-MS	n = 2	5.05	1.67	25.74	1.10	2.85	0.58	6.13	0.00	8.21	0.55
20	GC-IRMS		2.59	0.02	29.12	0.34	2.91	0.01	6.42	0.01	11.17	0.23
22.5	GC-MS	n = 1	5.83		23.40		3.11		6.01		8.86	
27	GC-MS	n = 1	4.52		30.59		2.79		5.66		9.79	
30	GC-MS	n = 2	2.82	0.11	23.87	0.49	2.03	0.04	6.00	0.00	6.45	0.05
30	GC-IRMS		2.55	0.02	23.84	0.19	2.49	0.01	6.27	0.06	8.84	0.02
35	GC-IRMS		2.00	0.05	23.67	0.74	2.34	0.03	6.26	0.00	8.10	0.41
40	GC-MS	n = 2	4.13	0.13	28.79	0.82	2.59	0.04	5.90	0.03	8.35	0.04
Average of sections		**Count**										
0-5 mm		5	3.26	1.39	30.59	2.26	2.62	0.35	6.03	0.50	8.78	0.69
>10 mm		10	3.55	1.28	26.85	3.34	2.60	0.32	6.11	0.23	8.40	1.40
≥30 mm		4	2.88	0.90	25.04	2.50	2.36	0.25	6.11	0.19	7.94	1.04

distance (mm)	machine	runs	Leu (%)	stdev	Ile (%)	stdev	Pro (%)	stdev	Asp (%)	stdev	Glu (%)	stdev
1	GC-MS	n = 5	3.28	0.05	1.65	0.07	8.50	0.16	14.06	0.14	5.26	0.04
2.8	GC-MS	n = 3	3.84	0.30	2.57	0.44	6.89	0.53	11.98	0.19	4.83	0.06
3	GC-IRMS		3.58	0.07	0.60	0.02	6.98	0.12	11.91	0.12	6.52	0.14
4.2	GC-MS	n = 3	3.20	0.10	1.48	0.16	8.28	0.27	11.89	0.23	4.58	0.03
4.5	GC-IRMS		3.60	0.04	0.89	0.01	6.43	0.09	11.74	0.07	5.07	0.04
6.9	GC-MS	n = 1	2.11		0.89		6.31		11.25		3.90	
7.5	GC-MS	n = 2	3.25	0.02	1.53	0.00	7.31	0.06	10.48	0.01	3.79	0.00
7.5	GC-IRMS		3.82	0.02	0.94	0.15	6.45	0.00	9.39	0.02	4.79	0.03
8.5	GC-MS	n = 3	3.47	0.03	2.17	0.08	6.06	0.17	9.47	0.09	2.96	0.01
11	GC-MS	n = 3	2.49	0.11	1.20	0.14	8.46	0.20	11.15	0.11	5.28	0.04
15	GC-IRMS		3.73	0.05	0.66	0.01	6.27	0.06	9.80	0.06	4.52	0.04
18	GC-MS	n = 2	3.60	0.45	2.25	0.70	7.05	0.81	10.29	0.52	3.90	0.03
20	GC-IRMS		4.05	0.02	1.54	0.01	6.74	0.01	11.36	0.03	5.14	0.09
22.5	GC-MS	n = 1	3.81		2.69		5.90		9.43		3.93	
27	GC-MS	n = 1	3.44		2.06		7.26		10.96		4.28	
30	GC-MS	n = 2	3.26	0.03	1.36	0.05	7.92	0.07	11.75	0.04	4.54	0.02
30	GC-IRMS		4.15	0.05	1.07	0.10	6.78	0.06	10.30	0.03	4.75	0.02
35	GC-IRMS		3.39	0.14	1.09	0.07	5.94	0.15	9.62	0.07	4.17	0.11
40	GC-MS	n = 2	3.42	0.03	2.06	0.05	6.29	0.03	9.67	0.01	3.09	0.03
Average of sections		**Count**										
0-5 mm		5	3.50	0.26	1.44	0.76	7.42	0.92	12.32	0.98	5.25	0.75
>10 mm		10	3.54	0.47	1.60	0.64	6.86	0.84	10.43	0.82	4.36	0.64
≥30 mm		4	3.56	0.41	1.39	0.47	6.73	0.86	10.34	0.99	4.14	0.74

distance (mm)	machine	runs	Phe (%)	stdev	Tyr (%)	stdev	Lys (%)	stdev
1	GC-MS	n = 5	1.05	0.04	2.42	0.12	14.14	0.20
2.8	GC-MS	n = 3	1.53	0.22	3.57	0.08	13.54	0.53
3	GC-IRMS		1.30	0.02	2.63	0.10	13.34	1.27
4.2	GC-MS	n = 3	1.01	0.07	3.30	0.10	14.38	0.11
4.5	GC-IRMS		1.01	0.02	6.51	0.09	14.26	0.29
6.9	GC-MS	n = 1	0.39		2.23		14.62	
7.5	GC-MS	n = 2	0.89	0.00	4.59	0.04	17.31	0.39
7.5	GC-IRMS		1.06	0.01	6.03	0.03	15.21	0.07
8.5	GC-MS	n = 3	0.84	0.01	3.95	0.05	16.26	0.54
11	GC-MS	n = 3	0.67	0.07	2.74	0.40	16.37	0.33
15	GC-IRMS		0.60	0.01	9.76	0.14	19.21	0.05
18	GC-MS	n = 2	1.32	0.31	5.74	0.24	17.87	1.63
20	GC-IRMS		1.09	0.06	4.41	0.12	13.45	0.42
22.5	GC-MS	n = 1	1.61		7.11		18.30	
27	GC-MS	n = 1	1.22		3.62		13.82	
30	GC-MS	n = 2	0.98	0.01	6.67	0.06	22.34	0.23
30	GC-IRMS		0.74	0.15	9.16	0.12	19.04	0.14
35	GC-IRMS		0.91	0.07	13.38	0.28	19.13	0.52
40	GC-MS	n = 2	0.89	0.01	6.32	0.09	18.49	0.41
Average of sections		**Count**						
0-5 mm		5	1.18	0.23	3.69	1.65	13.93	0.46
>10 mm		10	1.00	0.32	6.89	3.18	17.80	2.66
≥30 mm		4	0.88	0.10	8.88	3.25	19.75	1.75

Appendix Table 2-7.1. Statistics comparing binned regions of mol% data for the Subfossil Coral Outer vs Inner (0-5 mm vs >10 mm) using a t-Test (Two-Sample Assuming Unequal Variances). Highlight means that the comparison is significantly different in mean values (p value 0.05 or better).

Outer vs Inner Subfossil Coral	Alanine		Glycine		Threonine		Serine		Valine	
0-5 mm vs >10 mm	*0-5 mm*	*>10 mm*	*0-5 mm*	*>10 mm*	*0-5 mm*	*>10 mm*	*0-5 mm*	*>10 mm*	*0-5 mm*	*>10 mm*
Mean Mol%	3.26	3.55	30.59	26.85	2.62	2.60	6.03	6.11	8.78	8.40
Variance	1.94	1.64	5.09	11.16	0.12	0.10	0.25	0.05	0.47	1.95
Observations	5	10	5	10	5	10	5	10	5	10
Difference (Outer - Inner)	-0.30		3.74		0.02		-0.09		0.38	
Hypothesized Mean Difference	0		0		0		0		0	
Degree of freedom	7		11		7		5		13	
t Stat	-0.40		2.56		0.13		-0.36		0.70	
P(T<=t) one-tail	0.35		0.01		0.45		0.37		0.25	
t Critical one-tail	1.89		1.80		1.89		2.02		1.77	
P(T<=t) two-tail	0.70		0.03		0.90		0.73		0.50	
t Critical two-tail	2.36		2.20		2.36		2.57		2.16	

Outer vs Inner Subfossil Coral	Leucine		Isoleucine		Proline		Aspartic Acid		Glutamic Acid	
0-5 mm vs >10 mm	*0-5 mm*	*>10 mm*	*0-5 mm*	*>10 mm*	*0-5 mm*	*>10 mm*	*0-5 mm*	*>10 mm*	*0-5 mm*	*>10 mm*
Mean Mol%	3.50	3.54	1.44	1.60	7.42	6.86	12.32	10.43	5.25	4.36
Variance	0.07	0.22	0.58	0.41	0.84	0.70	0.96	0.68	0.57	0.41
Observations	5	10	5	10	5	10	5	10	5	10
Difference (Outer - Inner)	-0.03		-0.16		0.55		1.88		0.89	
Hypothesized Mean Difference	0		0		0		0		0	
Degree of freedom	13		7		7		7		7	
t Stat	-0.18		-0.40		1.14		3.69		2.27	
P(T<=t) one-tail	0.43		0.35		0.15		0.00		0.03	
t Critical one-tail	1.77		1.89		1.89		1.89		1.89	
P(T<=t) two-tail	0.86		0.70		0.29		0.01		0.06	
t Critical two-tail	2.16		2.36		2.36		2.36		2.36	

Outer vs Inner Subfossil Coral	Phenelyenaline		Tyrosine		Lysine	
0-5 mm vs >10 mm	*0-5 mm*	*>10 mm*	*0-5 mm*	*>10 mm*	*0-5 mm*	*>10 mm*
Mean Mol%	1.18	1.00	3.69	6.89	13.93	17.80
Variance	0.05	0.10	2.71	10.14	0.21	7.05
Observations	5	10	5	10	5	10
Difference (Outer - Inner)	0.18		-3.20		-3.87	
Hypothesized Mean Difference	0		0		0	
Degree of freedom	11		13		10	
t Stat	1.24		-2.57		-4.48	
P(T<=t) one-tail	0.12		0.01		0.00	
t Critical one-tail	1.80		1.77		1.81	
P(T<=t) two-tail	0.24		0.02		0.00	
t Critical two-tail	2.20		2.16		2.23	

Appendix Table 2-7.2. Statistics comparing binned regions of mol% data for the Modern Coral vs Subfossil coral (>10 mm) using a t-Test (Two-Sample Assuming Unequal Variances). Highlight means that the comparison is significantly different in mean values (p value 0.05 or better).

Modern vs Subfossil Coral	Alanine		Glycine		Threonine		Serine		Valine	
Modern vs >10 mm Subfossil	*Modern*	*>10 mm*	*Modern*	*>10 mm*	*Modern*	*>10 mm*	*Modern*	*>10 mm*	*Modern*	*>10 mm*
Mean Mol%	2.45	3.55	52.41	26.85	2.20	2.59	4.98	6.11	4.22	8.40
Variance	0.04	1.64	5.75	11.16	0.13	0.10	0.27	0.05	0.33	1.95
Observations	9	10	9	10	9	19	9	10	9	10
Difference (Modern - Subfossil)	-1.11		25.56		-0.39		-1.13		-4.19	
Hypothesized Mean Difference	0		0		0		0		0	
Degree of freedom	10		16		14		11		12	
t Stat	-2.69		19.29		-2.84		-6.03		-8.70	
P(T<=t) one-tail	0.01		0.00		0.01		0.00		0.00	
t Critical one-tail	1.81		1.75		1.76		1.80		1.78	
P(T<=t) two-tail	0.02		0.00		0.01		0.00		0.00	
t Critical two-tail	2.23		2.12		2.14		2.20		2.18	

Modern vs Subfossil Coral	Leucine		Isoleucine		Proline		Aspartic Acid		Glutamic Acid	
Modern vs >10 mm Subfossil	*Modern*	*>10 mm*	*Modern*	*>10 mm*	*Modern*	*>10 mm*	*Modern*	*>10 mm*	*Modern*	*>10 mm*
Mean Mol%	2.09	3.54	1.18	1.60	3.68	6.86	7.74	10.43	2.66	4.36
Variance	0.08	0.22	0.11	0.41	0.05	0.70	1.92	0.68	0.34	0.41
Observations	9	10	9	10	9	10	9	10	9	10
Difference (Modern - Subfossil)	-1.45		-0.42		-3.18		-2.70		-1.70	
Hypothesized Mean Difference	0		0		0		0		0	
Degree of freedom	15		14		10		13		17	
t Stat	-8.21		-1.80		-11.59		-5.09		-6.03	
P(T<=t) one-tail	0.00		0.05		0.00		0.00		0.00	
t Critical one-tail	1.75		1.76		1.81		1.77		1.74	
P(T<=t) two-tail	0.00		0.09		0.00		0.00		0.00	
t Critical two-tail	2.13		2.14		2.23		2.16		2.11	

Modern vs Subfossil Coral	Phenelyenaline		Tyrosine		Lysine	
Modern vs >10 mm Subfossil	*Modern*	*>10 mm*	*Modern*	*>10 mm*	*Modern*	*>10 mm*
Mean Mol%	0.66	1.00	4.81	6.89	11.09	17.80
Variance	0.01	0.10	6.04	10.14	5.00	7.05
Observations	9	10	9	10	9	10
Difference (Modern - Subfossil)	-0.35		-2.08		-6.71	
Hypothesized Mean Difference	0		0		0	
Degree of freedom	10		17		17	
t Stat	-3.36		-1.60		-5.98	
P(T<=t) one-tail	0.00		0.06		0.00	
t Critical one-tail	1.81		1.74		1.74	
P(T<=t) two-tail	0.01		0.13		0.00	
t Critical two-tail	2.23		2.11		2.11	

Appendix Table 2-7.3. Statistics comparing binned regions of mol% data for the Modern Coral vs Subfossil coral (>10 mm) when Glycine of Subfossil coral is set to modern values (Subfossil coral Gly +25.6%), using a t-Test (Two-Sample Assuming Unequal Variances). Highlight means that the comparison is significantly different in mean values (p value 0.05 or better). Gly of Subfossil coral adjusted utilizing the average offset between average modern and average >10mm Subfossil coral gly mol% values (+25.6%), then mol% was recalculated for all amino acids, before performing t-Test.

Modern vs Subfossil (Gly*) Coral	Alanine		**Glycine - Altered**		Threonine		Serine		Valine	
Modern vs >10 mm Subfossil	*Modern*	*>10 mm*	*Modern*	*>10 mm*	*Modern*	*>10 mm*	*Modern*	*>10 mm*	*Modern*	*>10 mm*
Mean Mol%	2.45	2.31	52.41	52.41	2.20	1.69	4.98	3.98	4.22	5.47
Variance	0.04	0.69	5.75	11.16	0.13	0.04	0.27	0.02	0.33	0.83
Observations	9	10	9	10	9	10	9	10	9	10
Difference (Modern - Inner)	0.13		0.00		0.51		1.00		-1.25	
Hypothesized Mean Difference	0		0		0		0		0	
Degree of freedom	10		16		13		9		15	
t Stat	0.49		0.00		3.78		5.58		-3.63	
P(T<=t) one-tail	0.32		0.50		0.00		0.00		0.00	
t Critical one-tail	1.81		1.75		1.77		1.83		1.75	
P(T<=t) two-tail	0.63		1.00		0.00		0.00		0.00	
t Critical two-tail	2.23		2.12		2.16		2.26		2.13	

Modern vs Subfossil (Gly*) Coral	Leucine		Isoleucine		Proline		Aspartic Acid		Glutamic Acid	
Modern vs >10 mm Subfossil	*Modern*	*>10 mm*	*Modern*	*>10 mm*	*Modern*	*>10 mm*	*Modern*	*>10 mm*	*Modern*	*>10 mm*
Mean Mol%	2.09	2.30	1.18	1.04	3.68	4.46	7.74	6.79	2.66	2.84
Variance	0.08	0.09	0.11	0.17	0.05	0.30	1.92	0.29	0.34	0.17
Observations	9	10	9	10	9	10	9	10	9	10
Difference (Modern - Inner)	-0.22		0.14		-0.78		0.95		-0.18	
Hypothesized Mean Difference	0		0		0		0		0	
Degree of freedom	17		17		12		10		14	
t Stat	-1.58		0.83		-4.20		1.93		-0.74	
P(T<=t) one-tail	0.07		0.21		0.00		0.04		0.23	
t Critical one-tail	1.74		1.74		1.78		1.81		1.76	
P(T<=t) two-tail	0.13		0.42		0.00		0.08		0.47	
t Critical two-tail	2.11		2.11		2.18		2.23		2.14	

Modern vs Subfossil (Gly*) Coral	Phenelyenaline		Tyrosine		Lysine	
Modern vs >10 mm Subfossil	*Modern*	*>10 mm*	*Modern*	*>10 mm*	*Modern*	*>10 mm*
Mean Mol%	0.66	0.65	4.81	4.48	11.09	11.58
Variance	0.01	0.04	6.04	4.29	5.00	2.98
Observations	9	10	9	10	9	10
Difference (Modern - Inner)	0.00		0.33		-0.49	
Hypothesized Mean Difference	0		0		0	
Degree of freedom	12		16		15	
t Stat	0.04		0.31		-0.53	
P(T<=t) one-tail	0.49		0.38		0.30	
t Critical one-tail	1.78		1.75		1.75	
P(T<=t) two-tail	0.97		0.76		0.60	
t Critical two-tail	2.18		2.12		2.13	

Appendix Table 2-8. Modern Coral Nitrogen CSIA-AA values and parameters that appear in the manuscript. TP is calculated according to McMahon et al. 2018 which uses a coral specific correction factor (see methods chapter 2).

Samples	Depth (mm)	0.6			1.8			7.1			14.9		
	Year BP	1970			1893			1562			1067		
		Measured		Normalized	Measured		Normalized	Measured		Normalized	Measured		Normalized
		δ15N (‰)	stdev	δ15N (‰)	δ15N (‰)	stdev	δ15N (‰)	δ15N (‰)	stdev	δ15N (‰)	δ15N (‰)	stdev	δ15N (‰)
Trophic	Glx	24.25	0.24	10.91	24.17	0.21	9.94	26.06	0.05	10.17	24.08	0.22	9.56
	Asx	13.88	0.33	0.54	14.46	0.09	0.24	15.53	0.14	-0.36	15.34	0.38	0.82
	Ala	23.13	0.72	9.79	22.55	0.02	8.32	24.38	0.78	8.49	23.82	1.15	9.30
	Ile	21.06	0.20	7.72	25.83	0.32	11.60	25.30	0.21	9.41	22.94	0.77	8.42
	Leu	24.14	0.45	10.80	24.51	0.29	10.28	26.49	0.20	10.60	19.95	0.54	5.43
	Pro	25.46	0.10	12.12	25.72	0.07	11.49	28.14	0.20	12.25	27.45	0.22	12.93
	Val	22.06	0.47	8.72	24.63	0.03	10.40	26.13	0.69	10.24	24.87	0.13	10.35
Intermediate	Gly	11.10	0.08	-2.23	10.17	0.04	-4.06	11.59	0.01	-4.29	12.15	0.04	-2.37
	Ser	7.49	0.01	-5.85	10.70	0.44	-3.53	12.66	0.20	-3.23	11.75	0.51	-2.77
Source	Lys	4.57	0.04	-8.77	6.24	0.27	-7.98	7.40	0.14	-8.49	7.23	0.06	-7.29
	Tyr	3.93	0.15	-9.41	5.21	1.29	-9.01	4.96	0.39	-10.92	4.00	0.71	-10.52
	Phe	6.56	0.53	-6.78	6.03	0.40	-8.20	8.69	0.28	-7.20	6.65	0.89	-7.87
Metabolic	Thr	-14.22	0.99	-27.56	-15.29	0.16	-29.52	-10.78	0.87	-26.67	-11.48	2.29	-26.00
Averages	Avg THAA	13.34	0.29	0.00	14.22	0.33	0.00	15.89	0.28	0.00	14.52	0.61	0.00
	Avg Trophic	22.00	3.86	8.66	23.12	3.97	8.90	24.57	4.15	8.69	22.63	3.92	8.12
	Avg Source	5.02	1.37	-8.32	5.83	0.54	-8.40	7.02	1.89	-8.87	5.96	1.72	-8.56
Parameters	Trophic - Source	16.98			17.29			17.56			16.68		
	∑V	2.59			2.64			2.64			2.85		
	∑V - no Ile	2.79			2.78			3.00			3.29		
	TP "Coral Calc"	3.33			3.39			3.29			3.29		

Average of recent millennia, excluding the 1970 point				
	Average Measured		Average Normalized	
	δ15N (‰)	stdev	δ15N (‰)	stdev
Glx	24.77	0.31	9.89	0.31
Asx	15.11	0.59	0.31	0.51
Ala	23.58	0.52	8.98	0.69
Ile	24.69	1.63	9.29	1.69
Leu	23.65	2.90	9.28	2.57
Pro	27.10	0.72	12.20	0.59
Val	25.21	0.08	9.93	0.81
Gly	11.30	1.05	-3.24	1.09
Ser	11.70	0.38	-3.84	1.37
Lys	6.96	0.60	-8.13	0.65
Tyr	4.72	1.01	-9.97	0.91
Phe	7.12	0.51	-7.51	0.64
Thr	-12.52	1.87	-27.44	1.53
Avg THAA	14.88	0.00		
Avg Trophic	23.44	0.40		
Avg Source	6.27	0.24		
Trophic - Source	17.18	0.45		
∑V	2.71	0.12		
∑V - no Ile	3.02	0.26		
TP "Coral Calc"	3.32	0.06		

Appendix Table 2-9. Subfossil Coral Nitrogen CSIA-AA values and parameters that appear in the manuscript. TP is calculated according to McMahon et al. 2018 which uses a coral specific correction factor (see methods).

Samples	Depth (mm)	1			2.8			3		
	Year BP	9705			9780			9789		
		Measured		Normalized	Measured		Normalized	Measured		Normalized
		δ15N (‰)	stdev	δ15N (‰)	δ15N (‰)	stdev	δ15N (‰)	δ15N (‰)	stdev	δ15N (‰)
Trophic	Glx	16.51	0.32	-1.12	16.23	0.04	-0.40	24.27	0.30	6.50
	Asx	18.87	0.36	1.23	18.52	0.16	1.88	19.63	0.30	1.86
	Ala	28.51	1.54	10.87	28.59	1.35	11.95	31.69	2.09	13.93
	Ile	30.90	0.71	13.26	30.89	0.54	14.26	34.48	0.80	16.71
	Leu	32.21	0.98	14.58	29.90	0.95	13.26	25.52	1.46	7.75
	Pro	30.31	0.27	12.68	31.83	0.27	15.19	32.87	0.20	15.10
	Val	32.46	0.26	14.83	29.15	0.05	12.51	28.92	0.42	11.16
Intermediate	Gly	16.51	0.32	-1.12	16.23	0.04	-0.40	16.79	0.19	-0.97
	Ser	18.37	0.67	0.74	18.00	0.28	1.37	9.94	1.27	-7.82
Source	Lys	10.19	1.49	-7.44	8.54	0.39	-8.10	9.67	0.07	-8.09
	Tyr	11.36	0.51	-6.27	8.43	0.56	-8.20	3.23	1.73	-14.54
	Phe	9.19	1.11	-8.44	11.33	0.80	-5.31	8.76	1.73	-9.01
Metabolic	Thr	-26.17	1.15	-43.80	-31.36	0.74	-48.00	-14.82	1.10	-32.58
Averages	Avg THAA	17.63	15.75	0.00	16.64	16.78	0.00	17.76	14.18	0.00
	Avg Trophic	27.11	6.60	9.48	26.44	6.32	9.81	28.19	5.32	10.43
	Avg Source	10.25	1.09	-7.38	9.43	1.64	-7.20	7.22	3.49	-10.55
Parameters	Trophic - Source	16.86			17.01			20.98		
	∑V	5.38			5.18			4.34		
	∑V - no Ile	5.02			4.76			3.44		
	TP "Coral Calc"	1.96			1.65			3.04		

Samples	Depth (mm)	10			15			20		
	Year BP	10081			10289			10498		
		Measured		Normalized	Measured		Normalized	Measured		Normalized
		δ15N (‰)	stdev	δ15N (‰)	δ15N (‰)	stdev	δ15N (‰)	δ15N (‰)	stdev	δ15N (‰)
Trophic	Glx	26.57	0.35	6.62	25.59	0.76	6.70	25.11	0.47	4.79
	Asx	18.00	0.18	-1.95	17.89	0.19	-1.01	18.68	0.13	-1.63
	Ala	28.40	0.53	8.45	26.79	0.64	7.89	28.02	0.56	7.71
	Ile	38.29	0.25	18.35	37.95	2.00	19.05	38.57	1.57	18.26
	Leu	27.93	0.78	7.98	28.83	0.07	9.93	29.31	0.43	9.00
	Pro	31.83	0.73	11.88	31.61	0.88	12.72	31.49	0.21	11.18
	Val	29.48	0.29	9.53	28.07	0.27	9.17	30.02	0.08	9.71
Intermediate	Gly	17.10	0.05	-2.85	15.36	0.12	-3.54	15.06	0.03	-5.25
	Ser	14.67	0.28	-5.28	13.81	0.02	-5.09	13.18	0.42	-7.13
Source	Lys	9.89	0.24	-10.06	8.77	0.16	-10.13	9.61	0.13	-10.71
	Tyr	10.58	0.90	-9.37	6.68	0.22	-12.21	12.29	0.52	-8.02
	Phe	11.09	0.90	-8.86	8.90	0.22	-9.99			
Metabolic	Thr	-4.49	0.25	-24.44	-4.57	1.51	-23.47	-7.59	0.05	-27.90
Averages	Avg THAA	19.95	11.73	0.00	18.90	12.10	0.00	20.31	12.63	0.00
	Avg Trophic	28.64	6.09	8.69	28.10	6.08	9.21	28.74	6.07	8.43
	Avg Source	10.52	0.60	-9.43	8.12	1.24	-10.78	10.95	1.90	-9.36
Parameters	Trophic - Source	18.12			19.99			17.79		
	∑V	3.91			4.02			4.12		
	∑V - no Ile	2.72			2.70			2.98		
	TP "Coral Calc"	3.04			3.20					

Samples	Depth (mm)	25			30			35		
	Year BP	10706			10915			11123		
		Measured		Normalized	Measured		Normalized	Measured		Normalized
		δ15N (‰)	stdev	δ15N (‰)	δ15N (‰)	stdev	δ15N (‰)	δ15N (‰)	stdev	δ15N (‰)
Trophic	Glx	25.88	0.45	7.24	25.70	0.78	6.66	24.90	0.50	6.68
	Asx	17.57	0.40	-1.07	17.53	0.18	-1.51	16.54	0.60	-1.67
	Ala	25.73	0.63	7.09	28.65	1.33	9.62	28.28	1.84	10.07
	Ile	34.46	0.40	15.82	37.71	4.73	18.67	30.40	1.32	12.19
	Leu	29.95	0.45	11.31	23.32	0.86	4.28	30.04	0.41	11.83
	Pro	30.72	0.70	12.07	30.20	0.64	11.16	28.35	1.39	10.14
	Val	29.04	0.21	10.39	27.79	0.39	8.75	29.99	0.28	11.77
Intermediate	Gly	15.56	0.04	-3.08	16.53	0.15	-2.51	15.31	0.06	-2.90
	Ser	14.78	0.28	-3.86	11.98	1.72	-7.06	15.06	0.24	-3.15
Source	Lys	8.42	0.71	-10.22	9.14	0.26	-9.90	6.59	0.37	-11.63
	Tyr	9.12	0.22	-9.52	9.74	1.05	-9.30	9.59	0.93	-8.63
	Phe	8.40	0.22	-10.24	10.95	1.05	-8.09	8.87	0.93	-9.34
Metabolic	Thr	-7.30	0.21	-25.94	-1.73	0.72	-20.77	-7.14	1.39	-25.36
Averages	Avg THAA	18.64	12.02	0.00	19.04	10.97	0.00	18.21	11.68	0.00
	Avg Trophic	27.62	5.35	8.98	27.27	6.23	8.23	26.93	4.95	8.72
	Avg Source	8.65	0.41	-9.99	9.94	0.92	-9.10	8.35	1.57	-9.86
Parameters	Trophic - Source	18.97			17.33			18.58		
	∑V	3.91			4.36			3.55		
	∑V - no Ile	2.93			2.92			3.22		
	TP "Coral Calc"	3.30			2.94			3.11		

		Subfossil Coral 0-5 mm				Subfossil Coral >10 mm			
		Average Measured		Average Normalized		Average Measured		Normalized >10 mm	
		δ15N (‰	stdev	δ15N (‰)	stdev	δ15N (‰)	stdev	δ15N (‰	stdev
Trophic	Glx	19.64	4.56	1.94	3.78	25.62	0.59	6.45	0.84
	Asx	18.55	0.82	0.85	1.23	17.70	0.70	-1.47	0.37
	Ala	28.95	1.56	11.25	1.89	27.65	1.14	8.47	1.16
	Ile	32.36	3.12	14.66	2.30	36.23	3.22	17.06	2.64
	Leu	29.52	3.34	11.82	4.01	28.23	2.53	9.05	2.74
	Pro	31.61	1.04	13.91	1.74	30.70	1.30	11.52	0.90
	Val	30.57	1.77	12.87	2.17	29.06	0.95	9.89	1.07
Intermediate	Gly	16.44	0.24	-1.26	0.96	15.82	0.81	-3.35	0.99
	Ser	16.00	3.67	-1.70	4.17	13.91	1.18	-5.26	1.62
Source	Lys	9.07	0.97	-8.63	1.10	8.74	1.18	-10.44	0.64
	Tyr	8.81	3.51	-8.89	3.26	9.67	1.84	-9.51	1.44
	Phe	10.06	2.31	-7.64	1.89	9.64	1.27	-9.31	0.87
Metabolic	Thr	-21.46	8.73	-39.17	7.82	-5.47	2.30	-24.65	2.42
Averages	Avg THAA	17.70	1.03			19.18	0.80		
	Avg Trophic	27.31	0.73			27.89	0.74		
	Avg Source	9.32	1.74			9.42	1.20		
Parameters	Trophic - Sou	18.00	1.92			18.46	0.94		
	∑V	4.92	0.77			3.98	0.27		
	∑V - no Ile	4.31	1.17			2.91	0.19		
	TP "Coral Ca	2.26	0.54			3.12	0.14		

Appendix Table 2-10.1. Statistics comparing binned regions of nitrogen CSIA-AA data for the Subfossil Coral Outer vs Inner (0-5mm vs >10 mm) from Cross Seamount using a t-Test (Two-Sample Assuming Unequal Variances). Highlight means that the comparison is significantly different in mean values (p value 0.05 or better).

Outer vs Inner Subfossil	Glx		Asx		Ala		Ile		Leu	
0-5 mm vs >10 mm	*0-5 mm*	*>10 mm*	*0-5 mm*	*>10 mm*	*0-5 mm*	*>10 mm*	*0-5 mm*	*>10 mm*	*0-5 mm*	*>10 mm*
Mean δ^{15}N (‰)	19.64	25.62	18.55	17.70	28.95	27.65	32.36	36.23	29.52	28.23
Variance	20.78	0.35	0.67	0.49	2.44	1.31	9.72	10.39	11.16	6.39
Observations	5	6	5	6	5	6	5	6	5	6
Hypothesized Mean Difference	0		0		0		0		0	
Difference (Outer - Inner)	-5.98		0.84		1.30		-3.87		1.29	
df	4		8		7		9		7	
t Stat	-2.91		1.81		1.55		-2.02		0.71	
P(T<=t) one-tail	0.02		0.05		0.08		0.04		0.25	
t Critical one-tail	2.13		1.86		1.89		1.83		1.89	
P(T<=t) two-tail	0.04		0.11		0.16		0.07		0.50	
t Critical two-tail	2.78		2.31		2.36		2.26		2.36	

Outer vs Inner Subfossil	Pro		Val		Gly		Ser		Lys	
0-5 mm vs >10 mm	*0-5 mm*	*>10 mm*	*0-5 mm*	*>10 mm*	*0-5 mm*	*>10 mm*	*0-5 mm*	*>10 mm*	*0-5 mm*	*>10 mm*
Mean δ^{15}N (‰)	31.61	30.70	30.57	29.06	16.44	15.82	16.00	13.91	9.07	8.74
Variance	1.08	1.70	3.12	0.91	0.06	0.65	13.44	1.39	0.95	1.39
Observations	5	6	5	6	5	6	5	6	5	6
Hypothesized Mean Difference	0		0		0		0		0	
Difference (Outer - Inner)	0.91		1.51		0.62		2.09		0.34	
df	9		6		6		5		9	
t Stat	1.29		1.71		1.79		1.22		0.52	
P(T<=t) one-tail	0.12		0.07		0.06		0.14		0.31	
t Critical one-tail	1.83		1.94		1.94		2.02		1.83	
P(T<=t) two-tail	0.23		0.14		0.12		0.28		0.62	
t Critical two-tail	2.26		2.45		2.45		2.57		2.26	

Outer vs Inner Subfossil	Tyr		Phe		Thr	
0-5 mm vs >10 mm	*0-5 mm*	*>10 mm*	*0-5 mm*	*>10 mm*	*0-5 mm*	*>10 mm*
Mean δ^{15}N (‰)	8.81	9.67	10.06	9.64	-21.46	-5.47
Variance	12.30	3.39	5.34	1.62	76.18	5.27
Observations	5	6	5	5	5	6
Hypothesized Mean Difference	0		0		0	
Difference (Outer - Inner)	-0.86		0.42		-15.99	
df	6		6		4	
t Stat	-0.49		0.36		-3.98	
P(T<=t) one-tail	0.32		0.37		0.01	
t Critical one-tail	1.94		1.94		2.13	
P(T<=t) two-tail	0.64		0.73		0.02	
t Critical two-tail	2.45		2.45		2.78	

Appendix Table 2-10.2. Statistics comparing binned regions of nitrogen CSIA-AA data for the Modern (excluding industrial revolution) vs Subfossil (>10mm) using a t-Test (Two-Sample Assuming Unequal Variances). Highlight means that the comparison is significantly different in mean values (p value 0.05 or better).

	Glx		Asx		Ala		Ile		Leu	
Modern vs >10 mm Subfossil	*Modern*	*>10 mm*	*Modern*	*>10 mm*	*Modern*	*>10 mm*	*Modern*	*>10 mm*	*Modern*	*>10 mm*
Mean δ^{15}N (‰)	24.77	25.62	15.11	17.70	23.58	27.65	24.69	36.23	23.65	28.23
Variance	1.25	0.35	0.32	0.49	0.88	1.31	2.37	10.39	11.23	6.39
Observations	3	6	3	6	3	6	3	6	3	6
Hypothesized Mean Difference	0		0		0		0		0	
Difference (Modern - Subfossil)	-0.85		-2.59		-4.06		-11.54		-4.58	
df	3		5		5		7		3	
t Stat	-1.24		-5.95		-5.69		-7.27		-2.09	
P(T<=t) one-tail	0.15		0.00		0.00		0.00		0.06	
t Critical one-tail	2.35		2.02		2.02		1.89		2.35	
P(T<=t) two-tail	0.30		0.00		0.00		0.00		0.13	
t Critical two-tail	3.18		2.57		2.57		2.36		3.18	

	Pro		Val		Gly		Ser		Lys	
Modern vs >10 mm Subfossil	*Modern*	*>10 mm*	*Modern*	*>10 mm*	*Modern*	*>10 mm*	*Modern*	*>10 mm*	*Modern*	*>10 mm*
Mean δ^{15}N (‰)	27.10	30.70	25.21	29.06	11.30	15.82	11.70	13.91	6.96	8.74
Variance	1.56	1.70	0.65	0.91	1.05	0.65	0.97	1.39	0.39	1.39
Observations	3	6	3	6	3	6	3	6	3	6
Hypothesized Mean Difference	0		0		0		0		0	
Difference (Modern - Subfossil)	-3.60		-3.86		-4.52		-2.21		-1.78	
df	4		5		3		5		7	
t Stat	-4.02		-6.36		-6.68		-2.97		-2.95	
P(T<=t) one-tail	0.01		0.00		0.00		0.02		0.01	
t Critical one-tail	2.13		2.02		2.35		2.02		1.89	
P(T<=t) two-tail	0.02		0.00		0.01		0.03		0.02	
t Critical two-tail	2.78		2.57		3.18		2.57		2.36	

	Tyr		Phe		Thr	
Modern vs >10 mm Subfossil	*Modern*	*>10 mm*	*Modern*	*>10 mm*	*Modern*	*>10 mm*
Mean δ^{15}N (‰)	4.72	9.67	7.12	9.64	-12.52	-5.47
Variance	0.41	3.39	1.94	1.62	5.89	5.27
Observations	3	6	3	5	3	6
Hypothesized Mean Difference	0		0		0	
Difference (Modern - Subfossil)	-4.94		-2.52		-7.05	
df	7		4		4	
t Stat	-5.90		-2.56		-4.18	
P(T<=t) one-tail	0.00		0.03		0.01	
t Critical one-tail	1.89		2.13		2.13	
P(T<=t) two-tail	0.00		0.06		0.01	
t Critical two-tail	2.36		2.78		2.78	

Appendix Table 2-10.3. Statistics comparing binned regions of nitrogen CSIA-AA data for the Subfossil Coral Outer vs Inner (0-5mm vs >10 mm) from Cross Seamount, HI using data normalized to THAA and a t-Test (Two-Sample Assuming Unequal Variances). Highlight means that the comparison is significantly different in mean values (p value 0.05 or better).

Outer vs Inner Subfossil Coral	Glx		Asx		Ala		Ile		Leu	
0-5 mm vs >10 mm	*0-5 mm*	*>10 mm*	*0-5 mm*	*>10 mm*	*0-5 mm*	*>10 mm*	*0-5 mm*	*>10 mm*	*0-5 mm*	*>10 mm*
Mean δ15N (‰)	1.94	6.45	0.85	-1.47	11.25	8.47	14.66	17.06	11.82	9.05
Variance	14.30	0.71	1.52	0.14	3.57	1.34	5.30	6.98	16.06	7.49
Observations	5	6	5	6	5	6	5	6	5	6
Difference (Outer - Inner)	-4.51		2.32		2.78		-2.40		2.76	
Hypothesized Mean Difference	0		0		0		0		0	
Degree of freedom	4		5		6		9		7	
t Stat	-2.61		4.06		2.87		-1.61		1.31	
P(T<=t) one-tail	0.03		0.00		0.01		0.07		0.12	
t Critical one-tail	2.13		2.02		1.94		1.83		1.89	
P(T<=t) two-tail	0.06		0.01		0.03		0.14		0.23	
t Critical two-tail	2.78		2.57		2.45		2.26		2.36	

Outer vs Inner Subfossil Coral	Pro		Val		Gly		Ser		Lys	
0-5 mm vs >10 mm	*0-5 mm*	*>10 mm*	*0-5 mm*	*>10 mm*	*0-5 mm*	*>10 mm*	*0-5 mm*	*>10 mm*	*0-5 mm*	*>10 mm*
Mean δ15N (‰)	13.91	11.52	12.87	9.89	-1.26	-3.35	-1.70	-5.26	-8.63	-10.44
Variance	3.04	0.80	4.73	1.15	0.93	0.98	17.36	2.63	1.20	0.41
Observations	5	6	5	6	5	6	5	6	5	6
Difference (Outer - Inner)	2.38		2.98		2.09		3.56		1.81	
Hypothesized Mean Difference	0		0		0		0		0	
Degree of freedom	6		6		9		5		6	
t Stat	2.76		2.79		3.54		1.80		3.26	
P(T<=t) one-tail	0.02		0.02		0.00		0.07		0.01	
t Critical one-tail	1.94		1.94		1.83		2.02		1.94	
P(T<=t) two-tail	0.03		0.03		0.01		0.13		0.02	
t Critical two-tail	2.45		2.45		2.26		2.57		2.45	

Outer vs Inner Subfossil Coral	Tyr		Phe		Thr	
0-5 mm vs >10 mm	*0-5 mm*	*>10 mm*	*0-5 mm*	*>10 mm*	*0-5 mm*	*>10 mm*
Mean δ15N (‰)	-8.89	-9.51	-7.64	-9.31	-39.17	-24.65
Variance	10.63	2.08	3.56	0.76	61.12	5.84
Observations	5	6	5	5	5	6
Difference (Outer - Inner)	0.62		1.67		-14.52	
Hypothesized Mean Difference	0		0		0	
Degree of freedom	5		6		5	
t Stat	0.39		1.79		-4.00	
P(T<=t) one-tail	0.36		0.06		0.01	
t Critical one-tail	2.02		1.94		2.02	
P(T<=t) two-tail	0.71		0.12		0.01	
t Critical two-tail	2.57		2.45		2.57	

Appendix Table 2-10.4. Statistics comparing binned regions of nitrogen CSIA-AA data for the Modern (excluding industrial revolution) vs Subfossil (>10 mm) using data normalized to THAA and a t-Test (Two-Sample Assuming Unequal Variances). Highlight means that the comparison is significantly different in mean values (p value 0.05 or better).

Normalized data	Glx		Asx		Ala		Ile		Leu	
Modern vs >10 mm Subfossil	*Modern*	*>10 mm*	*Modern*	*>10 mm*	*Modern*	*>10 mm*	*Modern*	*>10 mm*	*Modern*	*>10 mm*
Mean δ15N (‰)	9.89	6.45	0.23	-1.47	8.71	8.47	9.81	17.06	8.77	9.05
Variance	0.09	0.71	0.35	0.14	0.27	1.34	2.66	6.98	8.39	7.49
Observations	3	6	3	6	3	6	3	6	3	6
Difference (Modern - Subfossil)	0		0		0		0		0	
Hypothesized Mean Difference	3.45		1.70		0.24		-7.24		-0.28	
Degree of freedom	7		3		7		6		4	
t Stat	8.90		4.59		0.42		-5.06		-0.14	
P(T<=t) one-tail	0.00		0.01		0.34		0.00		0.45	
t Critical one-tail	1.89		2.35		1.89		1.94		2.13	
P(T<=t) two-tail	0.00		0.02		0.69		0.00		0.89	
t Critical two-tail	2.36		3.18		2.36		2.45		2.78	

Normalized data	Pro		Val		Gly		Ser		Lys	
Modern vs >10 mm Subfossil	*Modern*	*>10 mm*	*Modern*	*>10 mm*	*Modern*	*>10 mm*	*Modern*	*>10 mm*	*Modern*	*>10 mm*
Mean δ15N (‰)	12.23	11.52	10.33	9.89	-3.57	-3.35	-3.17	-5.26	-7.92	-10.44
Variance	0.52	0.80	0.01	1.15	1.10	0.98	0.15	2.63	0.36	0.41
Observations	3	6	3	6	3	6	3	6	3	6
Difference (Modern - Subfossil)	0		0		0		0		0	
Hypothesized Mean Difference	0.70		0.44		-0.22		2.09		2.52	
Degree of freedom	5		5		4		6		4	
t Stat	1.27		1.00		-0.30		2.99		5.79	
P(T<=t) one-tail	0.13		0.18		0.39		0.01		0.00	
t Critical one-tail	2.02		2.02		2.13		1.94		2.13	
P(T<=t) two-tail	0.26		0.36		0.78		0.02		0.00	
t Critical two-tail	2.57		2.57		2.78		2.45		2.78	

Normalized data	Tyr		Phe		Thr	
Modern vs >10 mm Subfossil	*Modern*	*>10 mm*	*Modern*	*>10 mm*	*Modern*	*>10 mm*
Mean δ15N (‰)	-10.15	-9.51	-7.76	-9.31	-27.40	-24.65
Variance	1.02	2.08	0.26	0.76	3.49	5.84
Observations	3	6	3	5	3	6
Difference (Modern - Subfossil)	0		0		0	
Hypothesized Mean Difference	-0.64		1.55		-2.75	
Degree of freedom	6		6		5	
t Stat	-0.78		3.18		-1.88	
P(T<=t) one-tail	0.23		0.01		0.06	
t Critical one-tail	1.94		1.94		2.02	
P(T<=t) two-tail	0.47		0.02		0.12	
t Critical two-tail	2.45		2.45		2.57	

Appendix Table 2-11. Modern coral carbon isotope CSIA-AA results.

		Measured		Normalized	Measured		Normalized	Measured		Normalized	Measured		Normalized
		$\delta^{13}C$ (‰)	stdev	δ13C (‰)	$\delta^{13}C$ (‰)	stdev	δ13C (‰)	$\delta^{13}C$ (‰)	stdev	δ13C (‰)	$\delta^{13}C$ (‰)	stdev	δ13C (‰)
Essential	Phe	-24.66	0.31	-13.11	-23.08	1.54	-10.02	-24.29	0.67	-12.12	-23.87	0.16	-11.28
	Thr	-3.16	0.20	8.38	-15.56	0.80	-2.51	-10.02	0.30	2.15	-4.84	0.34	7.75
	Ile	-16.46	0.64	-4.92	-20.40	0.34	-7.35	-16.96	0.70	-4.79	-16.70	0.13	-4.11
	Leu	-22.58	0.31	-11.04	-19.24	0.39	-6.19	-22.34	0.26	-10.17	-23.05	0.20	-10.46
	Val	-17.73	0.63	-6.19	-18.19	0.30	-5.14	-20.62	0.17	-8.45	-20.12	0.64	-7.53
	Lys	-21.66	0.19	-10.12	-15.77	0.17	-2.72	-14.82	0.31	-2.66	-24.04	1.00	-11.45
Non-Essential	Asp	-10.52	0.19	1.02	-13.19	0.40	-0.14	-11.78	0.20	0.39	-11.30	0.16	1.29
	Glu	-10.55	0.31	0.99	-10.76	0.23	2.29	-9.13	0.22	3.03	-10.83	0.33	1.76
	Pro	-12.06	0.15	-0.52	-12.04	1.22	1.01	-12.22	0.34	-0.06	-11.80	0.37	0.79
	Ala	-6.52	0.59	5.03	-5.75	0.52	7.31	-11.74	0.28	0.42	-8.73	0.57	3.86
	Ser	8.77	0.77	20.31	-2.92	0.39	10.13	10.80	0.65	22.96	8.93	0.50	21.52
	Gly	-1.38	0.18	10.16	0.30	0.08	13.35	-2.86	0.02	9.30	-4.72	0.17	7.87
Avg THAA		-11.54	9.87		-13.05	7.22		-12.17	9.44		-12.59	9.76	
Avg Essential		-17.71	7.76		-18.71	2.86		-18.17	5.29		-18.77	7.38	
Avg Non-essential		-5.38	7.94		-7.39	5.45		-6.16	9.02		-6.41	7.95	
mol% weighted THAA		-9.23			-9.39			-9.49			-10.70		

		Modern Coral Averages Excluding the Industrial Revolution			
		Average Measured		Average Normalized	
		δ13C (‰)	stdev	δ13C (‰)	stdev
Essential	Phe	-23.74	0.62	-11.14	1.06
	Thr	-10.14	5.36	2.46	5.14
	Ile	-18.02	2.06	-5.42	1.71
	Leu	-21.54	2.03	-8.94	2.39
	Val	-19.64	1.28	-7.04	1.71
	Lys	-18.21	5.07	-5.61	5.06
Non-Essential	Asp	-12.09	0.98	0.51	0.72
	Glu	-10.24	0.96	2.36	0.64
	Pro	-12.02	0.21	0.58	0.56
	Ala	-8.74	3.00	3.86	3.44
	Ser	5.60	7.44	18.20	7.03
	Gly	-2.43	2.54	10.17	2.84
	Avg THAA	-12.60	0.44		
	Avg Essential	-18.55	0.33		
	Avg Non-essential	-6.65	0.65		
	mol% weighted THAA	-9.86	0.73		

Appendix Table 2-12. Subfossil coral carbon isotope CSIA-AA results.

	Depth (mm)	3			4.5			7.5		
	Year BP	9789			9851			9976		
		Measured		Normalized	Measured		Normalized	Measured		Normalized
		$\delta^{13}C$ (‰)	stdev	δ13C (‰)	$\delta^{13}C$ (‰)	stdev	δ13C (‰)	$\delta^{13}C$ (‰)	stdev	δ13C (‰)
Essential	Phe	-21.89	0.64	-10.17	-21.35	0.79	-9.59	-24.96	0.34	-11.41
	Thr	-7.22	1.64	4.50	-6.15	0.13	5.62	-6.74	0.91	6.80
	Ile	-15.89	1.44	-4.16	-11.97	0.66	-0.20	-16.30	0.64	-2.76
	Leu	-22.49	1.54	-10.77	-25.77	0.35	-14.00	-25.92	0.11	-12.38
	Val	-21.53	1.19	-9.81	-18.65	0.27	-6.89	-15.96	0.55	-2.42
	Lys	-16.30	1.80	-4.57	-15.91	0.55	-4.15	-16.92	0.59	-3.37
Non-Essential	Asp	-11.87	1.29	-0.15	-10.71	0.36	1.05	-12.69	0.58	0.86
	Glu	-11.90	1.48	-0.18	-9.79	0.19	1.98	-12.24	0.70	1.31
	Pro	-11.85	1.35	-0.12	-12.77	0.17	-1.01	-15.98	0.81	-2.44
	Ala	-7.55	1.16	4.17	-10.38	0.59	1.38	-10.47	0.91	3.07
	Ser	12.57	1.26	24.30	3.15	0.22	14.91	-4.62	1.67	8.92
	Gly	-4.78	1.29	6.94	-0.88	0.19	10.89	0.28	0.19	13.83
Avg THAA		-11.73	9.68		-11.77	8.16		-13.54	7.65	
Avg Essential		-17.55	5.83		-16.63	6.96		-17.80	7.01	
Avg Non-essential		-5.90	9.51		-6.90	6.43		-9.29	6.00	
mol% weighted THAA		-12.04			-11.78			-12.74		

	Depth (mm)	10			15			20		
	Year BP	10081			10289			10498		
		Measured		Normalized	Measured		Normalized	Measured		Normalized
		$\delta^{13}C$ (‰)	stdev	δ13C (‰)	$\delta^{13}C$ (‰)	stdev	δ13C (‰)	$\delta^{13}C$ (‰)	stdev	δ13C (‰)
Essential	Phe	-22.57	0.57	-9.34	-19.87	0.88	-9.14	-18.59	1.19	-9.53
	Thr	-9.16	1.08	4.07	-7.06	0.39	3.67	-6.98	0.35	2.08
	Ile	-17.73	0.77	-4.50	-12.63	0.18	-1.89	-15.17	0.64	-6.10
	Leu	-24.95	0.33	-11.72	-23.47	0.76	-12.73	-21.42	0.71	-12.35
	Val	-18.14	1.32	-4.91	-18.41	0.62	-7.67	-12.50	0.10	-3.44
	Lys	-14.16	1.09	-0.92	-15.68	0.68	-4.95	-14.12	0.32	-5.06
Non-Essential	Asp	-8.84	0.72	4.40	-9.49	0.15	1.25	-7.45	0.79	1.62
	Glu	-8.19	1.02	5.04	-11.27	0.09	-0.54	-6.90	0.89	2.17
	Pro	-13.28	0.96	-0.05	-11.34	0.24	-0.61	-10.18	0.52	-1.12
	Ala	-21.03	2.90	-7.79	-9.73	0.42	1.00	-11.09	0.82	-2.02
	Ser	3.16	1.84	16.40	13.38	0.41	24.12	11.01	0.32	20.07
	Gly	-3.89	0.37	9.34	-3.25	0.23	7.48	4.61	0.25	13.67
Avg THAA		-13.23	8.25		-10.73	9.47		-9.07	9.17	
Avg Essential		-17.79	5.69		-16.19	5.79		-14.80	5.00	
Avg Non-essential		-8.68	8.21		-5.28	9.62		-3.33	9.00	
mol% weighted THAA		-12.62			-11.50			-8.44		

	Depth (mm)	25			30			35		
	Year BP	10706			10915			11123		
		Measured		Normalized	Measured		Normalized	Measured		Normalized
		$\delta^{13}C$ (‰)	stdev	δ13C (‰)	$\delta^{13}C$ (‰)	stdev	δ13C (‰)	$\delta^{13}C$ (‰)	stdev	δ13C (‰)
Essential	Phe	-24.83	1.40	-15.25	-22.23	0.95	-12.88	-20.20	0.92	-8.01
	Thr	0.39	0.38	9.96	-2.70	0.27	6.65	-9.59	1.47	2.59
	Ile	-7.50	1.46	2.07	-12.74	0.22	-3.40	-19.54	1.32	-7.35
	Leu	-20.85	0.32	-11.28	-21.33	0.34	-11.98	-25.83	1.49	-13.64
	Val	-17.89	0.06	-8.32	-15.67	0.13	-6.32	-17.49	0.30	-5.30
	Lys	-15.32	1.09	-5.75	-15.29	0.43	-5.94	-14.25	0.64	-2.06
Non-Essential	Asp	-6.58	0.13	2.99	-6.53	0.19	2.81	-8.46	0.88	3.73
	Glu	-14.97	0.20	-5.40	-9.64	0.13	-0.29	-6.32	0.64	5.87
	Pro	-10.14	0.34	-0.57	-10.23	0.32	-0.88	-14.05	1.39	-1.87
	Ala	-9.23	0.89	0.34	-6.48	0.20	2.87	-20.00	2.68	-7.81
	Ser	16.16	0.18	25.73	13.06	0.09	22.41	8.96	2.75	21.15
	Gly	-4.10	0.06	5.47	-2.39	0.09	6.96	0.51	0.60	12.70
Avg THAA		-9.57	10.86		-9.35	9.57		-12.19	9.84	
Avg Essential		-14.33	9.27		-14.99	7.06		-17.82	5.54	
Avg Non-essential		-4.81	10.90		-3.70	8.68		-6.56	10.31	
mol% weighted THAA		-11.13			-10.50			-11.18		

		Subfossil Coral 0-5 mm				Subfossil Coral >10 mm			
		Average Measured		Average Normalized		Average Measured		Average Normalized	
		δ13C (‰)	stdev	δ13C (‰)	stdev	δ13C (‰)	stdev	δ13C (‰)	stdev
Essential	Phe	-21.62	0.38	-9.88	0.41	-21.38	2.26	-10.69	2.77
	Thr	-6.69	0.76	5.06	0.79	-5.85	3.91	4.84	2.97
	Ile	-13.93	2.77	-2.18	2.80	-14.22	4.28	-3.53	3.35
	Leu	-24.13	2.31	-12.39	2.29	-22.97	2.09	-12.28	0.83
	Val	-20.09	2.03	-8.35	2.06	-16.68	2.27	-5.99	1.82
	Lys	-16.10	0.27	-4.36	0.30	-14.80	0.70	-4.11	2.10
Non-Essential	Asp	-11.29	0.82	0.45	0.85	-7.89	1.23	2.80	1.20
	Glu	-10.85	1.49	0.90	1.52	-9.55	3.21	1.14	4.15
	Pro	-12.31	0.66	-0.56	0.63	-11.54	1.73	-0.85	0.61
	Ala	-8.97	2.00	2.78	1.97	-12.93	6.07	-2.24	4.59
	Ser	7.86	6.67	19.61	6.64	10.96	4.52	21.65	3.28
	Gly	-2.83	2.76	8.92	2.79	-1.42	3.40	9.27	3.29
Avg THAA		-11.75	0.03			-10.69	1.70		
Avg Essential		-17.09	0.65			-15.99	1.53		
Avg Non-essential		-6.40	0.71			-5.39	1.98		
mol% weighted THAA		-11.91	0.19			-10.89	1.39		

Appendix Table 2-13.1. Statistics comparing binned regions of carbon CSIA-AA for the Subfossil Coral Outer vs Inner (0-5 mm vs >10 mm) using a t-Test (Two-Sample Assuming Unequal Variances). Highlight means that the comparison is significantly different in mean values (p value 0.05 or better).

Outer vs Inner Subfossil	Phe		Thr		Ile		Leu	
0-5 mm vs >10 mm	*0-5 mm*	*>10 mm*	*0-5 mm*	*>10 mm*	*0-5 mm*	*>10 mm*	*0-5 mm*	*>10 mm*
Mean $\delta^{13}C$ (‰)	-21.62	-21.38	-6.69	-5.85	-13.93	-14.22	-24.13	-22.97
Variance	0.15	5.09	0.57	15.32	7.69	18.28	5.36	4.39
Observations	2	6	2	6	2	6	2	6
Hypothesized Mean Difference	0		0		0		0	
Difference (Outer - Inner)	-0.24		-0.84		0.29		-1.16	
df	6		6		3		2	
t Stat	-0.25		-0.50		0.11		-0.63	
P(T<=t) one-tail	0.41		0.32		0.46		0.30	
t Critical one-tail	1.94		1.94		2.35		2.92	
P(T<=t) two-tail	0.81		0.64		0.92		0.59	
t Critical two-tail	2.45		2.45		3.18		4.30	

Outer vs Inner Subfossil	Val		Lys		Asp		Glu	
0-5 mm vs >10 mm	*0-5 mm*	*>10 mm*	*0-5 mm*	*>10 mm*	*0-5 mm*	*>10 mm*	*0-5 mm*	*>10 mm*
Mean $\delta^{13}C$ (‰)	-20.09	-16.68	-16.10	-14.80	-11.29	-7.89	-10.85	-9.55
Variance	4.14	5.14	0.07	0.49	0.68	1.50	2.23	10.33
Observations	2	6	2	6	2	6	2	6
Hypothesized Mean Difference	0		0		0		0	
Difference (Outer - Inner)	-3.41		-1.30		-3.40		-1.30	
df	2		5		3		4	
t Stat	-1.99		-3.77		-4.44		-0.77	
P(T<=t) one-tail	0.09		0.01		0.01		0.24	
t Critical one-tail	2.92		2.02		2.35		2.13	
P(T<=t) two-tail	0.18		0.01		0.02		0.48	
t Critical two-tail	4.30		2.57		3.18		2.78	

Outer vs Inner Subfossil	Pro		Ala		Ser		Gly	
0-5 mm vs >10 mm	*0-5 mm*	*>10 mm*	*0-5 mm*	*>10 mm*	*0-5 mm*	*>10 mm*	*0-5 mm*	*>10 mm*
Mean $\delta^{13}C$ (‰)	-12.31	-11.54	-8.97	-12.93	7.86	10.96	-2.83	-1.42
Variance	0.43	2.98	4.01	36.88	44.42	20.42	7.61	11.53
Observations	2	6	2	6	2	6	2	6
Hypothesized Mean Difference	0		0		0		0	
Difference (Outer - Inner)	-0.77		3.96		-3.10		-1.41	
df	5		6		1		2	
t Stat	-0.92		1.39		-0.61		-0.59	
P(T<=t) one-tail	0.20		0.11		0.33		0.31	
t Critical one-tail	2.02		1.94		6.31		2.92	
P(T<=t) two-tail	0.40		0.21		0.65		0.61	
t Critical two-tail	2.57		2.45		12.71		4.30	

Appendix Table 2-13.2. Statistics comparing binned regions of carbon CSIA-AA for the Modern Coral vs Subfossil coral (>10 mm) using a t-Test (Two-Sample Assuming Unequal Variances). Highlight means that the comparison is significantly different in mean values (p value 0.05 or better).

Modern vs Inner Subfossil	Phe		Thr		Ile		Leu	
Modern vs >10 mm Subfossil	*Modern*	*>10 mm*	*Modern*	*>10 mm*	*Modern*	*>10 mm*	*Modern*	*>10 mm*
Mean $\delta^{13}C$ (‰)	-23.97	-21.38	-8.39	-5.85	-17.63	-14.22	-21.80	-22.97
Variance	0.46	5.09	31.36	15.32	3.45	18.28	3.01	4.39
Observations	4	6	4	6	4	6	4	6
Hypothesized Mean Difference	0		0		0		0	
Difference (Modern - Inner)	-2.59		-2.54		-3.41		1.17	
df	6		5		7		7	
t Stat	-2.64		-0.79		-1.73		0.96	
P(T<=t) one-tail	0.02		0.23		0.06		0.18	
t Critical one-tail	1.94		2.02		1.89		1.89	
P(T<=t) two-tail	0.04		0.47		0.13		0.37	
t Critical two-tail	2.45		2.57		2.36		2.36	

Modern vs Inner Subfossil	Val		Lys		Asp		Glu	
Modern vs >10 mm Subfossil	*Modern*	*>10 mm*	*Modern*	*>10 mm*	*Modern*	*>10 mm*	*Modern*	*>10 mm*
Mean $\delta^{13}C$ (‰)	-19.16	-16.68	-19.08	-14.80	-11.70	-7.89	-10.32	-9.55
Variance	2.02	5.14	20.11	0.49	1.26	1.50	0.64	10.33
Observations	4	6	4	6	4	6	4	6
Hypothesized Mean Difference	0		0		0		0	
Difference (Modern - Inner)	-2.48		-4.27		-3.81		-0.77	
df	8		3		7		6	
t Stat	-2.13		-1.89		-5.06		-0.56	
P(T<=t) one-tail	0.03		0.08		0.00		0.30	
t Critical one-tail	1.86		2.35		1.89		1.94	
P(T<=t) two-tail	0.07		0.16		0.00		0.59	
t Critical two-tail	2.31		3.18		2.36		2.45	

Modern vs Inner Subfossil	Pro		Ala		Ser		Gly	
Modern vs >10 mm Subfossil	*Modern*	*>10 mm*	*Modern*	*>10 mm*	*Modern*	*>10 mm*	*Modern*	*>10 mm*
Mean $\delta^{13}C$ (‰)	-12.03	-11.54	-8.18	-12.93	6.39	10.96	-2.17	-1.42
Variance	0.03	2.98	7.23	36.88	39.42	20.42	4.57	11.53
Observations	4	6	4	6	4	6	4	6
Hypothesized Mean Difference	0		0		0		0	
Difference (Modern - Inner)	-0.49		4.74		-4.56		-0.75	
df	5		7		5		8	
t Stat	-0.69		1.68		-1.25		-0.43	
P(T<=t) one-tail	0.26		0.07		0.13		0.34	
t Critical one-tail	2.02		1.89		2.02		1.86	
P(T<=t) two-tail	0.52		0.14		0.27		0.68	
t Critical two-tail	2.57		2.36		2.57		2.31	

Appendix Table 2-13.3. Statistics comparing binned regions of carbon CSIA-AA for the Subfossil Coral Outer vs Inner (0-5 mm vs >10 mm) using normalized data and a t-Test (Two-Sample Assuming Unequal Variances). Highlight means that the comparison is significantly different in mean values (p value 0.05 or better).

Outer vs Inner Subfossil	Phe		Thr		Ile		Leu	
Norm: 0-5 mm vs >10 mm	*0-5 mm*	*>10 mm*	*0-5 mm*	*>10 mm*	*0-5 mm*	*>10 mm*	*0-5 mm*	*>10 mm*
Mean $\delta^{13}C$ (‰)	-9.88	-10.69	5.06	4.84	-2.18	-3.53	-12.39	-12.28
Variance	0.17	7.68	0.62	8.82	7.85	11.25	5.23	0.69
Observations	2	6	2	6	2	6	2	6
Hypothesized Mean Difference	0		0		0		0	
Difference (Outer - Inner)	0.82		0.22		1.35		-0.10	
df	6		6		2		1	
t Stat	0.70		0.17		0.56		-0.06	
P(T<=t) one-tail	0.26		0.44		0.32		0.48	
t Critical one-tail	1.94		1.94		2.92		6.31	
P(T<=t) two-tail	0.51		0.87		0.63		0.96	
t Critical two-tail	2.45		2.45		4.30		12.71	

Outer vs Inner Subfossil	Val		Lys		Asp		Glu	
Norm: 0-5 mm vs >10 mm	*0-5 mm*	*>10 mm*	*0-5 mm*	*>10 mm*	*0-5 mm*	*>10 mm*	*0-5 mm*	*>10 mm*
Mean $\delta^{13}C$ (‰)	-8.35	-5.99	-4.36	-4.11	0.45	2.80	0.90	1.14
Variance	4.26	3.30	0.09	4.40	0.72	1.45	2.32	17.24
Observations	2	6	2	6	2	6	2	6
Hypothesized Mean Difference	0		0		0		0	
Difference (Outer - Inner)	-2.35		-0.25		-2.35		-0.24	
df	2		6		3		5	
t Stat	-1.44		-0.28		-3.02		-0.12	
P(T<=t) one-tail	0.14		0.40		0.03		0.45	
t Critical one-tail	2.92		1.94		2.35		2.02	
P(T<=t) two-tail	0.29		0.79		0.06		0.91	
t Critical two-tail	4.30		2.45		3.18		2.57	

Outer vs Inner Subfossil	Pro		Ala		Ser		Gly	
Norm: 0-5 mm vs >10 mm	*0-5 mm*	*>10 mm*	*0-5 mm*	*>10 mm*	*0-5 mm*	*>10 mm*	*0-5 mm*	*>10 mm*
Mean $\delta^{13}C$ (‰)	-0.56	-0.85	2.78	-2.24	19.61	21.65	8.92	9.27
Variance	0.39	0.38	3.89	21.03	44.04	10.73	7.77	10.82
Observations	2	6	2	6	2	6	2	6
Hypothesized Mean Difference	0		0		0		0	
Difference (Outer - Inner)	0.28		5.02		-2.04		-0.36	
df	2		5		1		2	
t Stat	0.56		2.15		-0.42		-0.15	
P(T<=t) one-tail	0.32		0.04		0.37		0.45	
t Critical one-tail	2.92		2.02		6.31		2.92	
P(T<=t) two-tail	0.63		0.08		0.75		0.90	
t Critical two-tail	4.30		2.57		12.71		4.30	

Appendix Table 2-13.4. Statistics comparing binned regions of carbon CSIA-AA for the Modern Coral vs Subfossil coral (>10 mm) using normalized data and a t-Test (Two-Sample Assuming Unequal Variances). Highlight means that the comparison is significantly different in mean values (p value 0.05 or better).

Modern vs Inner Subfossil	Phe		Thr		Ile		Leu	
Norm: Modern vs >10 mm	*Modern*	*>10 mm*	*Modern*	*>10 mm*	*Modern*	*>10 mm*	*Modern*	*>10 mm*
Mean $\delta^{13}C$ (‰)	-11.6346	-10.6932	3.943058	9.270746	-5.2923	-3.52919	-9.46668	-12.2839
Variance	1.716248	7.677913	26.37145	10.82148	2.000805	11.24882	4.901155	0.693061
Observations	4	6	4	6	4	6	4	6
Hypothesized Mean Difference	0		0		0		0	
Difference (Modern - Inner)	-0.94135		-5.32769		-1.76311		2.817184	
df	8		5		7		4	
t Stat	-0.72014		-1.83862		-1.14405		2.432951	
P(T<=t) one-tail	0.24597		0.062685		0.145106		0.035876	
t Critical one-tail	1.859548		2.015048		1.894579		2.131847	
P(T<=t) two-tail	0.49194		0.12537		0.290211		0.071752	
t Critical two-tail	2.306004		2.570582		2.364624		2.776445	

Modern vs Inner Subfossil	Val		Lys		Asp		Glu	
Norm: Modern vs >10 mm	*Modern*	*>10 mm*	*Modern*	*>10 mm*	*Modern*	*>10 mm*	*Modern*	*>10 mm*
Mean $\delta^{13}C$ (‰)	-6.82732	-5.9936	-6.73818	-4.11273	0.639143	2.798657	2.018229	1.143111
Variance	2.13476	3.30143	22.13354	4.399604	0.412768	1.449302	0.74072	17.24334
Observations	4	6	4	6	4	6	4	6
Hypothesized Mean Difference	0		0		0		0	
Difference (Modern - Inner)	-0.83372		-2.62545		-2.15951		0.875118	
df	8		4		8		6	
t Stat	-0.80079		-1.04878		-3.67797		0.500348	
P(T<=t) one-tail	0.22319		0.176732		0.003119		0.317325	
t Critical one-tail	1.859548		2.131847		1.859548		1.94318	
P(T<=t) two-tail	0.446381		0.353464		0.006237		0.634649	
t Critical two-tail	2.306004		2.776445		2.306004		2.446912	

Modern vs Inner Subfossil	Pro		Ala		Ser		Gly	
Norm: Modern vs >10 mm	*Modern*	*>10 mm*	*Modern*	*>10 mm*	*Modern*	*>10 mm*	*Modern*	*>10 mm*
Mean $\delta^{13}C$ (‰)	0.305327	-1.00815	4.152198	-2.23652	18.72997	21.64648	10.17112	9.270746
Variance	0.511666	0.279134	8.235718	21.03418	34.06276	10.73269	5.381613	10.82148
Observations	4	5	4	6	4	6	4	6
Hypothesized Mean Difference	0		0		0		0	
Difference (Modern - Inner)	1.313478		6.388713		-2.91651		0.900373	
df	5		8		4		8	
t Stat	3.0642		2.708292		-0.90856		0.507385	
P(T<=t) one-tail	0.013984		0.013364		0.207488		0.312787	
t Critical one-tail	2.015048		1.859548		2.131847		1.859548	
P(T<=t) two-tail	0.027968		0.026729		0.414975		0.625573	
t Critical two-tail	2.570582		2.306004		2.776445		2.306004	

Chapter 3 Tables

Appendix Table 3-1. Radiocarbon data and age model for Kingman 1 and Kingman 2 corals.

CAMS#	depth (mm)	Fmodern		14C (yrs BP)		Age modeled (yr CE)
Kingman 1						
166969	0.7	1.0827	0.0045	>Modern		1965
166970	3.6	0.9372	0.0032	520	30	1810
166971	5.8	0.9251	0.0032	625	30	1688
166972	7.2	0.9335	0.0036	555	35	1602
166973	9	0.9197	0.0038	670	35	1467
166974	10.9	0.8575	0.0030	1235	30	1241
Kingman 2						
166975	0.1	0.8176	0.0033	1615	35	932
166976	3.9	0.8196	0.0031	1600	35	763
166977	7.6	0.7896	0.0037	1900	40	591
166978	11.4	0.7834	0.0035	1960	40	426
166979	17.2	0.7610	0.0028	2195	30	168
166980	21	0.7568	0.0033	2240	35	-5

Appendix Table 3-2. Bulk isotopic data and C/N ratios for the Kingman 1, live collected coral.

Depth (mm)	Year CE	δ13C (‰)	δ15N (‰)	C/N Ratio
0.1	2007	-17.19	15.43	2.80
0.2	2001	-17.38	15.77	2.81
0.3	1995	-17.30	16.33	2.77
0.4	1990	-16.84	16.76	2.79
0.5	1984	-16.72	16.62	2.74
0.6	1978		16.69	2.79
0.7	1972	-16.79	16.66	2.77
0.8	1965	-16.73	16.77	2.79
0.9	1959	-16.61	16.65	2.74
1	1953	-16.50	16.78	2.74
1.1	1947	-16.55	16.99	2.84
1.2	1941	-16.41	17.41	2.70
1.3	1936	-16.49	17.33	2.77
1.4	1931	-16.52	17.15	2.84
1.5	1926	-16.32	17.05	2.74
1.6	1920	-16.41	17.05	2.76
1.7	1915	-16.43	16.98	2.72
1.8	1910	-16.24	17.08	2.74
1.9	1904	-16.38	17.11	2.71
2	1899	-16.33	17.05	2.72
2.1	1894	-16.34	17.47	2.72
2.2	1888	-16.11	17.49	2.72
2.3	1883	-16.11	17.68	2.71
2.4	1878	-16.15	17.70	2.74
2.5	1872	-16.22	17.33	2.74
2.6	1867	-16.11	17.17	2.71
2.7	1862	-16.13	17.05	2.73
2.8	1856	-16.23	17.09	2.73
2.9	1851	-15.95	17.26	2.72
3	1846	-15.96	17.51	2.71
3.1	1841	-15.70	17.61	2.72
3.2	1836	-15.82	17.65	2.69
3.3	1831	-15.64	17.68	2.70
3.4	1825	-15.68	17.75	2.72
3.5	1820	-15.56	17.61	2.70

Depth (mm)	Year CE	δ13C (‰)	δ15N (‰)	C/N Ratio
3.6	1815	-15.73	17.73	2.74
3.7	1810	-15.71	17.67	2.72
3.8	1804	-15.67	17.74	2.71
3.9	1799	-15.71	17.72	2.72
4	1793	-15.71	17.71	2.73
4.1	1788	-15.89	17.89	2.72
4.2	1782	-15.93	17.72	2.78
4.3	1777	-16.09	17.37	2.71
4.4	1771	-15.85	17.47	2.72
4.5	1766	-15.86	17.64	2.72
4.6	1760	-15.91	17.39	2.71
4.7	1755	-15.84	17.48	2.72
4.8	1749	-15.97	17.71	2.75
4.9	1744	-15.83	17.65	2.73
5	1738	-15.69	17.55	2.70
5.1	1732	-15.86	17.41	2.74
5.2	1727	-15.75	17.57	2.74
5.3	1721	-15.66	17.55	2.69
5.4	1716	-15.84	17.57	2.73
5.5	1710	-15.79	17.64	2.71
5.6	1705	-15.92	17.43	2.70
5.7	1699		17.30	2.70
5.8	1693	-15.89	17.06	2.70
5.9	1688	-15.93	17.25	2.72
6	1682	-15.88	17.37	2.72
6.1	1676	-15.86	17.71	2.67
6.2	1670	-16.11	17.87	2.69
6.3	1664	-15.95	17.86	2.68
6.4	1658	-15.72	17.50	2.69
6.5	1652	-15.83	17.55	2.69
6.6	1646	-15.91	17.51	2.67
6.7	1640	-15.71	17.57	2.68
6.8	1634	-15.75	17.44	2.65
6.9	1628	-15.66	17.79	2.67

Depth (mm)	Year CE	δ13C (‰)	δ15N (‰)	C/N Ratio
7	1622	-15.72	17.74	2.68
7.1	1616	-15.65	17.89	2.68
7.2	1609	-15.70	17.75	2.70
7.3	1602	-15.78	17.43	2.67
7.4	1595	-15.79	17.59	2.69
7.5	1589	-15.78	17.20	2.64
7.6	1582	-15.62	17.57	2.68
7.7	1574	-15.64	17.80	2.68
7.8	1566	-15.90	17.58	2.66
7.9	1559	-15.65	17.68	2.69
8	1551	-15.67	17.50	2.71
8.1	1543	-15.84	17.65	2.66
8.2	1536	-15.95	17.53	2.71
8.3	1528	-16.06	17.35	2.69
8.4	1520	-16.02	17.61	2.69
8.5	1513	-16.01	17.60	2.73
8.6	1505	-15.83	17.77	2.68
8.7	1497	-15.69	18.05	2.73
8.8	1490	-15.80	17.70	2.74
8.9	1482	-15.65	17.43	2.73
9	1475	-15.53	17.31	2.81
9.1	1467	-15.83	17.05	2.69
9.2	1455	-15.74	16.76	2.69
9.3	1443	-15.99	16.61	2.70
9.4	1432	-16.12	16.75	2.70
9.5	1420	-15.93	16.63	2.71
9.6	1408	-16.19	16.62	2.68
9.7	1396	-16.06	16.97	2.71
9.8	1383	-16.12	17.16	2.72
9.9	1371	-16.04	17.37	2.73
10	1359	-16.06	17.45	2.76
10.1	1347	-15.96	17.72	2.76
10.2	1335	-16.03	17.86	2.75
10.3	1323	-16.31	17.46	2.72
10.4	1311	-16.44	17.96	2.64
10.5	1300	-16.11	17.40	2.67
10.6	1288	-15.98	17.50	2.67
10.7	1276	-16.07	17.38	2.65
10.8	1264	-16.36	17.09	2.69
10.9	1253	-16.12	17.12	2.71
11	1241	-16.07	17.05	2.71

Appendix Table 3-3. Bulk isotopic data and C/N ratios for the Kingman 2, subfossil coral. Note that the outermost 2.5 mm data should be excluded from environmental analysis as C/N ratios and acidity tests indicate degradation of the skeleton.

Depth (mm)	Year CE	δ13C (‰)	δ15N (‰)	C/N
0.1	932	-14.65	17.01	3.30
0.2	927	-14.49	17.70	3.03
0.3	923	-14.69	17.70	3.00
0.4	918	-14.73	17.41	2.99
0.5	914	-14.94	17.37	3.06
0.6	910	-14.84	17.71	3.00
0.7	905	-14.94	17.78	2.95
0.8	901	-14.91	17.75	3.02
0.9	896	-14.87	17.92	2.96
1	892	-15.16	17.69	2.95
1.1	887	-15.21	17.63	2.88
1.2	883	-15.05	17.49	2.91
1.3	878	-15.11	17.63	2.90
1.4	874	-15.17	17.73	2.92
1.5	869	-15.18	17.66	2.93
1.6	865	-15.35	17.87	2.89
1.7	861			2.93
1.8	856	-15.25	18.01	2.89
1.9	852	-15.12	18.04	2.88
2	847	-15.22	18.01	2.90
2.1	843	-15.50	17.90	2.86
2.2	839	-15.34	17.78	2.91
2.3	834	-15.37	17.83	2.90
2.4	830	-15.69	17.85	2.89
2.5	826	-15.64	17.81	2.92
2.6	821	-15.48	17.81	2.88
2.7	817	-15.56	17.80	2.86
2.8	812	-15.59	17.71	2.85
2.9	808	-15.60	17.58	2.87
3	803	-15.44	17.73	2.91
3.1	799	-15.31	17.41	2.88
3.2	794	-15.44	17.27	2.89
3.3	790	-15.35	17.18	2.90
3.4	786	-15.38	17.61	2.92
3.5	781	-15.52	17.18	2.83

Depth (mm)	Year CE	δ13C (‰)	δ15N (‰)	C/N Ratio
3.6	777	-15.55	18.10	2.88
3.7	772	-15.24	17.98	2.97
3.8	768	-15.16	18.26	2.91
3.9	763	-15.29	17.78	2.90
4	759			2.91
4.1	754	-15.52	17.58	2.93
4.2	749	-15.29	17.39	2.95
4.3	745	-15.32	17.25	2.99
4.4	740	-15.35	17.38	2.88
4.5	735	-15.27	17.33	2.88
4.6	731			2.92
4.7	726			2.88
4.8	721	-15.15	17.44	2.93
4.9	717	-15.25	17.51	2.96
5	712	-15.28	17.42	2.93
5.1	707	-15.19	17.03	2.87
5.2	703	-15.33	17.29	2.87
5.3	698	-15.26	17.16	2.87
5.4	693	-15.35	17.39	2.86
5.5	689	-15.40	17.30	2.87
5.6	684	-15.49	17.58	2.81
5.7	679	-15.24	17.78	2.89
5.8	675	-15.23	17.41	2.87
5.9	670	-15.29	17.71	2.85
6	665	-15.10	17.69	2.86
6.1	661	-15.29	17.86	2.86
6.2	656	-15.33	17.88	2.85
6.3	651	-15.42	17.74	2.84
6.4	647	-15.42	17.58	2.82
6.5	642	-15.55	17.75	2.82
6.6	638	-15.60	17.47	2.82
6.7	633	-15.40	17.15	2.81
6.8	628	-15.59	17.55	2.83
6.9	624	-15.53	17.68	2.83

Depth (mm)	Year CE	δ13C (‰)	δ15N (‰)	C/N Ratio
7	619	-15.60	17.69	2.85
7.1	614	-15.45	17.38	2.84
7.2	610	-15.34	17.49	2.85
7.3	605	-15.50	17.26	2.83
7.4	600	-15.54	17.02	2.81
7.5	596	-15.68	16.96	2.82
7.6	591	-15.52	16.96	2.85
7.7	587	-15.62	16.67	2.85
7.8	582	-15.65	16.80	2.86
7.9	578	-15.56	16.57	2.85
8	574	-15.59	16.77	2.85
8.1	569	-15.48	16.73	2.79
8.2	565	-15.57	16.98	2.83
8.3	561	-15.49	17.11	2.80
8.4	556	-15.45	17.41	2.84
8.5	552	-15.45	17.29	2.80
8.6	547	-15.41	17.13	2.79
8.7	543	-15.58	17.29	2.83
8.8	539	-15.73	17.42	2.81
8.9	535	-15.58	17.29	2.82
9	530	-15.61	17.48	2.86
9.1	526	-15.79	17.10	2.84
9.2	522	-15.72	17.15	2.83
9.3	517	-15.70	16.96	2.84
9.4	513	-15.73	17.37	2.82
9.5	509	-15.57	17.29	2.80
9.6	504	-15.48	17.09	2.82
9.7	500	-15.62	17.30	2.84
9.8	496	-15.56	17.18	2.80
9.9	491	-15.76	17.29	2.78
10	487	-15.51	17.42	2.78
10.1	483	-15.68	17.26	2.79
10.2	479	-15.76	17.02	2.78

Depth (mm)	Year CE	δ13C (‰)	δ15N (‰)	C/N Ratio
10.3	474	-15.65	17.24	2.79
10.4	470	-15.78	17.07	2.80
10.5	466	-15.74	17.05	2.77
10.6	461	-15.98	16.90	2.80
10.7	457	-15.77	16.93	2.80
10.8	452	-15.67	16.83	2.81
10.9	448	-15.88	17.00	2.81
11	444	-15.62	17.06	2.83
11.1	439	-15.89	16.99	2.83
11.2	435	-15.89	16.74	2.84
11.3	430	-15.88	16.85	2.86
11.4	426	-15.95	16.68	2.81
11.5	422	-15.92	16.78	2.81
11.6	417	-15.85	16.70	2.84
11.7	413	-15.96	16.71	2.78
11.8	408	-15.98	16.70	2.78
11.9	404	-16.11	16.83	2.93
12	399	-15.97	16.67	2.92
12.1	395	-16.03	16.65	2.90
12.2	390	-16.13	16.61	2.85
12.3	386	-15.96	16.70	2.92
12.4	382	-16.02	16.73	2.93
12.5	377	-15.86	16.85	2.92
12.6	373	-16.02	16.91	2.93
12.7	369	-15.93	16.70	2.95
12.8	364	-15.89	16.96	2.92
12.9	360		17.09	2.94
13	355			2.93
13.1	351	-15.82	17.23	2.94
13.2	346	-16.06	17.03	2.92
13.3	342	-15.97	17.01	2.99
13.4	337	-15.96	17.24	2.91
13.5	333	-15.86	17.15	2.90
13.6	328	-15.92	17.05	2.85
13.7	324	-15.95	16.97	2.83

Depth (mm)	Year CE	δ13C (‰)	δ15N (‰)	C/N Ratio
13.8	319	-16.04	17.02	2.88
13.9	315	-16.03	16.79	2.89
14	310	-16.07	16.83	2.87
14.1	306	-16.13	16.75	2.86
14.2	301	-15.84	16.74	2.90
14.3	297	-16.06	16.98	2.88
14.4	292	-15.93	16.82	2.91
14.5	288	-15.99	16.84	2.92
14.6	283	-15.81	16.95	2.90
14.7	279	-16.04	16.79	2.90
14.8	275	-15.88	16.83	2.87
14.9	270	-15.94	16.67	2.87
15	266	-15.95	16.77	2.85
15.1	261	-15.92	16.38	2.86
15.2	257	-16.17	16.52	2.85
15.3	252	-16.14	16.71	2.86
15.4	248	-16.17	17.08	2.86
15.5	243	-16.12	16.76	2.86
15.6	239	-16.14	17.03	2.86
15.7	235	-16.11	17.06	2.81
15.8	230	-16.14	16.98	2.86
15.9	226	-16.04	16.74	2.86
16	221	-16.13	16.84	2.84
16.1	217	-16.04	16.50	2.86
16.2	212	-16.16	16.55	2.84
16.3	208	-15.96	16.36	2.84
16.4	203	-16.18	16.22	2.86
16.5	199	-16.28	16.16	2.84
16.6	194	-16.14	16.50	2.82
16.7	190	-16.26	16.53	2.83
16.8	186	-16.34	16.39	2.84
16.9	181			2.83
17	177	-16.35	16.33	2.83

Depth (mm)	Year CE	δ13C (‰)	δ15N (‰)	C/N Ratio
17.1	172	-16.33	16.68	2.85
17.2	168	-16.35	16.49	2.85
17.3	163		16.37	2.84
17.4	159	-15.94	16.59	2.83
17.5	154	-16.23	16.53	2.83
17.6	150	-16.10	16.34	2.83
17.7	145	-16.31	16.45	2.80
17.8	141	-16.37	16.89	2.64
17.9	136	-16.32	16.64	2.80
18	132	-16.27	16.56	2.82
18.1	127	-16.30	16.76	2.79
18.2	123	-16.33	16.66	2.66
18.3	118	-16.22	16.69	2.75
18.4	114	-16.31	16.62	2.72
18.5	109	-16.32	16.52	2.75
18.6	105	-16.32	16.40	2.75
18.7	100	-16.32	16.61	2.73
18.8	96	-16.39	16.63	2.74
18.9	91	-16.31	16.61	2.74
19	86	-16.27	16.57	2.74
19.1	82	-16.26	16.52	2.74
19.2	77	-16.34	16.49	2.76
19.3	73	-16.25	16.31	2.75
19.4	68	-16.28	16.31	2.75
19.5	63	-16.26	16.15	2.73
19.6	59	-16.21	15.79	2.76
19.7	54	-16.08	15.93	2.73
19.8	50	-16.06	15.86	2.72
19.9	45	-16.20	16.25	2.72
20	41	-16.28	16.49	2.71
20.1	36	-16.34	16.41	2.75
20.2	32	-16.21	16.34	2.72
20.3	27	-16.26	16.55	2.73
20.4	23	-16.15	16.20	2.72
20.5	18	-16.19	16.73	2.72
20.6	14	-16.24	16.62	2.71
20.7	9	-16.20	16.56	2.69
20.8	4	-16.16	16.47	2.70
20.9	0	-16.26	16.52	2.65
21	-5	-16.21	16.90	2.66

Appendix Table 3-4. CSIA-AA nitrogen values and parameters for the live collected Kingman 1 coral from the Line Islands. As these samples are a compilation of adjacent growth layers, the estimate for age has an error of 20-30 years.

	Year CE	1995		1820		1652		1420		1288	
	Depth	0.3		3.5		6.5		9.5		10.6	
	Year analyzed	2019		2019		2022		2019		2022	
		$\delta^{15}N$	±	$\delta^{15}N$	±	$\delta^{15}N$	±	$\delta^{15}N$	±	$\delta^{15}N$	±
Trophic	*Glx	28.20	0.16	30.28	0.47	30.20	0.56	28.92	0.52	29.85	0.15
	Asx	19.46	0.20	20.65	0.26	20.16	0.22	19.71	0.14	20.19	0.15
	Ala	23.13	0.72	32.68	1.95	29.60	2.37	24.71	3.25	31.52	1.73
	Ile	27.79	1.08	33.74	0.29	31.83	0.55	29.53	2.10	32.89	0.13
	Leu	30.06	0.50	33.23	0.33	33.28	0.65	29.70	0.89	34.10	0.26
	Pro	32.94	0.18	35.28	0.19	33.55	1.05	32.71	0.29	33.66	0.46
	Val	22.06	0.47	33.82	0.19	34.16	0.61	24.96	0.09	34.85	0.65
Intermed.	Gly	11.10	0.08	17.62	0.15	18.79	0.22	17.42	0.06	18.63	0.07
	Ser	7.49	0.01	20.09	0.18	17.89	0.24	19.50	0.49	18.53	0.14
Source	Lys	10.61	0.65	12.91	1.22	9.81	0.63	12.16	0.26	11.16	0.32
	Tyr	11.27	0.51	12.97	0.17	10.79	0.17	11.23	0.36	11.79	0.29
	Phe	8.54	0.54	11.13	0.86	8.96	0.93	6.98	0.75	7.40	0.40
Metabolic	Thr	-14.22	0.99	-29.17	0.43	-25.98	1.00	-9.30	0.35	-27.40	0.37
	Avg (Tr-Src)	16.43	0.39	16.44	0.58	17.15	0.56	13.72	0.64	17.51	0.34
	Glu-Phe	19.65	0.56	19.15	0.98	21.25	1.09	21.94	0.91	22.45	0.43
	avg all trophics:	26.23	0.21	31.38	0.30	30.40	0.41	27.18	0.57	31.01	0.28
	avg all source:	10.14	0.33	12.34	0.50	9.85	0.38	10.12	0.29	10.11	0.20
Paramaters	TP "classic"	3.14	0.07	3.07	0.13	3.35	0.14	3.44	0.12	3.51	0.06
	TP "multi trophic"	3.93	0.07	3.85	0.13	4.18	0.14	4.30	0.12	4.38	0.06
	TP "coral specific"	3.59	0.11	3.52	0.17	3.80	0.27	3.89	0.15	3.95	0.12
	∑V	4.02		3.38		3.21		3.47		3.42	

Appendix Table 3-5. CSIA-AA nitrogen values and parameters for the subfossil Kingman 2 coral from the Line Islands. As these samples are a compilation of adjacent growth layers, the estimate for age has an error of 20-30 years.

	Year CE	707		552		422		159	
	Depth	5.1		8.5		11.5		17.4	
	Year analyzed	2022		2022		2022		2019	
		$\delta^{15}N$	±	$\delta^{15}N$	±	$\delta^{15}N$	±	$\delta^{15}N$	±
Trophic	*Glx	29.75	0.18	30.12	0.07	29.44	0.53	29.48	0.08
	Asx	20.35	0.20	20.76	0.18	20.25	0.09	20.31	0.04
	Ala	31.34	1.55	31.64	2.06	32.31	2.44	29.00	0.92
	Ile	32.80	0.69	33.41	0.47	33.35	0.32	31.99	0.27
	Leu	35.16	0.19	35.26	0.37	34.79	0.25	31.57	0.31
	Pro	34.17	0.25	33.82	0.73	33.40	0.37	33.35	0.19
	Val	35.30	0.30	35.50	0.45	35.57	0.60	30.04	0.31
Intermed.	Gly	18.76	0.07	18.44	0.33	20.05	0.26	18.17	0.15
	Ser	18.19	0.09	18.47	0.22	18.35	0.11	19.28	0.99
Source	Lys	10.53	0.23	11.18	0.09	11.45	0.17	12.65	0.22
	Tyr	12.31	0.17	13.01	0.05	13.09	1.64	12.58	0.58
	Phe	7.62	0.49	7.83	0.16	7.43	0.33	10.08	0.35
Metabolic	Thr	-28.94	1.21	-26.94	1.86	-25.82	0.76	-24.65	2.28
	Avg (Tr-Src)	17.79	0.32	17.71	0.34	17.22	0.67	14.84	0.28
	Glu-Phe	22.13	0.53	22.29	0.17	22.01	0.62	19.40	0.36
	avg all trophics:	31.27	0.25	31.50	0.33	31.30	0.38	29.39	0.15
	avg all source:	10.15	0.19	10.67	0.06	10.66	0.56	11.77	0.24
Paramaters	TP "classic"	3.46	0.07	3.49	0.02	3.45	0.08	3.11	0.05
	TP "multi trophic"	4.33	0.07	4.35	0.02	4.31	0.08	3.89	0.05
	TP "coral specific"	3.91	0.11	3.93	0.14	3.90	0.10	3.55	0.08
	∑V	3.55		3.46		3.69		2.71	

Bibliography

Altabet, M.A. (2006). Isotopic Tracers of the Marine Nitrogen Cycle: Present and Past. *Hdb Env Chem* **2**, 251–293.

Altabet, M. A. (2001). Nitrogen isotopic evidence for micronutrient control of fractional NO3- utilization in the equatorial Pacific. *Limnol. Oceanogr.* **46**, 368–380.

Altabet M. A. (1988) Variations in nitrogen isotopic composition between sinking and suspended particles: implications for nitrogen cycling and particle transformation in the open ocean. *Deep Sea Research Part A. Oceanographic Research Papers* **35**, 535–554.

Ambrose S.H. and Norr L. (1993) Experimental Evidence for the Relationship of the Carbon Isotope Ratios of Whole Diet and Dietary Protein to Those of Bone Collagen and Carbonate. In *Prehistoric Human Bone* (eds. J. B. Lambert, G. Grupe). *Springer.* pp. 1–38.

Antonov, J.I., Seidov, D., Boyer, T.P., Locarnini, R.A., Mishonov, A. V., Garcia, H.E., Baranova, O.K., Zweng, M.M., Johnson, D.R. (2010). World Ocean Atlas 2009, Volume 2: Salinity, NOAA Atlas NESDIS 69. 10.1182/blood-2011-06-357442

Arellano-Torres, E. (2010). Paleoceanography of the https://doi.org/Eastern Tropical North Pacific on Millennial Timescales. Univ. Edinburgh. Dissertation: https://www.era.lib.ed.ac.uk/handle/1842/4634

Baines, S.B., Twining, B.S., Vogt, S., Balch, W.M., Fisher, N.S. and Nelson, D.M. (2011). Elemental composition of equatorial Pacific diatoms exposed to additions of silicic acid and iron. *Deep Sea Research Part II: Topical Studies in Oceanography* **58** (3-4), 512-523.

Batista F. C., Ravelo C. A., Crusius J., Casso M. A., and McCarthy M. D. (2014) Compound specific amino acid $\delta^{15}N$ in marine sediments: A new approach for studies of the marine nitrogen cycle. *Geochimica et Cosmochimica Acta* **142**, 553–569.

Berger, A., Loutre, M.F. (1991). Insolation values for the climate of the last 10 million years. Quat. Sci. Rev. 10, 4, 297-317.

Beaufort, L., de Garidel-Thoron, T., Mix, A.C. and Pisias, N.G. (2001). ENSO-like forcing on oceanic primary production during the late Pleistocene. *Science* **293** (5539), 2440-2444.

Bidigare, R.R., Hanson, K.L., Buesseler, K.O., Wakeham, S.G., Freeman, K.H., Pancost, R.D., Millero, F.J., Steinberg, P., Popp, B.N., Latasa, M., Landry, M.R., Laws, E.A. (1999). Iron-stimulated changes in ^{13}C fractionation and export by equatorial Pacific phytoplankton: Toward a paleogrowth rate proxy. *Paleoceanography* **14** (5), 589-595.

Blaauw, M., Christen, J.A. (2011). Flexible paleoclimate age-depth models using an autoregressive gamma process. *Bayesian Anal.* **6**, 457–474.

Boyce, D.G., Lewis, M.R., Worm, B. (2010). Global phytoplankton decline over the past century. *Nature* **466**, 591–596.

Boyer T. P., Garcia H. E., Locarnini R. A.; Zweng M. M., Mishonov A. V., Reagan J. R., Weathers K. A., BaranovaO. K., Seidov D., Smolyar I. V. (2018). World Ocean Atlas 2018. Temperature and Dissolved Oxygen averaged over years 1955-2010 at 400m. *NOAA National Centers for Environmental Information*, https://accession.nodc.noaa.gov/NCEI-WOA18 (accessed July-4-2021).

Brainard RE, Acoba T, Asher MAM, Asher JM, Ayotte PM, Barkley HC, DesRochers A, Dove D, Halperin AA, Huntington B, Kindinger TL, Lichowski F, Lino KC, McCoy KS,Oliver T, Pomeroy N, Suka R, Timmers M, Vargas-Ángel B, Venegas RM, Wegley Kelly L, Williams ID, Winston M, Young CW, Zamzow J (2019) Coral Reef Ecosystem Monitoring Report for the Pacific Remote Islands Marine National Monument 2000–2017. Pacific Islands Fisheries Science Center, *PIFSC Special Publication*, SP-19-006. 820 p.

Broccoli, A.J., Dahl, K.A. and Stouffer, R.J. (2006). Response of the ITCZ to Northern Hemisphere cooling. *Geophysical Research Letters*, **33**(1).

Brzezinski, M.A., Krause, J.W., Church, M.J., Karl, D.M., Li, B., Jones, J.L. and Updyke, B. (2011). The annual silica cycle of the North Pacific subtropical gyre. *Deep Sea Research Part I: Oceanographic Research Papers*, **58** (10), 988-1001.

Casciotti, K.L., Trull, T.W., Glover, D.M., Davies, D. (2008). Constraints on nitrogen cycling at the subtropical North Pacific Station ALOHA from isotopic measurements of nitrate and particulate nitrogen. *Deep. Res. Part II Top. Stud. Oceanogr.* **55**, 1661–1672.

Catão A. J. L. and López-Castillo A. (2018) On the degradation pathway of glyphosate and glycine. *Environmental Science: Processes and Impacts* **20**, 1148-1157.

Chang, A.S., Pedersen, T.F., Hendy, I.L. (2008). Late Quaternary paleoproductivity

history on the Vancouver Island margin, western Canada: a multiproxy geochemical study. *Can. J. Earth Sci.* **45**, 1283–1297. https://doi.org/10.1139/E08-054

Chavez, F.P., Messié, M., Pennington, J.T. (2011). Marine primary production in relation to climate variability and change. *Ann. Rev. Mar. Sci.* **3**, 227–260. https://doi.org/10.1146/annurev.marine.010908.163917

Chavez, F. P., Buck, K. R., Service, S. K., Newton, J., & Barber, R. T. (1996). Phytoplankton variability in the central and eastern tropical Pacific. *Deep Sea Research Part II: Topical Studies in Oceanography*, **43** (4-6), 835-870.

Chavez, F. P. & Toggweiler, J. R. (1995) Physical estimates of global new production: The upwelling contribution, in: C. P. Summerhayes, K.-C. Emeis, M. V. Angel, R. L. Smith & B. Zeitzschel (Eds) Upwelling in the ocean: Modern processes and ancient records. New York, *John Wiley & Sons*, 313-320.

Chikaraishi Y., Ogawa N.O., Kashiyama Y., Takano Y., Suga H., Tomitani A., Miyashita H., Kitazato H., and Ohkouchi N. (2009) Determination of aquatic food-web structure based on compound-specific nitrogen isotopic composition of amino acids. *Limnology and Oceanography: Methods* **7**, 740–750.

Clement, A.C., Seager, R., Cane, M.A. (2000). Suppression of El Niño during the Mid-Holocene by changes in the Earth's orbit. *Paleoceanography* **15**, 731–77.

Clement, A.C., Seager, R. and Cane, M.A. (1999). Orbital controls on the El Nino/Southern Oscillation and the tropical climate. *Paleoceanography*, **14**(4), pp.441-456.

Coale, K.H., Fitzwater, S.E., Gordon, R.M., Johnson, K.S. and Barber, R.T. (1996). Control of community growth and export production by upwelled iron in the equatorial Pacific Ocean. *Nature*, **379** (6566), pp.621-624.

Cobb, K.M., Charles, C.D., Cheng, H., Edwards, R.L. (2003). El Nino / Southern Oscillation and tropical El Nino Pacific climate during the last millennium. *Nature* **424**, 271–276.

Corno, G., Karl, D.M., Church, M.J., Letelier, R.M., Lukas, R., Bidigare, R.R., Abbott, M.R. (2007). Impact of climate forcing on ecosystem processes in the North Pacific Subtropical Gyre. *J. Geophys. Res.* **112**, 1–14.

Costa, K.M., Jacobel, A.W., McManus, J.F., Anderson, R.F., Winckler, G. and Thiagarajan, N. (2017). Productivity patterns in the equatorial Pacific over the last 30,000 years. *Global Biogeochemical Cycles*, **31** (5), pp.850-865.

Dandonneau, Y., Deschamps, P.Y., Nicolas, J.M., Loisel, H., Blanchot, J., Montel, Y., Thieuleux, F. and Bécu, G. (2004). Seasonal and interannual variability of ocean color and composition of phytoplankton communities in the North Atlantic, equatorial Pacific and South Pacific. *Deep Sea Research Part II: Topical Studies in Oceanography*, **51** (1-3), pp.303-318.

Dauwe B., Middelburg J. J., Herman P. M. J., and Heip C.H.R. (1999) Linking diagenetic alteration of amino acids and bulk organic matter reactivity. *Limnology and Oceanography* **44**, 1809–1814.

Deutsch, C., Sarmiento, J.L., Sigman, D.M., Gruber, N., Dunne, J.P., 2007. Spatial coupling of nitrogen inputs and losses in the ocean. *Nature*, **445** (7124), 163-167.

Deutsch, C., Berelson, W., Thunell, R., Weber, T., Tems, C., McManus, J., Crusius, J., Ito, T., Baumgartner, T., Ferreira, V. and Mey, J. (2014). Centennial changes in North Pacific anoxia linked to tropical trade winds. *Science*, **345** (6197), 665-668.

Di Lorenzo, E., Schneider, N., Cobb, K.M., Franks, P.J.S., Chhak, K., Miller, J., McWilliams, J.C., Bograd, S.J., Arango, H., Curchitser, E., Powell, T.M., Rivière, P. (2008). North Pacific Gyre Oscillation links ocean climate and ecosystem change. *Geophys. Res. Lett.* 35, 2–7.

Diaz, H.F., Giambelluca, T.W. (2012). Changes in atmospheric circulation patterns associated with high and low rainfall regimes in the Hawaiian Islands region on multiple time scales. *Glob. Planet. Change* **98–99**, 97–108.

Dore, J.E., Brum, J.R., Tupas, L.M., Karl, D.M. (2002). Seasonal and interannual variability in sources of nitrogen supporting export in the oligotrophic subtropical North Pacific *Ocean. Limnol. Oceanogr.* **47**, 1595–1607.

Dore, J.E., Lukas, R., Sadler, D.W., Church, M.J., Karl, D.M. (2009). Physical and biogeochemical modulation of ocean acidification in the central North Pacific. *Proc. Natl. Acad. Sci.* **106**, 12235–12240.

Druffel, E.R.M., Griffin, S., Witter, A., Nelson, E., Southon, J., Kashgarian, M., and Vogel, J. (1995). Gerardia: Bristlecone pine of the deep-sea? *Geochim. Cosmochim. Acta* **59**, 5031-5036.

Druffel, E.R.M., Griffin, S., Guilderson, T.P., Kashgarian, M., Southon, J., Schrag, D.P. (2001). Changes of subtropical North Pacific radiocarbon and correlation with climate variability. *Radiocarbon* **43** (1), 15-25.

Dubois, N., Oppo, D.W., Galy, V.V., Mohtadi, M., Van Der Kaars, S., Tierney, J.E., Rosenthal, Y., Eglinton, T.I., Lückge, A. and Linsley, B.K. (2014). Indonesian vegetation response to changes in rainfall seasonality over the past 25,000 years. *Nature Geoscience*, **7** (7), pp.513-517.

Dubois, N., Kienast, M., Kienast, S., Normandeau, C., Calvert, S.E., Herbert, T.D., Mix, A., 2011. Millennial-scale variations in hydrography and biogeochemistry in the Eastern Equatorial Pacific over the last 100 kyr. *Quat. Sci. Rev.* **30**, 210–223.

Edinger E. N. and Sherwood O. A. (2012). Applied taphonomy of gorgonian and antipatharian corals in Atlantic Canada: experimental decay rates, field observations, and implications for assessing fisheries damage to deep-sea coral habitats. *Neues Jahrbuch fur Geologie und Palaontologie-Abhandlungen*, **265**, 199.

Ehrlich H. (2010) Chitin and collagen as universal and alternative templates in biomineralization. *International Geology Review* **52**, 661-699.

Ehrlich, H., Etnoyer, P., Litvinov, S.D., Olennikova, M.M., Domaschke, H., Hanke, T., Born, R., Meissner, H., Worch, H. (2006). Biomaterial structure in deep-sea bamboo coral (*Anthozoa: Gorgonacea: Isididae*): perspectives for the development of bone implants and templates for tissue engineering. *Materwiss. Werksttech.* **37**, 552–557.

Emmer, E., Thunell, R.C. (2000). Nitrogen isotope variations in Santa Barbara Basin sediments: Implications for denitrification in the eastern tropical North Pacific during the last 50,000 years. *Paleoceanography* **15**, 377–387.

Finkel, Z. V., Beardall, J., Flynn, K.J., Quigg, A., Rees, T.A. V, Raven, J.A. (2010). Phytoplankton in a changing world: Cell size and elemental stoichiometry. *J. Plankton Res.* **32**, 119–137.

Feely, R.A., Gammon, R.H., Taft, B.A., Pullen, P.E., Waterman, L.S., Conway, T.J., Gendron, J.F. and Wisegarver, D.P., 1987. Distribution of chemical tracers in the eastern equatorial Pacific during and after the 1982–1983 El Niño/Southern Oscillation event. *Journal of Geophysical Research: Oceans*, **92** (C6), pp.6545-6558.

Fiedler, P.C., Talley, L.D. (2006). Progress in Oceanography Hydrography of the eastern tropical Pacific : A review. Progress in Oceanography: A review of Eastern Tropical Pacific Oceanography, 69, 143-180.

Fry, B., & Wainright, S.C. (1991). Diatom sources of ^{13}C-rich carbon in marine food webs. *Mar. Ecol. Prog. Ser.*, 149-157.

Galbraith, E.D., Kienast, M., Pedersen, T.F., Calvert, S.E. (2004). Glacial-interglacial modulation of the marine nitrogen cycle by high-latitude O_2 supply to the global thermocline. *Paleoceanography* **19**, 1–12.

Ganeshram, R.S., Pedersen, T.F., Calvert, S.E., McNeill, G.W., Fontugne, M.R. (2000). Glacial-interglacial variability in denitrification in the world's oceans: Causes and consequences. *Paleoceanography* **15**, 361–376.

Ganeshram, R.S., Pedersen, T.F., Calvert, S.E., Murray, J.W. (1995). Large changes in oceanic nutrient inventories from glacial to interglacial periods. *Nature* **376**, 755–758.

Germain L.R., Koch P.L., Harvey J., McCarthy M.D. (2013). Nitrogen isotope fractionation in amino acids from harbor seals: Implications for compound-specific trophic position calculations. *Mar. Ecol. Prog. Ser.* **482**, 265–277. https://doi.org/10.3354/meps10257

Glynn D. S., McMahon K. W., Guilderson T. P., and McCarthy M. D. (2019) Major shifts in nutrient and phytoplankton dynamics in the North Pacific Subtropical Gyre over the last 5000 years revealed by high-resolution proteinaceous deep-sea coral $\delta^{15}N$ and $\delta^{13}C$ records. *Earth and Planetary Science Letters* **515**, 145–153.

Glynn, D. S., McMahon, K. W., Sherwood, O. A., Guilderson, T. P., & McCarthy, M. D. (2022). Investigating preservation of stable isotope ratios in subfossil deep-sea proteinaceous coral skeletons as paleo-recorders of biogeochemical information over multimillennial timescales. *Geochimica et Cosmochimica Acta*, **338**, 264-277.

Goldberg W. M. (1974) Evidence of a sclerotized collagen from the skeleton of a gorgonian coral. *Comparative Biochemistry and Physiology Part B: Comparative Biochemistry* **49**, 525–526.

Goldberg W. M. (1976) Comparative study of the chemistry and structure of gorgonian and antipatharian coral skeletons. *Marine Biology* **35**, 253–267.

Goodfriend G. A. (1997) Aspartic acid racemization and amino acid composition of the organic endoskeleton of the deep-water colonial anemone Gerardia : Determination of longevity from kinetic experiments. *Geochimica et Cosmochimica Acta* **61**, 1931–1939.

Griffiths, M.L., Kimbrough, A.K., Gagan, M.K., Drysdale, R.N., Cole, J.E., Johnson, K.R., Zhao, J.X., Cook, B.I., Hellstrom, J.C. and Hantoro, W.S. (2016). Western Pacific hydroclimate linked to global climate variability over the past two millennia. *Nature communications,* **7** (1), pp.1-9.

Gruber, N. (2016). Elusive marine nitrogen fixation. *Proceedings of the National Academy of Sciences,* **113** (16), 4246-4248.

Guidi, L., Chaffron, S., Bittner, L., Eveillard, D., Larhlimi, A., Roux, S., Darzi, Y., Audic, S., Berline, L., Brum, J.R., Coelho, L.P., Espinoza, J.C.I., Malviya, S., Sunagawa, S., Dimier, C., Kandels-Lewis, S., Picheral, M., Poulain, J., Searson, S., Stemmann, L., Not, F., Hingamp, P., Speich, S., Follows, M., Karp-Boss, L., Boss, E., Ogata, H., Pesant, S., Weissenbach, J., Wincker, P., Acinas, S.G., Bork, P., De Vargas, C., Iudicone, D., Sullivan, M.B., Raes, J., Karsenti, E., Bowler, C., Gorsky, G. (2016). Plankton networks driving carbon export in the oligotrophic ocean. *Nature* **532**, 465–470.

Guilderson, T.P., McCarthy, M.D., Dunbar, R.B., Englebrecht, A., Roark, E.B. (2013). Late Holocene variations in Pacific surface circulation and biogeochemistry inferred from proteinaceous deep-sea corals. *Biogeosciences* **10**, 6019–6028.

Guilderson T. P., Schrag D. P., Druffel E. R. M., Reimer R. W. (2021) Postbomb Subtropical North Pacific Surface Water Radiocarbon History. *Journal of Geophysical Research: Oceans* **126**, e2020JC016881.

Haug, G.H. (2001). Southward Migration of the Intertropical Convergence Zone Through the Holocene. *Science* **293**, 1304–1308.

Heaton T. J., Köhler P., Butzin M., Bard E., Reimer R. W., Austin W.E.N., Bronk Ramsey C., Grootes P.M., Hughen K. A., Kromer B., Reimer P. J., Adkins J., Burke A., Cook M. S., Olsen J., Skinner L. C. (2020) Marine20 - The Marine Radiocarbon Age Calibration Curve (0-55,000 cal BP). *Radiocarbon* **62**, 779–820.

Hendy, J. (2021). Ancient protein analysis in archaeology. Science Advances, 7(3), eabb9314.

Hendy, I.L., Pedersen, T.F. (2006). Oxygen minimum zone expansion in the Eastern Tropical North Pacific during deglaciation. *Geophys. Res. Lett.* **33**, 1–5.

Hendy, I.L., Pedersen, T.F., Kennett, J.P., Tada, R. (2004). Intermittent existence of a southern Californian upwelling cell during submillennial climate change of the last 60 kyr. *Paleoceanography* **19**, 1–15.

Hernes, P.J., Benner, R. (2002). Transport and diagenesis of dissolved and particulate terrigenous organic matter in the North Pacific Ocean. *Deep. Res. Part I Oceanogr. Res. Pap.* **49**, 2119–2132.

Hill T. M., Myrvold C. R., Spero H. J., and Guilderson T. P. (2014) Evidence for benthic-pelagic food web coupling and carbon export from California margin bamboo coral archives. *Biogeosciences* **11**, 3845–3854.

Hinga, K.R., Arthur, M.A., Pilson, M.E.Q., Whitaker, D. (1994). Carbon isotope fractionation by marine phytoplankton in culture: The effects of CO_2 concentration, pH, temperature, and species. *Global Biogeochem. Cycles* **8**, 91–102.

Holl S. M., Schaefer J., Goldberg W. M., Kramer K. J., Morgan T. D., and Hopkins T. L. (1992) Comparison of Black Coral Skeleton and Insect Cuticle by combination of Carbon-13 NMR and Chemical Analyses. *Archives of Biochemistry and Biophysics,* **292,** 107-111.

Horii, S., Takahashi, K., Shiozaki, T., Hashihama, F. and Furuya, K. (2018). Stable isotopic evidence for the differential contribution of diazotrophs to the epipelagic grazing food chain in the mid-Pacific Ocean. *Global Ecology and Biogeography,* **27** (12), pp.1467-1480.

Howell, P., Pisias, N., J.Ballance, J. Baughman, and L. Ochs (2006). ARAND Time-Series Analysis Software, Brown University, Providence RI.

Ingalls A. E., Lee C., and Druffel E. R. M. (2003) Preservation of organic matter in mound-forming coral skeletons. *Geochimica et Cosmochimica Acta* **67**, 2827–2841.

Jia, G., Li, Z., 2011. Easterly denitrification signal and nitrogen fixation feedback documented in the western Pacific sediments. *Geophys. Res. Lett.* **38**, L24605, 1-4.

Johnson, G. C., Sloyan, B. M., Kessler, W. S., & McTaggart, K. E. (2002). Direct measurements of upper ocean currents and water properties across the tropical Pacific during the 1990s. *Progress in Oceanography,* **52** (1), 31-61.

Kaiser K. and Benner R. (2009) Biochemical composition and size distribution of organic matter at the Pacific and Atlantic time-series stations. *Marine Chemistry* **113**, 63-77.

Kao, S.J., Liu, K.K., Hsu, S.C., Chang, Y.P., Dai, M.H. (2008). North Pacific-wide spreading of isotopically heavy nitrogen during the last deglaciation: Evidence from the western Pacific. *Biogeosciences* **5**, 1641–1650. https://doi.org/10.5194/bg-5-1641-2008

Kao, H.Y. and Yu, J.Y., 2009. Contrasting eastern-Pacific and central-Pacific types of ENSO. *Journal of Climate,* **22** (3), pp.615-632.

Kang, J.H., Kim, W.S. and Chang, K.I. (2008). Latitudinal distribution of mesozooplankton in the off-equatorial northeastern Pacific before and after the 1998/99 La Niña event. *Marine environmental research*, **65** (3), pp.218-234.

Karl, D.M., Letelier, R., Hebel, D., Tupas, L., Dore, J., Christian, J., Winn, C. (1995). Ecosystem changes in the North Pacific subtropical gyre attributed to the 1991-92 El Niño. *Nature* **373**, 230–234.

Karl, D., Leteller, R., Tupas, L., Dore, J., Christian, J., Hebel, D., (1997). The role of nitrogen fixation in biogeochemical cycling in the subtropical North Pacific Ocean. *Nature* **388**, 533–538.

Karl, D.M. (1999). Minireviews: A Sea of Change: Biogeochemical Variability in the North Pacific Subtropical Gyre. *Ecosystems* **2**, 181–214.

Karl, D.M., Bidigare, R.R., Letelier, R.M. (2001). Long-term changes in plankton community structure and productivity in the North Pacific Subtropical Gyre: The domain shift hypothesis. *Deep Sea Res. Part II Top. Stud. Oceanogr.* **48**, 1449–1470.

Karl, D., Michaels, A., Bergman, B., Capone, D., Carpenter, E., Letelier, R., Lipschultz, F., Paerl, H., Sigman, D., Stal, L. (2002). Dinitrogen fixation in the world's oceans. *Biogeochemistry* **57–58**, 47–98.

Karl, D.M., Church, M.J., Dore, J.E., Letelier, R.M., Mahaffey, C. (2011). Predictable and efficient carbon sequestration in the North Pacific Ocean supported by symbiotic nitrogen fixation. *PNAS* **109**, 6, 1842-1849.

Keeling, C.D., Brix, H., Gruber, N. (2004). Seasonal and long-term dynamics of the upper ocean carbon cycle at Station ALOHA near Hawaii. *Global Biogeochem. Cycles* **18**, 1–26.

Kienast, M. (2000). Unchanged nitrogen isotopic composition of organic matter in the South China Sea during the last climatic cycle: Global implications. *Paleoceanography* **15**, 244–253.

Kienast, M., Lehmann, M.F., Timmermann, A., Galbraith, E., Bolliet, T., Holbourn, A., Normandeau, C., Laj, C., (2008). A mid-Holocene transition in the nitrogen dynamics of the western equatorial Pacific: Evidence of a deepening thermocline? *Geophys. Res. Lett.* **35**, 1–5.

Kienast, S.S., Calvert, S.E., Pedersen, T.F., (2002). Nitrogen isotope and productivity variations along the northeast Pacific margin over the last 120 kyr: Surface and subsurface paleoceanography. *Paleoceanography* **17** (4), 7-1.

Kim, M. S., Lee, W. S., Suresh Kumar, K., Shin, K. H., Robarge, W., Kim, M., & Lee, S. R. (2016). Effects of HCl pretreatment, drying, and storage on the stable isotope ratios of soil and sediment samples. Rapid Communications in Mass Spectrometry, 30(13), 1567-1575.

Koutavas, A. and Lynch-Stieglitz, J., (2004). Variability of the marine ITCZ over the eastern Pacific during the past 30,000 years. In The Hadley circulation: Present, past and future (pp. 347-369). Springer, Dordrecht.

Krull E. S., Baldock J. A., and Skjemstad J.O. (2003) Importance of mechanisms and processes of the stabilization of soil organic matter for modelling carbon turnover. *Functional Plant Biology* **30**, 207–222.

Lambrides, A.B.J., Weisler, M.I., (2018). Late Holocene Marshall Islands Archaeological Tuna Records Provide Proxy Evidence for ENSO Variability in the Western and Central Pacific Ocean. *J. Isl. Coast. Archaeol.* **13**, 531–562.

Langton, S.J., Linsley, B.K., Robinson, R.S., Rosenthal, Y., Oppo, D.W., Eglinton, T.I., Howe, S.S., Djajadihardja, Y.S., Syamsudin, F., (2008). 3500 yr record of centennial-scale climate variability from the Western Pacific Warm Pool. *Geology* **36**, 795–798.

LaRowe D. E. and Van Cappellen P. (2011) Degradation of natural organic matter: A thermodynamic analysis. *Geochimica et Cosmochimica Acta* **75**, 2030-2042.

Larsen T., Ventura M., Andersen N., O'Brien D. M., Piatkowski U., and McCarthy, M. D. (2013). Tracing carbon sources through aquatic and terrestrial food webs using amino acid stable isotope fingerprinting. *PloS one* **8**, e73441.

Laws, E.A., Popp, B.N., Bidigare, R.R., Kennicutt, M.C., Macko, S.A., (1995). Dependence of phytoplankton carbon isotopic composition on growth rate and $[CO_2]$aq: theoretical considerations and experimental results. *Geochim. Cosmochim. Acta* **59**, 1131–1138.

Le Campion Alsumard T., Golubic S., and Hutchings P. (1995) Microbial endoliths in skeletons of live and dead corals: Porites lobata (Moorea, French Polynesia). *Marine Ecology Progress Series* **117**, 149–158.

Lee, K.E., Slowey, N.C., Herbert, T.D., (2001). Glacial sea surface temperatures in the subtropical North Pacific: A comparison of Uk_{37}', $\delta^{18}O$, and foraminiferal assemblage temperature estimates. *Paleoceanography* **16**, 268–279.

Lehmann M. F., Bernasconi S. M., Barbieri A., and McKenzie J. A. (2002) Preservation of organic matter and alteration of its carbon and nitrogen

isotope composition during simulated and in situ early sedimentary diagenesis. *Geochimica et Cosmochimica Acta* **66**, 3573–3584.

Linsley, B.K., Dunbar, R.B., Dassié, E.P., Tangri, N., Wu, H.C., Brenner, L.D. and Wellington, G.M., (2019). Coral carbon isotope sensitivity to growth rate and water depth with paleo-sea level implications. *Nature Communications*, **10** (1), 1-9.

Locarini, R.A., Mishonov, A. V., Antonov, J.I., Boyer, T.P., Garcia, H.E., Baranova, O.K., Zweng, M.M., Johnson, D.R., (2010). World Ocean Atlas 2009, Volume 1: Temperature, World.

Lu, Z., Liu, Z., Zhu, J., Cobb, K.M., (2018). A review of paleo El Niño-Southern Oscillation. *Atmosphere* **9**, 4, 130.

Mantua, N.J., Hare, S.R., Zhang, Y., Wallace, J.M. and Francis, R.C. (1997). A Pacific interdecadal climate oscillation with impacts on salmon production. *Bulletin of the American Meteorological Society*, **78** (6), pp.1069-1080.

Martin, J.H., Knauer, G.A., Karl, D.M., Broenkow, W.W. (1987). VERTEX: carbon cycling in the northeast Pacific. *Deep Sea Res. Part A, Oceanogr. Res. Pap.* **34**, 267–285.

Martiny, A. C., Vrugt, J. A., & Lomas, M. W. (2014). Concentrations and ratios of particulate organic carbon, nitrogen, and phosphorus in the global ocean. *Scientific data*, **1**(1), 1-7.

Masotti, I., Moulin, C., Alvain, S., Bopp, L., Tagliabue, A., & Antoine, D. (2011). Large-scale shifts in phytoplankton groups in the Equatorial Pacific during ENSO cycles. *Biogeosciences*, **8** (3), 539-550.

Massana, R., Logares, R. (2013). Eukaryotic versus prokaryotic marine picoplankton ecology. *Environ. Microbiol.* **15**, 5, 1254-1261.

Mateo, M. A., Serrano, O., Serrano, L., & Michener, R. H. (2008). Effects of sample preparation on stable isotope ratios of carbon and nitrogen in marine invertebrates: implications for food web studies using stable isotopes. *Oecologia*, **157** (1), 105-115.

McCarthy M. D., Benner R., Lee C. and Fogel M. L. (2007) Amino acid nitrogen isotopic fractionation patterns as indicators of heterotrophy in plankton, particulate, and dissolved organic matter. *Geochimica et Cosmochimica Acta* **71**, 4727–4744.

McCarthy M. D., Lehman J., and Kudela R. (2013) Compound-specific amino acid $\delta^{15}N$ patterns in marine algae: Tracer potential for cyanobacterial vs. eukaryotic organic nitrogen sources in the ocean. *Geochimica et Cosmochimica Acta* **103**, 104-120.

McKay, J.L., Pedersen, T.F., Kienast, S.S. (2004). Organic carbon accumulation over the last 16 kyr off Vancouver Island, Canada: Evidence for increased marine productivity during the deglacial. *Quat. Sci. Rev.* **23**, 261–281.

McMahon K. W., Fogel M. L., Elsdon T. S., and Thorrold, S. R. (2010). Carbon isotope fractionation of amino acids in fish muscle reflects biosynthesis and isotopic routing from dietary protein. *Journal of Animal Ecology* **79**, 1132-1141.

McMahon, K. M, McCarthy, M., Sherwood, O., Larsen, T., Guilderson, T., (2015). Millennial-scale plankton regime shifts in the subtropical North Pacific Ocean. *Science* **350**, 1530–1533.

McMahon K. W. and McCarthy M. D. (2016) Embracing variability in amino acid $\delta^{15}N$ fractionation: Mechanisms, implications, and applications for trophic ecology. *Ecosphere* **7**, 1–26.

McMahon K. W., Williams B., Guilderson T. P., Glynn D. S., and McCarthy M. D. (2018) Calibrating amino acid $\delta^{13}C$ and $\delta^{15}N$ offsets between polyp and protein skeleton to develop proteinaceous deep-sea corals as paleoceanographic archives. *Geochimica et Cosmochimica Acta* **220**, 261-275.

McMahon, K. M., Williams, B., Guilderson, T.P., Glynn, D.S., and McCarthy, M.D., (2017). Calibrating amino acid $\delta^{13}C$ and $\delta^{15}N$ offsets between polyp and protein skeleton to develop deep-sea proteinaceous corals as paleoceanographic archives. *Geochimica et Cosmochimica*, **220**, 261-27.

McPhaden, M. J., & Zhang, D. (2002). Slowdown of the meridional overturning circulation in the upper Pacific Ocean. *Nature*, **415** (6872), 603-608.

Monnin, E., Steig, E. J., Siegenthaler, U., Kawamura, K., Schwander, J., Stauffer, B., Stocker, T.F., Morse, D.L., Barnola, J.M., Bellier, B., Raynaud, D., Fischer, H., (2004). Evidence for substantial accumulation rate variability in Antarctica during the Holocene, through synchronization of CO_2 in the Taylor Dome, Dome C and DML ice cores. *Earth and Planetary Science Letters*, **224** (1-2), 45-54.

Montoya, J.P., McCarthy, J.J. (1995). Isotopic fractionation during nitrate uptake by phytoplankton growth in continuous culture. *J. Plankton Res.* **17**, 439–464.

Moore, J.K., Doney, S.C., Glover, D.M. and Fung, I.Y., 2001. Iron cycling and nutrient-limitation patterns in surface waters of the World Ocean. Deep Sea Research Part II: Topical Studies in Oceanography, 49(1-3), pp.463-507.

Moy, C.M., Seltzer, G.O., Rodbell, D.T., Anderson, D.M., 2002. Variability of El Niño Southern Oscillation activity at millennial timescales during the Holocene epoch. Nature 420, 162–165.

Nielsen J. M., Popp B. N., and Winder M. (2015). Meta-analysis of amino acid stable nitrogen isotope ratios for estimating trophic position in marine organisms. *Oecologia* **178**, 631-642.

Noé S. U. and Dullo W. C. (2006). Skeletal morphogenesis and growth mode of modern and fossil deep-water isidid gorgonians (Octocorallia) in the West Pacific (New Zealand and Sea of Okhotsk). *Coral reefs,* **25**, 303-320.

Noé S., Lembke-Jene L., Reveillaud J., and Freiwald A. (2007). Microstructure, growth banding and age determination of a primnoid gorgonian skeleton (Octocorallia) from the late Younger Dryas to earliest Holocene of the Bay of Biscay. *Facies*, **53**, 177-188.

Ohkouchi N., Chikaraishi Y., Close H. G., Fry B., Larsen T., Madigan D. J., McCarthy M. D., McMahon K. W., Nagata T., Naito Y. I., Ogawa N. O., Popp B. N., Steffan S., Takano Y., Tayasu I., Wyatt A. S. J., Yamaguchi Y. T., and Yokoyama Y. (2017) Advances in the application of amino acid nitrogen isotopic analysis in ecological and biogeochemical studies. *Organic Geochemistry* **113**, 150-174.

Oppo, D.W., Rosenthal, Y. and Linsley, B.K. (2009). 2,000-year-long temperature and hydrology reconstructions from the Indo-Pacific warm pool. *Nature,* **460** (7259), 1113-1116.

Park, J.Y., Kug, J.S., Park, J., Yeh, S.W. and Jang, C.J., (2011). Variability of chlorophyll associated with El Niño–Southern Oscillation and its possible biological feedback in the equatorial Pacific. *Journal of Geophysical Research: Oceans,* **116** (C10).

Pei, Q., Zhang, D.D., Li, J., Lee, H.F., (2017). Proxy-based Northern Hemisphere temperature reconstruction for the Mid-to-Late Holocene. *Theor. Appl. Climatol.* 130, 1043–1053.

Pena, L.D., Cacho, I., Ferretti, P. and Hall, M.A., (2008). El Niño–Southern Oscillation–like variability during glacial terminations and interlatitudinal teleconnections. *Paleoceanography,* **23** (3).

Pennington, J.T., Mahoney, K.L., Kuwahara, V.S., Kolber, D.D., Calienes, R., Chavez, F.P., (2006). Primary production in the eastern tropical Pacific: A review. *Prog. Oceanogr.* **69**, 285–317.

Pichevin, L.E., Ganeshram, R.S., Francavilla, S., Arellano-Torres, E., Pedersen, T.F., Beaufort, L., 2010. Interhemispheric leakage of isotopically heavy nitrate in the eastern tropical Pacific during the last glacial period. *Paleoceanography* **25**, 1–15.

Pichevin, L.E., Reynolds, B.C., Ganeshram, R.S., Cacho, I., Pena, L., Keefe, K., Ellam, R.M., (2009). Enhanced carbon pump inferred from relaxation of nutrient limitation in the glacial ocean. *Nature* **459,** 1114–1117.

Polovina, J.J., Howell, E. A., Abecassis, M., (2008). Ocean's least productive waters are expanding. *Geophys. Res. Lett.* **35**, 2–6.

Popp, B.N., Laws, E. a., Bidigare, R.R., Dore, J.E., Hanson, K.L., Wakeham, S.G., (1998). Effect of Phytoplankton Cell Geometry on Carbon Isotopic Fractionation. *Geochim. Cosmochim. Acta* **62**, 69–77.

Quay, P., Stutsman, J., (2003). Surface layer carbon budget for the subtropical N. Pacific: $\delta^{13}C$ constraints at station ALOHA. *Deep. Res. Part I Oceanogr. Res. Pap.* **50**, 1045–1061.

Quay, P., Sonnerup, R., Westby, T., Stutsman, J., McNichol, A. (2003). Changes in the $^{13}C/^{12}C$ of dissolved inorganic carbon in the ocean as a tracer of anthropogenic CO_2 uptake. *Global Biogeochem. Cycles* **17,** 1004, 1-20.

Quay, P. D., Sonnerup, R., Munro, D., and Sweeney, C., (2017). Anthropogenic CO_2 accumulation and uptake rates in the Pacific Ocean based on changes in the $^{13}C/^{12}C$ of dissolved inorganic carbon. *Global Biogeochem. Cycles* **31**, 59-80.

Ramirez M. D., Besser A. C., Newsome S. D., and McMahon K. W. (2021) Meta-analysis of primary producer amino acid δ15N values and the influence on trophic position estimation. *Methods Ecol Evol.* **12**, 1750–1767.

Rafter, P.A., Charles, C.D. (2012). Pleistocene equatorial Pacific dynamics inferred from the zonal asymmetry in sedimentary nitrogen isotopes. *Paleoceanography* **27**, 1–8.

Rafter, P. A., & Sigman, D. M. (2016). Spatial distribution and temporal variation of nitrate nitrogen and oxygen isotopes in the upper equatorial Pacific Ocean. *Limnology and Oceanography,* **61**(1), 14-31.

Rafter, P. A., Sigman, D. M., & Mackey, K. R. (2017). Recycled iron fuels new

production in the eastern equatorial Pacific Ocean. Nature communications, 8(1), 1-10.

Rau, G.H., Takahashi, T., Des Marais, D.J. (1989). Latitudinal variations in plankton $\delta^{13}C$: implications for CO_2 and productivity in past oceans. *Nature* **341**, 516–518.

Rau, G.H., Riebesell, U., Wolf-Gladrow, D. (1996). A model of photosynthetic ^{13}C fractionation by marine phytoplankton based on diffusive molecular CO_2 uptake. *Mar. Ecol. Prog. Ser.* **133**, 275–285.

Rau, G.H., Takahashi, T., Desmarais, D.J., Repeta, D.J., Martin, J.H. (1992). The relationship between $\delta^{13}C$ of organic matter and [CO_2 (aq)] in ocean surface water: Data from a JGOFS site in the northeast Atlantic Ocean and a model. *Geochim. Cosmochim. Acta* **56**, 1413–1419.

Reimer, P.J., Brown, T. a, Reimer, R.W. (2004). Discussion: Reporting and Calibration of Post-Bomb ^{14}C Data. *Radiocarbon* **46**, 1299–1304.

Reimer, P.J., Bard, E., Bayliss, A., Beck, J.W., Blackwell, P.G., Ramsey, C.B., Buck, C.E., Cheng, H., Edwards, R.L., Friedrich, M., Grootes, P.M., Guilderson, T.P., Haflidason, H., Hajdas, I., Hatté, C., Heaton, T.J., Hoffmann, D.L., Hogg, A.G., Hughen, K.A., Kaiser, K.F., Kromer, B., Manning, S.W., Niu, M., Reimer, R.W., Richards, D.A., Scott, E.M., Southon, J.R., Staff, R.A., Turney, C.S.M., van der Plicht, J. (2013). IntCal13 and Marine13 Radiocarbon Age Calibration Curves 0–50,000 Years cal BP. *Radiocarbon* **55**, 1869–1887.

Roark E. B., Guilderson T. P., Dunbar R. B., and Ingram B. L. (2006) Radiocarbon-based ages and growth rates of Hawaiian deep-sea corals. *Marine Ecology Progress Series* **327**, 1–14.

Roark, E.B., Guilderson, T.P., Dunbar, R.B., Fallon, S.J., Mucciarone, D. A. (2009). Extreme longevity in proteinaceous deep-sea corals. *Proc. Natl. Acad. Sci. U.S.A.* **106,** 5204–5208.

Robinson, R.S., Martinez, P., Pena, L.D., Cacho, I. (2009). Nitrogen isotopic evidence for deglacial changes in nutrient supply in the eastern equatorial Pacific. *Paleoceanography* **24**, PA4213, 1-12.

Rodionov, S.N. (2004). A sequential algorithm for testing climate regime shifts. *Geophys. Res. Lett.* **31** (9). Regime shift program available at: https://www.beringclimate.noaa.gov/regimes/

Rodionov, S.N. (2006). Use of prewhitening in climate regime shift detection. *Geophys. Res. Lett.* **33** (12).

Romanek, C. S., Grossman, E. L., and Morse, J.W. (1992). Carbon isotopic fractionation in synthetic aragonite and calcite: Effects of temperature and precipitation rate. *Geochimica et Cosmochiica Acta*, **56**, 419-430.

Rustic, G. T., Koutavas, A., Marchitto, T. M., & Linsley, B. K. (2015). Dynamical excitation of the tropical Pacific Ocean and ENSO variability by Little Ice Age cooling. *Science*, **350** (6267), 1537-1541.

Sachs, J.P., Sachse, D., Smittenberg, R.H., Zhang, Z., Battisti, D.S. and Golubic, S., (2009). Southward movement of the Pacific intertropical convergence zone AD 1400–1850. *Nature Geoscience*, **2** (7), pp.519-525.

Saino T. and Hattori A. (1980) ^{15}N natural abundance in oceanic suspended particulate matter. *Nature* **283**, 752–754.

Saino T. and Hattori A. (1987) Geographical variation of the water column distribution of suspended particulate organic nitrogen and its ^{15}N natural abundance in the Pacific and its marginal seas. *Deep Sea Research Part A, Oceanographic Research Papers* **34**, 807–827.

Sauthoff W. (2016) Nitrogen Isotopes of Amino Acids in Marine Sediment: A Burgeoning Tool to Assess Organic Matter Quality and Changes in Supplied Nitrate ^{15}N. University of California Santa Cruz, Master's Thesis.

Schiff, J.T., Batista, F.C., Sherwood, O.A., Guilderson, T.P., Hill, T.M., Ravelo, A.C., McMahon, K.W., Mccarthy, M.D. (2014). Compound specific amino acid $\delta^{13}C$ patterns in a deep-sea proteinaceous coral: Implications for reconstructing detailed $\delta^{13}C$ records of exported primary production. *Mar. Chem.* **166**, 82–91.

Schmittner, A., & Somes, C. J. (2016). Complementary constraints from carbon (^{13}C) and nitrogen (^{15}N) isotopes on the glacial ocean's soft-tissue biological pump. *Paleoceanography*, **31** (6), 669-693.

Schneider, T., Bischoff, T., Haug, G.H. (2014). Migrations and dynamics of the intertropical convergence zone. *Nature* **513**, 45–53.

Scott, K.M., Henn-Sax, M., Harmer, T.L., Longo, D.L., Frame, C.H., Cavanaugh, C.M. (2007). Kinetic isotope effect and biochemical characterization of form IA RubisCO from the marine cyanobacterium Prochlorococcus marinus MIT9313. *Limnol. Oceanogr.* **52**, 2199–2204.

Shen Y., Guilderson T. P., Sherwood O. A., Castro C. G., Chavez F. P. and McCarthy M. D. (2021) Amino acid $\delta^{13}C$ and $\delta^{15}N$ patterns from sediment trap time series and deep-sea corals: Implications for biogeochemical and ecological

reconstructions in paleoarchives. *Geochimica et Cosmochimica Acta* **297**, 288–307.

Sherwood O. A., Scott D. B. and Risk M. J. (2006) Late Holocene radiocarbon and aspartic acid racemization dating of deep-sea octocorals. *Geochimica et Cosmochimica Acta* **70**, 2806–2814.

Sherwood O. A. and Edinger E. N. (2009) Ages and growth rates of some deep-sea gorgonian and antipatharian corals of Newfoundland and Labrador. *Canadian Journal of Fisheries and Aquatic Sciences* **66**, 142–152.

Sherwood O. A., Thresher R. E., Fallon S. J., Davies D. M. and Trull T.W. (2009) Multi-century time-series of ^{15}N and ^{14}C in bamboo corals from deep Tasmanian seamounts: Evidence for stable oceanographic conditions. *Marine Ecology Progress Series* **397**, 209–218.

Sherwood O. A., Lehmann M. F., Schubert C. J., Scott D. B. and McCarthy M. D. (2011) Nutrient regime shift in the western North Atlantic indicated by compound-specific $\delta^{15}N$ of deep-sea gorgonian corals. *Proceedings of the National Academy of Sciences of the United States of America* **108**, 1011–1015.

Sherwood O. A., Guilderson T. P., Batista F. C., Schiff J. T. and McCarthy M.D. (2014) Increasing subtropical North Pacific Ocean nitrogen fixation since the Little Ice Age. *Nature* **505**, 78–81.

Sigman, D.M., DiFiore, P.J., Hain, M.P., Deutsch, C., Karl, D.M., Bo, V. (2009). Sinking organic matter spreads the nitrogen isotope signal of pelagic denitrification in the North Pacific. *Geophysical Research Letters* **36**, L08605, 1-5.

Silfer J. A., Engel M. H., Macko S. A. and Jumeau E. J. (1991) Stable carbon isotope analysis of amino acid enantiomers by conventional isotope ratio mass spectrometry and combined gas chromatography/isotope ratio mass spectrometry. *Analytical Chemistry* **63**, 370–374.

Somes, C. J., A. Schmittner, E. D. Galbraith, M. F. Lehmann, M. A. Altabet, J. P. Montoya, R. M. Letelier, A. C. Mix, A. Bourbonnais, and M. Eby (2010), Simulating the global distribution of nitrogen isotopes in the ocean, Global *Biogeochem. Cycles*, **24**, GB4019.

Strzepek K. M., Thresher R. E., Revill A. T., Smith C. I., Komugabe A. F. and Fallon S. F. (2014) Preservation effects on the isotopic and elemental composition of skeletal structures in the deep-sea bamboo coral Lepidisis spp. (Isididae). *Deep-Sea Research Part II: Topical Studies in Oceanography* **99**, 199–206.

Stuiver, M., Polach, H.A. (1977). Discussion Reporting of ^{14}C Data. *Radiocarbon* **19**, 355–363.

Stuiver, M., Reimer, P.J., and Reimer, R.W. (2021). CALIB 8.2 [WWW program] at http://calib.org.

Sun X. and Turchyn A. V. (2014) Significant contribution of authigenic carbonate to marine carbon burial. *Nature Geoscience* **8**, 1–4.

Takahashi, T., Sutherland, S.C., Wanninkhof, R., Sweeney, C., Feely, R.A., Chipman, D.W., Hales, B., Friederich, G., Chavez, F., Sabine, C., Watson, A., Bakker, D.C.E., Schuster, U., Metzl, N., Yoshikawa-Inoue, H., Ishii, M., Midorikawa, T., Nojiri, Y., Körtzinger, A., Steinhoff, T., Hoppema, M., Olafsson, J., Arnarson, T.S., Tilbrook, B., Johannessen, T., Olsen, A., Bellerby, R., Wong, C.S., Delille, B., Bates, N.R., de Baar, H.J.W. (2009). Climatological mean and decadal change in surface ocean pCO_2, and net sea-air CO_2 flux over the global oceans. *Deep. Res. Part II Top. Stud. Oceanogr.* **56**, 8-10, 554-577.

Tans, P.P., I.Y. Fung, and T. Takahashi (1990). Observational constraints on the global atmospheric CO_2 budget. *Science*, **247**, 1431-1439,

Tesdal, J.E., Galbraith, E.D., Kienast, M. (2013). Nitrogen isotopes in bulk marine sediment: Linking seafloor observations with subseafloor records. *Biogeosciences* **10**, 101–118.

Thompson, L.G., Mosley-Thompson, E., Davis, M.E., Zagorodnov, V.S., Howat, I.M., Mikhalenko, V.N. and Lin, P.N. (2013). Annually resolved ice core records of tropical climate variability over the past~ 1800 years. *Science,* **340** (6135), 945-950.

Thunell, R.C., Kepple, A.B. (2004). Glacial-Holocene $\delta^{15}N$ record from the Gulf of Tehuantepec, Mexico: Implications for denitrification in the eastern equatorial Pacific and changes in atmospheric N_2O. *Global Biogeochem. Cycles* **18**, 1–12.

Trenberth, K.E. and Smith, L. (2006). The vertical structure of temperature in the tropics: Different flavors of El Niño. *Journal of climate*, **19** (19), 4956-4973.

Turk, D., Lewis, M.R., Harrison, G.W., Kawano, T. and Asanuma, I. (2001). Geographical distribution of new production in the western/central equatorial Pacific during El Niño and non-El Niño conditions. *Journal of Geophysical Research: Oceans*, **106** (C3), 4501-4515.

Vogel, J.S., Nelson, D.E., Southon, J.R. (1987). ^{14}C background levels in an accelerator mass spectrometry system. *Radiocarbon* **29**, 323–333.

Voss, M., Dippner, J.W., Montoya, J.P. (2001). Nitrogen isotope patterns in the oxygen-deficient waters of the Eastern Tropical North Pacific Ocean. *Deep. Res. Part I Oceanogr. Res. Pap.* **48**, 1905–1921.

Wang, C. and Fiedler, P.C. (2006). ENSO variability and the eastern tropical Pacific: A review. *Progress in Oceanography*, **69**(2-4), pp.239-266.

Williams B. (2020). Proteinaceous corals as proxy archives of paleo-environmental change. *Earth-Science Reviews **209***, 103326.

Williams B. and Grottoli A. G. (2010) Recent shoaling of the nutricline and thermocline in the western tropical Pacific. *Geophysical Research Letters* **37**, 2–6.

Wu, H.C., Dissard, D., Douville, E., Blamart, D., Bordier, L., Tribollet, A., Le Cornec, F., Pons-Branchu, E., Dapoigny, A. and Lazareth, C.E. (2018). Surface ocean pH variations since 1689 CE and recent ocean acidification in the tropical South Pacific. *Nature Communications,* **9** (1), 1-13.

Yamashita Y. and Tanoue E. (2003) Distribution and alteration of amino acids in bulk DOM along a transect from bay to oceanic waters. *Marine Chemistry* **82**, 145-160.

Yan, H., Sun, L., Wang, Y., Huang, W., Qiu, S., Yang, C., 2011. A record of the Southern Oscillation Index for the past 2,000 years from precipitation proxies. *Nat. Geosci.* **4**, 611–614.

Yang, S., Gruber, N., Long, M. C., & Vogt, M. (2017). ENSO driven variability of denitrification and suboxia in the Eastern Tropical Pacific Ocean. *Global Biogeochemical Cycles*, **31**, 1470–1487,

Young, J.N., Bruggeman, J., Rickaby, R.E.M., Erez, J., Conte, M. (2013). Evidence for changes in carbon isotopic fractionation by phytoplankton between 1960 and 2010. *Global Biogeochem. Cycles* **27**, 505–515.

Zaiontz C. (2019) Real Statistics Resource Pack software (Release 6.2). Copyright (2013 – 2019) www.real-statistics.com

Zaunbrecher, L.K., Cobb, K.M., Beck, J.W., Charles, C.D., Druffel, E.R., Fairbanks, R.G., Griffin, S. and Sayani, H.R. (2010). Coral records of central tropical Pacific radiocarbon variability during the last millennium. *Paleoceanography*, **25** (4).

Zhang, X. and Dam, H.G. (1997). Downward export of carbon by diel migrant mesozooplankton in the central equatorial Pacific. *Deep Sea Research Part II: Topical Studies in Oceanography*, **44** (9-10), 2191-2202.

Zhang, R.H., Rothstein, L.M. and Busalacchi, A.J. (1998). Origin of upper-ocean warming and El Niño change on decadal scales in the tropical Pacific Ocean. *Nature*, **391**(6670), pp.879-883.

Zubkov, M. V. (2014). Faster growth of the major prokaryotic versus eukaryotic CO_2 fixers in the oligotrophic ocean. *Nat. Commun.* 5, 1–6.